



QUANTITATIVE EXPERIMENTAL CHARACTERIZATION AND MATHEMATICAL MODELING OF MIXED CULTURE DYNAMICS

—

**ANALYSIS OF A MEDICALLY RELEVANT THREE-SPECIES
MIXED CULTURE IN A CHEMOSTAT**

Dissertation

zur Erlangung des akademischen Grades
Doktoringenieurin
(Dr.-Ing.)

von Dipl.-Ing. & Dipl.-Biol. Julia K. Schmidt
geb. am 12.10.1971 in Bad Oeynhausen

genehmigt durch die Fakultät für Verfahrens- und Systemtechnik
der Otto-von-Guericke-Universität Magdeburg

Gutachter:

Prof. Dr.-Ing. Udo Reichl

Prof. Dr. rer. nat. Thomas Bley

Promotionskolloquium am 17.10.2008

Forschungsberichte aus dem Max-Planck-Institut
für Dynamik komplexer technischer Systeme

Band 25

Julia K. Schmidt

**Quantitative Experimental Characterization and
Mathematical Modeling of Mixed Culture Dynamics**

Analysis of a Medically Relevant Three-Species Mixed Culture
in a Chemostat

Shaker Verlag
Aachen 2008

Bibliographic information published by the Deutsche Nationalbibliothek

The Deutsche Nationalbibliothek lists this publication in the Deutsche Nationalbibliografie; detailed bibliographic data are available in the Internet at <http://dnb.d-nb.de>.

Zugl.: Magdeburg, Univ., Diss., 2008

Copyright Shaker Verlag 2008

All rights reserved. No part of this publication may be reproduced, stored in a retrieval system, or transmitted, in any form or by any means, electronic, mechanical, photocopying, recording or otherwise, without the prior permission of the publishers.

Printed in Germany.

ISBN 978-3-8322-7776-5

ISSN 1439-4804

Shaker Verlag GmbH • P.O. BOX 101818 • D-52018 Aachen

Phone: 0049/2407/9596-0 • Telefax: 0049/2407/9596-9

Internet: www.shaker.de • e-mail: info@shaker.de

Danksagung

Die vorliegende Arbeit entstand während meiner Tätigkeit als wissenschaftliche Mitarbeiterin des Lehrstuhls Bioprozesstechnik der Fakultät für Verfahrens- und Systemtechnik der Otto-von-Guericke-Universität am Max-Planck-Institut für Dynamik komplexer technischer Systeme in Magdeburg. Allen, die zum Gelingen der Arbeit beigetragen haben, danke ich herzlich. Ganz besonderer Dank gilt:

Prof. Dr.-Ing. U. Reichl für die Möglichkeit zur Promotion an seinem Lehrstuhl und die Überlassung des spannenden Themas zur weitestgehend freien Gestaltung und selbstständigen Bearbeitung.

Prof. Dr. rer. nat. T. Bley für die Übernahme des Zweitgutachtens.

Dr. Yvonne Genzel für ihre ganz besondere Unterstützung meiner Arbeiten, ihre stets offene Tür zur Diskussion konzeptioneller Fragestellungen und gute Zusammenarbeit in gemeinsamen Projekten.

Liane Geisler für ihre unschätzbare Verlässlichkeit, gute Laune und Energie im Labor und ihre Hilfe bei der Durchführung der T-RFLP-Analysen und Kultivierungen.

Bastian Schäfer, Julia Rausenberger und Lars Regestein für ihr großes Engagement im Rahmen ihrer Diplomarbeiten und den damit geleisteten Beitrag zu dieser Arbeit.

Allen Kollegen in der Gruppe Bioprozesstechnik und am Max-Planck-Institut für die freundschaftliche Arbeitsatmosphäre, gegenseitige Unterstützung und stetige Bereitschaft zur Diskussion, insbesondere Andreas Bock, Dr. Boris Hundt, Bernd Kalbfuß-Zimmermann, Dr. Lars Möhler, Christian Riedele, Joachim Ritter, Josef Schulze-Horsel, Jana Schwarzer, Henrik Sommer, Diana Vester und Anke Zimmermann.

Prof. Dr. rer. nat. D. Flockerzi für vertiefende Diskussionen zur mathematischen Betrachtung der Konkurrenz und Koexistenz im Chemostat.

Prof. Dr. rer. nat. B. König und Prof. Dr. med. W. König für die großzügige Bereitstellung experimenteller Möglichkeiten am Institut für Medizinische Mikrobiologie in der Anfangszeit dieser Arbeit.

Dem Kultusministerium des Landes Sachsen-Anhalt für die Finanzierung eines Teils der vorliegenden Arbeit (Forschungsprojekt FKZ: 3572A/0604T).

Meinen Eltern für ihre Unterstützung und ihr Vertrauen in mich und die Möglichkeit, meinen Weg nach meinen Vorstellungen gehen zu können.

Kurzfassung

Das Ziel der vorliegenden Arbeit war die Charakterisierung der Wachstumsdynamik einer definierten drei-Spezies Mischkultur im Chemostat mittels experimenteller Untersuchungen und mathematischer Modellbildung. Es gibt zahlreiche rein experimentelle Untersuchungen mit zwei-Spezies Systemen und mindestens ebenso viele rein mathematische Analysen zur Konkurrenz im Chemostat mit bis zu unendlich vielen Spezies. Über die Verknüpfung beider Herangehensweisen wurde bislang kaum berichtet. Das gewählte Modellsystem aus *Staphylococcus aureus* (*S. a.*), *Burkholderia cepacia* (*B. c.*) und *Pseudomonas aeruginosa* (*P. a.*) ist motiviert durch Mischinfektionen in Lungen von Mukoviszidose Patienten (Cystische Fibrose).

Zur Bestimmung absoluter und speziespezifischer Zellzahlen aus Mischkulturen, insbesondere für mehr als zwei Stämme, existierte bislang keine Methode, abgesehen von arbeitsaufwendigen Selektivplattenverdünnungen. Im Rahmen der Arbeit wurde eine quantitative T-RFLP Analysemethode etabliert und validiert, die eine für die mathematische Modellierung notwendige hohe Datenqualität, das heißt Reproduzierbarkeit und Genauigkeit, gewährleistet. Die Linearität der Methode innerhalb des Messbereichs von 10^4 bzw. 10^6 cfu/mL (speziesabhängig) bis 10^{10} cfu/mL für log-transformierte Zellzahlen wurde gezeigt. Der maximale Fehler war (Mittelwert \pm Standardabweichung (cfu/mL log-transformiert)) $8,60\pm 0,39$ für zwei-Spezies Proben und $6,95\pm 0,20$ für drei-Spezies Proben.

Ein experimentelles Protokoll zur Generierung reproduzierbarer Mischkulturen unter definierten und kontrollierbaren Bedingungen in Rührreaktoren wurde etabliert. Für Mischkultivierungen mit drei Spezies wurde eine stabile Koexistenz von *B. c.* und *P. a.* über mehr als 35 Volumenaustausche im Chemostat ($D = 0,2 \text{ h}^{-1}$) gefunden. Zusätzlich wurde das Vorhandensein von *S. a.* unterhalb der T-RFLP Detektionsgrenze mit Selektivplatten noch am Ende der Kultivierungsdauer nachgewiesen. In Mischkulturexperimenten mit zwei Spezies, *S. a.* und *B. c.*, war das Ergebnis nicht eindeutig, es könnte sowohl eine stabile Koexistenz oder ein sehr langsames Auswaschen von *S. a.* vorgelegen haben.

Die erstellten Modelle basierten auf dem klassischen Chemostatmodell mit Monod-Kinetik für Konkurrenz um ein Substrat. Über den Vergleich der erzielten experimentellen Daten und Modellsimulationen für bestimmte erweiterte Annahmen zu Eigenschaften sowohl der Mischkulturen (Chemostat) als auch der Reinkulturen (Batch und Chemostat) wurden potentielle Interaktionen zwischen den Spezies identifiziert. Es wurde so auch überprüft,

welche der Interaktionen für die beobachtete Koexistenz von zwei oder sogar drei Spezies verantwortlich sein könnte. Für diese Simulationsanalyse wurden ausschließlich Parameter verwendet, die auf separaten Einzelspezies-Experimenten und -Modellen beruhen.

Eine Acetat-Biotrophie zwischen *S. a.* als Produzent und *B. c.* bzw. *P. a.* als Verbraucher wurde für einen zwei- und einen drei-Spezies Chemostaten simuliert, konnte jedoch für biologisch sinnvolle Parametersätze die experimentell gefundene Koexistenz nicht erklären.

Die Nutzung von Glucose und Aminosäuren als Mischsubstrat wurde modelliert und für *S. a.* abhängiges Wachstum und unabhängiges Wachstum für *B. c.* (mit Diauxie) und *P. a.* angenommen. Für die Mischsubstratkinetik wurden zwei Varianten verglichen, gekoppelte Verwertung (ein $\mu_{max,199,i}$) und entkoppelte Verwertung (je ein $\mu_{max,Glc,i}$ und ein $\mu_{max,AA,i}$). Nur die zweite Variante simulierte die Koexistenz zwischen *B. c.* und *P. a.* und Auswaschen von *S. a.* und ergab damit eine sehr gute Übereinstimmung zu dem experimentellen Befund des drei-Spezies Experiments.

Eine mögliche drei-Spezies Koexistenz, wie sie aus den Resultaten der Selektivplatten für *S. a.* abzuleiten wäre, konnte durch Erweiterungen des Mischsubstratmodells mit weiteren Annahmen zu möglichen Interaktionen erklärt werden: a) Konkurrenz um Valin als einem dritten Substrat und b) Biotrophie mit einem noch nicht identifizierten Stoffwechselprodukt, das von *P. a.* gebildet wird. Weitere experimentelle Untersuchungen zur Bestätigung und Quantifizierung dieser Annahmen sind jedoch notwendig.

Im Rahmen des Projekts wurde gezeigt, dass der Vergleich zwischen der mathematischen Beschreibung eines Mischkulturchemostats und experimenteller Daten die Identifizierung potentieller Interaktionen zwischen den Spezies ermöglicht. Eine wichtige Voraussetzung dafür boten die mittels der etablierten T-RFLP Methode reproduzierbaren und genauen Zellzahlbestimmungen der Mischkulturkeimzahlen. Die Untersuchung wurde mit Stämmen durchgeführt, die im Gegensatz zu den in der Literatur beschriebenen Systemen keine gezielt gewählten und insgesamt unbekannte Wachstumscharakteristika hatten. Die detaillierte experimentelle Analyse und genaue mathematische Beschreibung der Reinkulturen stellte sich daher als weitere wichtige Bedingung bei den durchgeführten Untersuchungen heraus.

List of Contents

1	INTRODUCTION	1
2	THEORY	5
2.1	MEDICAL BACKGROUND: INFECTIONS IN CYSTIC FIBROSIS PATIENTS	5
2.1.1	HEREDITARY DISEASE CYSTIC FIBROSIS	5
2.1.2	MIXED CULTURE STUDIES FOR CF RELEVANT BACTERIA	5
2.1.3	PHYSIOLOGY AND NUTRIENT REQUIREMENTS OF CF RELEVANT BACTERIA	6
2.1.3.1	<i>Staphylococcus aureus</i>	6
2.1.3.2	<i>Burkholderia cepacia</i>	7
2.1.3.3	<i>Pseudomonas aeruginosa</i>	7
2.2	GROWTH OF SINGLE MICROBIAL SPECIES	9
2.2.1	SINGLE NUTRIENT CONTROLLED KINETICS	9
2.2.1.1	Growth with a Single Substrate	9
2.2.1.2	Maintenance	9
2.2.1.3	Inhibition	10
2.2.2	USE OF MIXED SUBSTRATES	10
2.2.2.1	Diauxic Growth	11
2.2.2.2	Multiple Substrate Growth	11
2.2.3	BATCH AND CONTINUOUS PROCESS MODE MODELS	12
2.3	MIXED CULTURES OF BACTERIA	13
2.3.1	THE STRUGGLE FOR EXISTENCE – A HISTORICAL INTRODUCTION	13
2.3.2	APPROACHES TO MIXED CULTURES IN DIFFERENT SCIENTIFIC FIELDS	13
2.3.3	INTERSPECIES INTERACTIONS	15
2.3.4	EXPERIMENTAL STUDIES OF INTERACTIONS	17
2.4	COMPETITION AND COEXISTENCE IN THE CHEMOSTAT	18
2.4.1	THE BASICS OF THE CHEMOSTAT PROCESS	18
2.4.2	COMPETITIVE EXCLUSION PRINCIPLE VERSUS PARADOX OF THE PLANKTON	19
2.4.3	MATHEMATICAL CHEMOSTAT MODELS OF MIXED CULTURES	20
2.4.3.1	Resource-Consumer-Models and Interference-Competition-Models	20
2.4.3.2	Model Assumptions for Circumvention of the CEP	20
2.4.3.3	Experimental Verifications of Mathematical Assumptions	22
2.5	QUANTIFICATION OF CELL NUMBERS IN MIXED CULTURE SAMPLES	22
2.5.1	MOLECULAR BIOLOGICAL ENUMERATION METHODS	23
2.5.2	TERMINAL-RESTRICTION FRAGMENT LENGTH POLYMORPHISM (T-RFLP) ANALYSIS	24
2.6	ASPECTS OF MATHEMATICAL MODELING AND MODEL VALIDATION	25
2.6.1	INTRODUCTION OF SOME BASICS ON PARAMETER IDENTIFICATION	25
2.6.2	DETERMINATION OF KINETIC AND STOICHIOMETRIC GROWTH PARAMETERS	26
3	MATERIALS AND METHODS	29
3.1	BUFFERS AND SOLUTIONS	29
3.1.1	WORKING SOLUTIONS FOR CULTURE MEDIA	29
3.1.2	WORKING SOLUTIONS FOR ANALYTICS	30
3.1.3	WORKING SOLUTIONS FOR T-RFLP AND PREPARATION OF IQS	30
3.2	MEDIA	32
3.2.1	LIQUID CULTURE MEDIA	32
3.2.1.1	Chemically Defined Full Media	32
3.2.1.2	Complex Medium (Laura-Bertani)	33
3.2.2	SOLID CULTURE MEDIUM	34
3.2.2.1	General Complex Agar Media	34

3.2.2.2	Selective Agar Media	34
3.3	MICROORGANISMS	34
3.3.1	MAIN STRAINS FOR CULTIVATION EXPERIMENTS	34
3.3.2	OTHER STRAINS	34
3.3.3	STRAIN KEEPING AND WORKING STOCK PREPARATION	35
3.4	CULTIVATION METHODS	35
3.4.1	CULTIVATION ON AGAR PLATES	35
3.4.2	MICROAEROBILIC AGAR PLATE CULTIVATIONS OF <i>CAMPYLOBACTER JEJUNI</i>	35
3.4.3	SHAKE FLASK CULTIVATIONS	35
3.4.3.1	Shake Flasks and Shake Flask Incubator	35
3.4.3.2	Batch Cultivations in Shake Flasks	36
3.4.4	2 L STIRRED TANK BIOREACTOR (2 L STR)	36
3.4.4.1	Set-up of 2 L Stirred Tank System	36
3.4.4.2	Batch Cultivation in 2 L Stirred Tank Reactor	38
3.4.4.3	Chemostat Cultivation in Stirred Tank Reactor	39
3.4.5	SMALL SCALE PARALLEL STIRRED TANK BIOREACTOR (SMALL SCALE STR)	40
3.4.5.1	Set-up of Small Scale STR	40
3.4.5.2	Batch Cultivation in Small Scale STR	41
3.4.5.3	Chemostat Cultivation in Small Scale STR	42
3.5	ANALYTICAL ASSAYS	42
3.5.1	CELL ENUMERATION FOR SINGLE-SPECIES SAMPLES	42
3.5.2	CELL ENUMERATION FOR MIXED SPECIES SAMPLES (T-RFLP ANALYSIS METHOD)	43
3.5.2.1	Generation of 16S rDNA Fragments from Bacteria Samples	43
3.5.2.2	Analysis of the 16S rDNA Fragment Mixture	45
3.5.2.3	Calculation of Cell Numbers from Fragment Analysis Data	47
3.5.3	METABOLIC SUBSTRATES AND PRODUCTS	49
3.6	MATHEMATICAL MODELING OF THE BACTERIAL CULTURES	50
3.6.1	CHARACTERIZATION OF MODEL TYPE AND MODELING METHOD	50
3.6.2	MATLAB MODELING AND SIMULATION SOFTWARE	50
3.6.3	PARAMETER ESTIMATION METHODS	50
4	RESULTS	53
4.1	ESTABLISHMENT OF THE CULTIVATION PROTOCOL	53
4.1.1	POOL OF BACTERIAL STRAINS	53
4.1.2	SELECTION OF A FULL AND CHEMICALLY DEFINED CULTURE MEDIUM	53
4.1.3	SCALE-UP AND IMPACT OF AERATION	54
4.2	QUANTIFICATION OF SPECIES SPECIFIC CELL NUMBERS IN MIXED CULTURES	56
4.2.1	REPRODUCIBILITY OF THE QUANTITATIVE T-RFLP ANALYSIS METHOD	56
4.2.2	LINEARITY AND HOMOGENEITY OF VARIANCES FOR SINGLE-SPECIES (S. A.)	59
4.2.3	RECOVERY OF T-RFLP QUANTIFICATIONS IN MIXED SPECIES DILUTION SERIES	60
4.2.4	REPRODUCIBILITY BETWEEN DIFFERENT RUNS OF QUANTITATIVE T-RFLP	66
4.2.5	QUANTITATIVE T-RFLP FOR MONITORING CULTIVATION EXPERIMENTS	67
4.2.6	SUMMARY	69
4.3	SINGLE-SPECIES GROWTH: <i>S. AUREUS</i>, <i>B. CEPACIA</i>, AND <i>P. AERUGINOSA</i>	71
4.3.1	EXPERIMENTS ON GROWTH DYNAMICS	71
4.3.1.1	Growth Dynamics of <i>S. aureus</i>	71
4.3.1.2	Growth Dynamics of <i>B. cepacia</i>	74
4.3.1.3	Growth Dynamics of <i>P. aeruginosa</i>	77
4.3.1.4	Chemostat at Different Dilution Rates	79
4.3.2	EXPERIMENTS ON PROPERTIES POTENTIALLY RELEVANT IN INTERACTIONS	83
4.3.2.1	Uptake of Acetate	83
4.3.2.2	Influence of pH value	85
4.3.2.3	Functions of Glucose and Amino Acids as Growth Substrates	85
4.3.3	SUMMARY OF THE EXPERIMENTAL RESULTS OF SINGLE-SPECIES CHARACTERISTICS	88

4.3.4	SINGLE-SPECIES MATHEMATICAL MODELS	91
4.3.4.1	Growth on One Substrate: Glucose	91
4.3.4.2	Growth on Two Substrates: Glucose and Acetate	92
4.3.4.3	Growth on One Substrate: Amino Acids	94
4.3.4.4	Growth on Two Substrates: Glucose and Amino Acids	95
4.3.5	SUMMARY OF RESULTS FOR MATHEMATICAL MODELING OF SINGLE-SPECIES GROWTH	110
4.4	INVESTIGATION OF BIOTROPY ON ACETATE	112
4.4.1	TWO-SPECIES CHEMOSTAT EXPERIMENTS	112
4.4.2	MATHEMATICAL MODELS OF TWO-SPECIES CHEMOSTAT	114
4.4.2.1	Two-Species Chemostat Model without Acetate Biotrophy	114
4.4.2.2	Two-Species Chemostat Model with Acetate Biotrophy	115
4.4.3	SUMMARY	118
4.5	INVESTIGATION OF SPECIES INTERACTIONS IN A THREE-SPECIES CHEMOSTAT	119
4.5.1	THREE-SPECIES CHEMOSTAT EXPERIMENTS IN 2 L STIRRED TANK	119
4.5.2	THREE-SPECIES CHEMOSTAT EXPERIMENTS IN SMALL SCALE STR	123
4.5.3	MATHEMATICAL MODELS OF THREE-SPECIES CHEMOSTAT	125
4.5.3.1	Three-Species Chemostat Model with Single Substrate Competition	125
4.5.3.2	Three-Species Chemostat Model with Acetate Biotrophy	126
4.5.3.3	Three-Species Chemostat Models with Mixed Substrate Growth	128
4.5.3.4	Studies of the Properties of Model Variant No. 2 to Explain Coexistence	133
4.5.3.5	Chemostat Model Variants to Generate Three-Species Coexistence	135
4.5.4	SUMMARY	140
5	DISCUSSION	145
5.1	SYSTEMS ANALYSIS BY COMBINING MATHEMATICAL MODELING AND EXPERIMENTS	145
5.2	CELL NUMBER QUANTIFICATION WITH T-RFLP	148
5.2.1	REQUIREMENTS FOR MIXED CULTURE CELL ENUMERATION	148
5.2.2	EVALUATION OF ERROR WITHIN T-RFLP QUANTIFICATION	149
5.2.3	MEANS OF IMPACT ON T-RFLP QUANTIFICATION QUALITY AND RANGE	149
5.2.4	APPLICATION OF T-RFLP FOR MONITORING CULTIVATIONS	152
5.2.5	BENEFIT OF T-RFLP QUANTIFICATION FOR MIXED CULTURE STUDIES	153
5.3	GROWTH CHARACTERISTICS OF THE SINGLE SPECIES	154
5.3.1	SINGLE-SPECIES EXPERIMENTS WITH <i>S. AUREUS</i> , <i>B. CEPACIA</i> , AND <i>P. AERUGINOSA</i>	154
5.3.1.1	Acetate, Pyruvate and Influence of pH Value	155
5.3.1.2	Growth on Two Substrates: Glucose and Amino Acids	156
5.3.1.3	Other Substrates and Metabolites	157
5.3.2	MODEL ASSUMPTIONS AND SIMULATION RESULTS FOR THE SINGLE-SPECIES	158
5.3.2.1	Estimated Kinetic Parameters for Growth on Glucose	158
5.3.2.2	Mixed Substrate Kinetics for Glucose and Amino Acids	158
5.4	APPARENT COEXISTENCE PHENOMENON IN THE MIXED CULTURES	162
5.4.1	MIXED CULTURES WITH ACETATE AS ADDITIONAL CARBON SOURCE	163
5.4.2	EVALUATION OF MIXED CULTURE WITH MULTIPLE SUBSTRATE USE	165
5.4.3	EXPLANATIONS FOR A POSSIBLE THREE-SPECIES COEXISTENCE	167
5.5	COMPARISON TO THE ORIGINAL SYSTEM - CF LUNGS	168
6	SUMMARY	171
7	OUTLOOK	173
8	REFERENCES	175
9	APPENDIX	181

List of Symbols, Abbreviations and Indices

Symbols

AA	Concentration of amino acids	(g/L)
A	Peak area in fragment analysis	
Ace	Concentration of acetate	(g/L)
c_j	Concentration of component j	(g/L); (cfu/L); (mol/L)
cyc	Number of PCR cycles	(-)
d	Diameter of reactor vessel	(m)
D	Dilution rate	(h ⁻¹)
d_0	Eccentric diameter	(m)
f	Efficiency parameter of PCR in T-RFLP	(-)
F	Dilution factor	(-)
F_x	Dilution factor of the x th dilution step	(-)
Glc	Concentration of glucose	(g/L)
h	Relative humidity	(%)
H	Height of reactor vessel	(m)
i	Number of species in the mixed culture	(-)
I	Inhibitor Concentration	(g/L)
K_i	Inhibition constant	(g/L)
K_s	Substrate affinity, half-saturation (Monod) constant	(g/L)
m	Specific maintenance rate	(h ⁻¹)
\dot{m}_L	Mass flow of liquid medium feed	(g/h)
n	Revolutions per minute	(rpm)
N	Cell number of a bacterial species	(cfu)
$N_{\text{counted cells}}$	Cell number in a counting chamber	(-)
$N_{\text{small squares}}$	Small squares used in a counting chamber	(-)
OTR	Oxygen transfer rate	(mol/(L·h))
p	Pressure	(bar)
p_j	Partial pressure of component j	(bar)
$p_{O_2,L}$	Partial pressure of oxygen in the liquid phase	(% air saturation)
Pr	Concentration of hypothetical product	(g/L)
q	Aeration rate (vvm) ($=\dot{V}_G/V_L$)	(L/(L·min))
R	General gas constant 0.08314	(L·bar/(mol·°K))
r_P	Product formation rate ($=dP/dt$)	(g/(L·min))
r_X	Biomass formation rate ($=dX/dt$)	(cfu/(L·min))
S	Substrate concentration	(g/L)
S_1	Concentration of substrate 1 in mixed substrates	(g/L)
S_2	Concentration of substrate 2 in mixed substrates	(g/L)
S_{\min}	Minimum maintenance substrate concentration	(g/L)
T	Temperature	(°C)
t	Time	(h)
V	Nominal volume of vessel	(L)
\dot{V}_G	Aeration; volume flow of gaseous medium	(NL/h)
V_L	Filling volume of vessel; working volume	(L)
F_L	Volume flow of liquid medium	(L/h)
V_{plated}	Volume spread on dilution plate	(L)
V_{dilution}	Volume of the dilution steps	(L)

Val	Concentration of valine	(g/L)
X	Concentration of cell	(cfu/L) or (AU)
y _j	Mol fraction of component j in gaseous phase	(-)
Y _{X/S}	Yield coefficient of cells from substrate S	(cfu/L)/(g/L) or AU/(g/L)
Y _{P/X}	Yield coefficient of a product from cells	(g/L)/(cfu/L) or (g/L)/AU
z	Number of 16S rRNA gene copies per cell	(-)
α	Parameter of cell associated product formation	((g/(L·min))/(cfu/L)
β	Parameter of growth associated product formation (= Y _{P/X})	(g/L)/AU or (g/L)/(cfu/L)
μ	Specific growth rate	(h ⁻¹)
μ _{max}	Maximum specific growth rate	(h ⁻¹)
ρ _{L,medium}	Density of liquid medium	(g/L)

Abbreviations

AA	Amino acids
ANOVA	Analysis of variance
AU	Arbitrary units (used for optical density values)
<i>B. c.</i>	<i>Burkholderia cepacia</i>
Cas	Casamino acids
CEP	Competitive exclusion principle
CF	Cystic fibrosis
CFTR	Cystic fibrosis transmembrane conductance regulator
CSTR	Continuous stirred tank reactor
cfu	Colony forming units
CIP	Cleaning in place
CO ₂	Carbon dioxide
conc.	Concentration
const.	Constant
crit.	Critical
CV	Coefficient of variation
DMEM	Dulbecco's modified eagle medium
DNA	Deoxyribonucleic acid
DSMZ	German strain collection of microorganisms and cells (Deutsche Stammsammlung für Mikroorganismen und Zellen)
EQ	Efficiency quotient in T-RFLP analysis
Glc	Glucose
GMEM	Glasgow minimal eagle medium
IQS	Internal quantification standard
KCl	Potassium chloride
LB	Laura-Bertani
M199	Medium number 199
Met	Methionine
mRNA	Messenger RNA
Na/K	Sodium/potassium
NaOH	Sodium hydroxide
NTA	Nitrilotriacetate
OD ₆₅₀	Optical density at a wavelength of 650 nm

P	Phosphate
PCR	Polymerase chain reaction
<i>P. a.</i>	<i>Pseudomonas aeruginosa</i>
RNA	Ribonucleic acid
<i>S. a.</i>	<i>Staphylococcus aureus</i>
SD	Standard deviation
SES	Sum of error squares
<i>S. m.</i>	<i>Stenotrophomonas maltophilia</i>
STR	Stirred tank reactor
TPE	Tris-buffer, phosphoric acid and EDTA-buffer
T-RFLP	Terminal restriction fragment length polymorphism
ZNGI	Zero net growth isocline

Indices

AA	Amino acids
Ace	Acetate
air	Standard air composition
Cas	Casamino acids
CO ₂	Carbon dioxide
crit	Critical = point of washout in chemostat
F	Feed
g	Number of plates in dilution plating
G	Gas
Glc	Glucose
i	Number of species in the mixed culture <i>S.a.</i> , <i>B.c.</i> or <i>P.a.</i>
in	Incoming
IQS	Internal quantification standard (<i>C. jejuni</i>) in T-RFLP
j	Component j
L	Liquid phase
Met	Methionine
N ₂	Nitrogen
n	Number of substrates in mixed substrate assumptions
O ₂	Oxygen
out	Outgoing
P	Product
Pr	Hypothetical metabolic product
S	Substrate
S ₁	Substrate 1 of mixed substrates
S ₂	Substrate 2 of mixed substrates
S _n	Substrate n of mixed substrates
species	Bacterial species in T-RFLP quantification
Val	Valine
x	Number of dilution steps in dilution plating
X	Biomass, cell number
199	Determined for medium M199+P+NTA, namely not individually only for glucose or only amino acids as substrate
650	At a wavelength of 650 nm

1 Introduction

Under natural conditions bacteria commonly do not grow as pure but as mixed cultures of different species. Mixed cultures and their behavior have been treated by many disciplines, ranging from *in situ* ecological microbiology over mathematical biology to biotechnological processes and medical microbiology. Research of mixed cultures in ecological microbiology focuses on the diversity of species in a natural environment and its dynamics. In mathematical biology theoretical conditions of mixed cultures are analyzed by the use of mathematical models [3, 48, 64, 82, 112, 132]. The main topic is the contradiction between competition on the one hand and the observed coexistence in mixed populations on the other hand [50, 67].

In addition to the theoretical and experimental observations some technical use of bacterial communities already exists. In biotechnology, the special properties of bacterial mixed cultures are employed to degrade mixtures of toluene and phenol. The characteristics of the bacterial system are the basis for defining the optimum operating point of the bioreactor [121]. The systematic utilization of bacterial communities plays an important role in the remediation of industrial wastewaters of carbon and nitrogen with the help of suspended biofilm microcarriers [142]. The detailed characterization of such heterogeneous microbial systems is of great interest in a growing number of application fields.

Bacterial mixed cultures in the medical-clinical field are not of use, but in contrast very problematic, for example due to their undesired growth on catheters or intubation tubes. The elimination of these infestations is difficult and can only be successful, if the properties of the mixed culture as a whole were taken into account [21].

Mixed cultures are highly relevant in the successive secondary infections in patients suffering from the genetic disease cystic fibrosis (CF) (mucoviscidosis) [118]. It generates a malfunction of the secretory epithelium of all exocrine glands leading to increased secretion, increased viscosity of mucus and a change in mucus and secretions compositions in the lungs of patients. Manifestations of bacteria in these secretion liquids are the reason for a recidivating or chronic bronchitis, peribronchitis, pneumonie and bronchiectasia. These infections lead to the most frequent (80 %) cause of death of patients due to lung failure by immune reactions [158].

CF patients are infected with more than one bacterial species (mixed infections), mainly *Staphylococcus aureus*, *Burkholderia cepacia*, *Pseudomonas aeruginosa*, *Stenotrophomonas maltophilia*, or *Haemophilus influenzae*. These mixed infections cause special difficulties for

therapy, because tested efficacies of antibiotics against one strain cannot be transferred equivalently to the mixed culture [38]. Additionally, mixed infection composition varies depending on therapeutic history and patient's age [118]. Systematic studies on the prediction of the potency of antibiotics on mixed infections obviously cannot be performed on the lung cultures either of one unique patient or of several different patients as “parallel and reproducible” experiments. Therefore, an *in vitro* laboratory cultivation system is desirable, in which in contrast to the lungs environmental conditions are defined and controllable.

Traditional laboratory methodology uses pure cultures for strain characterization. A transfer of findings from such experiments to describe growth in the presence of other species is hardly possible. The limitation is the lack of characterization and knowledge of interaction mechanisms both inside the community and also outside with its environment, which still have to be understood. For example competition might take place, which can be direct (interference competition) or indirect (resource competition). The first could be formation of an inhibitor by one species [12] the latter could be competition for the same substrate [68].

An important prerequisite for studies on mixed cultures is the monitoring of the population dynamics to obtain quantitative data. Cell numbers and relevant metabolites should be monitored. Up to now, in contrast to numerous theoretical considerations on the dynamics of mixed cultures based on mathematical models, complex microbial communities have hardly been studied in laboratories, as cell quantification methods and protocols for defined mixed cultivations are not available. Therefore, quantitative experimental data for validation of such models are hardly reported for more than two species. In particular, studies of bacterial population dynamics with absolute cell numbers of more than two species are rare [41, 42, 93, 94].

The aim of the presented work was the establishment of a methodology for quantitative analysis of a bacterial mixed culture consisting of at least three species. The focus was on identification of interactions of species with arbitrary and rather unknown growth characteristics. A new approach using the comparison of experiment and model simulation was applied on selected strains from the CF context as a model mixed culture.

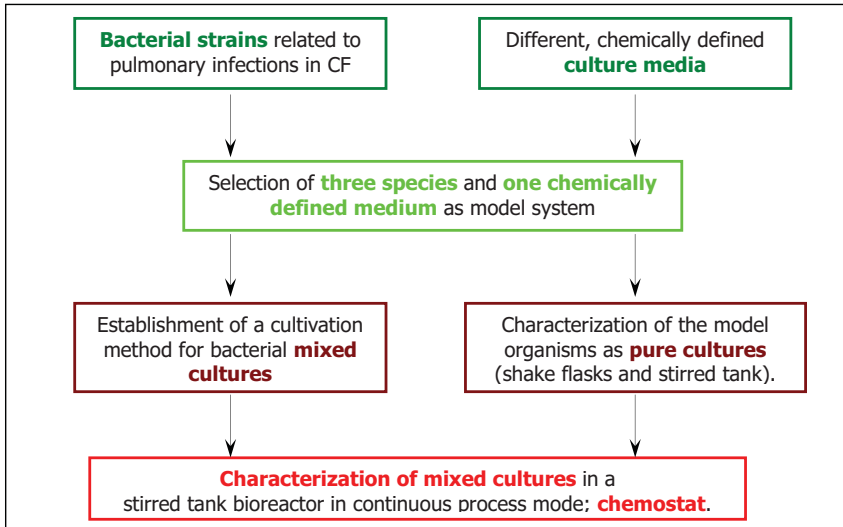


Figure 1.1: Overview on experimental tasks of the mixed culture investigations

The concept comprised the following tasks (Fig. 1.1):

1. A reproducible laboratory model system of a medically relevant community had to be established as such a system to represent important properties of the patient's mixed infections does not exist to date. The laboratory set-up had to provide reproducibility and control.
2. A new method for quantification of species specific cell numbers in a mixed sample was required for monitoring of the population dynamics. This method had to be established and applied based on the molecular biological T-RFLP analysis method (terminal restriction fragment length polymorphism).
3. Growth properties of pure cultures and possible interspecies interactions were to be identified by combining experiment and mathematical modeling.
4. A mathematical model for the three-species system had to be formulated for the validation of the model assumptions with the respective experimental data. On the one hand, the mathematical description of the experimental results would serve for goal-oriented experimental planning. On the other hand, it would support the gaining basic knowledge on the growth dynamics of a mixed culture (Fig. 1.2).

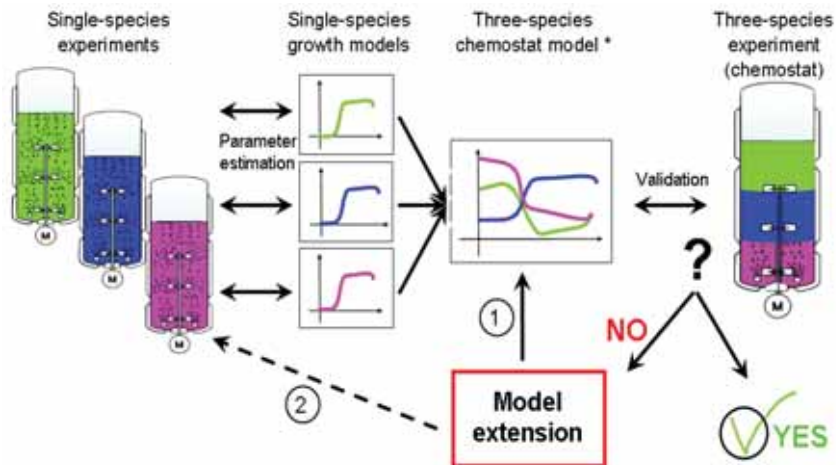


Figure 1.2: Flow scheme of the iteratively mathematical modeling approach: comparison of experimental results and simulation leads to validation of the mixed culture model (yes) or to extension of the mixed culture model (no) based on theoretical consideration for interspecies interactions (1) or additional pure culture properties (2). The result is a quantitative description of species interactions and mixed culture growth dynamics.

* Classic chemostat model [48]

2 Theory

2.1 Medical Background: Infections in Cystic Fibrosis Patients

2.1.1 Hereditary Disease Cystic Fibrosis

Cystic fibrosis (CF), also mucoviscidosis, is a disease caused by a malfunction of the secretory epithelium of all exocrine glands. It was first described in 1938 for CF of pancreas and is an autosomal recessive and monogenetic hereditary disease of the Caucasian population [115]. CF is the most abundant genetic disease in Europe; one in 2000 newborns is homozygous. Mutations in the CF-gene cause dysfunctionality of the CFTR (CF transmembrane conductance regulator) in epithelial cells [71]. This leads to increased secretion, increased viscosity of mucus and a change in mucus and secretions compositions. The main clinical features may include chronic obstructive pulmonary disease, exocrine pancreatic insufficiency, high content of Na^+ and Cl^- in sweat, and male infertility. A bacterial colonization of the secretion liquid of exocrine glands of the lung often is the cause for a recidivating or chronic bronchitis, peribronchitis, pneumonia and bronchiectasia. The strains *P. a.* and *B. c.* were reported as most abundant pulmonal infectants in older patients [146] and the strain *S. a.* in young patients and infants [115]. The alginate producing variants of *P. a.* are associated with a rapid decline in lung function. Once established within the CF airways, *P. a.* is very resistant to eradication by chemotherapy. *B. c.* infections have become more abundant since the last decade and as chronic infections often are associated with an adverse clinical course [24]. Further details on pathogenicity of *P. a.* in CF can be found in [58, 59]. A comprehensive overview on mixed culture infections and the roles of the different species in CF disease is given in [39].

2.1.2 Mixed Culture Studies for CF Relevant Bacteria

CF patients' lungs are usually infected with more than one bacterial species. However, only within the last decade a focus has been set onto possible interactions between members of the mixed infections, which were mainly studied for their potential impact on pathogenicity. A possible interaction between *B. c.* and *P. a.* related to exoproducts of *B. c.* was pointed out [95]. In the presence of *P. a.* a significant increase of siderophores, lipases and proteases was found. By diffusion of N-acyl-homoserine lactones so-called "communication" between *P. a.* and *B. c.* takes place [119]. These signaling molecules control expression of virulence factors and biofilm formation. They are assumed to serve as universal language for the two organisms and this has been proposed to play an important role in pathogenesis of the mixed

consortium [29]. As a synergistic interaction the rate of adhesion of *B. c.* towards epithelial cells of the respiration tract was increased by *P. a.*. Its exoproducts led to enhanced release of receptors on the cell surface [123]. As a direct interaction N-acyl-homoserine lactones of *P. a.* have been found to antagonize growth and production of virulence factor of *S. a.*. This has suggested a competitive advantage for *P. a.* in niches of growth occupied with *S. a.*, namely wounds or lungs of CF patients [116]. A more rapid emergence of colonization with *P. a.* in patients receiving prophylaxis against *S. a.* would be a possible indirect interaction [39].

2.1.3 Physiology and Nutrient Requirements of CF Relevant Bacteria

2.1.3.1 *Staphylococcus aureus*

S. a. is an early infectant of CF patients, namely infants and young children. *S. a.* is a gram-positive bacterium in the shape of cocci that sometimes aggregate to chains or grape-like structures. It does not form spores, is pigmented yellowish and grows in layers [13]. *S. a.* is facultative anaerobic.

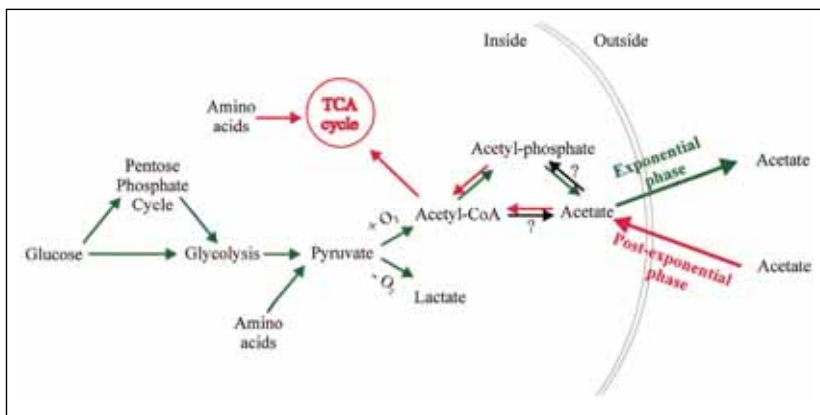


Figure 2.1: Scheme of the glucose metabolism of *S. a.*; green arrows = pathways during exponential growth phase, red arrows = reactions during stationary growth phase, black arrows with question marks indicate not well known pathways (from [137]).

A criterion of selection and reason for the high rate of food poisoning caused by *S. a.* is its very high salt, namely osmolarity tolerance, up to saturation (20 % NaCl) [152]. The optimal pH value for growth of *S. a.* is about 7; its optimal growth temperature is 37 °C. Glucose is degraded via the pentose-phosphate-way and glycolysis to pyruvate and then metabolized depending on the growth conditions [152]. Under anaerobic conditions pyruvate is reduced to lactate [70, 74], while under aerobic conditions decarboxylation to acetyl-coA takes place

[35]. Generation of ATP is partly realized through degradation of acetyl-coA towards acetate. An outstanding property of *S. a.* is the auxotrophy for several amino acids. The number and composition of these amino acids vary with the specific strain. However, when tested for five different *S. a.* strains, all were auxotrophic for valine [107]. The maximum specific growth rates in tryptic soy broth vary with the strain from $\mu_{max} = 0.81 \text{ h}^{-1}$ to 1.81 h^{-1} [137], no values for K_S were presented.

2.1.3.2 *Burkholderia cepacia*

Only little is known about pathogenesis of *B. c.* in CF patients and there are discussions, if *B. c.* is a true pathogen or just a marker of severe lung disease [39]. The mechanism of colonization of the respiration tract of CF patients is not yet fully understood. Adhesion to the mucosa epithelium seems to be the first step, facilitated by the fimbriae on the surface of *B. c.* [75]. The high resistance of *B. c.* to a large number of antibiotics makes its treatment in CF patients difficult.

B. c. are gram-negative rods, aerobic, with flagellae, non-spore forming and belong to the pseudomonad rRNA group II [13]. They possess a versatile carbon source metabolism for up to a 100 different carbon sources, namely a number of sugars, fatty acids, alcohols and amino acids, even Penicillin G [9]. The temperature optimum of the species is at 30°C [15], a pH optimum has not been reported. *B. c.* is urease-negative and catalase- and oxidase-positive. The production of energy is mainly achieved chemoorganotrophically through respiration and with O_2 as final electron acceptor. No parameter values for μ_{max} or K_S have been presented for *B. c.*. By production of siderophores (transport and extracellular storage of three-valent iron) bacteria compete with iron binding proteins of the host for free iron-ions. This seems to correlate with the ability of some bacteria to establish infections. *B. c.* expresses at least three siderophore-mediated iron-transport systems: pyochelin, cepabactin and azurechelin [135]. Pyochelin seems to be most important for clinical manifestations of the *B. c.* infections in CF patients. *B. c.* produces extra cellular components such as proteases, gelatinases, hemolysins lipases and exopolysaccharides [39]. The function of these products as possible virulence factors has not been clarified yet. The production of extra cellular virulence factors is regulated by “quorum-sensing” based on cell density (N-acyl-homoserine lactones) [81].

2.1.3.3 *Pseudomonas aeruginosa*

P. a. is a late, but the most critical infectant of CF patients, especially associated with increased decline of patient’s health [58, 59]. Due to its frequency and worldwide abundance as a cause for CF lung infection *P. a.* is called CF leading strain [133]. In 75-90 % of all

patients a chronic lung infection develops with this bacterium [111]. Different hypothesis exist for the pathogenicity of *P. a.*. Some authors stress a special adherence of *P. a.* towards CF epithelial cells [22]. A more recent theory assumes special growth conditions as cause for growth of *P. a.* in the CF lung. Inhaled organisms reach the mucus in an active or passive manner, form micro colonies and reduce the p_{O_2} . During the following anaerobic growth phase they possibly use nitrite as final electron acceptor. Bacteria adapt to the conditions in the CF lung by forming micro colonies in anaerobic plaques of mucus [156]. As in *B. c.* the production of extra cellular virulence factors in *P. a.* is controlled by “quorum sensing” [134].

P. a. is an aquatic bacterium, forms blue-green pus, responsible for skin- and lung-infections (also nosocomial). The gram-negative rods of *P. a.* form a polysaccharide (alginate) capsule for protection against the environment. Flagellae, fimbriae and pili facilitate surface adhesion (biofilm) and motility [124]. Strains are sorted into mucoid and non-mucoid strains referring to the ability and tendency of strains to form biofilms. The production of alginate is increased by higher osmolarity, higher p_{O_2} , the presence of ethanol, or nitrogen limitation [26]. Low p_{O_2} has been reported to have a positive effect on growth, and to lead to higher cell densities. As a possible explanation this has been related to a decrease of O_2 mass transfer in STR cultivations by an increased secretion of polysaccharides and proteins [122].

The metabolism of *P. a.* is chemoorganotroph for a high number of carbon sources with O_2 as final electron acceptor. Hexoses are degraded via the Entner-Doudoroff-way. *P. a.* belongs to the bacteria group of non-fermenters; this means its use of glucose is obligatorily aerobic. Denitrification serves as anaerobic oxidation with nitrate, nitrite or arginine as terminal electron acceptor and molecular nitrogen as final metabolic product [124]. Growth of *P. a.* in general depends on availability of iron and O_2 . No pH or temperature optimum has been reported for *P. a.*.

Table 2.1: Growth parameters for *P. a.* cultivation on glucose found in literature

Reference	$\mu_{max} (h^{-1})$	$K_{S,Sn} (g/L)$	maintenance rate $m (h^{-1})$
Beyenal et al. [10]	0.29	<i>Glc</i> 0.0269*	0.0078
		<i>O₂</i> 0.00118	
Bakke et al. [6]	0.4	<i>Glc</i> 2	-
Robinson et al. [120]	0.45	<i>Glc</i> 2	-

* The reported $K_{S,Glc}$ value is very low in comparison to the other two references: the model used was based on double substrate limitation (S1 glucose and S2 O_2) and used Tessier instead of Monod kinetic

2.2 Growth of Single Microbial Species

Pure cultures are very rare under natural conditions and so is growth on only one substrate. However, it has become established practice to characterize growth properties of isolated species under well-defined laboratory conditions. For their description single-species growth kinetics as for example the selected ones presented in the following are used [44].

2.2.1 Single Nutrient Controlled Kinetics

2.2.1.1 Growth with a Single Substrate

Monod [99] introduced the concept to describe microbial growth as substrate-controlled (eqn. 2.1). The kinetic relates the specific growth rate (μ) of a microbial population (X) to the substrate concentration (S). The kinetic parameters, maximum specific growth rate (μ_{max}) and substrate affinity (K_s), are assumed as constant, but depend on strain, medium and growth conditions, e.g. pH, temperature, p_{O_2} .

eqn. 2.1

$$\mu = \frac{\mu_{max} \cdot S}{S + K_s} \quad [99]$$

Alternative kinetic expressions for single nutrient growth have been formulated as reviewed by Kovarova-Kovar and Egli [73]. However, for the last half century all kinetics were dominated by Monod's concept and basically adapt the dependence of μ and S [69]. For a detailed presentation and discussion of variants of the Monod model see [5, 8, 69, 73].

2.2.1.2 Maintenance

When cells are metabolically active, but not growing or dividing, they may still take up substrate. This effect was not considered in the original Monod equation (eqn. 2.1). For the first time Herbert [52] proposed an extension of eqn. 2.1 with a maintenance rate (m) (eqn. 2.2). The formation of biomass based on ($X \cdot \mu$) is thereby reduced by a constant value of m . This results in a portion of the substrate necessary only for maintenance (solve for S : if $\mu = 0$, then $m = \mu_{max} \cdot S / (K_s + S)$). The higher S and consequently μ , the lower the ratio of μ to m . For alternative expressions, which were formulated additionally see [73].

eqn. 2.2

$$\mu = \frac{\mu_{max} \cdot S}{K_s + S} - m \quad [52]$$

2.2.1.3 Inhibition

If microbial growth is reduced by the presence of a substance, namely an inhibitor concentration (I), this is termed inhibition. There are different ways of inhibition: a) by an excess concentration of the substrate, for example alcohol or acid, b) competitive inhibition and c) non-competitive inhibition. For the three kinds the respective model formulations are given below. In the equations K_I denotes the inhibition constant of the inhibitor I .

a) Substrate excess inhibition results in a decrease of $\mu(S)$ again after a maximum, instead of constant μ_{max} , with increasing substrate concentration S .

eqn. 2.3

$$\mu = \frac{\mu_{max} \cdot S}{K_S + S + S^2/K_I} \quad [8]$$

b) Competitive inhibition occurs, when the inhibitor (I) and the required enzyme compete for the same spatial structure of the substrate (S). The inhibitory effect can be diminished by increasing substrate concentration S .

eqn. 2.4

$$\mu = \frac{\mu_{max} \cdot S}{S + K_S \cdot (1 + I/K_I)} \quad [2]$$

c) Non-competitive inhibition occurs, when the inhibitor (I) changes the spatial structure of the required enzyme or prevents substrate uptake or use in another way. An increase of the substrate concentration (S) has no effect on the inhibitory activity. A typical example for this kind of inhibition is product inhibition, for which a number of kinetics have been published.

eqn. 2.5

$$\mu = \frac{\mu_{max} \cdot S}{S + K_S} \cdot \left(\frac{K_I}{I + K_I} \right) \quad [8]$$

2.2.2 Use of Mixed Substrates

The kinetics for substrate-controlled growth on one single compound, for example glucose or lactose as carbon source, has been investigated in laboratory systems. In natural ecosystems conditions are more complex and microorganisms can use as many of the carbon sources as present in the respective site. Additionally, it was realized in different industrial processes more than the one theoretically considered substrate was taken up as energy source by the organisms [76]. This led to the characterization of growth kinetics of microorganisms on more than one substrate, namely mixed substrates.

2.2.2.1 Diauxic Growth

Diauxic growth is the sequential use of two carbon sources (mixed substrates) (S_1 and S_2). It mostly leads to bi-phasic growth, as growth on the second substrate only starts after depletion of the first. Typically, the organism is assumed to grow first on the substrate providing the higher maximum specific growth rate and then to switch to the next substrate with some lag-time for change of the enzymatic « equipment ». However, diauxic growth without lag-time has been observed [44]. Mathematically the sequential growth on two substrates can either be formulated with the help of an inhibitor or a repressor approach. The inhibitor approach combines the assumption of independent growth on two substrates with S_1 as a non-competitive inhibitor (eqn. 2.7) on S_2 (eqn. 2.5).

2.2.2.2 Multiple Substrate Growth

The sequential use of carbon sources under batch conditions (2.2.2.1) was regarded as a contrast to simultaneous multiple substrate uptake under continuous cultivation conditions. The sequential uptake was evaluated as a special case of mixed substrate use, which depending on the physiology of the organism and the environmental can as well be simultaneously as multiple substrate [44]. If mixed substrates are considered, their relation with regard to growth control can be assumed to be dependent (eqn. 2.6; eqn. 2.9) or independent (eqn. 2.7; eqn. 2.8) of each other. The formulations use either one μ_{max} for the dependent growth on two or more substrates (S_n) or specific maximum growth rates $\mu_{max,S1}$, $\mu_{max,S1}$ or $\mu_{max,Sn}$ on the single substrates. The affinity constants always refer to only one of the substrates ($K_{S,S1}$, $K_{S,S2}$ or $K_{S,Sn}$).

Two substrates...			
...dependent (interactively essential)	$\mu = \mu_{max} \cdot \left(\frac{S_1}{K_{S,S1} + S_1} \cdot \frac{S_2}{K_{S,S2} + S_2} \right)$	[96]	eqn. 2.6
...independent, low concentrations	$\mu = \frac{\mu_{max,S1} \cdot S_1}{K_{S,S1} + S_1} + \frac{\mu_{max,S2} \cdot S_2}{K_{S,S1} + S_2}$	[44]	eqn. 2.7
...independent	$\mu = \frac{1}{n} \cdot \sum_n \frac{\mu_{max,Sn} \cdot S_n}{K_{S,Sn} + S_n}$	[10]	eqn. 2.8
...reduction of uptake in presence of 2nd resource	$\mu = \frac{\mu_{max,S1} \cdot S_1}{K_{S,S1} + S_1 + a_{S2} \cdot S_2} + \frac{\mu_{max,S2} \cdot S_2}{K_{S,S2} + S_2 + a_{S1} \cdot S_1}$	[157]	eqn. 2.9
...one growth controlling (‘Liebig’s Law of the Minimum’) (perfectly essential)	$\mu = \min_{n=1,...,k} \{ \mu(S_n) \}$	[44]	eqn. 2.10

Gottschal [43] introduced a concept of mixed substrate growth to distinguish between growth on more than one substrate, without giving kinetic formulations, for a) different metabolic purposes, such as glucose and O_2 , and b) the same metabolic use, such as glucose and fructose. For a) only one of the substrates would be rate limiting, for b) both substrates would contribute to substrate-controlled growth. Simultaneous uptake of two substrates, but growth control by the one present at lower concentration is accounted for by eqn. 2.10.

Growth of organisms on a mixture of 20 substrates at very low concentrations, of which none supported growth as a single nutrient at that concentration, was observed. This surprising result was evaluated as important for growth under environmental situations [73]. The simultaneous uptake of multiple substrates at low concentrations, of which all contribute to cell formation and to the growth rate, can be described most appropriately by eqn. 2.7 [44]. For a detailed discussion and experimental examples see [43, 49, 73].

2.2.3 Batch and Continuous Process Mode Models

The general mass balance for a component j with the concentration c_j in an ideal reactor with its concentration $c_{j,in}$ in the feed and $c_{j,out}$ in the harvest is given in eqn. 2.11). The incoming and outgoing volume flows are denoted by $F_{L,in}$ and $F_{L,out}$, respectively. For the biomass formation rate (r_X) proportionality between specific growth rate (μ) and biomass concentration (X) is assumed (eqn. 2.12). The product formation rate (r_P) is expressed as in eqn. 2.13. For completely growth associated product formation $\beta=0$, for product formation by non-growing cells $\alpha=0$ needs to be assumed [86].

eqn. 2.11

$$\frac{d(V_L \cdot c_j)}{dt} = F_{L,in} \cdot c_{j,in} + r_j - F_{L,out} \cdot c_{j,out}$$

eqn. 2.12

$$r_X = \mu \cdot X$$

eqn. 2.13

$$r_P = (\alpha + \beta \cdot \mu) \cdot X$$

For a batch process, a closed system ($F_{L,in} = F_{L,out} = 0$) and a constant filling volume V_L are assumed. For the biomass balance eqn. 2.11 and eqn. 2.12 are reduced to eqn. 2.14. For the balance of the limiting substrate (S) eqn. 2.11 is reduced to eqn. 2.15 by introduction of the growth yield ($Y_{X/S}$) (eqn. 2.17). For the product balance and with the assumption that the relation of Luedeking and Piret (eqn. 2.13) [86] is valid, eqn. 2.11 is reduced to eqn. 2.17

eqn. 2.14

$$\frac{dX}{dt} = \mu \cdot X$$

eqn. 2.15

$$\frac{dS}{dt} = -\frac{\mu \cdot X}{Y_{X/S}}$$

eqn. 2.16

$$\frac{dP}{dt} = (\alpha + \beta \cdot \mu) \cdot X$$

eqn. 2.17

$$Y_{X/S} = \frac{dX}{dS}$$

The chemostat is one mode of continuous processes; others are the turbidostat or the oxidostat. It consists of a culture vessel with homogenously mixed content (often an STR), to which fresh medium is added ($F_{L,in} = F_{L,out} = F_L = \text{const.}$) and the liquid volume is kept constant by some mechanism of overflow-removal ($V_L = \text{const.}$) (Figure 2.2). The system is thus open. The dilution rate (D) is the flow rate related to the liquid volume (eqn. 2.20). The biomass and substrate balances are expressed as in eqn. 2.18 and eqn. 2.19. S_{in} and S_{out} denote the substrate concentrations in the feed and in the harvest. For an ideal stirred tank $S_{out} = S$ is assumed, with S giving the concentration in the reactor. At steady state of the system ($d/dt = 0$) the growth rate equals the dilution rate $\mu = D$.

eqn. 2.18

$$\frac{dX}{dt} = (\mu - D) \cdot X$$

eqn. 2.19

$$\frac{dS}{dt} = -\frac{\mu \cdot X}{Y_{X/S}} + D \cdot (S_{in} - S)$$

eqn. 2.20

$$D = \frac{F_L}{V_L}$$

2.3 *Mixed Cultures of Bacteria*

2.3.1 The Struggle for Existence – a Historical Introduction

Gause [36] was the first experimenter, who systematically studied a mixed culture under laboratory conditions. He aimed to elucidate the dynamics in ecosystems, the struggle for existence, by characterization of the underlying elementary processes. Already Gause [36] stressed the importance of the exact knowledge of growth of single-species for description of the mixed culture behavior. However at that time, the works of Monod [99] to describe single-species microbial growth for example were not yet available.

The work of Gause [36] can be seen as a starting point for mixed culture studies with laboratory methods and he already emphasized the importance of mathematical methods. Fredrickson [33] gave a review on mixed culture studies and following Gause's concept he demanded defined populations and knowledge about essential medium components. Gottschal [43] stressed the importance of identified species and of controlled experimental conditions.

2.3.2 Approaches to Mixed Cultures in Different Scientific Fields

Mixed cultures are relevant in many ways, which is reflected in the numerous methodologies by which they are investigated in several scientific disciplines. In the following a brief overview on the different approaches will be given.

In **medical microbiology, terrestrial and aquatic microbial ecology** material of patients, soil or water samples are analyzed with respect to species composition. The diversity of organisms is mostly characterized as changes of species' numbers as ratios [87, 151]. The disappearance or appearance of certain organisms depending on parameters such as medical treatment, age of patients, as well as state of pollution of soil or water, or annual seasons. Analytics mainly comprise molecular biological methods, such as single strand conformation polymorphism (SSCP) [27], denaturing-gradient gel electrophoresis (DGGE) [90], restriction fragment length polymorphism (RFLP) [90], DNA sequencing for final identification of strains through correlation with bands from SSCP or DGGE analysis [127], multiplex PCR [150], and fluorescent *in situ* hybridization (FISH) [57].

Theoretical microbial ecology seeks to analyze microbial community interactions not in natural environment, but with laboratory systems. The general concept is to quantify one selected interaction at a time, which afterwards can be combined to a complete system description. Co-cultivation of only two species of a community is a frequent approach, for which two strains are chosen for their specific physiological properties. Possible interactions are formulated as hypothesis and sometimes as a mathematical model. Typical experiments focus on the result of long term composition, for example which strain persists or in what ratio two species form [44]. Differentiating determination of cell numbers over time for two-species growth has been reported only in one study, where selective dilution plating was applied. However, reproducibility of data from dilution plating has proved as problematic [151]. Nine bacterial species were investigated in a mixed chemostat culture to gain insight into the ecosystem of dental plaque; no mathematical model was presented [94].

The chemostat occupies a central place in **mathematical biology**, its importance relates to the many models it represents, lakes, waste water treatment, or bioprocesses. For the description of the growth dynamics in the chemostat differential equation systems are formulated of up to an infinite number of species [132]. Interactions like competition, food-chains or negative effects by inhibitors are expressed mathematically. Mostly, the investigation of the equation system itself for conditions for constant or oscillating stable coexistence and special mathematical properties is the aim. So far, the model assumptions for three or more species have not been validated experimentally [79, 83, 110]. For two-species models experimental validations are reported (2.4.3.3).

In **biotechnological processes** mixed cultures are mostly considered on the whole [55], and if the process is modeled, the mixed culture is simulated as one culture [154]. Application fields

are waste water treatment, detoxification, food technology and biofilms, for which species compositions has hardly been considered. However, a two-species system for production of Nisin has been characterized and quantified by selective dilution plating. A model based control of pH and p_{O_2} for increased productivity has been implemented successfully [130]. Quantitative definition of an undefined inoculum from a waste water plant has been reported. However, only ratios for the groups of aerobic and denitrifying bacteria in the mixed culture have been given [159].

2.3.3 Interspecies Interactions

When bacterial populations grow together they might interact with each other in various ways. Reviews on classification and dynamics of interaction between pairs of microbial populations can be found in [34]. Additionally, Marsh and Bowden [91] gave an overview focusing mainly on biofilm mode of growth. The growth mode of microorganisms as suspension or biofilm and the habitat, *in situ* (natural) or laboratory (cultivation process), was not of importance for the interaction systematics. Depending on the scientific discipline wording and meaning may vary, therefore a summary of selected definitions and their origin is given in Table 2.2 and Table 2.3.

Indirect interactions have been defined by Fredrickson [34] as those taking effect by change of the abiotic environment, direct as effected by physical contact. In a mixed culture one or a combination of binary interactions, namely between two species, might take place. Fredrickson [34] noted quantitative knowledge on each of the interactions was necessary, but might even not be sufficient for quantitative description of the dynamics of a more than two-species system.

Table 2.2: Binary interactions and relationships between two species A and B (I)

Effect of B on growth of A	Effect of A on growth of B	Remarks	Interaction
<i>Indirect interactions</i> [34]			
-	-	Negative effects by removal of resources	COMPETITION
-	0		
-	-	Negative effects by production of toxins or inhibitors	ANTAGONISM
-	0		AMENSALISM
-	+	Negative effects by production of lytic agents ; positive effects by solubilization of biomass	ECCRINOLYSIS
+	0	Positive effects by production of a stimulus for growth of A by B (host) (commensal) or by removal of an inhibitor for growth of A by B.	COMMENSALISM
+	+	As ‘commensalism’ and presence of both populations <u>not</u> necessary for growth of both	PROTO-COOPERATION
+	+	As ‘commensalism’ and presence of both populations <u>is</u> necessary for growth of either	MUTUALISM
<i>Direct interactions</i> [34]			
-	+	B feeds on A	FEEDING (INCL. PREDATION AND SUSPENSION FEEDING)
-	+	The parasite (B) penetrates the body of its host (A) and therein converts the host’s biomaterial or activities in its own	
+	+(0)	A and B are in physical contact ; interaction highly specific	SYMBIOSIS
-	-	Competition for space	CROWDING

Table 2.3: Binary interactions and relationships between two species A and B (II)

Term		Definition
<i>Population relationships</i> [91]		
SPATIAL	OBLIGATE	A requires physical contact with B throughout most or all its life history
	FACULTATIVE	A can complete its life history apart from B
TEMPORAL	ALLELOCHEMICAL	Chemical compounds produced by A evoke a behavioral or growth response in B
	BEHAVIOURAL	The behavior of A and B is required for establishment or maintenance of association
	CYCLICAL	Physical association is periodically interrupted and reformed
METABOLIC	PERMANENT	Physical association is required throughout the life history of each partner
	METABOLITE	A metabolic product of A (amino acid, carbohydrate, nucleotide) is semiochemical (invokes a response) in B
	BIOTROPHY	A requires a nutrient that is a metabolic product of B
	SYMBIOTROPHY, NECROTROPHY	A's nutritional needs are completely met by B, which remains alive (parasitism), or is weakened or killed (parasitism, pathogenesis)
GENETIC	GENE-PRODUCT TRANSFER	Protein or RNA synthesized off the genome of A is used by B
	GENE TRANSFER	Genes of A are transferred to the genome of B

2.3.4 Experimental Studies of Interactions

The examples listed below have been experimentally achieved and except for very few examples have not been analyzed mathematically. Enhancements of bacterial activity (synergy) due to interactions take place, for example by biotrophy [91] or the exploitation of the metabolic product of one species by a second species [96]. Even „communication“ between groups of bacteria via quorum-sensing to synchronize responses towards environmental input signals were observed [119]. Mathematically mostly one interaction is analyzed, whereas in reality many types of interactions will occur simultaneously [44].

Examples of two or three species and two substrates

Coexistence in a chemostat was reported for *Bacillus cereus* and *Candida tropicalis* competing for two substitutable resources, glucose and fructose [157]. A mixed culture of *Pseudomonas* sp. and *Klebsiella aerogenes* under competition for glucose and p-

hydroxybenzoate was studied, in which *K. aerogenes* outcompeted the first [113]. Coexistence of three species by using a mixotroph-obligate heterotrophic system on two non-substitutable substrates, acetate and thiosulfate has been generated [41]. A similar example has been studied for two *Clostridium* species [77] and for two *E. coli* strains [28].

Examples of mutually interdependent community members

Coexistence was found for a riboflavin-producing *S. cerevisiae* and a riboflavin-requiring *L. casei* while the two competed for glucose at the same time (commensalism + competition) [96]. Lactate served as a mediator in two other examples: commensalism in mixed cultures of *Propionibacterium shermanii* growing on lactate produced by *Lactobacillus plantarum* from glucose [78]; and the same scenario for *Streptococcus mutans* and *Veillonella alcalescens*, two strains studied for their relevance in dental plaque [97].

Examples of additional effects

Effects of natural systems were transferred for characterization of their impact into chemostat studies. These were for example the presence of inert particles, change of temperature or, a very important factor, spatially and temporarily discontinuous growth conditions.

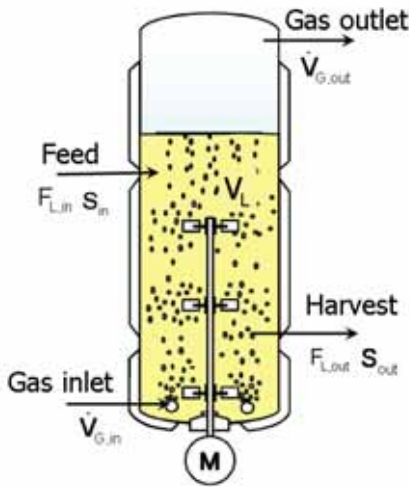
2.4 Competition and Coexistence in the Chemostat

The chemostat was often stated as the best laboratory idealization of natural systems for population studies [61, 153]. The authors have pointed out its advantages for a) reduction of complexity and b) the generated nutrient limitation similar to the ‘real’ system. The main interaction, which is studied, is competition for one or more substrates. The chemostat therefore is applied in an extensive number of experimental studies in microbial ecology and of completely theoretical competition models in mathematical biology [45]. In the following the theory of competition in the chemostat and examples for its experimental and theoretical applications in mixed culture studies will be introduced. The demand was not only mathematical formulations for mixed culture competition should be formulated, but that they should also be tested experimentally [34].

2.4.1 The Basics of the Chemostat Process

Already Gause [36] applied a manual sequential batch mode as simple continuous process mode and the technical development of the chemostat later enabled the realization of continuous cultivation for pure and mixed culture studies. The chemostat as a rather simple principle was first mathematically conceived and technically described simultaneously and independently by Novick and Szilard [106] and by Monod [100]. The dynamics of single-

species growth taking into account additional kinetics, for example diauxic growth or growth in the presence of inhibitors as established for batch cultures have very rarely been discussed. However, the use of multiple substrates in chemostat cultures has been dealt with quite frequently by introduction of the respective kinetics (2.2.2) for example into the classic chemostat competition model (Figure 2.2). A review focusing on mixed cultures on mixed substrates was presented by Gottschal [46]. The importance of the yield coefficient $Y_{X/S}$ for the outcome of mixed substrate competition, which has no impact on single substrate competition, was stated [76]. For comprehensive reviews see [44-46, 73].



Chemostat competition model (Monod)
eqn. 2.21

$$\frac{dX_i}{dt} = \left(\frac{\mu_{\max,i} \cdot S}{K_{S,i} + S} \right) \cdot X_i - D \cdot X_i \quad i = 1, \dots, n$$

$$S = S_{out}$$

$$\frac{dS}{dt} = -\frac{1}{Y_{X/S,i}} \cdot \frac{\mu_{\max,i} \cdot S}{K_{S,i} + S} \cdot X_i + (S_{in} - S) \cdot D$$

$$Y_{X/S,i} = \frac{X_i}{S_{in} - S}$$

$$D = \frac{F_{L,in}}{V_L}$$

$$V_L = \text{const.}$$

$$F_{L,in} = F_{L,out} = F_L$$

Figure 2.2: Principle scheme (left) of a continuous stirred tank reactor (CSTR) and the mathematical model (right) of a chemostat with competition of i species for one substrate S . For the assumption of an ideal reactor S equals S_{out} .

2.4.2 Competitive Exclusion Principle versus Paradox of the Plankton

The basic idea of the “struggle for existence” [36] (2.3.1) was formulated mathematically for the first time in the “competitive exclusion principle (CEP)” [50]. The CEP states “ i species cannot live together simultaneously on fewer than i resources”. The obvious biodiversity of nature poses a contradiction to this strict mathematical law, as obviously even in environments poor of substrates many species coexist, for example plankton at the surface of the sea. Accordingly, Hutchinson [67] formulated the theory of the “paradox of the plankton” to point out this seeming discrepancy. In the following years up to now these two important theories have formed two contrary poles. Between them mathematicians and biologists have

either tried to confirm the CEP or they have searched for assumptions to circumvent the CEP and by this to explain the observed diversity of species theoretically. Mathematical models were formulated and their dynamical behavior was analyzed for a better understanding of the basic nature of competition [16, 61, 63, 155].

2.4.3 Mathematical Chemostat Models of Mixed Cultures

The mathematical foundations of the standard chemostat competition model (2.4.1, eqn. 2.21) were presented by Smith and Waltman [132] based on the theories of nonlinear differential equations and dynamical systems.

2.4.3.1 Resource-Consumer-Models and Interference-Competition-Models

The chemostat models proposed in literature can be divided in two categories based on the interaction mode that is assumed: a) resource-consumer models and b) interference-competition models.

a) Resource-consumer-models assume an indirect interaction via competition for shared resources. The general model predicts that each species i will continue to grow as long as the resource availability exceeds the λ_i -value of the population [48]. The so-called break-even concentration λ_i of the substrate S is, defined as $\mu(\lambda) \cdot D = 0$, namely $\lambda_i = K_{S,i} \cdot D / (\mu_{max,i} \cdot D)$. The resources can either be abiotic, for example carbon, O_2 , hydrogen, nitrogen, or non self reproducing resources, for example phosphorus, or biotic. Biotic resources are self reproducing and change the model fundamentally (Lotka-Volterra-, predator-prey-models). The assumption of a predator and prey relation obviously is rarely appropriate for microbial communities. Instead of one resource mixed substrates, are considered for example by Tilman [143]. The author distinguishes between essential and substitutable (non-essential) resources, for which the model predictions are changed accordingly.

b) Interference-competition-models consider a direct interaction between species, namely toxin production. For an unknown interspecies interaction a ‘black-box’ term was implemented into the standard chemostat model, but without a precise biological motivation given by the authors of these studies [84, 92].

2.4.3.2 Model Assumptions for Circumvention of the CEP

As mentioned above, a high number of theoretical studies deal with variations or additional assumptions for mathematical models to circumvent the CEP and thereby to understand species diversity. In the following part the focus will be on resource-consumer models, as competition for a shared substrate almost always is assumed to occur (2.4.3.1). Depending on

the scientific field of the research group the ways to circumvent the CEP are either biologically or mathematical motivated. The biological ones are often quite complex and analytical results are therefore hard to establish. The mathematical ones often try to prove general results, which lead to simplified and thereby very unlikely biological assumptions.

Periodically operated chemostat

Models with time-variant substrate input are studied to represent two systems more realistically. Natural communities are assumed to be confronted with time-dependent substrate conditions, for example due to the four seasons, and waste-water treatment plants have to cope with varied compositions of input streams.

Three types of models can be distinguished: 1) variation of input concentration S_{in} , 2) variation of dilution rate D or 3) combination of both. For all three types the possibility of coexistence of two species has been proven. Two species living on one substrate were shown to coexist for an optimal amplitude of oscillation of the input concentration [62, 131]. For specific operation conditions of the dilution rate D coexistence for three species was shown mathematically [79]. Feedback control of the dilution rate D as a function of the state of the chemostat mathematically ensured coexistence of two species, but not of three or more species [23]. Coexistence of i species on one substrate has been proven to be possible for very specific assumptions by Wolkowicz and Zhao [155]. Interestingly, the mathematical analysis for this last example resulted in a possible coexistence of three species with sustained oscillations of D , whereas two species for the same parameter value set did not coexist.

Multiple nutrients

Different types of abiotic resources are considered perfectly essential (eqn. 2.7, eqn. 2.10) or interactively essential (eqn. 2.6). Levin [80] proposed an extension of the CEP concluding that i species cannot coexist on fewer than i resources. Passarge and Huisman [110] reviewed the graphical method of zero net growth isoclines to determine, whether coexistence of two species is possible depending on their individual growth parameters for the two substrates. The possibility of coexistence of two species on one substrate perfectly essential for one species and one common substrate for both species was verified mathematically by deFreitas [25]. The possibility of coexistence for a system as before combined with commensalism was shown mathematically by Miura et al. [98]. Vayenas and Pavlou [147] gave a suitable parameter set for the coexistence of three species on three interactively essential resources. Huisman and Weissing [64] showed oscillations (non-equilibrium) for three species on three essential resources assuming cyclic displacement of species. The same authors studied a

model for three species on three interactively essential resources and found coexistence after additional implementation of a parameter α , if each species consumes most of the resource, for which it is the worst competitor [65]. A range of purely mathematical studies can be found on the topic of multiple species on multiple resources, for which the question remains unanswered, whether the underlying constraints for the specific nutrient limitations are realistically chosen for or can even be found in nature [110, 132].

2.4.3.3 Experimental Verifications of Mathematical Assumptions

Theoretical propositions for modifications or generalizations were made in order to achieve coexistence of i species competing for fewer than i or even one resource (2.4.3). These theories aimed to solve the discrepancy between the CEP and the paradox of the plankton. What are missing in the theoretical studies are experimental verifications of the proposed mathematical models. This lack of experiments accounts for the chemostat models which circumvent the CEP, but also for the affirmation of the higher dimensional case of the CEP itself. For a two-species mixed culture the CEP was confirmed experimentally by Hansen and Hubbell [48]. In recent literature the necessity, but also difficulties of quantitative experimental approaches to mixed cultures, are underlined. Laboratory experiments and fieldwork are regarded as the challenges of future ecological research [110]. Especially for three-species systems it is pointed out that mathematical models provide the basis for an experimental study of a system of three microbial populations. The results obtained from the analysis of the model equations should be verified experimentally afterwards. But so far, no experimental study exists with a microbial system of three or more species, which was especially chosen in accordance to the mathematical assumptions as was stated by Vayenas and Pavlou [147].

2.5 *Quantification of Cell Numbers in Mixed Culture Samples*

For a quantitative monitoring of mixed culture growth, the determination of species-specific cell numbers is required. As already mentioned only very few experimental studies with three species and absolute cell number monitoring were found (2.3). Selective dilution plating for cell enumeration was applied exclusively for them. Conventional selective dilution plating methods, in particular, are not applicable to any mixed culture as selective media might not be available for each community member. Of course, depending on the composition of the respective species selective agars might be at hand. However, if dealing with three or more species, selective dilution plating is extremely laborious. The use of fluorescent

oligonucleotide probes has been reported for two-species mixed culture quantification [121]. However, if more than two species in a mixed culture have been investigated this method has only been applied for the determination of relative population composition [18].

In general, enumeration methods for microbial communities fall into the categories molecular biological, biochemical and microbiological. For a complete overview on the methods used to date see [138]. As can be seen from the examples given above, most of these methods are not applied for quantitative monitoring of mixed culture growth dynamics. They are mainly used for analysis of species diversity or number of different species in natural samples, such as for example soil, water, sputum, or biofilms.

2.5.1 Molecular Biological Enumeration Methods

Molecular biological enumeration methods have several advantages in community studies compared to biochemical or microbiological assays. They include no cultivation steps and therefore no unintended species selection, are time-efficient and highly sensitive. Therefore, a selection of them will be presented in the following.

Real-time PCR: The increase of the specific or unspecific PCR product, depending on the choice of DNA probe, in PCR amplification reactions is determined via the related increase of fluorescence intensity. By correlation to a DNA quantification standard the concentration of the specific DNA is determined in each PCR reaction batch [56].

Competitive PCR: An internal DNA standard of known concentration is spiked into a sample of unknown DNA concentration (DNA template) in several dilution steps. The sequence of the standard is similar to the template so amplification is assumed to be similar for both. The unknown concentration is derived from the ratio between amplicon amount of the standard and of the DNA template. Analysis of mixed samples is laborious, as for each template sequence an individual primer pair needs to be designed. Several PCR runs are required for each concentration measurement [40].

FISH = Fluorescent *In Situ* Hybridization: Sequence specific fluorescently marked DNA probes emit fluorescence signals at excitation at the DNA goal point. This is detected locally and can be quantified by image analysis [57, 90].

Flow cytometer analysis: Bacteria are fluorescently marked and thereby can be detected as well as quantified species-specific by the respective experimental device. For quantification a suitable marking and data analysis protocol needs to be established, the methodological protocol has to be adapted individually for each mixed bacterial system [102, 128, 129, 149].

2.5.2 Terminal-Restriction Fragment Length Polymorphism (T-RFLP) Analysis

Among the molecular biological methods, the terminal-restriction fragment length polymorphism (T-RFLP) analysis is the only one, which allows quantitative studies [138]. PCR amplification for an abundant DNA sequence, the 16S rRNA gene, is performed on a genomic DNA mixture from a mixed culture sample. It involves tagging one end of PCR products by the use of a fluorescent molecule attached to a primer. The amplified product mixture is then cut by a restriction enzyme. As a result of species specific differences in the DNA sequence, restriction sites lead to different fragment length. Terminal restriction fragments (T-RFs) are separated by electrophoresis and visualized by fluorescence. T-RFLP analysis provides quantitative data about each T-RF detected, including size in base pairs and intensity of fluorescence (peak height).

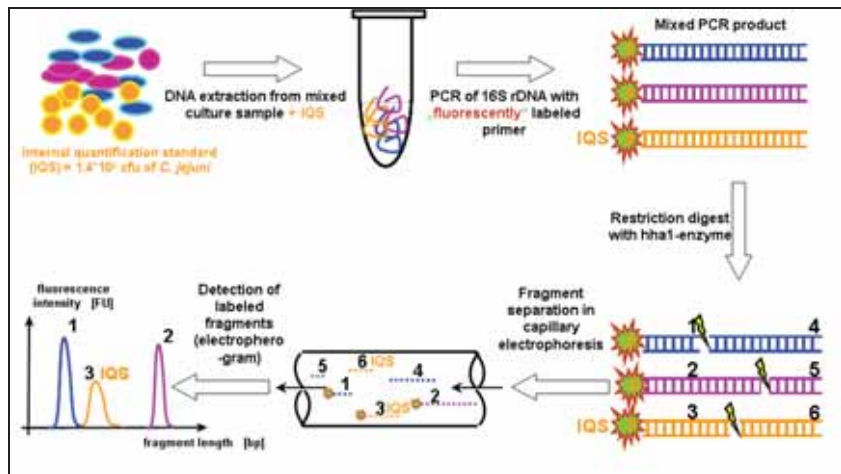


Figure 2.3: Flow scheme of the quantitative T-RFLP analysis method for enumeration of absolute and species specific cell numbers (graphic adapted from V. Grüntzig et al., Center for Microbial Ecology, Michigan State University East Lansing, Michigan, 48824)

The possibility for quantification of single-species cell numbers with a T-RFLP analysis method adapted to a capillary DNA sequencer was presented [145]. This method has been advanced and established for the quantification of absolute and species-specific cell numbers of the three-species mixed culture for and within the presented project [126] (Figure 2.3).

2.6 *Aspects of Mathematical Modeling and Model Validation*

2.6.1 **Introduction of Some Basics on Parameter Identification**

Mathematical models often consist of dependent and independent variables for which relations are formulated based on observations in reality for these variables. The relation can be either mechanistic or empirical. If a variable is assumed to be constant for a certain experimental constellation it is called a model parameter. The value of the parameter is determined by fitting it to the experimental values of the dependent and independent variables for a chosen model assumption (model equations) and the respective initial conditions. The mathematical method for the fit depends on the applied model equations. Linear equations with linear parameters, namely linear for the independent variable, can be solved by linear regression methods. Non-linear equations with linear parameters can be solved by non-linear regression. Equations with non-linear parameters, namely non-linear for the independent variable, can be solved by iterative methods, for example the simplex method. These imply the disadvantage of identifying local minima as a solution. An alternative are evolutionary methods, which are reported to identify global minima. More details and description of different solving methods can be found in [47]. The experimental data themselves as well as the applied mathematical methods are of importance for the quality of model fits and the possibility to discriminate between variants of a model. The difficulty of formulating models of increasing complexity and their validation with data exhibiting much scatter was discussed in a review on growth kinetics of suspended microorganisms [73]. The major importance of good data quality was pointed out for its application in useful mathematical modeling.

The determined parameter values therefore are not absolutely true. As mentioned above its error, namely deviation to the unknown «real» value, depends on the one hand on the deviation of the experimental data due to the measuring method. On the other hand the parameter deviates due to “lack of fit”, meaning the influence of the chosen model assumptions and their formulation, as well as the applied mathematical fitting methods. The deviation of the experimental data can be quantified by statistical methods, for example the F-test, and then the respective analytical protocol can be improved for a reduction of the analytical error. The chosen model assumption and formulation can be tested with respect to the quality of the simulation in accordance to the experimental data. For this the sum of error squares (SEQ) value is a common method used for the evaluation and comparison of the quality of fit.

- a) The fit for two different model formulations and one data set can be evaluated to decide between two hypotheses on a system property and to determine, which of them might be closer to reality.
- b) The fit of one model formulation to two or more experimental set-ups is evaluated for its ability to predict experimental results for a changed set-up.

For case a) the parameter values resulting from the fit may change, for case b) the values would be expected to stay constant to verify model validity.

2.6.2 Determination of Kinetic and Stoichiometric Growth Parameters

The influences of chosen mathematical protocols for the determination of kinetic and stoichiometric parameters of the Monod model are presented in the following. The kinetic parameters μ_{max} and K_S of the Monod growth kinetic (eqn. 2.1) and the stoichiometric parameter $Y_{X/S}$ are determined from experimental data. The required data sets over time are the dependent variable for the specific growth rate (μ) and the independent substrate variable for the substrate-controlled growth (S). As μ cannot be directly measured experimentally it needs to be determined indirectly, for example from the directly measured variable for cell numbers (X). Basically, the following methods for the parameter identification are presented and discussed in the appropriate literature.

- I. The yield coefficient $Y_{X/S}$ is calculated from the biomass value X formed and the substrate amount S depleted during a time period Δt . The yield coefficient is often assumed to be constant for the whole growth phase, but this is not necessarily true as discussed by Gottschal and Dijkhuizen [44] and Pirt [113].
- II. Linear regression on transformation plots, for example of Eadie-Hofstee, Lineweaver-Burk or “direct linear” plots result in values for parameters μ_{max} and K_S . As pointed out by Kovarova-Kovar and Egli [73] such transformations affect the quality of determined parameter values negatively.
- III. Non-linear optimization of fit of μ_{max} and K_S to the data of biomass X and substrate S by applying the respective balances for dX/dt and dS/dt and one kinetic expression for μ as given in (2.2.3) for batch or continuous formulation depending on the experiment. When the parameters μ_{max} and K_S are fitted to a set of experimental data, K_S is known to vary with μ_{max} . Consequently the question of whether the observed changes in Monod kinetic parameters between different authors are a result of this high correlation between them is still unanswered [73].

- IV. A direct calculation for μ_{max} is derived from the solution of the biomass balance (eqn. 2.14) and a Monod kinetic (eqn. 2.1) for exponential growth in a batch culture, namely $\mu = \mu_{max}$. The maximum specific growth rate μ_{max} is determined by linear (eqn. 2.22)) or nonlinear (eqn. 2.23)) regression.
- V. An approach for optimal experimental design of fed-batch experiments to increase the quality of parameter estimation of μ_{max} and K_S was first presented by Munack [103], where an optimal feeding rate based on the Fisher information matrix was calculated and applied. The method was improved later concerning the necessary computation time by introducing simple equations [7].

eqn. 2.22

$$\ln\left(\frac{X}{X_0}\right) = \mu_{max} \cdot t$$

eqn. 2.23

$$X = X_0 \cdot e^{(\mu_{max} \cdot t)}$$

In a batch cultivation μ is commonly determined from the directly measured variable for cell numbers X with eqn. 2.14. This implies a difficulty for the determination of K_S , because most data points will be available at a substrate concentration much higher than K_S (during exponential growth phase). The phase of substrate concentrations around K_S is commonly very short and thus not many data points contribute to the fitting exercise. The resulting problem in the fit is insensitive to variation of K_S and dominated by μ_{max} . One solution to the problem is use of a chemostat process. For a chemostat in steady state the dilution rate D ($< \mu_{max}$) is equal to the specific growth rate μ of the cultivated microorganisms. This can be used to obtain the data S and the respective specific growth rates μ for optimized fit of K_S (eqn. 2.1).

3 Materials and Methods

All methods and protocols described in the following were performed in compliance to the standard rules of sterile and good practice for laboratory work.

3.1 Buffers and Solutions

3.1.1 Working Solutions for Culture Media

Table 3.1: Preparation of NaOH solution (0.6 M)

Compound	Molar weight	ad 1 L ultrapure water
NaOH (sodium hydroxide)	40 g/mol	24 g

Table 3.2 Preparation of NTA solution (0.25 M)

Compound	Molar weight	ad 1 L NaOH solution (0.6 M)
Nitrilotriacetate (NTA)	191.14 g/mol	47.8 g

The NTA amount was dissolved in 900 mL of NaOH solution (0.6 M) (Table 3.1), cooled down to room temperature and filled up to 1 L with NaOH solution (0.6 M).

Table 3.3: Preparation of sodium dihydrogen phosphate stock solution (1.5 M)

Compound	Molar weight	ad 200 mL ultrapure water
Sodium dihydrogen phosphate (NaH_2PO_4)	137.99 g/mol	41.4 g

Table 3.4: Preparation of dipotassium hydrogen phosphate stock solution (1.5 M)

Compound	Molar weight	ad 400 mL ultrapure water
Dipotassium hydrogen phosphate (K_2HPO_4)	174.18 g/mol	104.51 g

Table 3.5: Preparation of Na/K-phosphate buffer (1.5 M, pH 7.0)

Compound	Amount	Final conc.
Sodium dihydrogen phosphate solution (1.5 M) (Table 3.3)	200 mL	1.5 M
Dipotassium hydrogen phosphate solution (1.5 M) (Table 3.4)	400 mL	1.5 M

For preparation of a 1.5 M sodium-/potassium phosphate buffer (Table 3.5) the two phosphate solutions were mixed in the ratio 1:2. The pH value was then at pH 7, if not, it was titrated using the solutions until pH 7.0 was reached.

Table 3.6: Preparation of glucose stock solution (200 g/L)

Compound	Molar weight	ad 1 L ultrapure water
α -D-(+)-Glucose Monohydrate	180.16 g/mol	200 g

The glucose stock solution was autoclaved separately prior to its use for media preparation (20 min, 121 °C) and stored at room temperature.

Table 3.7: Preparation of acetate stock solution (100 g/L)

Compound	Molar weight	ad 1 L ultrapure water
Sodium acetate (NaHCO_3)	82.04 g/mol	100 g

The acetate stock solution was autoclaved (20 min, 121 °C) prior to its use in sterile filtered media preparations and stored at 4 °C.

Table 3.8: Preparation of casamino acid stock solution (200 g/L)

Compound	Molar weight	ad 100 mL ultrapure water
Casamino acids	--	20 g

The casamino acid stock solution was sterile filtered (0.2 μm) before use.

Table 3.9: L-Methionine stock solution (100 mM)

Compound	Molar weight	ad 10 mL ultrapure water
L-Methionine	149.21 g/mol	1 mM

The L-Methionine stock solution was sterile filtered (0.2 μm) before use.

3.1.2 Working Solutions for Analytics

Table 3.10: Physiological salt solution (1 % m/v))

Compound	Molar weight	ad 100 mL ultrapure water
NaCl	58.44 g/mol	1 g

Table 3.11: HCl/Formalin solution for inactivation of bacteria

Denomination	Volume added to 5 mL of HCl stock solution (0.1 M)
Formalin stock solution (37 %)	25 μL

3.1.3 Working Solutions for T-RFLP and Preparation of IQS

Table 3.12: Preparation of phosphate buffered saline (PBS)

Compound	Molar weight	ad 1 L ultrapure water
Sodium chloride (NaCl)	58.44 g/mol	8 g
Potassium chloride (KCl)	74.55 g/mol	0.2 g
Disodium hydrogen phosphate (Na_2HPO_4)	137.99 g/mol	1.15 g
Dipotassium hydrogen phosphate (K_2HPO_4)	174.18 g/mol	0.2 g

Table 3.13: Preparation of Tris-HCl solution (1 M, pH 8.0)

Compound	Molar weight	Ad 1 L ultrapure water
Tris-HCl	157.6 g/mol	157.6 g

Adjust to pH 8.0 by addition of TRIS powder.

Table 3.14: Preparation of EDTA solution (0.5 M)

Compound	Molar weight	ad 100 mL ultrapure water
EDTA	372.24 g/mol	18.6 g

Table 3.15: Preparation of lysis buffer

Compound	ad 1 L ultrapure water	Final concentration
Tris-HCl (1 M, pH 8.0)	20 mL	20 mM
EDTA (0.5 M)	4 mL	2 mM
Triton X-100	12 mL	1.2 % (v/v)

Table 3.16: Preparation of lysozyme solution (100 mg/mL)

Compound	Molar weight	ad 1 mL 10 mM Tris-HCl (pH 8)
Lysozyme	14 kDa	100 mg

Table 3.17: Preparation of lysostaphin solution (1 mg/mL)

Compound	Molar weight	ad 1 mL 50 mM Tris-HCl, 145 mM NaCl (pH 7.5)
Lysostaphin	-	1 mg

Table 3.18: Preparation of RNAase A solution (20 mg/mL)

Compound	Molar weight	ad 1 mL ultra pure water
RNAase A	-	20 mg

Table 3.19: Preparation of TPE buffer

Compound	Molar weight	ad 1 L ultrapure water	Final concentration
TRIS	121.14	10.8 g	890 mM
EDTA	372.24 g/mol	74.4 mg	2 mM

Adjust to pH 7.5 with about 25 mL of phosphoric acid (85 % (v/v)) (H₃PO₄).

Table 3.20: Preparation of 5x loading buffer for PCR gel electrophoresis

Compound	Add to 1 L or volume needed	Final concentration
Glycerol	500 mL	50 % (v/v)
TPE buffer	500 mL	50 % (v/v)
Bromphenolic blue	Some small pieces	-
Xylencyanol	Some small pieces	-

3.2 Media

3.2.1 Liquid Culture Media

3.2.1.1 Chemically Defined Full Media

M199+P+NTA and MEM α +P+NTA medium

Table 3.21: Preparation of M199+P+NTA medium

Compound	ad 1 L ultrapure water	final concentration
M199 basal powder	16.06 g (as indicated by manufacturer for 1 L)	-
NTA	16 mL NTA-solution (0.6 M) (Table 3.2)	4 mM
Phosphate buffer	25 mL Sodium-Phosphate-buffer (1.5 M, pH 7.0) (Table 3.5)	37.5 mM

Table 3.22: Preparation of MEM α +P+NTA medium

Compound	Ad 1 L ultrapure water	Final concentration
MEM α basal powder	x g (as indicated by manufacturer for 1 L)	-
NTA	16 mL NTA solution (0.6 M)	4 mM
Phosphate buffer	25 mL S-P-phosphate buffer (1.5 M, pH 7.0)	37.5 mM

After dissolving all components for M199+P+NTA medium (Table 3.21), MEM α +P+NTA medium (Table 3.22), respectively, in 800 mL of ultrapure water the pH was about 6.8 and not further adjusted. After filling the solution with ultrapure water up to 1 L it was sterile filtered (0.2 μ m) and stored at 4 °C in the dark.

Other chemically defined media

Apart from the M199+P+NTA and MEM α +P+NTA media other defined media based on commercially available cell culture media were used for cultivation experiments. For preparation of variants of GMEM medium, additives as given in Table 3.23 were dissolved together with GMEM basal powder in the required amounts. With the phosphate buffer (Table 3.5) for GMEM+P a white precipitate formed, which was removed during sterile filtration in the medium preparation (3.2.1.1). The precipitate, presumably insoluble salts of phosphate and alkaline earth metals, in this case calcium and magnesium [101], was prevented by addition of the complex forming agent nitrilotriacetic acid (NTA) in GMEM+P-Glc+NTA.

Table 3.23: Variants based on GMEM basal medium with different additives

Abbreviation of variant	Additives ad 13.9 g GMEM basal and 1 L ultrapure water	Final concentrations of additives
GMEM	1.1 g glucose 4.4 g NaHCO ₃	6 g/L glucose 4.4 g/L NaHCO ₃
GMEM+P	1.1 g glucose 25 mL phosphate buffer (1.5 M)	6 g/L glucose 37.5 mM phosphate buffer
GMEM+P-Glc	25 mL phosphate buffer (1.5 M)	37.5 mM phosphate buffer
GMEM+P-Glc+NTA	25 mL phosphate buffer (1.5 M) 16 mL NTA solution (0.6 M)	37.5 mM phosphate buffer 4 mM NTA
GMEM+P-Glc+NTA+Cas	25 mL phosphate buffer (1.5 M) 16 mL NTA solution (0.6 M) 10 mL casamino acid (50 g/L)	37.5 mM phosphate buffer 4 mM NTA-solution 0.5 g/L casamino acids
GMEM+P-Glc+NTA+Met	25 mL phosphate buffer (1.5 M) 16 mL NTA solution (0.6 M) 16.8 µL L-methionine (100 mM)	37.5 mM phosphate buffer 4 mM NTA-solution 0.268 mM L-methionine

Table 3.24: Other chemically defined media applied in cultivation experiments

Abbreviation	Basal medium	Comments
DMEM	**	contained NaHCO ₃ as buffer
Ham's F12	**	--

** no preparation necessary (ready to use liquid medium)

All chemically defined media (Table 3.23, Table 3.24) were sterile filtered (0.2 µm membrane filter) after addition of all components and mixed with the required amount of ultrapure water.

3.2.1.2 Complex Medium (Laura-Bertani)

After preparation of LB medium as given in Table 3.25 the solution was autoclaved (121 °C, 20 min) and stored afterwards at room temperature. For experiments with LB medium containing glucose, acetate or casamino acids sterile glucose stock solution (Table 3.6), acetate stock solution (Table 3.7) or casamino acid stock solution (Table 3.8), respectively, was added as indicated to reach the final concentrations as indicated in the results part (1).

Table 3.25: LB medium

Compound	ad 1 L ultrapure water	Final concentration
Tryptone	10 g	10 g/L
Yeast Extract	5 g	5 g/L
NaCl	5 g	5 g/L

3.2.2 Solid culture medium

3.2.2.1 General Complex Agar Media

LB agar

For preparation of LB agar plates 15 g of Agar were added to the liquid LB medium compounds (Table 3.25) before filling up to 1 L. After autoclavation the LB agar solution was cooled down to approximately 60 °C under stirring for 10 to 15 min. Under the laminar flow box the liquid LB agar was poured into sterile petri dishes in aliquots of about 25 mL.

Columbia blood agar and chocolate blood agar

Columbia blood agar and chocolate blood agar were commercially available agar plates (Table 9.1). They contain blood as complex compound to provide good growth conditions for a broad range especially of medically relevant bacteria.

3.2.2.2 Selective Agar Media

<i>Cepacia</i> agar	: selective for <i>B. c.</i>
Chapman agar	: selective for <i>S. a.</i>
PCN agar	: selective for <i>P. a.</i>
Charcoal agar	: selective for <i>Campylobacter jejuni</i>

3.3 Microorganisms

3.3.1 Main Strains for Cultivation Experiments

S. a. ATCC 29213 (Institute of Medical Microbiology, University of Magdeburg, Germany).

B. c. DSM 7288 (German strain collection of microorganisms and cells, DSMZ).

P. a. PAO 1 (Institute of Microbiology, TU Munich, Germany).

3.3.2 Other Strains

S. a. DSM 20231 (DSMZ).

B. c. LMG 16656 (Institute of Microbiology, TU Munich, Germany).

P. a. ATCC 27853 (DSMZ).

Alcaligenes xylosoxidans DSM 2403,

Stenotrophomonas maltophilia DSM 50170,

Campylobacter jejuni (clinical isolate) (all: Institute of Medical Microbiology, University of Magdeburg, Germany).

3.3.3 Strain Keeping and Working Stock Preparation

Stocks of the strains were stored at -80 °C in Microbanks[®] that were prepared according to the manufacturer's protocol from freshly over night incubated agar plate cultures.

For glycerol stock preparation 20 mL broth of an over night standard shake flask cultivation were pelleted (15 min, 4000 rpm) and resuspended in approximately 4 mL of LB medium. From this suspension 1 mL and 0.8 mL of sterile glycerol (87 % (v/v)) were aliquoted into a cryotube. After 30 min of storage on ice for homogenization the stocks were stored at -70 °C.

Working cultures of the strains mostly used were kept at 4 °C on LB agar plates after overnight incubation at 37 °C and transferred every fortnight.

3.4 Cultivation Methods

3.4.1 Cultivation on Agar Plates

A small amount of bacterial cell material was taken from an agar plate, Microbank[®] or glycerol stock with the tip of an inoculation loop. The material on the loop was then carefully spread onto a new and sterile agar plate. After incubation at 37 °C over night plates were stored at 4 °C.

3.4.2 Microaerophilic Agar Plate Cultivations of *Campylobacter jejuni*

For cultivation of *Campylobacter jejuni* one Mikrobank[®] bead was transferred from a *C. jejuni* Mikrobank stock onto a new and sterile *Campylobacter* medium agar plate (charcoal agar). For the necessary microaerophilic conditions the plates were put in a 2.5 L anaerobic jar together with a freshly opened sachet of CampyGen[™], which generated a microaerophilic atmosphere by an oxidative reaction. The jar was closed directly after putting plates and sachet into it to prevent loss of the desired atmosphere.

3.4.3 Shake Flask Cultivations

3.4.3.1 Shake Flasks and Shake Flask Incubator

For shake flask experiments wide neck shake flasks without baffles and a nominal volume of 250 mL were used. As sterile barrier commercially available cotton plugs were used. Plugged empty shake flasks were autoclaved (20 min, 121 °C) prior to use.

Shake flask cultures were incubated in a humidified orbital shaking incubator. The eccentric diameter could be set by mechanical adjustment to 5.0 cm, 2.5 cm or 1.25 cm. Humidity was generated by a heated internal water reservoir and controlled by the internal cooling circuit,

which was activated manually by the respective circuit board switch (not mentioned in manual, information received directly by Kuhner, Basel, Switzerland).

3.4.3.2 Batch Cultivations in Shake Flasks

For pure culture shake flask experiments the culture medium was transferred into the shake flask with a 25 mL pipette under the laminar flow box. Cell material of a freshly grown overnight plate was suspended in 500 μ L of medium in a reaction tube (Eppendorf) for inoculation of the shake flask. After gentle homogenization (vortex) 200 μ L of the mixture was pipetted into the shake flask. Parallel cultures were incubated from one suspension mixture. Incubation in the shake flask incubator was done according to Table 3.26.

Table 3.26: Shake flask standard cultivation conditions

Process parameter	Unit	Set value
Volume of liquid media (V_L)	mL	20
Nominal volume of shake flask (V)	mL	250
Shaking frequency (n)	rpm	200
Shaking diameter (d_0)	cm	5.0
Incubation temperature (T)	$^{\circ}$ C	37
Relative humidity (h)	%	60

Samples of the shake flask cultures were taken under the laminar box. Supernatant and cells were separated by centrifugation (5 min, 13,000 rpm, 4 $^{\circ}$ C) and stored frozen at -4 $^{\circ}$ C. Standard analytics were optical density (3.5.1) of culture broth, b) pH measured from supernatant and c) glucose concentration from the supernatant after storage (3.5.3).

3.4.4 2 L Stirred Tank Bioreactor (2 L STR)

3.4.4.1 Set-up of 2 L Stirred Tank System

STR cultivations in 1 L and 2 L scale in either batch or chemostat mode were performed in a stand-alone STR of type Biostat B2 consisting of a glass vessel and a control unit.

The online parameters temperature, pH value, and oxygen partial pressure (p_{O_2}) were measured with Pt-100, 405 DPAS SC and InPro 6000 series probes, respectively. All process parameter values could be set and controlled with the control unit of the bioreactor. The control unit did not provide the option for recording of data, therefore an external process control system (PCS7) was integrated additionally. The control module provided power input for the stirrer motor, probe connectors, a thermostat for the cooling water jacket of the STR,

water inlet and outlet for the off-gas cooler and four integrated hose pumps for dosage of optional reagents. The integrated pumps were substituted with externally stand-alone feed-and harvest pumps. The standard module was exchanged by a thermal mass flow controller. The aeration went through a sterile filter before it was dispersed by a sparger ring. The off-gas was dehumidified by a water cooled (4 °C) condenser.

The O₂ and CO₂ in the off-gas were analyzed with the off-gas analysis modules Magnos 16 and Uras 14, respectively. The off-gas section between reactor and off-gas analysis was set up with a foam trap, a return valve in a bypass, and a flow meter. Optionally, for continuous processes the reactor and the substrate feed bottle were each positioned on a balance with digital data output connected to process control system (PCS 7).

Off-gas balances

The volumetric oxygen (OTR) and carbon dioxide transfer rate (CTR) were balanced from off-gas analysis data, namely O₂ and CO₂ mole fractions (y_{O_2} and y_{CO_2}). The eqn. 3.1, eqn. 3.2, and eqn. 3.3 are based on systems borders (Figure 3.1), for constant temperature ($T = 310.15 \text{ K}$), pressure ($p = 1.01 \text{ bar}$) and nitrogen as an inert air compound [139].

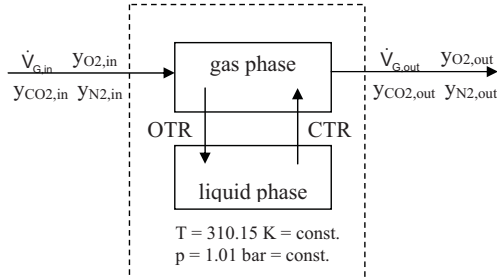


Figure 3.1: Scheme of off-gas balancing system borders and assumptions.

eqn. 3.1

$$OTR = \frac{\dot{V}_G \cdot p}{V_L \cdot R \cdot T} \cdot \left[y_{O_2,in} - \left(\frac{1 - y_{O_2,in} - y_{CO_2,in}}{1 - y_{O_2,out} - y_{CO_2,out}} \right) \cdot y_{O_2,out} \right]$$

eqn. 3.2

$$CTR = \frac{\dot{V}_G \cdot p}{V_L \cdot R \cdot T} \cdot \left[\left(\frac{1 - y_{O_2,in} - y_{CO_2,in}}{1 - y_{O_2,out} - y_{CO_2,out}} \right) \cdot y_{CO_2,out} - y_{O_2,in} \right]$$

eqn. 3.3

$$RQ = \frac{CTR}{OTR}$$

3.4.4.2 Batch Cultivation in 2 L Stirred Tank Reactor

The glass vessel was filled with 2 L of ultrapure water and the top cover was mounted with probes and equipment as given in Figure 3.2 and Table 3.27. The bioreactor and the connected equipment (sampling vessel, foam trap, inoculation vessel and tool) were autoclaved for 30 min at 120 °C.

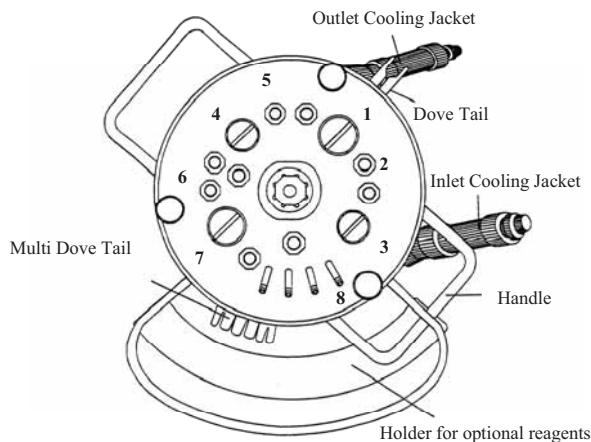


Figure 3.2: Assembly of top cover and connector positions for equipment used (from handbook Biostat® B, BBI Systems Sartorius).

Table 3.27: Positions of equipment in top cover after reactor assembly.

Position	Applied equipment
1	Off-gas cooler
2	Pt-100 temperature probe
3	pH electrode
4	pO ₂ probe
5	Aeration sparger
6	Sampling
7	Diaphragm for inoculation
8	Harvest

After autoclaving the water was poured out of the vessel under the laminar flow box, the top cover was mounted and probes and cooling system were connected. Sterile filtered culture medium was filled into a 2 L Schott bottle and pumped into the reactor via a sterile connection (STT coupling). For each cultivation the molar fractions $y_{O_2,in}$ and $y_{CO_2,in}$ were calculated under the assumption of ideal gas behavior from off-gas data (Magnos 16: O₂ in

vol % (v/v); Ureas 14: CO₂ in ppm) by multiplication with 10² and 10⁶, respectively. Standard cultivation conditions for STR cultivations in Biostat B2 are given in Table 3.28.

Inoculation

A pre-culture was cultivated in shaking flask under standard conditions (3.4.3.2) until an optical density of 1.0 AU was reached. The necessary pre-culture volume (1 % of reactor cultivation volume) was transferred into a 250 mL Schott bottle with inoculation device. After its connection to the reactor via a diaphragm (pos. 7, Table 3.27), the inoculum was pumped into the reactor.

Sampling

Samples were analyzed as given in 3.5.

Table 3.28: 2 L STR (Biostat B2) standard cultivation conditions

Process parameter	Unit	Set value
Working volume (V_L)	mL	1000
Nominal volume of stirred tank (V)	mL	2000
Stirrer speed (n)	rpm	500
Aeration (\dot{V}_G)	NL/h	120
Incubation temperature (T)	°C	37
No pH control		
No pO ₂ control		

3.4.4.3 Chemostat Cultivation in Stirred Tank Reactor

For continuous cultivations in chemostat mode the standard reactor set-up was extended with a feed and a harvest bottle. After autoclaving the bottles together with their connection equipment, medium was sterile filtered into the substrate feed bottle. Both bottles were connected to the reactor via sterile connectors and the tubing positioned into the external hose pumps. For harvest a silicon tube reached into the culture broth. The feed was led via silicon tubing to the middle of the reactor and near to the culture broth surface. Set-up routines as well as off-gas analysis were performed as described in 3.4.4.1 and 3.4.4.2.

Inoculation

Single-species chemostat cultures were inoculated as standard batch (3.4.4.2). For mixed chemostat experiments separate shake flask cultures of *B. c.*, *P. a.*, and *S. a.* were started with 2 h time delay each. An OD₆₅₀ of 1.0 AU was reached according to their growth

characteristics each of the precultures approximately at the same time, 6 h after start of *S. a.*. Equal volumes of precultures with OD₆₅₀ 1.0 AU were joined (1:1:1) ad 1 % (v/v) of V_L into the sterile inoculation vessel and transferred into the reactor. The cultivation was started as described for batch cultivation (3.4.4.2). The switch from batch to continuous process mode was defined by complete consumption of the main carbon source indicated by a significant increase of p_{O_2} and a drop in OTR. At this point the substrate feed was started manually via PCS7 interface. The feed mass flow (\dot{m}_L) was set and controlled via PCS7 through control of the feed pump speed. The controller used the weight decrease determined for the feed bottle as input signal. The mass flow value was calculated manually for the chosen flow rate (D) with eqn. 3.4. The density $\rho_{L,Medium}$ was determined experimentally with the weight ($mass_{medium}$) of a defined volume of medium (V_{medium}):

$$\rho_{L,Medium} = mass_{medium} / V_{medium} = 1.01063 \text{ g/L}.$$

eqn. 3.4

$$\dot{m}_L = D \cdot \rho_{L,Medium} \cdot V_L$$

3.4.5 Small Scale Parallel Stirred Tank Bioreactor (Small Scale STR)

3.4.5.1 Set-up of Small Scale STR

All STR cultivations with a working volume (V_L) of 200 mL in batch or chemostat mode were performed in a fedbatch pro[®] system, whose parallel reactors can be operated and controlled completely individually. The small scale STR cultivation system consisted of four glass vessels (stirrer-pro[®], $V = 450$ mL), a process control system (EasyAccess[®]) and six hardware modules: one temperature and agitation module (Bioblock[®]), one monitoring module (PH4PO4[®]), one gas-mixture module (MX4/4[®]), one off-gas analysis module (GA4[®]), two multi pump modules (MP8[®]). The gas mixture module was connected to the air, N₂, O₂, and CO₂ laboratory gas supply. The temperature control unit used the laboratory cooling water system.

Each vessel was equipped with a magnetic stirrer bar, a ceramic frit for submerge gassing, an off-gas cooler, a temperature sensor, a pH probe and a p_{O_2} probe. The pump modules, 16 dosage pumps, supplied 4 optional dosage feeds per reactor. Off-gas was lead into a small foam trap (250 mL bottle with some antifoam) before entering the off-gas analysis module. The off-gas analysis module measured O₂ and CO₂ contents in the off-gas and determined OTR, CTR and RQ values online.

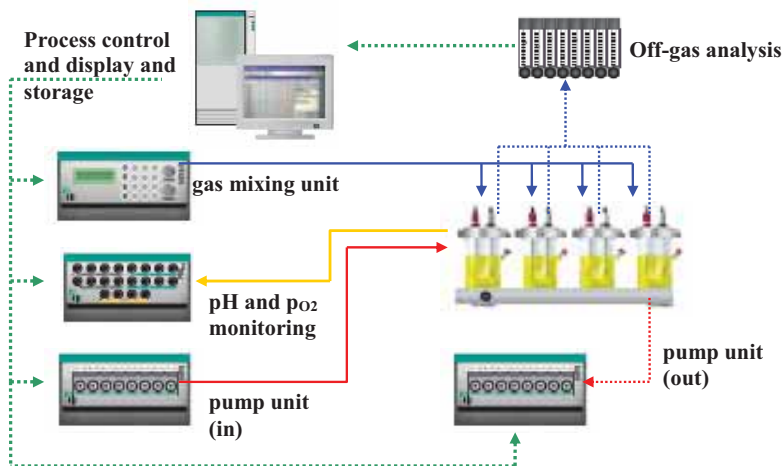


Figure 3.3: Flow scheme of small scale STR bioreactor set-up ([©]dasgip AG).

3.4.5.2 Batch Cultivation in Small Scale STR

Cultivations were prepared as according to the set-up procedures integrated in the process control system. After choice of process conditions (Table 3.29), the software leads through an interactive step-by-step calibration and configuration protocol. After calibration of pH electrodes, the reactors were assembled, filled with deionized water and autoclaved. In the meantime pump calibration and CIP (cleaning in place) of tubing was conducted. After autoclaving, the water was exchanged against the required medium volume. The reactor was positioned into the agitation and temperature control unit, the temperature probe was placed in its shaft, probes, aeration, and off-gas were connected. To start the process control with the defined experimental conditions the system was switched from ‘set-up’ to ‘control’ mode (Table 3.29).

Inoculation

Precultures were prepared as standard shake flask cultures (3.4.4.2). The inoculation volume (1 % (v/v) of V_L) was transferred into the reactor with a glass syringe (40 mm) via the ethanol wetted sampling septum on the side of the vessel. Immediately after inoculation the time point was marked and start of cultivation data monitoring was initiated in the process control.

Sampling

Analytics were done according to the experimental task (3.5).

Table 3.29: Small scale STR (dasgip fedbatch pro) standard cultivation conditions

Process parameter	Unit	Set value
Working volume (V_L)	mL	200
Nominal volume of STR (V)	mL	450
Stirrer speed (n)	rpm	300
Aeration (\dot{V}_G)	NL/h	0.5
Incubation temperature (T)	°C	37
No pH control		
No pO ₂ control		

3.4.5.3 Chemostat Cultivation in Small Scale STR

Continuous cultivations were started as batch cultivations (3.4.5.2) and switched to chemostat mode manually by activating feed and harvest pump via the process control interface. The time point of starting the continuous mode was defined by complete consumption of glucose indicated by the pO₂ and OTR signal. For chemostat operation mode a tube was mounted inside the reactor reaching through the top cover onto the required surface height representing 200 mL filling volume under process conditions (with gas hold-up) to control the filling volume. Outside, this tube was connected to a 10 L harvest bottle and positioned in one of the pumps of the system. The feed tubing was positioned in one of the system pumps and connected to the reactor via the sampling septum with a one-way syringe tip. The required volume flow (F_L) was controlled with the process control system. Drift of actual value compared to set value was checked, but no drift was observed.

3.5 Analytical Assays

3.5.1 Cell Enumeration for Single-Species Samples

Turbidometric determination of optical density

Turbidity was measured with a spectrophotometer at 650 nm in disposable cuvettes directly from culture broth after sampling. Undiluted samples with values above 0.4 AU were diluted with physiological salt solution (Table 3.10) to fit in the linear range (0.01 AU to 0.4 AU). After homogenization (vortex) the turbidity was measured against culture medium that was diluted correspondingly.

Determination of colony forming units by dilution plating

A 10-fold dilution series of a bacterial suspension with $x = 1, \dots, k$ dilution steps was prepared. 50 μ L (V_{plated}) of each dilution volume (V_{dilution}) in the range of $1:10^0$ to $1:10^{10}$ was spread on

agar plates (duplicates). The overall number of plates is denoted by $N_{plates} = 1 \dots g$. After incubation over night (37 °C) the colonies on each plate were counted ($N_{colonies,g}$) and the number of CFU in 1 mL (X) of the undiluted sample was calculated (eqn. 3.5). The dilution factor of each plate is given by F_x . Plates with less than 5 or more than 400 colonies were not considered for the calculation. The dilution plating allowed quantification in concentrations to a limit of about 20 cfu/mL.

eqn. 3.5

$$X = \frac{1}{N_{plates}} \sum_{g=1}^{N_{plates}} N_{colonies,g} \cdot F_x \cdot \frac{V_{dilution}}{V_{plated}}; g \text{ denotes the single plate; } x \text{ relates to the dilution step}$$

Abbe-Zeiss (Thoma-Zeiss) counting chamber

Prior to counting under the microscope, 500 µL of suspension were mixed with 500 µL of HCl/Formalin solution (Table 3.11) for inactivation of the bacteria. Of the mixture a little less than 8 µL were given onto the counting chamber slide and covered with the cover slip following the manufacturer's instruction. Bacteria were counted ($N_{counted\ cells}$) in 64 small squares ($= N_{small\ squares}$) in four diagonally arranged major squares of the counting chamber. The cell number X in the original sample before dilutions with an overall factor of F were applied was calculated according to eqn. 3.6.

eqn. 3.6

$$X = \frac{N_{counted\ cells}}{N_{small\ squares}} \cdot F \cdot 4 \cdot 10^6\ l/mL$$

3.5.2 Cell Enumeration for Mixed Species Samples (T-RFLP Analysis Method)

The quantitative T-RFLP analysis method used was published as part of the work presented [126]. It was based on a method by Trotha et al. [145].

Preparation of internal quantification standard (IQS)

As IQS 100 µL aliquots of a *Campylobacter jejuni* suspension ($OD_{600} \sim 0.4$ in 10 % (v/v) glycerol in PBS (Table 3.12)) were prepared and stored at -80 °C. The cell number of these aliquots was determined by dilution plating (3.5.1). The result (cfu/mL) was used as N_{IQS} in T-RFLP calculation (eqn. 3.7)) and adapted after every new IQS preparation.

3.5.2.1 Generation of 16S rDNA Fragments from Bacteria Samples

Extraction of genomic DNA from bacteria

After adding 1 mL of culture sample to an IQS, it was washed once with PBS. Therefore, it was pelleted (10 min, 13,000 rpm, 4° C), the supernatant was discarded, the pellet was

resuspended with PBS. After centrifugation (10 min, 13,000 rpm, 4° C) the pellet was kept and the supernatant was discarded again. For defined samples, the PBS washing step before pelleting could be omitted, because the samples were already prepared with PBS and no medium components could disturb the DNA extraction and PCR steps. The pellet was homogenized (vortexed) after addition of 100 µL lysis buffer (Table 3.15), 40 µL of lysozyme (Table 3.16) and 40 µL of lysostaphin solution (Table 3.17). After incubation (37 °C, 1.5 h) 20 µL of proteinase K was added and the mixture was incubated again (1 h, 56 °C). Enzyme activity was stopped (5 min, 95 °C), and 20 µL of RNAase A (Table 3.18) was added with subsequent incubation (30 min, 37 °C). After short centrifugation of the tubes (13,000 rpm) the DNA extraction was performed according to the manufacturer's protocol (QIAamp DNA Blood Mini Kit). DNA concentration of the resulting DNA extract was quantified at 260 nm in an ultra-microcuvette and stored at -4 °C for further use.

Polymerase chain reaction (PCR) of 16S rDNA

The following protocol was used for amplification of nearly complete 16S rRNA genes from the DNA extract. A 50 µL PCR reaction mixture contained: 5 µL 10x buffer, 4 µL MgCl₂ (25 mM), 0.5 µL primer 8f FAM (100 µM, AGA GTT TGA TCC TGG CTC AG), 0.5 µL primer 1492r (100 µM, TAG CTT GTT ACG ACT T), 4 µL dNTPs (2.5 mM each), 0.25 µL Takara Ex Taq DNA polymerase (5 U/µL), and 30 ng genomic template DNA. DNA amplification was performed with a thermocycler at the following settings (program No.35 "PCRTFLP"):

2 min at 94 °C,

35 cycles: (0.5 min at 50 °C / 1 min at 72 °C / 10 s at 94 °C),

1 min at 55 °C, then 5 min at 72 °C.

HPLC-grade water (LiChrosolv[®]) was used for all steps in sample preparation from PCR to fragment analysis. No BSA solution was used in PCR reactions as good data quality was noticed without. Primer amount for unlimited amplification was calculated and needed to be increased compared to the value reported in literature [145]. Specificity of PCR results and reproducibility of species quantification with T-RFLP analysis was optimal with a 1 °C/s heating gradient of the thermocycler, which was adjusted internally in the PCR cycler.

Amplicon verification and purification

Successful amplification of the 16S rDNA sequence was verified with analytical agarose gel electrophoresis (1 % (w/v) agarose in TPE buffer). The size of the bands of about 1,500 bp was determined and controlled by use of 1 kbp ladders. Amplicon mixture was purified from preparative gel electrophoresis (2 % (w/v) agarose in TPE buffer) after excision of bands

using a QIAquick Gel Extraction Kit according to the manufacturer's protocol. It was then stored at 4 °C or -20 °C for further use.

Restriction digest of the amplicon

After purification the amplicon mixtures were digested separately with *hhaI* endonuclease. The digestion mixture (10 µL) contained 5 µL of purified amplicon as well as 3.4 µL HPLC-grade water, 0.5 µL *hhaI* solution (10 U/µL), 1 µL NEB 4x buffer, and 0.1 µL BSA (10 mg/mL). Digestion was performed with a thermocycler (3 h, 37 °C, then 20 min, 65 °C, and finished at 8 °C (program No. 36 "HHAIVER").

3.5.2.2 Analysis of the 16S rDNA Fragment Mixture

The digestion mixture was separated on a Genetic Analyzer 3100Avant. For sample preparation 1 µL of the digested amplicon was mixed with 21 µL of HiDi formamide, 0.5 µL Genescan® 500 ROX sizing standard and 0.5 µL of an additional 780 bp sizing fragment. Fragment analysis was performed on a 50 cm capillary array with polymer POP 6 in fragment analysis mode with DataCollection software 2.0 (run parameters: oven temperature 50 °C; prerun voltage 12.2 kV; prerun time 180 s; injection voltage 1.5 kV; injection time 20 s; voltage number of steps 20 nk; voltage set-up interval 30 s; data delay time 1200 s; run voltage 12.2 kV; run time 6500 s). Length as well as related peak area of fragments was determined with GeneMapper software 3.5 (analysis type: microsatellite; peak detection algorithm: advanced; ranges: analysis full range and sizing partial size 50 to 600 bp; peak detection: peak amplitude; thresholds B:10, R:50, G:50, O:50, Y:50. Expected fragment sizes were derived from *in silico* analysis of the amplified 16S rDNA sequence (BLAST database) considering 27f and 1492r primer binding and *hhaI*-restriction sites. Also a Java® tool application of the ribosomal database project II (RDP version 8.1; <http://rdp8.cme.msu.edu/html/>) was used for fragment length estimation.

Sizing standard definitions for 16S rDNA fragment analysis

The standard definitions of GS 500 ROX sizing standards for fragment sizing with GeneMapper Software are (bp): 50, 75, 100, 139, 150, 160, 200, 245, 300, 340, 350, 400, 450, 490, 500, and 780 (custom made fragment). The resulting fragment lengths were not consistent with the theoretically expected ones for the respective species (Figure 3.4).

The sizing standard definitions were adapted to fit the specific electrophoresis run properties of 16S rDNA amplicon restriction fragments. The following sizing definitions were used instead (bp): 51, 76, 102, 140, 152, 161, 201, 247, 301, 337, 350, 401, 451, 492, 503, and 746.

Resulting fragment lengths were consistent with their nominal sizes over a wide range of fragment lengths (98 bp to 566 bp) (Figure 3.5).

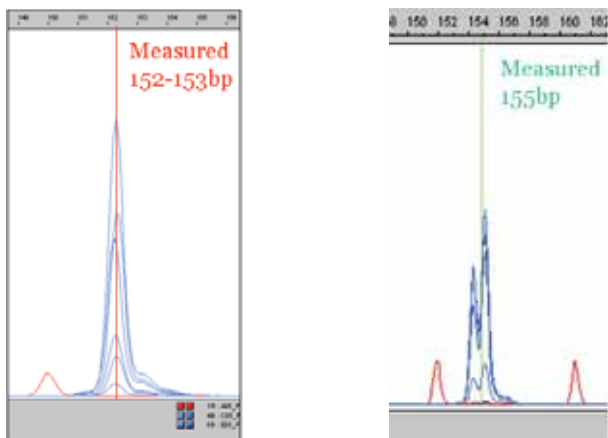


Figure 3.4: Fragment analysis peak of *P. a.* in the respective GeneMapper electropherogram. The theoretically expected value was 155 bp. Sizing standard definitions: standard (right) resulted in a length of 152-153 bp; adapted (left) resulted in the expected length of 155 bp.

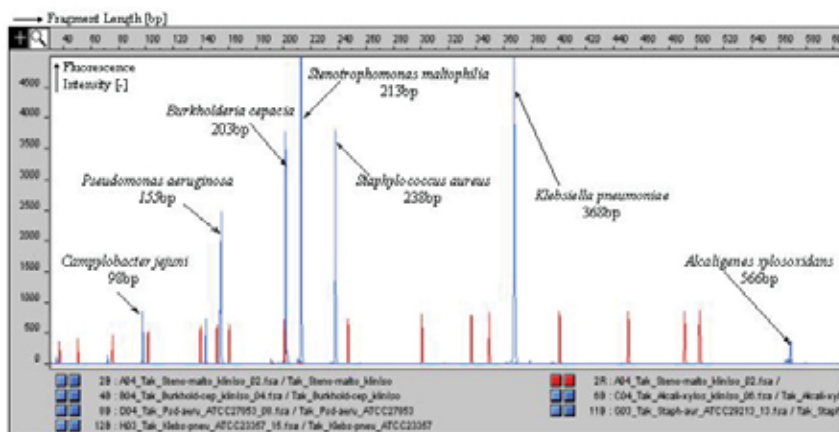


Figure 3.5: Sizing of fragments with adapted standard definitions for 16S rRNA gene T-RFLP. Electropherogram for seven species relevant in CF with their theoretically expected 16S DNA fragment lengths. The measured values were consistent in a range of 98-566 bp.

Different sizing results between manufacturer's and adapted standard definitions were probably caused by differences in DNA-sequences of sizing standard (non-16S DNA) and

sample fragments (16S rDNA). Sequence composition, namely biochemical properties, has great impact on separation in capillary electrophoresis (Applied Biosystems, pers. com.).

3.5.2.3 Calculation of Cell Numbers from Fragment Analysis Data

The following algorithm (eqn. 3.7) [85, 145] was used to calculate the absolute cell number ($N_{species}$) in the analyzed culture sample from the fragment analysis data, namely peak areas.

eqn. 3.7

$$N_{species} = e^{\ln(A_{species}/A_{IQS}) - cyc[\ln(f_{species}/f_{IQS})] + \ln(N_{IQS} \cdot z_{IQS})} / z_{species}$$

For calculation of concentrations, $N_{species}$ was divided by the sample volume. $A_{species}$ and A_{IQS} are the peak areas in the fragment analysis of the species of interest and the internal quantification standard (IQS), respectively. The number of cycles in the PCR was denoted by cyc and the absolute cell number of the IQS to which the sample was added was given by N_{IQS} . The species specific copy numbers of 16S rRNA genes per cell (genome), z_{IQS} and $z_{species}$, were taken from [<http://rrndb.cme.msu.edu/rrndb/servlet/controller?page=home>]. In case the strains of the databank and the mixed culture did not exactly match, the copy number of a different strain but same species was assumed to give reasonable estimates as proposed by Fogel et al. [32]. For T-RFLP cell number determinations the following copy numbers were used: *P. a.* 4 copies, *S. a.* 5 copies, *B. c.* 6 copies and *C. j.* 3 copies.

The efficiency parameters $f_{species}$ and their quotients ($EQ = f_{species}/f_{IQS}$), were determined from peak areas (T-RFLP) and dilution plating counts after parameter optimization (Nelder-Mead simplex (direct search) method (fminsearch), MatLab 6.1.0.450 - release 12.1) (Figure 3.6).

Eight independent, pooled 10-fold dilution series of the *B. c.*, *P. a.* and *S. a.* were quantified with T-RFLP method. The dilutions were prepared from 10^3 cfu/mL to 10^{10} cfu/mL for *P. a.* and *B. c.*, and 10^5 cfu/mL to 10^{10} cfu/mL for *S. a.*. No results were obtained for dilution steps 10^5 cfu/mL (*S. a.*), 10^3 cfu/mL (*B. c.*) and 10^4 cfu/mL (*P. a.*) due to loss of corresponding peaks. The dilution steps 10^3 cfu/mL and 10^4 cfu/mL (*P. a.*) and 10^{10} cfu/mL (*B. c.*) were considered not to be in the linear range (not shown, Figure 3.6). As reference the corresponding dilutions were calculated from the undiluted cell number determined by dilution plating for each strain.

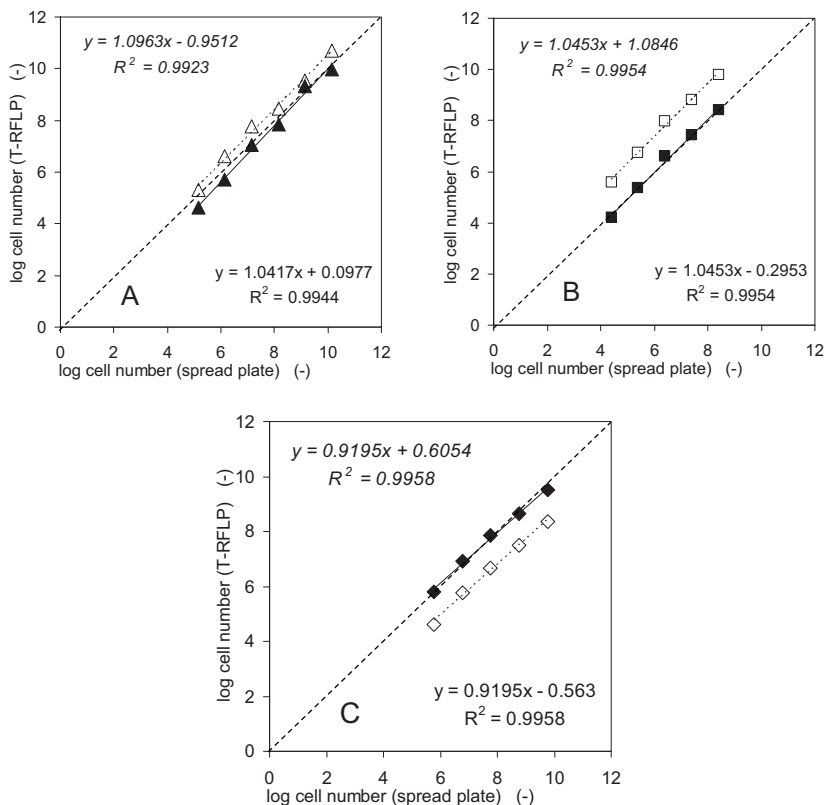


Figure 3.6: Determination of EQ from T-RFLP quantification of eight independent, pooled 10-fold dilution series. **Open symbols:** EQ from literature [145]: (A) 0.896 (*P.a.*) (B) 0.869 (*B.c.*) (C) 0.869 (*S.a.*). **Full symbols:** EQ optimized with dilution plate counts: (A) 0.9363 (*P.a.*) (B) 0.9522 (*B.c.*) (C) 0.8777 (*S.a.*). Linear regression and coefficient of variation: literature values [145] (lower right); optimized (upper left).

In contrast to Trotha et al. [145] the optimized EQ results were 0.9363 (*P.a.*), 0.9522 (*B.c.*), and 0.8777 (*S.a.*) obtained for best fit of quantifications (T-RFLP) to the references (dilution plating) (Figure 3.6). These optimized EQ values were kept constant for T-RFLP cell number calculations throughout the present work.

Conversion between quantitative T-RFLP and OD values

Conversion factors of OD_{650} to T-RFLP enumerations were determined as species specific quotients of T-RFLP result and OD value. A ten-fold dilution series ($1:10^0$ to $1:10^2$) of each bacterial strain was prepared. For each dilution OD_{650} (single replicate) and cell number

(cfu/mL) with quantitative T-RFLP (in duplicate for each sample) were measured. The mean of all six (four for *B. c.*) calculated quotients were used as conversion factor (mean \pm SD):

<i>S. a.</i>	$(1.130 \pm 0.303) \cdot 10^{09}$ (cfu/mL)/AU;
<i>B. c.</i>	$(1.849 \pm 0.712) \cdot 10^{08}$ (cfu/mL)/AU;
<i>P. a.</i>	$(4.157 \pm 1.844) \cdot 10^{08}$ (cfu/mL)/AU.

3.5.3 Metabolic Substrates and Products

Glucose and lactate

The extracellular concentrations of glucose and lactate were determined with an automated enzymatic quantification method (YSI 7100 MBS) with the validated method of the bioprocess engineering group (“SOP for glucose measurement with YSI 7100”). An assay validation with unweighted regression analysis for a range between 0.5 g/L and 5.0 g/L was performed for glucose measurements in the medium M199+P+NTA. The limit of detection was 0.052 g/L, the limit of quantification was 0.158 g/L, and the SD of the method was 0.016 g/L, meaning relative SD of the method was 0.57 %. An assay validation with unweighted regression analysis for a range between 0.3 g/L and 2.1 g/L was performed for lactate measurements in the medium M199+P+NTA. The limit of detection was 0.04 g/L, the limit of quantification was 0.122 g/L, and the SD of the method was 0.012 g/L, meaning relative SD of the method was 1.02 %.

Ammonia

The concentration of ammonia was determined with a Vitros DT60 II System Chemistry (“SOP for ammonia measurement”). The method was executed as validated in the bioprocess engineering group for a range between 0.5 and 6 mg/L. The limit of detection was 0.57 g/L, the limit of quantification 1.72 g/L, the SD of the method was 0.17 g/L, meaning a relative SD of the method of 5.23 %.

Amino acids

The concentrations of amino acids in cultivation supernatant were determined by anionic exchange liquid chromatography system (Dionex) based on change of the potential of a gold electrode [37] (“SOP for amino acid measurement”) as validated in the bioprocess engineering group.

Acetate and pyruvate

Acetate and pyruvate concentrations in the culture supernatant were analyzed by HPLC (Agilent 1100 series). The method was performed according to the standard method

established within the presented work in the bioprocess engineering group (“SOP HPLC for mixed communities”). For acetate a validation was performed in a range between 1 mM to 12 mM: the limit of detection was 0.05 mM, the limit of quantification was 0.17 mM, the SD of the method was 0.0165 mM, meaning a relative SD of the method of 0.57 %. For pyruvate the validation was performed in a range between 0.05 mM to 0.9 mM: the limit of detection was 0.008 mM, the limit of quantification was 0.024 mM, the SD of the method was 0.002 mM, meaning a relative SD of the method of 0.53 %.

3.6 Mathematical Modeling of the Bacterial Cultures

3.6.1 Characterization of model type and modeling method

The formulated models of the mixed culture were unstructured and segregated, the models of the pure cultures were unstructured and unsegregated. A deterministic modeling approach was chosen. The models consisted of non-linear ordinary differential equations, which were also non-linear in the parameters. The independent variables were cultivation time (t) for batch or dilution rate (D) for continuous processes. Dependent variables were the cell numbers (X_i), the substrate concentration (S), the glucose concentration (Glc), the acetate concentration (Ace), the amino acid concentration (AA), and the specific growth rate (μ). The parameters of the models were the maximum specific growth rates ($\mu_{max,i}$), the substrate affinities ($K_{S,i}$), the yield of cell number on a substrate ($Y_{X/S,i}$), the yield of product per cell ($Y_{P/X,i}$), and an inhibition constant (K_I). The index i relates to the three species S , a ., B , c ., P , a ..

3.6.2 MatLab Modeling and Simulation Software

The MatLab software version 7.0.4 was used for mathematical modeling, parameter estimations and simulations. Parameter values were optimized with an *ode* model fit to experimental data, the optimization criterion was the minimum sum of error squares (SEQ) (*fminsearch*). Two stop criteria for end of optimization were used: a) the resulting value of the optimized SES function did not change any more in its eighth position after the point ($TolFun = 1e^{-8}$), or b) stop after 1000 iterations. All parameters were varied to their fourth position after the point.

3.6.3 Parameter Estimation Methods

In order to determine μ_{max} independently of K_S and other parameters it was determined from the phase of exponential growth of a batch cultivation ($f = X(t)$). For this a nonlinear fit of the cell numbers during exponential growth (eqn. 2.23) to experimental data was applied (*lsqcurvefit*) (2.6.2).

The substrate affinity constant (K_S) was estimated first from batch experiments based on the Monod kinetic (eqn. 2.1) for the substrate of interest by optimization of SES (3.6.2). Furthermore for a more independent estimation of K_S chemostat experiments with varied dilution rates D were performed. The steady state for each D was assumed to be reached after at least 5 volume exchanges and was verified during the experiment by online data and by at least three successive samples with comparable results. For each chosen D , respectively specific growth rate (μ), the resulting substrate concentrations (Glc and AA) of glucose and amino acids in quasi steady state were measured. These data were used to optimize the model fit to experiments and determine K_S based on Monod kinetic (eqn. 2.1) over the whole range of the theoretical $f = \mu(S)$ diagram. For each D a time span of 24 h was applied in the optimization up to quasi steady state and afterwards the next D was used. The experimentally found values at D for wash out of the species from the chemostat were weighted by a factor of 100 in the optimized fit. This method of independent determination of μ_{max} and K_S was chosen to reduce correlation of μ_{max} and K_S [7]. The yield coefficients of cell number per substrate $Y_{X/Glc}$, $Y_{X/AA}$, and of product per cell $Y_{Ace/X}$ were determined either directly by a differential quotient or by parameter estimation during optimized model fit. Details will be given in the respective results chapter.

4 Results

4.1 Establishment of the Cultivation Protocol

As a first step towards the experimental characterization of a mixed culture, the experimental set-up for cultivations under defined and controllable conditions in an STR was established. At least three strains and an appropriate culture medium had to be chosen. Complex media components are subject to batch-to-batch variations and can lead to background noise in biochemical analytics. Therefore, the medium was supposed to be completely chemically defined to facilitate quantitative analysis of substrates and metabolites and support equally good growth of all strains.

4.1.1 Pool of Bacterial Strains

The pool of bacterial strains (3.3) was motivated by the pathogens mainly found in lungs of CF patients [39] (2.1). To reduce health risks during laboratory work no clinical isolates were chosen for selection experiments and *Haemophilus influenzae* was not considered. The final choice of strains was carried out in combination with the selection of a suitable culture medium as given in the following.

4.1.2 Selection of a Full and Chemically Defined Culture Medium

Minimal media typically used for bacteria were not suitable as they are developed to be species specific. Commercially available cell culture basal media do not contain complex additives, but a broad and varied range of biochemical compounds. Several commercially available cell culture basal media GMEM, Ham's F12, M199, and MEM α and variants of those (3.2.1.1) were therefore tested in single-species shake flask experiments (3.4.3.2).

Qualitative criteria for evaluation were:

- ⇒ complete glucose consumption correlated to the main phase of biomass formation to ensure the function of glucose as limiting substrate and main carbon and energy source
- ⇒ optimal exponential growth for biomass formation with uninhibited growth conditions
- ⇒ short lag phase.

The basal medium GMEM did not support bacterial growth. The preparation was therefore varied with phosphate (P) instead of carbonate buffer, less glucose (-Glc) and addition of nitrilotriacetate (NTA) to prevent precipitation of phosphates (+NTA). These variations of GMEM led to improved growth of all strains (Table 4.1). This established preparation protocol was applied for the basal media M199 and MEM α . The media M199+P+NTA and

MEM α +P+NTA, whose composition (Table 9.4) coincided best with the defined media compositions for *S. a.* [107, 152] and for *S. m.* [109] (Table 9.3) supported good growth of all eight species. Growth in MEM α +P+NTA of *S. a.* was very good. This was probably due to the supplement of nucleic acids in this preparation, which were not present in M199.

Table 4.1: Comparison of growth of bacterial strains in liquid media and standard shake flask (3.4.3.2): growth quality: / not tested; - very weak; 0 weak; + good; ++ very good

	GMEM	GMEM+P	GMEM+P-Glc	GMEM+P-Glc+NTA	Ham's F12	MEM α +P+NTA	M199+P+NTA	LB	LB+Glc
<i>A. xylosoxidans</i> DSM 2402	/	0	0	+	0	+	+	++	++
<i>B. c.</i> LMG 16656	-	0	0	++	0	+	+	++	++
<i>B. c.</i> DSM 7288	/	0	+	++	/	++	++	++	++
<i>S. a.</i> ATCC 29213	/	/	/	-	0	++	+	++	++
<i>S. a.</i> DSM 20231	-	/	/	/	0	++	+	++	++
<i>S. maltophilia</i> DSM 50170	/	0	0	-	+	-	+	++	++
<i>P. a.</i> PAO1	-	0		++	+	++	++	++	++
<i>P. a.</i> ATCC 27853	/	0	0	++	-	++	+	++	++

Eventually M199+P+NTA was chosen as the standard medium for all experiments in the presented project, as it supported good growth of more strains than MEM α +P+NTA. Thereby it would be possible later to increase the number of species in mixed culture experiments with M199+P+NTA. *B. c.* DSM 7288, *S. a.* ATCC 29213 and *P. a.* PAO 1 were the three best growing strains in M199+P+NTA and therefore were chosen for the mixed culture chemostat experiments.

4.1.3 Scale-Up and Impact of Aeration

Growth characteristics in shake flask (3.4.3.2) and 2 L STR (3.4.5.2) batch cultivations were compared. Surprisingly, for *S. a.* and *P. a.* growth in the STR gave about only half of the final biomass value compared to the shake flask cultivation. Growth conditions in shake flask and STR were comparable as in both systems no pH- and no pO₂-control was applied. A main difference was the aeration: submerge ($q = 1$ vvm) in the STR and surface mass transfer in the shake flask. Therefore, it was tested, whether an aeration effect could be responsible for the

difference. Different aeration rates in submerge mode were applied (0.416 vvm; 0.125 vvm; 0.0416 vvm) and one as surface mode (0.416 vvm) to *S. a.* small scale STR cultures (Figure 4.1).

For submerge aerated cultures of *S. a.* a decrease of volumetric aeration rate q (vvm) directly correlated to an increase of maximum biomass values. The surface aerated shake flask provided growth similar to the lowest submerge aerated STR (0.0416 vvm). The highest biomass formation was reached in the surface aerated STR (0.416 vvm).

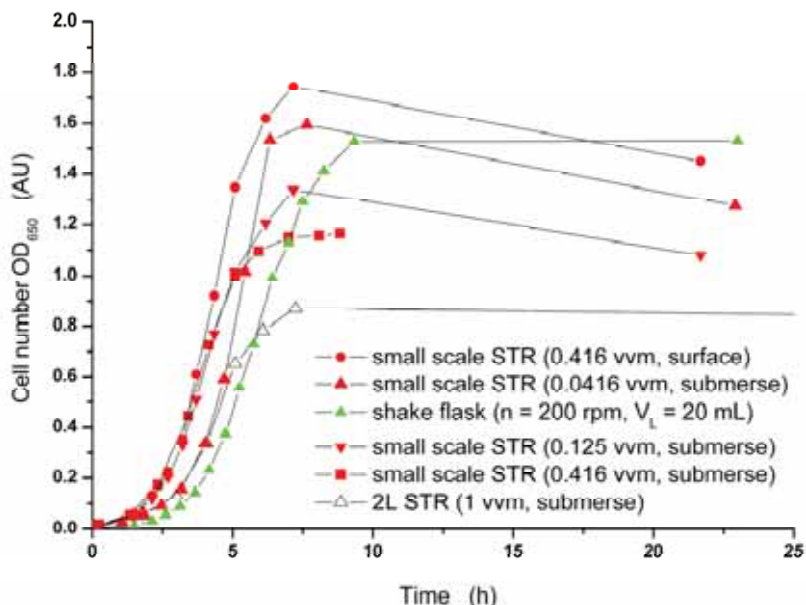


Figure 4.1: Biomass formation of *S. a.* in dependence of rate q (vvm) and mode (submerge / surface) of aeration in 2 L and small scale STR compared to shake flask.

In addition, the data of metabolic products of three cultivations were compared: low (surface) aeration in a shake flask, submerge aeration at 0.416 vvm and 1.0 vvm, both in STR cultivations (data not shown). It was found that not only cell number decreased with increasing aeration, but also the time course of the metabolic products acetate and pyruvate changed correspondingly. Their concentrations were significantly higher at higher aeration. This indicated a physiological effect by increased product formation instead of cells for high aeration.

A confirmation of the aeration effect on biomass formation of *S. a.* was demonstrated in chemostat cultures. Two parallel experiments for *S. a.* were performed with two submerge aeration rates: 0.083 vvm and 0.0416 vvm, respectively. The aeration with 0.083 vvm resulted in lower biomass values of *S. a.* compared to experiments with aeration of 0.0416 vvm. The wash-out point was at 0.4 h⁻¹ and at 0.7 h⁻¹ depending on the aeration rate, 0.083 vvm and 0.0416 vvm, respectively.

Experiments with *B. c.* and *P. a.* had similar results with an increased cell yield and increased μ at wash-out for lower aeration rates (data not shown).

Based on this and the experimental results obtained for *S. a.* (Figure 4.1) and *B. c.* an aeration rate of 0.0416 vvm (0.5 NL/h) in submerge mode for the small scale STR was chosen.

4.2 *Quantification of Species Specific Cell Numbers in Mixed Cultures*

Most species specific enumeration methods for mixed cultures are laborious or only qualitative, and therefore impede generation of quantitative data required for validation of mathematical models (2.5). For the present work a quantitative T-RFLP analysis of 16S rDNA [126] was adapted and evaluated for quantification of absolute and species specific cell numbers of *B. c.*, *P. a.* and *S. a.* (3.5.2).

Reference method for cell number quantification in single-species samples

For each strain cell numbers (cfu/mL) for the various dilution steps were calculated from dilution plating determinations of the respective undiluted suspension (3.5.1).

Reference method for cell number quantification in mixed species samples

As a reference for T-RFLP quantifications in defined mixed samples, cell numbers (cfu/mL) of the non-mixed and undiluted suspensions of the respective strains were determined by dilution platings (see above) and used for calculating theoretical concentrations in diluted samples. As an additional internal positive control, all single-species dilution samples were quantified by the T-RFLP method (duplicates from the same sample) and compared with the T-RFLP results obtained by mixed species analysis for evaluation of results recovery in mixed species sample analysis.

4.2.1 *Reproducibility of the Quantitative T-RFLP Analysis Method*

Reproducibility of capillary electrophoresis, that is to say exclusively the error introduced by the device, was checked by eight replicate runs (same capillary), prepared from one restriction digest. Quality loss due to capillary use was evaluated by repetition after 100 fragment

analysis runs. Reproducibility of T-RFLP sample preparation and quantification was determined for defined bacterial samples (single and mixed species) as well as for samples from actual cultivations.

Replicates of single-species quantification were produced from one suspension, which was divided into eight IQS tubes. Thereby errors introduced during the complete chain of sample preparation steps were taken into account. Replicates of defined mixed species were prepared from single-species suspensions, which introduced a potential error during the mixing step.

Duplicate samples of actual mixed culture samples from chemostat cultivation were taken as five samples within a time interval of 10 min, what was repeated the following day. The two sets of five replicates were processed at two different days in two independent series to evaluate reproducibility of the complete method (DNA extraction, PCR, restriction digestion, fragment analysis). The obtained basic statistical parameters are summarized in Table 4.2.

T-RFLP quantification, namely the precision of the sequencer, showed a very small CV of about 0.16 %, which did not increase after 100 measurement runs (about 0.04 %) (Table 4.2). In comparison, the error introduced by sample preparation was significantly higher with a CV in between 1.30 % (defined single-species samples) and 4.39 % (defined two-species samples). In general, two- and three-species replicates showed higher CV. However, the additional error introduced by the mixing of the appropriate samples has to be taken into account. Independent replicates taken from three-species cultures, which were not diluted before quantification, showed a maximum CV of 1.76 %. Therefore, the higher CV of defined samples compared to culture samples seemed to result rather from sample preparation than from quantification by the T-RFLP method itself. The higher CV in two-species mixtures compared to three-species (2.93 %) was unexpected and cannot be explained so far.

Table 4.2: Summary of statistical analyses of cell enumeration with quantitative T-RFLP, which was carried out in the present work. *

	Sample mean	Standard deviation (SD)	Coefficient of variation (CV) (%)	Percentage standard error of sample mean (%)
Error introduced by the device				
Genetic Analyzer (new capillaries, eight replicates) ^a	8.58	0.01	0.16	0.06
Genetic Analyzer (capillaries after 100 runs, eight replicates) ^a	8.63	0.00	0.04	0.01
Defined samples				
Single-species (<i>S. a.</i> values) lower working range (Figure 4.2) ^b	5.74	0.07	1.31	0.46
Single-species upper working range (Figure 4.2) ^b	9.67	0.13	1.30	0.46
Two-species (<i>S. a.</i> values) (<i>P. a.</i> spiked with <i>S. a.</i>) (Figure 4.3A) ^c	8.81	0.39	4.39	1.79
Two-species (<i>S. a.</i> values) (<i>P. a.</i> spiked with <i>S. a.</i>) (Figure 4.3A) ^c	8.64	0.34	3.89	1.59
Two-species (<i>P. a.</i> values) (<i>S. a.</i> spiked with <i>P. a.</i>) (Figure 4.3B) ^d	9.00	0.34	3.81	1.55
Three-species (<i>P. a.</i> values) <i>S. a.</i> spiked with <i>P. a.</i> and <i>B. c.</i> (Figure 4.6) ^e	7.81	0.16	2.0	0.89
Three-species (<i>B. c.</i> values) <i>S. a.</i> spiked with <i>P. a.</i> and <i>B. c.</i> (Figure 4.6) ^e	6.95	0.20	2.93	1.31
Culture samples (Chemostat; Figure 4.9)				
Three-species chemostat (<i>P. a.</i> values at time point (I)) ^f	7.18	0.12	1.71	0.77
Three-species chemostat (<i>B. c.</i> values at time point (I)) ^f	8.14	0.14	1.72	0.77
Three-species chemostat (<i>P. a.</i> values at time point (II)) ^f	7.63	0.13	1.76	0.79
Three-species chemostat (<i>B. c.</i> values at time point (II)) ^f	8.39	0.13	1.55	0.69

* All values log-transformed cell numbers (cfu/mL) (-); Calculation of statistical parameters Graphpad Prism software package (GraphPad software, San Diego, California, USA).

^a from the same restriction digest

^b eight independent replicates from the same bacterial suspension

^c six independent replicates from mixed bacterial suspensions (duplicate values)

^d six independent replicates from mixed bacterial suspensions

^e five independent replicates from mixed bacterial suspensions

^f five independently taken samples (every 5 min) from mixed bacterial chemostat (two time points I and II)

4.2.2 Linearity and Homogeneity of Variances for Single-Species (*S. a.*)

A defined dilution series of *S. a.* was prepared to investigate linearity and homogeneity of variances (F-test) at the upper and lower working range of the quantitative T-RFLP method. A *S. a.* shake flask culture broth in the end of the exponential growth phase was washed with PBS and adjusted to OD₆₅₀ of about 10 AU with PBS. Six independent ten-fold dilution series of *S. a.* suspension were prepared ($1:10^5$ to $1:10^0$). Individual samples at each dilution step were pooled to compensate for pipetting errors. Single replicates of each dilution step were quantified by the T-RFLP. Additionally, eight replicates were analyzed by quantitative T-RFLP from each the $1:10^0$ (upper working range), the $1:10^4$ and the $1:10^5$ dilutions (lower working range). Higher concentrations (10^{11} cfu/mL) were not considered for quantifications due to the loss of the *C. jejuni* peak (IQS) (data not shown).

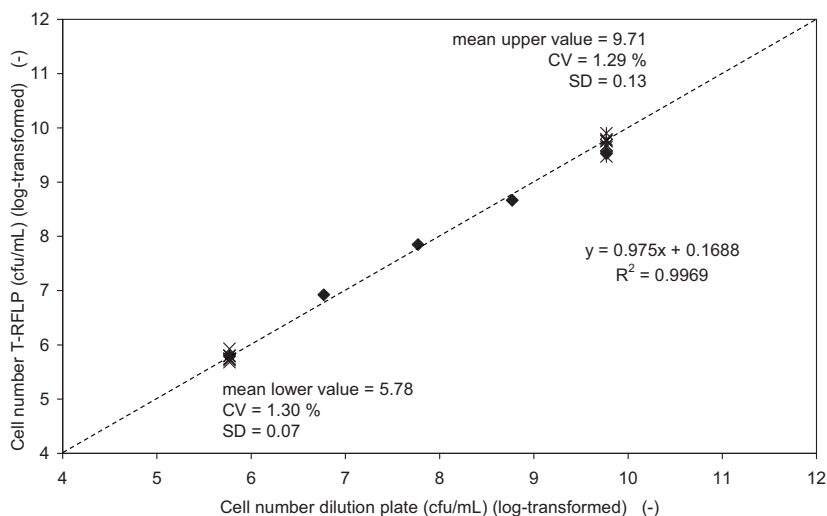


Figure 4.2: T-RFLP quantification of a single-species dilution series (*S. a.*): linear regression, reproducibility at the upper and lower limit range (eight independent replicates from a pooled dilution series)

The linear working range for the T-RFLP quantification of single-species dilution series of *S. a.* after logarithmic transformation of cell numbers obtained by the T-RFLP method is given in Figure 4.2. The lower working range was set to 10^6 cfu/mL as 10^5 cfu/mL could not be analyzed (loss of *S. a.* peak). Homogeneous variances at the lower (10^6 cfu/mL) and upper (10^{10} cfu/mL) working range were obtained (F-test; f_1 , $f_2 = 7$; 99%). The mean log-transformed values in the lower range were 5.78 and in the upper 9.71, respectively.

The residual SD of the linear regression was determined as 2.68. The percentage standard error of the sample mean of eight replicates was about 0.46 % in lower and upper range. Similar results were obtained for single-species T-RFLP quantifications of *P. a.* (linear range 10^5 to 10^{10} cfu/mL) and *B. c.* (linear range 10^4 to 10^9 cfu/mL).

4.2.3 Recovery of T-RFLP Quantifications in Mixed Species Dilution Series

Results obtained from single-species T-RFLP quantification do not necessarily correlate with results obtained for two or more species analysis for example due to possible PCR bias [88, 140]. For application in cultivation experiments, comparability of results obtained with T-RFLP for single-species and two- or three-species samples had to be assured. Therefore, defined samples with known cell numbers were prepared and analyzed. The single-species suspensions, which were used for preparation of the mixed samples, were applied as positive controls. As the preparation of the mixed samples involved no dilution, they should give the same cell number values as the single-species samples they were prepared from. Recovery after spiking of one-species samples with one or two other species was tested. The spiked dilution series were evaluated for differences of the slope of linear regression and quantification range differed compared to pure dilution series.

Two-species enumeration (*S. a.*, *P. a.*)

Independent and individually pooled dilution series ($1:10^5$ to $1:10^0$) of *S. a.* and *P. a.* (both undiluted at $OD_{650} \sim 10$ AU) were prepared. Mixed samples of *P. a.* with *S. a.* were derived by spiking 1 mL of *S. a.* ($1:10$ dilution) into 1 mL of each *P. a.* dilution step into the same IQS-tube. Mixed samples of *S. a.* with *P. a.* spikes were prepared correspondingly. Each of these mixed samples was prepared in duplicate; of which each was quantified by the T-RFLP.

The quantifications of *P. a.* dilutions from 10^7 to 10^{10} cfu/mL spiked with *S. a.* were comparable to the single-species results of *P. a.* (Figure 4.3A). For the 10^6 cfu/mL samples the duplicate values were very consistent. However, mixed sample results fitted in the linear range, but showed an unexpected difference of about 1 log-step between pure and mixed sample results. At 10^5 cfu/mL pure and mixed samples gave consistent results, but all four values were about 0.5 log-steps higher than expected. Quantifications of *P. a.* as spikes (10^9 cfu/mL) in *S. a.* dilution series gave similar values compared to spiked and unspiked *P. a.* dilutions (Figure 4.3A).

Altogether the deviations in the range 10^5 and 10^6 cfu/mL of the unspiked dilution series of *P. a.* were unexpected (compare Figure 3.6A for a standard result) and could not be

explained. If it had been a preparative error, the mixed samples should have been similarly skewed as original suspensions were the same.

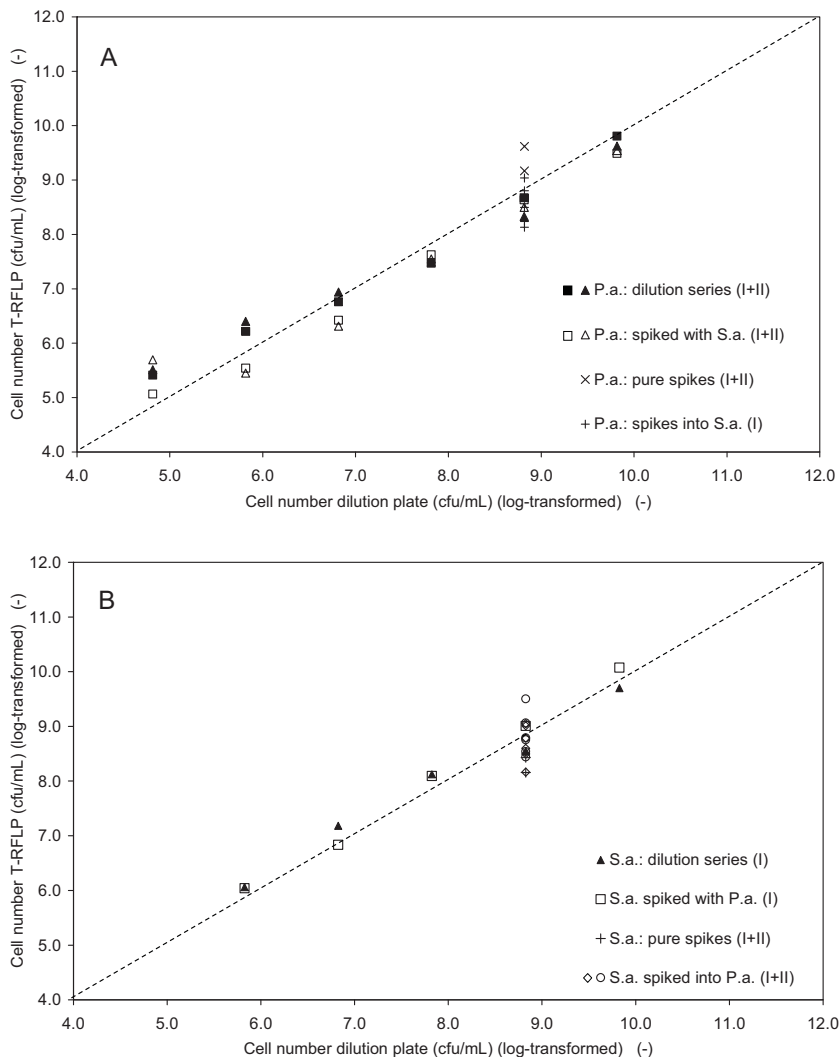


Figure 4.3: T-RFLP quantification of defined two-species mixtures: a 10-fold dilution of *P. a.* and *S. a.*, respectively, spiked with the corresponding second species. T-RFLP quantification of unspiked suspension as positive control. A: *P. a.* cell numbers (Table 4.3 for statistics), B: *S. a.* cell numbers (Table 4.4 for statistics); duplicates I/II as indicated.

For the quantifications of *S. a.* dilutions (10^6 to 10^{10} cfu/mL) spiked with *P. a.* good recovery of pure sample results was apparent (Figure 4.3B). Also, the values of *S. a.* spiked into *P. a.* samples correlated very well with the pure spike values as well as with the corresponding values (10^9 cfu/mL) in the dilution series (Figure 4.3B). The residual SD of the first order linear regression was determined as 2.74 (pure) and 2.55 (spiked) (Table 4.4). These values were in the same range as the residual SD of 2.68 obtained before in the single-species (*S. a.*) quantification (Figure 4.2).

No influence of the ratio between the two species on T-RFLP quantification was observed: varied *S. a.* numbers + constant *P. a.* numbers as well as constant *S. a.* numbers + varied *P. a.* numbers resulted in very similar values.

In addition, the two single-species (unspiked) and two-species (spiked with *S. a.*) dilution series of *P. a.* were fitted by first order linear regression (Table 4.3); correspondingly for *S. a.* (Table 4.4). For each species, the differences between both, the residual SD and the slopes of linear regression, were not significant (residual SD, F-test, $P = 99\%$; slope, t-test, $P = 95\%$). For the dilution series of both *P. a.* and *S. a.* the slope of linear regression for spiked samples was closer to the optimal value of 1.0 than for pure dilution samples (Table 4.3, Table 4.4). It was therefore assumed that no significant bias was introduced into the quantification due to the second species in PCR or other steps. Also, the quantification range (10^5 to 10^{10} cfu/mL for *P. a.*, 10^6 to 10^{10} cfu/mL for *S. a.*) was not reduced by spiking (Figure 4.2, Figure 4.3A & B). For efficiency, such evaluation was not performed with *B. c.* in two-species samples, but in three-species samples' evaluation as given below.

Table 4.3: Linear regression analysis of two-species T-RFLP evaluation (*P. a.*, Figure 4.3A)

<i>P. a.</i> dilutions	pure (I)	spiked (I)	pure (II)	spiked (II)
Linear regression	$0.77x + 1.75$	$0.85x + 0.99$	$0.86x + 1.54$	$0.93x + 0.75$
Residual SD	3.86	3.79	3.78	3.71
CV	0.98	0.93	0.98	0.99

Table 4.4: Linear regression analysis of two-species T-RFLP evaluation (*S. a.*, Figure 4.3B)

<i>S. a.</i> dilutions	pure (I)	spiked (I)
Linear regression	$0.87x + 1.15$	$1.02x - 0.01$
Residual SD	2.74	2.55
CV	0.98	0.99

Three-species enumeration (*S. a.*, *P. a.*, *B. c.*)

Independent and pooled dilutions ($1:10^5$ to $1:10^0$, $1:10^4$ to $1:10^0$ and $1:10^4$ to $1:10^0$, respectively) were prepared of *S. a.*, *P. a.* and *B. c.* suspensions (OD₆₅₀ about 10 AU).

Defined three-species mixed samples were prepared by spiking 1 mL of *P. a.* ($1:10^3$ dilution) together with 1 mL of *B. c.* ($1:10^3$ dilution) (each 10^8 cfu/mL) into 1 mL of each *S. a.* dilution step. The amount of required dilution was successively dosed into the same IQS tube. Before adding the next species, liquid volume was discarded after centrifugation (13,000 rpm, 4 °C).

The five dilution steps of single-species *S. a.* as well as the spiking suspensions of *B. c.* and *P. a.* were analyzed by T-RFLP as positive control for the resulting values from the three-species samples. The resulting values were compared to the values resulting from T-RFLP analysis of the five three-species samples (Figure 4.4 A, B and C).

Very good consistency between cell numbers of the defined three-species samples compared to the control values was found (Figure 4.4). The maximum differences in T-RFLP cell enumerations were 0.48, 0.20, and 0.20 (cfu/mL log-transformed). On the average the differences were 0.30 ± 0.16 , 0.09 ± 0.10 , and 0.16 ± 0.06 (mean \pm SD in cfu/mL log-transformed) for *S. a.*, *P. a.*, and *B. c.*, respectively. Obviously, no bias of data due to different number of species needs to be taken into account, as could have been expected due to the preferential amplification in mixed DNA templates compared to pure ones reported in literature [17]. As found for the two-species evaluation (Figure 4.3) the quantification range (10^6 to 10^{10} cfu/mL) was not narrowed by presence of two more species. The use of quantitative T-RFLP for comparison of cell numbers from single and mixed cultivations was therefore possible.

S. a. dilutions spiked with two additional species were fitted by first order linear regression (Figure 4.5). Slopes of the mixed samples were slightly higher than those of pure cultures (Table 4.5). However, individual slopes of linear regression (t-Test, $P = 95\%$) as well as residual SD (F-Test, $P = 99\%$) did not differ significantly. Differences between slopes of linear regression of mixed and pure dilution series were therefore evaluated as arbitrary.

Table 4.5: Linear regression analysis of three-species T-RFLP evaluation (*S. a.*, Figure 4.5, duplicates I and II as indicated)

<i>S. a.</i> dilutions	pure (I)	spiked with <i>P. a.</i> and <i>B. c.</i> (I)	pure (II) *	spiked with <i>P. a.</i> and <i>B. c.</i> (II)
Linear regression	$0.8830x + 1,3859$	$0.9470x + 0.9907$	$0.10325x + 0.1434$	$0.9859x + 0.5552$
Residual SD	2.72	2.65	2.96	2.60
CV	0.99	0.99	0.98	0.99

* result for undiluted suspension II ($10^{8.93}$) was not considered for regression, but as outlier

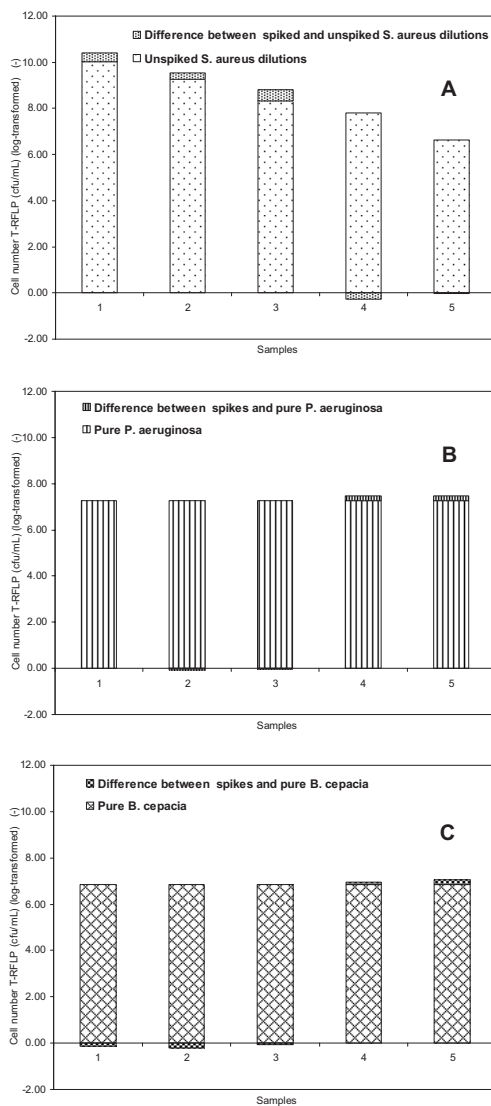


Figure 4.4: T-RFLP quantifications of defined three-species mixtures (mean of duplicates): Results of unspiked single-species samples and calculated differences to results of the spiked (three-species) samples are given; (A) five ten-fold *S. a.* dilutions ($10^{10.03}$ to $10^{6.63}$ cfu/mL); (B) spiked with constant number of *P. a.* ($10^{7.27}$ cfu/mL) and (C) spiked with constant number of *B. c.* ($10^{6.86}$ cfu/mL)

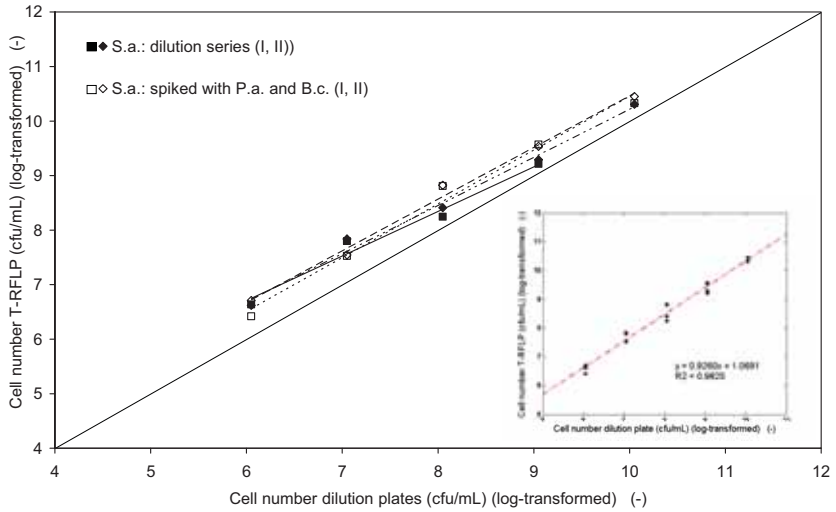


Figure 4.5: Linearity and recovery of T-RFLP results for *S. a.* dilution steps: single-species results (unspiked) and three-species (spiked with *B. c.* and *P. a.*). Linear regression over all samples (small graph). Independent duplicates as indicated I/ II. See Table 4.5 for statistics.

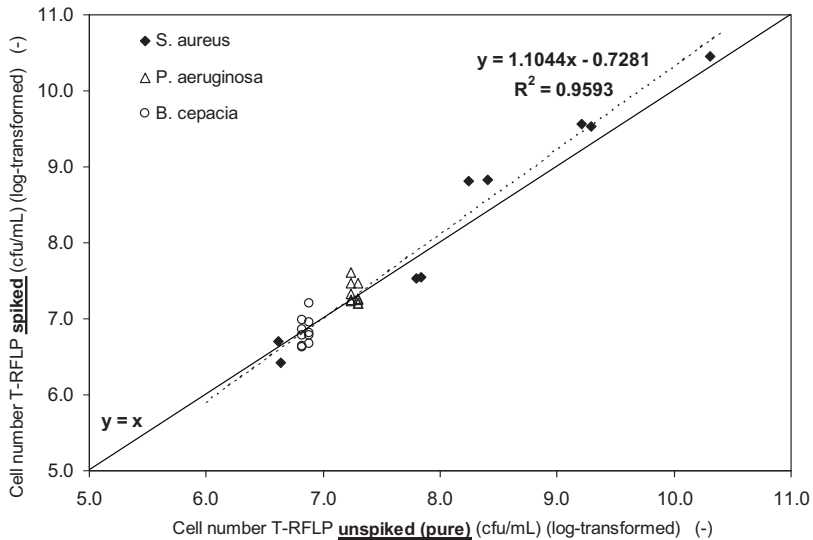


Figure 4.6: T-RFLP quantifications of *S. a.*, *P. a.* and *B. c.* from spiked samples (all three species) versus unspiked samples prepared in parallel (each single-species): comparison of results within the T-RFLP method. Table 4.5 for statistics.

Values obtained for the single-species (unspiked) and three-species mixtures (spiked) did not differ significantly (Figure 4.6). The resulting linear regressions and the values were close to each other and close to the ideal correlation (1.0), as for two-species (Figure 4.3A, B).

4.2.4 Reproducibility between Different Runs of Quantitative T-RFLP

Quantification results of cell number dynamics in cultivations performed during the complete period of time of this project presented had to be evaluated and compared. Therefore, results obtained in several completely independent data sets were collected over a period of 12 months to test for reproducibility of T-RFLP quantification in between runs (Table 4.6). As a representative result the dilution series of one of the species (*P. a.*) is presented (Figure 4.7).

Table 4.6: Linear regression of T-RFLP quantification between different series

Species	Linear regression overall	CV of the linear regression* (R^2)	mean of slopes**	SD of slopes	mean of intercepts
<i>P. a.</i>	$y = 1.00x - 0.30$	0.94	0.95	0.11	0.11
<i>S. a.</i>	$y = 0.97x + 0.50$	0.96	0.94	0.08	0.66
<i>B. c.</i>	$y = 0.93x + 0.31$	0.97	0.94	0.11	0.11

* over all experimental series

** slopes of the linear regressions determined for the individual experimental series

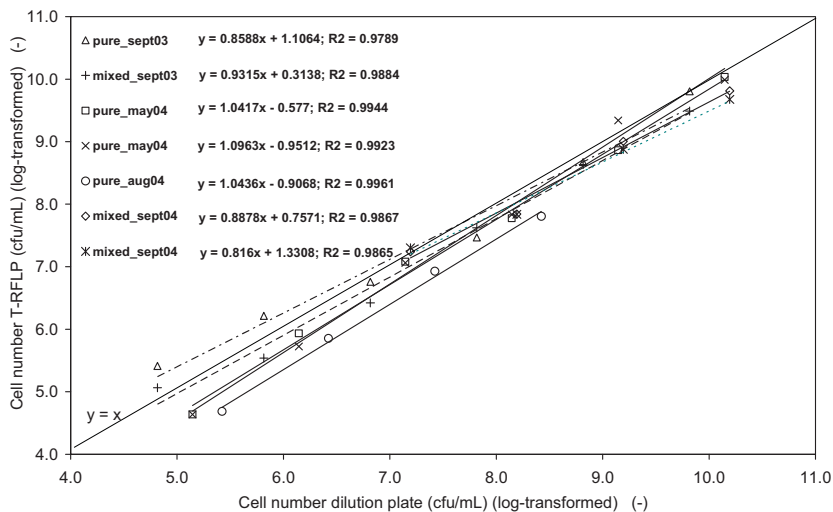


Figure 4.7: T-RFLP quantification of independent *P. a.* dilution series prepared from five different suspensions (two dilution series prepared in duplicate). Reference values were calculated from dilution plating results of the undiluted suspensions. Table 4.6 for statistics.

Altogether the evaluated quantitative T-RFLP gave very consistent results compared to the reference values. Percentage SD of the slopes of the different and independent dilution series were in the range of 8.53 to 11.95 %. There was a slightly higher variation between the data sets in the low quantification ranges, what was possibly due to propagation of dilution errors. It has to be kept in mind samples from shaken flasks and bioreactors will not be diluted before quantification. Therefore, dilution errors, which could not be avoided for preparing standard curves, are not relevant for monitoring continuous cultivations. Reproducibility could be assumed to be in the range reported in Table 4.2. Efficiency quotients and the number of rRNA gene copies were kept constant with very good consistency of results and T-RFLP quantification did not seem to vary in between experimental series or days.

4.2.5 Quantitative T-RFLP for Monitoring Cultivation Experiments

In the following the use of T-RFLP quantification for monitoring bacterial growth dynamics will be described. First, growth of *S. a.*, *P. a.* and *B. c.* was investigated as single-species cultures in shake flasks afterwards as a three-species culture under chemostat conditions.

Quantitative T-RFLP for monitoring of shake flask experiments

The results of T-RFLP quantifications of two shake flasks in parallel were compared to those of a third parallel flask with optical density (OD₆₅₀) as a standard laboratory method (Figure 4.8). Results of both methods are presented after logarithmic transformation. The number of intervals on the log-axis was kept equal for T-RFLP and OD in each figure to allow for an easier comparison of the increase in cell number determined with the two different methods.

The growth dynamics in the shake flask cultures, namely the time dependent characteristic, were very consistent with the two methods for *S. a.* and *P. a.* (Figure 4.8). The time course as well as cell numbers correlated well. However, for *B. c.* T-RFLP values were lower compared to the OD results during the exponential and early stationary growth phase (0 to 8 h). At present, this difference between both methods cannot be explained satisfactorily. The lower cell counts determined by T-RFLP analysis might result from an increase in size and mass of the cells during the early growth phase [53] and therefore indicate an initial increase in mass density rather than in number density. As both shake flasks analyzed by T-RFLP gave similar results, the difference between the two methods did not seem to be due to scatter in data. In preliminary experiments with *B. c.* some scatter in data was noticed for T-RFLP quantification. It was tested, whether use of plastic pipettes and Eppendorf tubes or glass ware for sample preparation had an impact on quantifications. However, this was not confirmed and data quality in later experiments with *B. c.* was similar to the other two species.

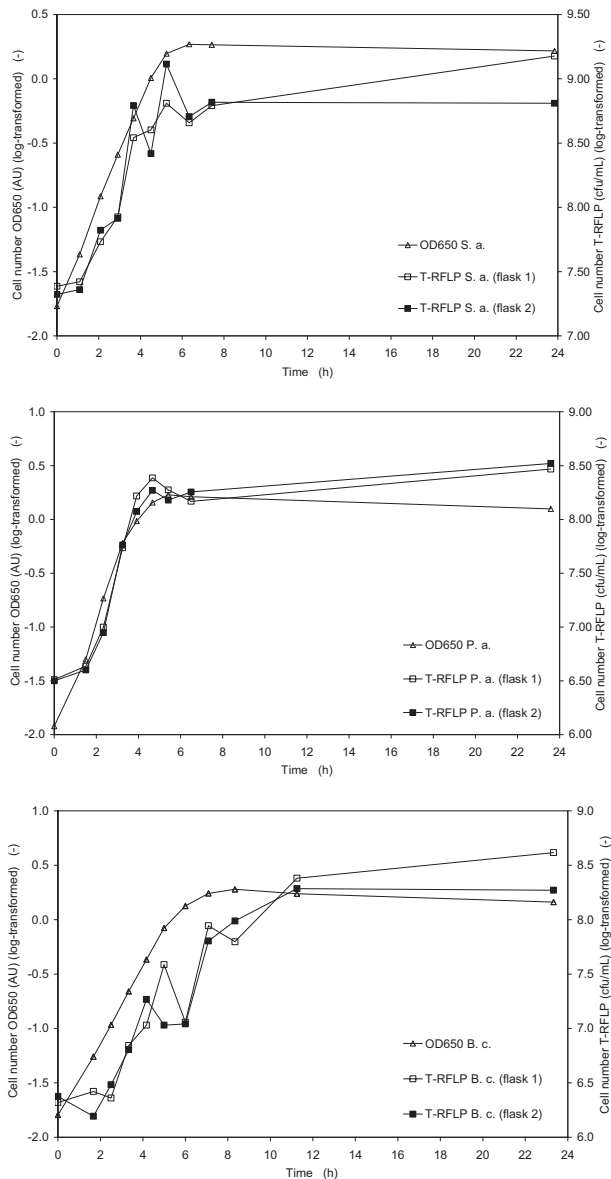


Figure 4.8: Comparison of OD and T-RFLP for monitoring shake flask cultivations of *S. a.* (top), *P. a.* (middle), and *B. c.* (bottom) in M199+P+NTA medium. Three flasks in parallel: two for T-RFLP and one for OD.

Quantitative T-RFLP for monitoring of three-species chemostat cultivation

Growth dynamics of a three-species chemostat culture of *P. a.*, *B. c.* and *S. a.* was monitored over a period of more than 170 h corresponding to 33 volume exchanges (Figure 4.9). After switching to continuous mode instationarity of glucose and OD measurements reflected adaptation of the bacteria to the new cultivation conditions (8 - 40 h). T-RFLP quantifications correlated correspondingly. While cell numbers of *P. a.* and *B. c.* remained at a comparatively high level over the whole period of time, cell numbers of *S. a.* dropped below the limit of quantification. If *S. a.* was completely washed out in the following or remained constant at a level below the quantification limit was not investigated in this period of the project. After about 40 h stability of glucose and OD values over time indicated that the culture had reached stationary conditions. However, cell numbers of *B. c.* were still instationary up to about 80 h of cultivation. Altogether the stationary phase was reflected remarkably well by the consistent results of quantitative T-RFLP of *P. a.* and *B. c.*, which did not show any outliers or scatter.

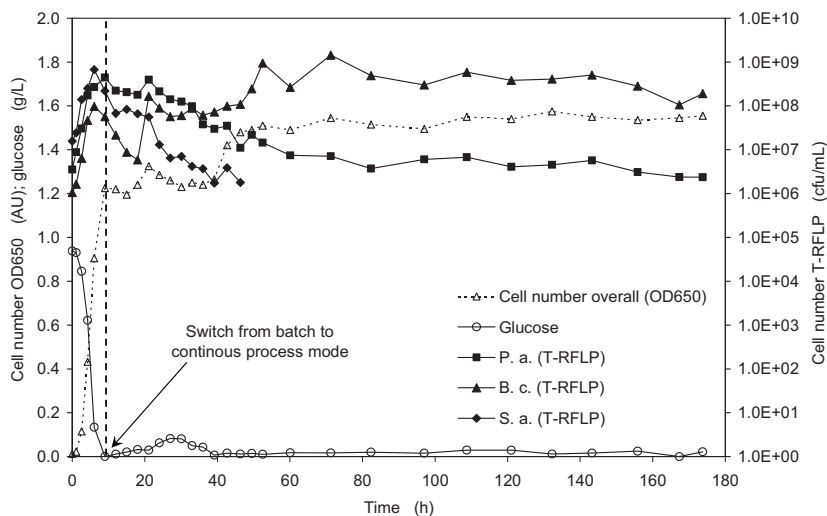


Figure 4.9: Growth dynamics in a three-species chemostat cultivation of *P. a.*, *B. c.* and *S. a.* monitored by the quantitative T-RFLP analysis. STR cultivation: $D = 0.2 \text{ h}^{-1}$; $V = 2.0 \text{ L}$; $V_L = 1.0 \text{ L}$; $q = 1.0 \text{ vvm}$; M199+P+NTA.

4.2.6 Summary

A quantitative T-RFLP method was evaluated and applied for specific and absolute cell number enumerations. The method was tested to be unbiased by quantitative sample composition and allowed reproducible enumerations of mixed cultures. For assay validation,

samples of defined concentration containing one, two or three species were quantified. Logarithmically transformed absolute cell numbers of single-species dilutions were linear within a lower working range of 10^4 to 10^6 cfu/mL (species-dependent) and an upper working range of 10^{10} cfu/mL. Quantifications of dilutions (10^6 to 10^{10} cfu/mL) spiked with one or two other species agreed well with the single-species positive controls. Differences between slopes of first order linear regression of the spiked and pure dilutions were insignificant. CV of defined mixed replicates was maximum 4.39 %, of a three-species chemostat it was maximum 1.76 %. T-RFLP monitoring of pure cultures in parallel shake flasks gave very consistent results with OD measurements.

Typical errors of T-RFLP analysis results were determined for defined samples (values in cfu/mL log-transformed (-)). The values can be used to evaluate experimental variations as due to measurement errors or due to actual growth characteristics. For single-species samples of about 5.7, the error was about ± 0.07 . The maximum error of ± 0.39 was determined for two-species samples with a mean of about 8.6. For three-species samples the error was ± 0.16 and ± 0.20 for sample means of 7.81 and 6.95, respectively.

The T-RFLP quantifications of actual cultivations were found to exhibit only very little error and variation. The error determined from actual chemostat culture samples with three species was ± 0.12 for a mean of 7.2 and ± 0.13 for a mean of 8.4. These values were low compared to the samples from defined samples, what was probably due to additional errors introduced by the sample preparation. Variations between values of growth dynamics larger than about 0.2 could therefore be assumed not to be caused by the measurement, but rather by the microbial culture itself.

4.3 Single-Species Growth: *S. aureus*, *B. cepacia*, and *P. aeruginosa*

The selected strains *S. a.* ATCC 29213, *B. c.* DSM 7288, and *P. a.* PAO1 are typically not used in bioprocesses. Therefore not much data are available in literature on the kinetics of the strains. However, the data were required for characterization of strains as the necessary basis for mathematical modeling, especially with regard to the mixed culture behavior. In order to obtain this basis cultivation experiments were performed in batch mode in shake flasks and in batch and continuous mode in 200 mL and 2 L scale. The mathematical models of single-species growth were formulated.

4.3.1 Experiments on Growth Dynamics

Growth dynamics of the strains were first studied in shake flask cultivations. However, shake flasks do not provide the possibility to monitor and control process parameters and, most important, can not be used in continuous mode. Therefore, growth dynamics for *S. a.*, *B. c.*, and *P. a.* were characterized in more detail in STR in preparation of chemostat experiments. In shake flasks and STR the focus was on dynamics of cell number and the potential formation of organic acids. Additionally, the oxygen consumption and amino acid consumption were measured in the 2 L STR and the small scale STR, respectively. The analysis was individually for all amino acids (3.5.3), however, as a first approach they were evaluated cumulatively. For the small scale STR cell numbers were determined as OD and the values in cfu/mL were calculated (3.5.2.3). This was convenient for their use in mathematical models and comparison to T-RFLP data from mixed cultures (cfu/mL).

4.3.1.1 Growth Dynamics of *S. aureus*

The cell formation of *S.a.* in shake flask, 2L STR and small scale STR showed similar characteristics during cultivation (Figure 4.10, Figure 4.11, and Figure 4.12). After a short lag phase, exponential growth was observed followed by a linear growth phase corresponding to the reduction of glucose concentration. In the shake flask and in small scale STR the cell number was comparable (shake flask = 1.53 AU (Figure 4.10); small scale STR = $1.8 \cdot 10^9$ cfu/mL (1.59 AU) (Figure 4.12). In 2 L STR, however, the growth rate decreased after 5.0 h and 0.53 g/L glucose was left and the maximum cell number (0.89 AU) was measured after 7 h, together with glucose of 0.15 g/L (Figure 4.11). This difference in cell number was presumably caused by impact of aeration (4.1.3).

The formation of acetate, max. 0.19 g/L (Figure 4.10), max. 0.21 g/L (Figure 4.11), max. 0.5 g/L (Figure 4.12), and of pyruvate max. 0.2 g/L (Figure 4.10), max. 0.2 g/L (Figure 4.11),

pyruvate was not analyzed in small scale STR due to problems with the HPLC analysis) by *S. a.* was observed. Acetate formation mainly took place during the exponential growth phase (I), pyruvate was released during the phase of linear growth before the steady state phase (II) (Figure 4.11). In small scale STR the final acetate concentration (about 0.5 g/L) was doubled compared to the cultivations in shake flask (Figure 4.10) and 2 L STR (Figure 4.11) and its formation continued until the end of cell number increase. These differences could not be explained in detail and were probably related to the influence of cultivation conditions on growth of *S. a.* (4.1.3). No other of the analyzed organic acids (3.5.3) was detected during cultivation of *S. a.*: formate, fumarate, malate, propionate, succinate, and lactate. The pH value decreased to about 6.5 during growth of *S. a.* correspondingly to the uptake of glucose (Figure 4.10). Ammonia release (max. 15 mg/L) correlated to acetate formation in the shake flask. However, in the 2 L STR release of ammonia was significantly higher (30 mg/L) and continued until the end of cell formation. This difference was presumably due to the impact of aeration (4.1.3).

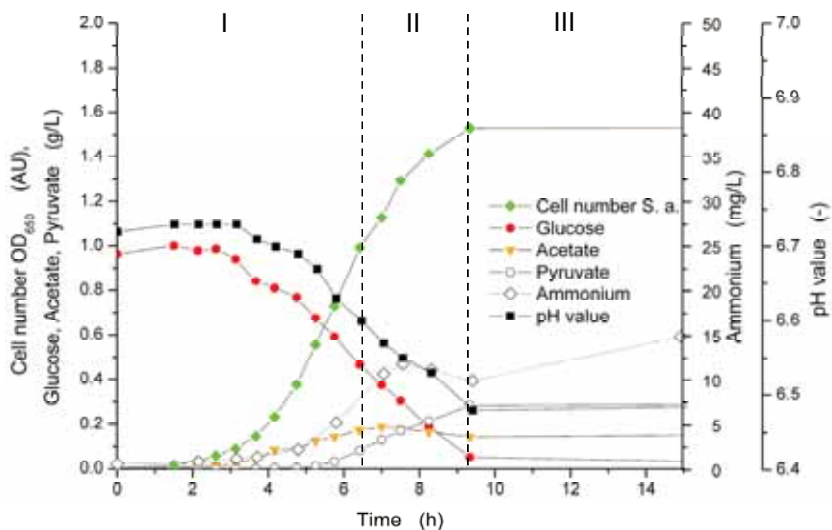


Figure 4.10: Growth of *S. a.* ATCC 29213 in shake flask cultivation. Three growth phases: (I) uptake of glucose and phase of exponential growth, (II) uptake of glucose and linear phase of growth, (III) stationary phase without depletion of glucose.

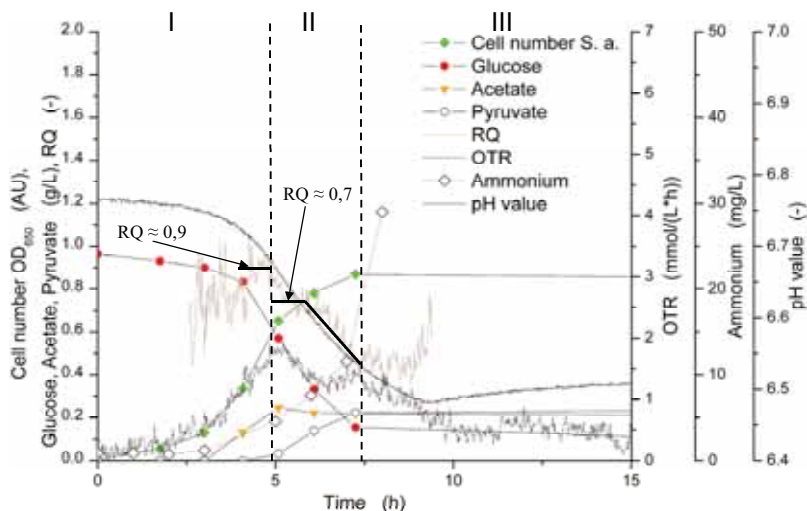


Figure 4.11: Batch growth characteristics of *S. a.* ATCC 29213 in a 2 L STR cultivation. Three growth phases: (I) uptake of glucose and phase of exponential growth, (II) uptake of glucose and linear phase of growth, (III) stationary phase without depletion of glucose.

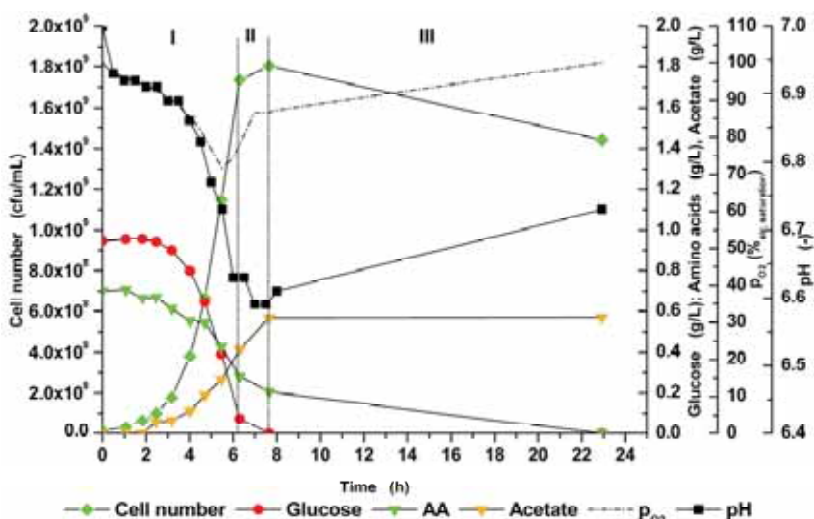


Figure 4.12: Growth of *S. a.* ATCC 29213 in small scale STR in M199+P+NTA. Three growth phases: (I) uptake of glucose until depletion of asparagine, glycine, valine, and serine, (II) uptake of glucose and amino acids, (III) uptake of amino acids after depletion of glucose.

The time courses of acetate and pyruvate formation corresponded with the OTR and RQ. Two peaks of the OTR of *S. a.* cultivation indicated two different physiological states (Figure 4.11, phase I and II) during glucose uptake. The first peak of OTR (1.94 mM/h at 5 h) correlated with the end of acetate formation. The formation of pyruvate started during the transition between exponential and stationary growth phase (4 to 7.5 h) and ended with the second OTR peak (1.52 mM/h at 7.3 h). After 10 h of cultivation the OTR value indicated a reduced metabolic activity (phase III) at a constantly low level of 0.4 mM/h. The overall O₂ uptake as calculated from OTR (3.4.4.1) was 12.5 mM O₂. As complete oxidation of 5.55 mM glucose would require stoichiometrically 16.65 mM O₂, this indicated formation of a less oxidized metabolic product by *S. a.* during growth on glucose. Due to technical problems in the off-gas tubing, the data were not monitored after 15 h. The RQ indicated two different metabolic activities during growth of *S. a.* on glucose correspondingly to the OTR. During the phase I the RQ was about 0.9, during phase II it decreased to 0.7 and afterwards it stayed at a level of about 0.4, when less O₂ was taken up. The low OTR in the final phase could not be explained and did not correlate with cell number formation of *S. a.*. However, in general such low RQ values (0.5) indicate the uptake of, for example amino acids.

Amino acids were taken up during glucose consumption and still after depletion of glucose until they were depleted (23 h) (Figure 4.12). The uptake of amino acids was expected due to auxotrophy of *S. a.* for amino acids [152]. Their uptake in the growth phase without increase in cell number correlated with an RQ of about 0.4 during stationary phase in the 2 L STR cultivation (Figure 4.11). The analysis of amino acids clearly showed the growth dependence of *S. a.* on specific amino acids, which is visualized in the division of the display into three phases I, II and III (Figure 4.12). At end of phase I, exponential growth phase, the amino acids asparagine, glycine, valine, and serine were depleted. In phase II no further cell formation took place, although several amino acids were still available.

4.3.1.2 Growth Dynamics of *B. cepacia*

The time courses of cultivations of *B. c.* in shake flask, 2L STR and small scale STR were comparable. Exponential growth was observed until depletion of glucose and growth continued after glucose depletion on second substrates up to the maximum cell number of 1.72 AU (Figure 4.13), 1.98 AU (Figure 4.14) and $3.2 \cdot 10^8$ cfu/mL (1.73 AU) (Figure 4.15). The second substrates for *B. c.* were not identified by HPLC analysis for sugars and organic acids (3.5.3). None of the analyzed organic acids (3.5.3) were detected during cultivation of *B. c.*: acetate, formate, fumarate, malate, propionate, pyruvate, succinate, and lactate.

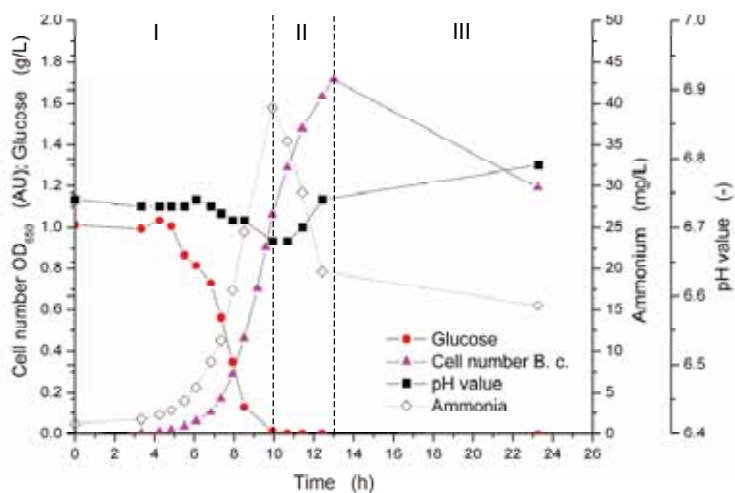


Figure 4.13: Growth of *B. c.* DSM 7288 in shake flask cultivation. Three growth phases: (I) growth up to depletion of glucose, (II) growth without glucose, (III) stationary phase.

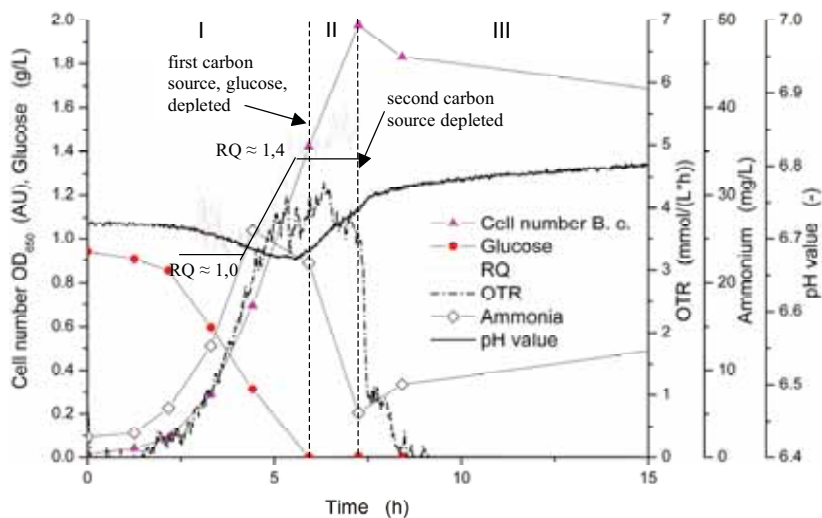


Figure 4.14: Batch growth characteristics of *B. c.* DSM 7288 in 2 L STR. Three growth phases: (I) growth up to depletion of glucose, (II) growth without glucose, (III) stationary phase.

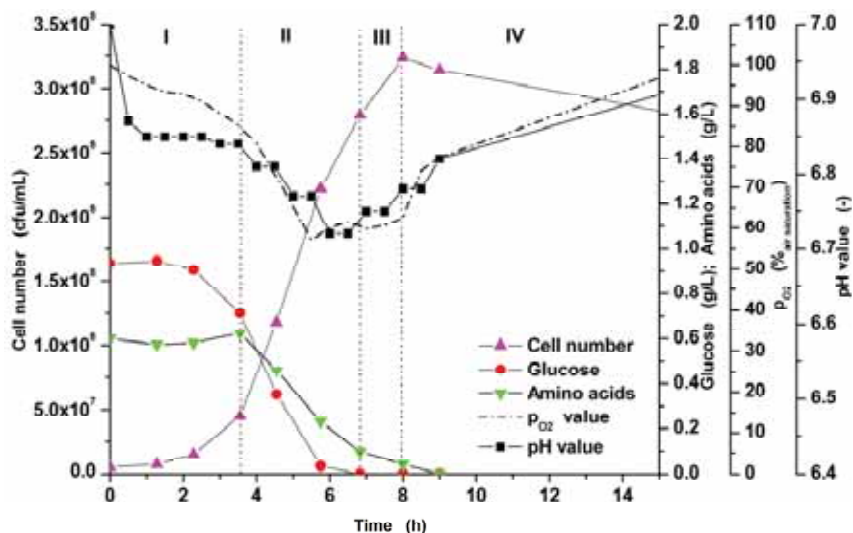


Figure 4.15: Growth of *B. c.* in small scale STR in M199+P+NTA. Four growth phases: (I) uptake of glucose, (II) uptake of glucose and amino acids, (III) uptake of amino acids after depletion of glucose, (IV) stationary phase (death).

In the *B. c.* culture the pH value decreased slightly from 6.75 to a minimum value of about 6.7 despite release of ammonia into the medium. Ammonia reached its maximum of 39.5 mg/L (Figure 4.13) at the same time point of glucose depletion (10 h).

During glucose consumption of *B. c.* the OTR reached a maximum of 4.2 mM/h. The O₂ uptake of 7 mM until depletion of 5.55 mM glucose was significantly less than stoichiometrically required (16.65 mM O₂). During further cell growth the OTR reached a second local maximum of 4.4 mM/h. The O₂ uptake until the end of growth (drop of OTR) was 14.8 mM altogether. The RQ time course of *B. c.* correlated with the consumption glucose (RQ = 1.0). In the second growth phase of *B. c.* the RQ changed to 1.4, which indicated a change of substrate releasing more carbon dioxide. Based on the O₂ consumption and the pH curve it was assumed this substrate was formed from glucose in the first growth phase and taken up again as carbon source in the second phase.

The curve of amino acids indicated their use as substrate. For the first 3.5 h no amino acids were taken up (I). Then, amino acids were taken up in parallel to glucose consumption (II) and further after the depletion of glucose, while cell formation still took place (III).

4.3.1.3 Growth Dynamics of *P. aeruginosa*

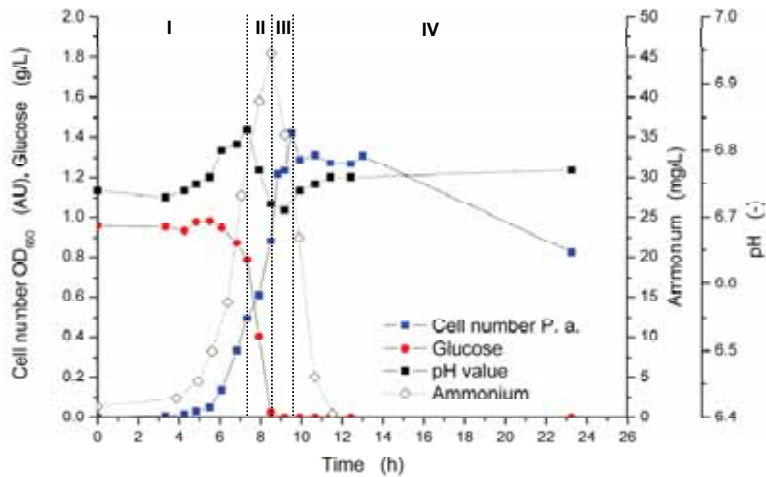


Figure 4.16: Growth of *P. a. PAO1* in shake flask cultivation. Four growth phases: (I) uptake of glucose, (II) strong uptake of glucose and decrease of pH value, (III) further increase of cell number after depletion of glucose, (IV) stationary phase.

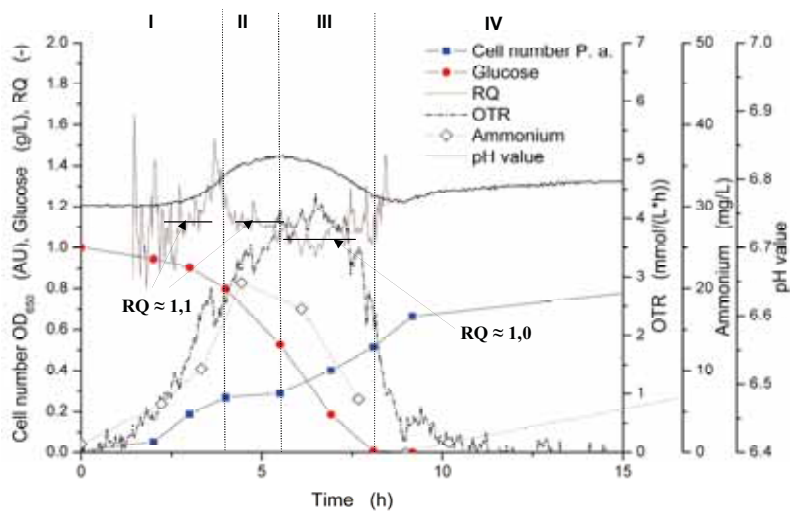


Figure 4.17: Batch growth of *P. a. PAO1* 2 L STR in 2 L STR. Four growth phases: (I) uptake of glucose (II) uptake of glucose and stagnation of cell number (III) further increase of cell number (IV) further increase after depletion of glucose.

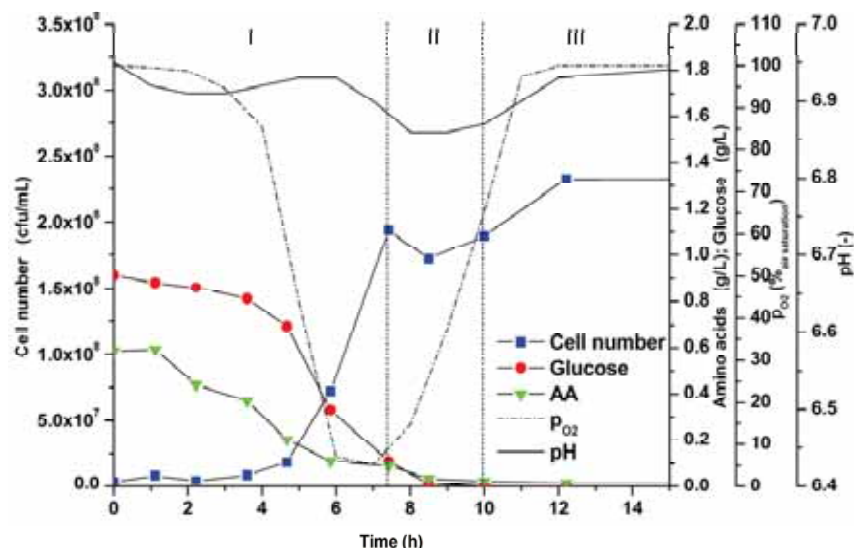


Figure 4.18: Growth of *P. a. PAO1* in small scale STR in M199+P+NTA. Three growth phases: (I) uptake of glucose and amino acids (II) uptake of glucose and amino acids and stagnation of cell number (III) further increase of cell number after depletion of amino acids and glucose.

Cultures of *P. a.* showed a significant biphasic growth (Figure 4.16, Figure 4.17, Figure 4.18), which was more prominent in the STR cultivations. After exponential growth cell formation stagnated when glucose concentration was low (0.2 g/L) (Figure 4.18, Phase II) followed by a second growth phase (Figure 4.18, Phase III). The maximum cell number, however, differed between shake flask (1.31 AU) (Figure 4.16), 2 L STR (0.94 AU) (23 h) (Figure 4.17) and small scale STR $2.3 \cdot 10^8$ cfu/mL (0.55 AU) (Figure 4.18). Comparably to *B. c.* growth of *P. a.* continued on other substrates after glucose depletion (Fig 17, 18). The second substrates for *P. a.* were not identified by HPLC analysis for sugars and organic acids (3.5.3). None of the analyzed organic acids (3.5.3) were detected during cultivation of *P. a.*: acetate, formate, fumarate, malate, propionate, pyruvate, succinate, lactate.

In *P. a.* cultures the pH value increased from 6.75 to a maximum value of app. 6.8 at the time point of maximum ammonia concentration (45.5 mg/L, Fig 16)) in the culture broth. Afterwards, the pH decrease correlated with strong glucose consumption. This indicated the formation of an acidic substance by *P. a.*. The pH value increased again after depletion of glucose, indicating an uptake of this acidic substance.

During glucose consumption (phase I) the OTR increased as expected and dropped at the transition to phase II indicating depletion of one substrate (Figure 4.17). The O_2 uptake during phase I was 2.7 mM. Further increase of OTR in phase II correlated with the continued glucose uptake, despite stagnation in cell formation. The O_2 uptake during phase II was 7.3 mM O_2 , what indicated the conversion of glucose into a metabolic product instead of biomass. The total O_2 uptake of *P. a.* was 20 mM. This could indicate the uptake of a second carbon and energy source from the medium apart from glucose by *P. a.*. The RQ correlated to the other cultivation data; during glucose consumption it was between 1.0 and 1.1. The p_{O_2} value reached its minimum of 5 % $_{air,sat.}$ at end of phase I before depletion of glucose and amino acids, what could be due to an unknown substrate used or metabolite formed by *P. a.*. This value was low in relation to the low cell number and glucose concentration (compare to *B. c.* and *S. a.*) and correlated to the OTR course (Figure 4.18). Surprisingly, the p_{O_2} increased already, while glucose and amino acids were still taken up, and also during the cell number stagnation phase, when the constant decrease of the two substrates continued.

The curve of amino acids indicated their use as a substrate. Amino acids were taken up parallel to glucose during the whole cultivation time.

4.3.1.4 Chemostat at Different Dilution Rates

Chemostat experiments at different dilution rates were conducted in small scale STR under standard conditions (3.4.5.3) for further characterization of growth of *S. a.*, *B. c.*, and *P. a.* by analysis of the resulting XD-curves and for the estimation of kinetic parameters for the mathematical analysis (3.6.3). The cultivation parameters cell number, glucose and amino acid concentrations, and pH value were determined during steady state for each dilution rate (Figure 4.19, Figure 4.20 and Figure 4.21). The cell number was determined as OD measurements (AU) (3.5.1) and converted into cfu/mL (3.5.2.3), and also with quantitative T-RFLP analysis (cfu/mL) (3.5.2). The values for $D = 0 \text{ h}^{-1}$ in the graphs are the values determined at the end of the batch phase, before the switch to continuous process mode.

After switch from batch to continuous process mode, the cell number of *S. a.* first decreased to about $1.2 \cdot 10^9$ cfu/mL (OD) or $4 \cdot 10^8$ cfu/mL (T-RFLP), respectively and then increased for dilution rates $D < 0.25 \text{ h}^{-1}$. The maximum value of $1.8 \cdot 10^9$ cfu/mL (OD) or $6 \cdot 10^8$ cfu/mL (T-RFLP), respectively, was reached for $0.25 \text{ h}^{-1} < D < 0.4 \text{ h}^{-1}$. The OD value correlated very well with the expected value based on the batch experiment (Figure 4.12) of $1.7 \cdot 10^9$ cfu/mL (OD). At higher dilution rates ($0.4 \text{ h}^{-1} < D < 0.5 \text{ h}^{-1}$) the cell number decreased, interrupted by a plateau phase at $D = 0.5$ to 0.6 h^{-1} . Washout was determined at $D_{crit} = 0.7 \text{ h}^{-1}$. The two

methods for cell number determination resulted in comparable time courses of X over D . However, the values determined by T-RFLP analysis were constantly lower than those calculated from OD measurements.

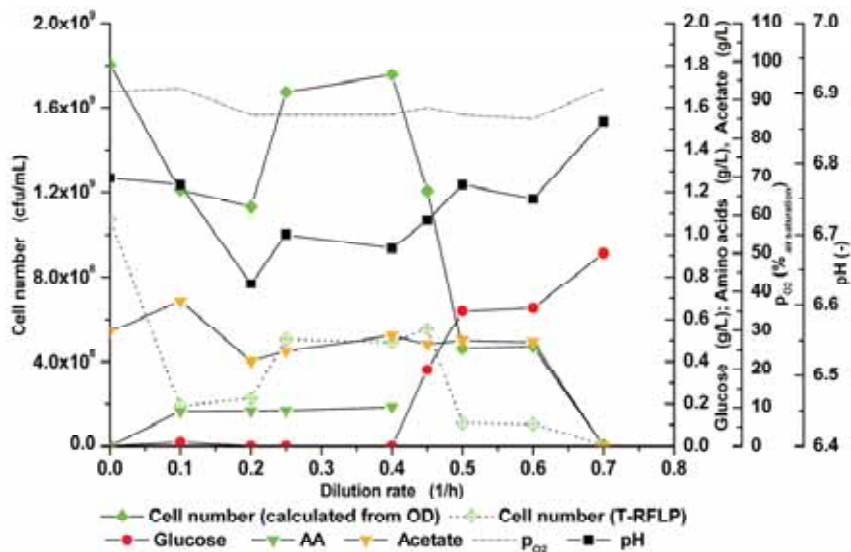


Figure 4.19: XD-diagram of *S. a.* ATCC 29213 growth in small scale STR. Values in quasi steady state for different dilution rates $D = (0.1; 0.2; 0.25; 0.4; 0.45; 0.5; 0.6; 0.7) \cdot (h^{-1})$. $D = 0 h^{-1}$ indicates values at the end of the batch phase.

The concentrations of glucose correlated to the cell numbers of *S. a.* For dilution rates below $0.45 h^{-1}$ glucose concentration did not increase significantly as expected for glucose as limiting substrate. For $D = 0.45 h^{-1}$ very abrupt one third of the fed glucose was not taken up any more. This was not expected for the assumption of glucose as limiting substrate.

For higher dilution rates some amino acids were taken up completely by *S. a.*, mainly glycine, serine, and valine. The overall amino acid concentration remained at about $0.2 g/L$ for all D up to $0.4 h^{-1}$. Unfortunately, no amino acids could be analyzed for $D > 0.4 h^{-1}$ due to technical problems the HPLC analysis device. At all dilution rates, except at the washout point D_{crit} , $0.5 g/L$ acetate was determined. This did not correlate with reduced cell numbers and glucose concentrations for the dilution rates $D = 0.45, 0.5$, and $0.6 h^{-1}$. The time course of the pO_2 of above $85 \%_{air,sat.}$ for all dilution rates indicated low O_2 uptake by *S. a.* and no O_2 limitation. The pH value did not show a significant dependence of the dilution rate.

After switch from batch to continuous process mode, the cell number of *B. c.* (Figure 4.20) increased for $D < 0.3 \text{ h}^{-1}$ to a maximum value of $3.2 \cdot 10^8 \text{ cfu/mL}$. This was comparable to $3.5 \cdot 10^8 \text{ cfu/mL}$ as expected from the cell yield in the batch experiment (Figure 4.15). At higher dilution rates ($0.7 \text{ h}^{-1} < D < 1.0 \text{ h}^{-1}$) the cell number of *B. c.* decreased to a plateau at about $1.7 \cdot 10^8 \text{ cfu/mL}$. At $D = 1.1$ and 1.2 h^{-1} the cell number remained nearly constant and dropped at the point of washout at about $D = 1.3 \text{ h}^{-1}$. The concentrations of glucose and amino acids in *B. c.* chemostat cultivations increased with higher values of D . This was expected from the Monod kinetic ($\mu = f(S)$) (2.2.1.1), which describes the increase of the limiting substrate S with increase of the specific growth rate (μ) for low substrate concentrations, when $\mu < \mu_{max}$. For *B. c.* the time course of the p_{O_2} correlated very well with the related cell numbers, except for the decrease between D of 0.3 and 0.7 h^{-1} , for which OD was constant. The pH value for *B. c.* did not show a significant dependence of the dilution rate (D), respective specific growth rate (μ). At the washout point the pH approached the value of the medium (7.6), as it was to be expected.

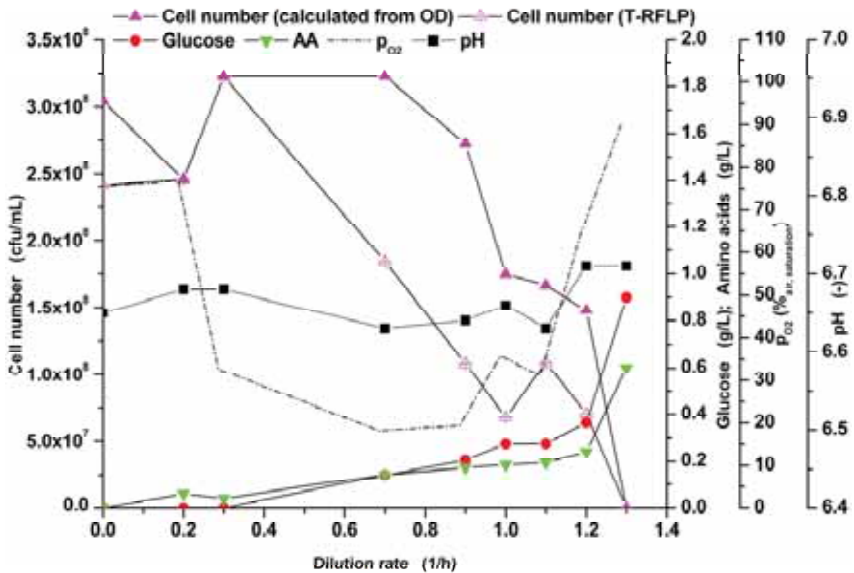


Figure 4.20: XD-diagram of *B. c.* chemostat growth in small scale STR. All values in quasi steady state for different dilution rates $D = (0.2; 0.3; 0.7; 0.9; 1.0; 1.1; 1.2; 1.3) \cdot (\text{h}^{-1})$. $D = 0 \text{ h}^{-1}$ indicates end of the batch phase.

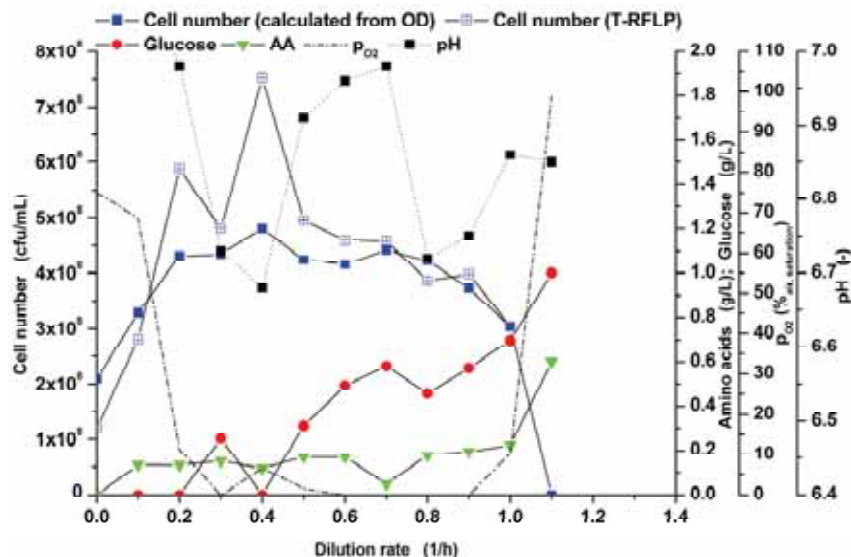


Figure 4.21: XD-diagram of *P. a.* chemostat growth in small scale STR. Values in quasi steady state for different dilution rates $D = (0.1; 0.2; 0.3; 0.4; 0.5; 0.6; 0.7; 0.8; 0.9; 1.0; 1.1) \cdot (\text{h}^{-1})$. $D = 0 \text{ h}^{-1}$ indicates end of the batch phase.

After switch from batch to continuous process mode, the cell number of *P. a.* (Figure 4.21) increased at small dilution rates ($D < 0.2 \text{ h}^{-1}$) to a maximum value of $4.3 \cdot 10^8 \text{ cfu/mL}$, which was double than expected from the batch experiment ($2.3 \cdot 10^8 \text{ cfu/mL}$) (Figure 4.18). The cell number of *P. a.* did not show a significant plateau, only at higher dilution rates the cell number decreased slightly ($0.8 \text{ h}^{-1} < D < 1.0 \text{ h}^{-1}$). The washout point was determined at about $D = 1.1 \text{ h}^{-1}$. The concentration of glucose in *P. a.* chemostat cultivations increased very much with increase of dilution rate. Already at a dilution rate $D = 0.7 \text{ h}^{-1}$ half of the fed glucose was not taken up any more. This was not expected, when considering the Monod kinetic ($\mu = f(S)$). At higher dilution rates some amino acids were not taken up, mainly isoleucine, glutamate, and aspartate. All other amino acids in M199+P+NTA medium were depleted at all dilution rates almost completely up to the washout point. This time course of p_{O_2} of *P. a.* did not correlate well with the cell numbers. This was probably due to the property of *P. a.* to decrease the mass transfer of O_2 at high O_2 supply [122], which led to a O_2 limitation of the *P. a.* cultivations at dilution rates $D > 0.3 \text{ h}^{-1}$. The low p_{O_2} could not be prevented by increased

aeration and stirring. The pH value showed an unstable behavior, which could possibly be related to the O₂ limitation at certain dilution rates.

For *B. c.* and *P. a.*, glucose at low dilution rates was below the amino acids and then increased more than the amino acid concentration. The similar increase of both substrates with increase of *D* indicated uptake of glucose and amino acids as mixed substrates. The higher concentration of glucose for higher dilution rates could mean glucose was not the limiting substrate then.

4.3.2 Experiments on Properties Potentially Relevant in Interactions

4.3.2.1 Uptake of Acetate

Acetate was found as metabolic product for *S. a.* and assumed to possibly lead to a commensalistic interaction in the mixed culture. By an enrichment of the medium M199+P+NTA with 1 g/L sodium acetate, it was tested, if *B. c.* or *P. a.* could take up acetate as additional carbon and energy source. Cultivations with acetate were performed in shake flask (data not shown) and small scale STR at standard conditions (3.4.5.2) for the two strains (Figure 4.22, Figure 4.23).

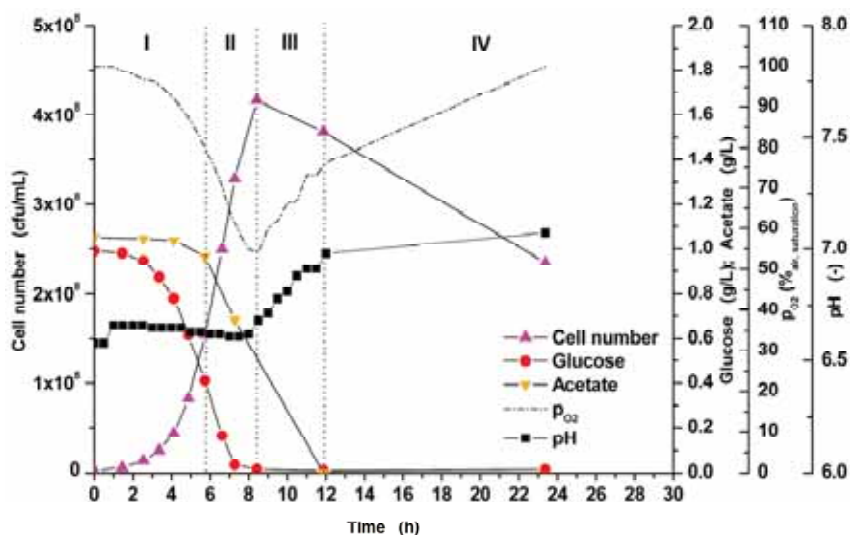


Figure 4.22: Growth of *B. c.* in M199+P+NTA medium supplemented with 1 g/L acetate in small scale STR. Four growth phases: (I) uptake of glucose, (II) uptake of glucose and acetate, (III) uptake of acetate and stagnation of cell number, (IV) stationary phase.

Acetate was completely taken up by *B. c.* and by *P. a.* during shake flask cultivations as well as in small scale STR. In the shake flask the increase in cell number of *B. c.* from acetate compared to growth without was 0.4 AU; in the small scale STR it was $0.92 \cdot 10^8$ cfu/mL (0.49 AU). For *B. c.* in both vessels a time-delay before start of acetate uptake occurred, *B. c.* depleted acetate after glucose.

In the shake flask the increase in cell number of *P. a.* compared to growth without acetate was 0.3 AU. Surprisingly, in the small scale STR experiment no increase in cell number of *P. a.* from acetate was observed. In comparison to the control without acetate ($2.3 \cdot 10^8$ cfu/mL (0.55 AU)) even less cells were formed ($1.7 \cdot 10^8$ cfu/mL). The uptake of acetate by *P. a.* was parallel to glucose; glucose and acetate were depleted at the same time point. Some further cells were formed by *P. a.* after acetate and glucose were depleted in shake flask and STR cultivations. However, in these experiments amino acids were not analyzed and it was not resolved, whether amino acids served as substrate together with acetate, as well.

It was concluded that *B. c.* and *P. a.* were able to use acetate as carbon- and energy source.

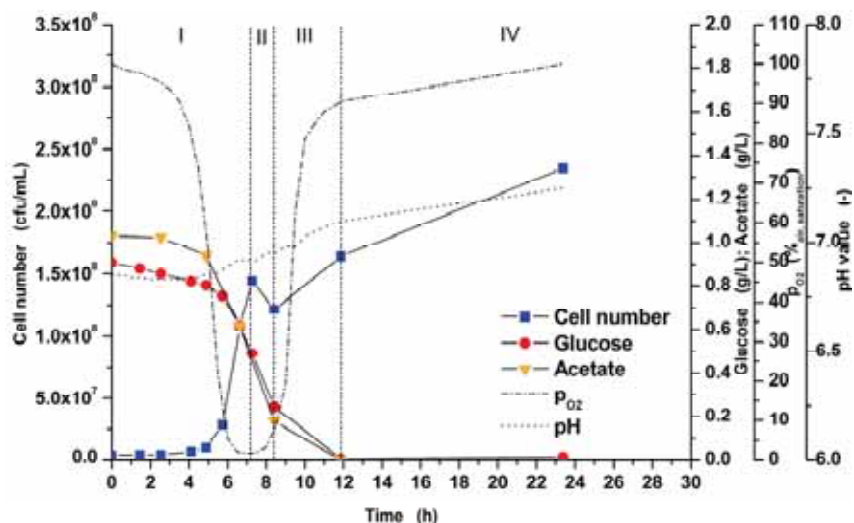


Figure 4.23: Growth of *P. a.* PAO1 in M199+P+NTA medium supplemented with 1 g/L acetate in small scale STR. Four growth phases: (I) uptake of glucose and acetate, (II) uptake of glucose and acetate and stagnation of cell number, (III) uptake of glucose and acetate up to depletion of both substrates, (IV) increase of cell number after depletion of glucose and acetate.

4.3.2.2 Influence of pH value

The organic acids acetate and pyruvate secreted by *S. a.* during its growth phase decreased the pH value in the cultivations. It was also found *S. a.* did not completely take up glucose during shake flask and 2 L STR cultivations. As a possible reason a pH effect on growth of *S. a.* was suspected. Additionally, the pH value could be affected by accumulation or depletion of acetate due to a possible acetate biotrophy in the mixed culture. Therefore, pH dependence of growth of *S. a.*, *B. c.* and of *P. a.* was investigated (Table 4.7). The adjustment of the pH value was performed with buffer solution to avoid possible molarity effects.

Table 4.7: Summary of shake flask cultures at different pH starting values 5.3, 6.5 and 7.0.

Results after exponential growth phase (h)	pH 5.3	pH 6.5	pH 7.0	Conclusion
<i>S. a.</i> (8 h)	1.2 AU, <i>Glc</i> left	1.8 AU, <i>Glc</i> depleted	1.8 AU, <i>Glc</i> depleted	Negative effect only at pH 5.3
<i>B. c.</i> (8 h)	1.6 AU, <i>Glc</i> depleted	2.1 AU*, <i>Glc</i> depleted	1.6 AU, <i>Glc</i> depleted	No significant effect
<i>P. a.</i> (9.5 h, 8 h, 7 h, respectively)	lag-phase 4.5 h 1.3 AU, <i>Glc</i> depleted	lag-phase 3.0 h, 1.5 AU, <i>Glc</i> depleted	lag-phase 2.2 h, 1.5 AU, <i>Glc</i> depleted	Negative effect only at pH 5.3

* this value was evaluated as outlier, as all other data was consistent for the three pH values

Except for the pH value of 5.3, which reduced growth of *S. a.* and *P. a.* compared to the other two pH values tested, no significant effect of the pH to the strains was found.

4.3.2.3 Functions of Glucose and Amino Acids as Growth Substrates

In the batch cultivations with M199+P+NTA amino acids were taken up by *S. a.*, *B. c.* and *P. a.*, respectively (Figure 4.12; Figure 4.15; Figure 4.18) (4.3.1). However, glucose was assumed as main and growth controlling substrate (2.2.1). Further growth experiments were conducted to elucidate the functions of the two substrates for the strains in more detail.

To obtain the required basis for estimation of the respective kinetic parameters growth only on amino acids was investigated with a customized M199 identical to standard M199, but without glucose. It was applied in batch cultivations in small scale STR (Figure 4.24, Figure 4.25 and Figure 4.26). After 22.75 h glucose was pulsed into each of the cultures (final concentration 1 g/L) to characterize growth only on glucose without amino acids.

Growth of *S. a.* only on amino acids had a first maximum cell number of $4.0 \cdot 10^8$ cfu/mL (0.35 AU) after 10 h cultivation and a second after 15 h as overall maximum value of $4.9 \cdot 10^8$ cfu/mL (0.42 AU). The decrease of amino acids correlated with the cell number

increase for the first 8 h. At the end of phase (I) the amino acids glycine, serine, valine, and proline were depleted and the amino acids were not taken up further during phase (II). The pulsed glucose was taken up completely, but the increase of cell number from $5 \cdot 10^8$ cfu/mL (0.44 AU) to $6 \cdot 10^8$ cfu/mL (0.53 AU) was insignificant. The amino acids still present were not taken up in combination with glucose (III). Summing up, the cell numbers formed from growth on amino acids (I) and on glucose (III) were $6 \cdot 10^8$ cfu/mL. This was lower than the cell number of *S. a.* in standard M199+P+NTA medium ($1.8 \cdot 10^9$ cfu/mL) (Figure 4.12). The cell number formed only on amino acids (0.42 AU per 0.8 g/L amino acids) was about the same as in the pulse experiment before (0.5 AU per 1 g/L amino acids) (data not shown). The results for medium without glucose confirmed that *S. a.* was capable to grow on amino acids. However, growth on glucose in presence of all necessary amino acid (Figure 4.12) was more effective and tripled the cell yield compared to the consecutive use of amino acids and glucose. The amino acids were assumed to be required for growth on glucose. This result was expected as the auxotrophy of *S. a.* for amino acids is well known from literature.

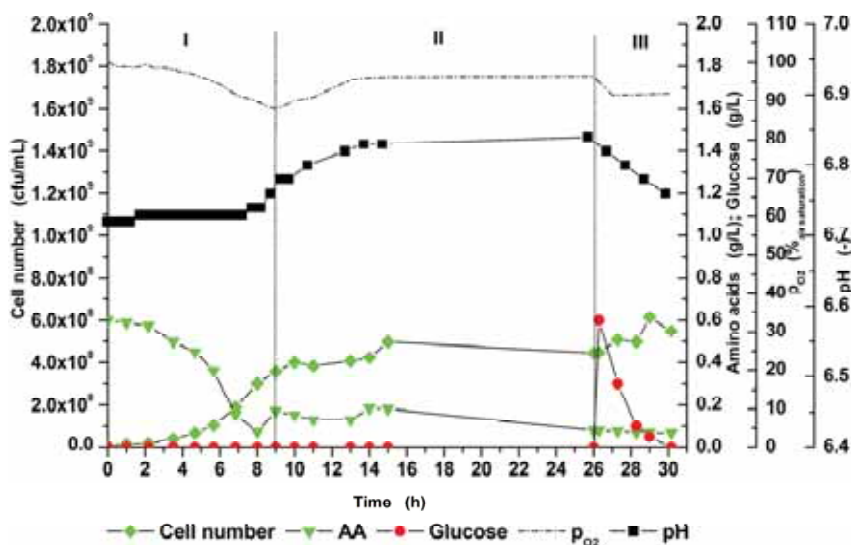


Figure 4.24: Batch cultivation of *S. a.* in M199+P+NTA in small scale STR without glucose: (I) growth on amino acids, (II) stationary phase without depletion of all amino acids, (III) afterwards a glucose pulse was set.

B. c. reached $1.8 \cdot 10^8$ cfu/mL (0.97 AU), and *P. a.* $1.6 \cdot 10^8$ cfu/mL (0.38 AU) from growth on amino acids (I). The decrease of amino acids correlated with increase of cell number and ended with the depletion of amino acids after 7.3 h (*B.c.*), 7.5 h (*P.a.*). The time course of p_{O_2} signal during growth of *B. c.* on amino acids was not bi-phasic as in standard M199+P+NTA medium (Figure 4.25). This could indicate diauxic growth on glucose and amino acids under standard conditions.

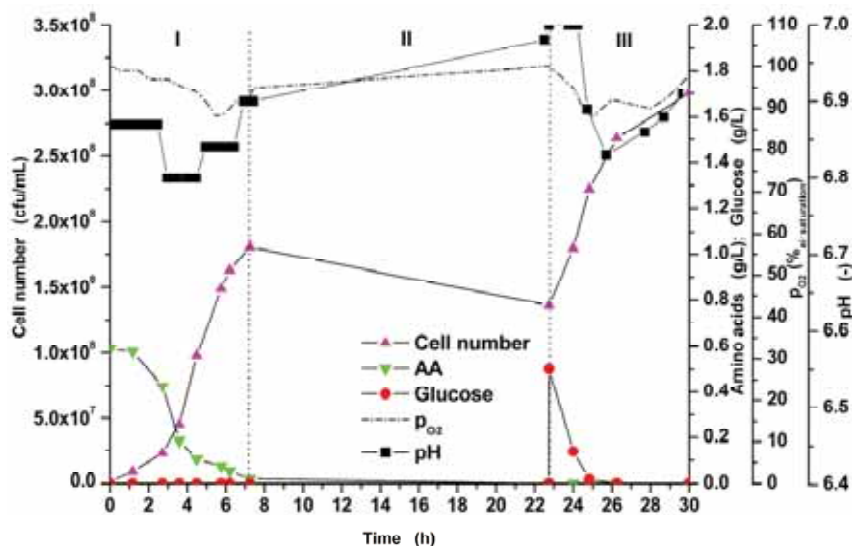


Figure 4.25: Growth of *B. c.* in custom M199+P+NTA without glucose in small scale STR: (I) growth on amino acids, (II) stationary phase, (III) afterwards a glucose pulse was set.

After the glucose pulse (II) the cell number of *B. c.* increased from $1.4 \cdot 10^8$ cfu/mL (0.76 AU) to $2.8 \cdot 10^8$ cfu/mL (1.51 AU), that of *P. a.* from $1.3 \cdot 10^8$ cfu/mL (0.31 AU) to $3.45 \cdot 10^8$ cfu/mL (0.83 AU). The result indicated for the two strains, the amino acids in standard medium were not required for growth on glucose.

The cell numbers of *B. c.* formed from amino acids (I) and glucose (III) in sum were $3.2 \cdot 10^8$ cfu/mL, comparable to the cell number of *B. c.* in standard M199+P+NTA (Figure 4.15). The cell numbers of *P. a.* formed from amino acids (I) and glucose (II) were in sum $3.45 \cdot 10^8$ cfu/mL (0.83 AU), which was about 50 % more than the cell number formed during the growth of *P. a.* in standard M199+P+NTA ($2.3 \cdot 10^8$ cfu/mL) (Figure 4.18). In summary, it was shown *B. c.* and *P. a.* grow on both substrates, amino acids and glucose, as independent

carbon and energy sources and that these two substrates contributed mainly to its cell number formation under standard cultivation conditions.

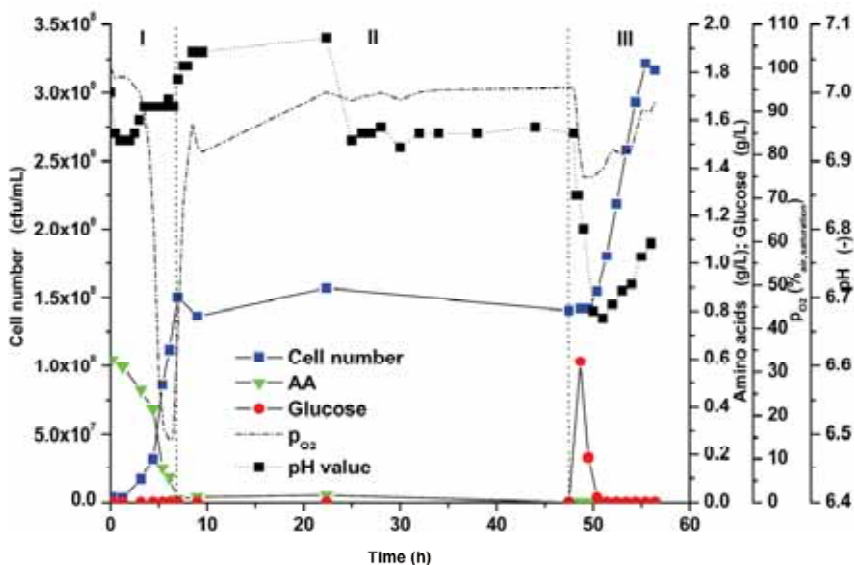


Figure 4.26: Growth of *P. a.* in custom M199+P+NTA without glucose in small scale STR: (I) growth on amino acids, (II) stationary phase, (III) afterwards a glucose pulse was set.

4.3.3 Summary of the Experimental Results of Single-Species Characteristics

An overview on the main experimental results from the single-species experiments is given in Table 4.8 for the cultivations under different conditions and in Table 4.9 for the investigations on special physiological properties. For *B. c.* the results indicated the formation of a metabolic product from glucose that was taken up again after depletion of glucose. For *P. a.* the results indicated an uptake of a substrate as carbon source additional to glucose.

Table 4.8: Summary of cultivation results under different process conditions for single-species experiments (4.3.1)

Cultivation experiment	<i>S. a.</i>	<i>B. c.</i>	<i>P. a.</i>
Shake flask	1.53 AU at glucose depletion after 10 h	0.91 AU at glucose depletion after 10 h 1.72 AU after 13 h	0.77 AU at glucose depletion after 8.5 h 1.31 AU after 9.5 h
	pH decrease	Slight pH decrease, increase after glucose depletion	Slight pH increase then pH decrease and increase after glucose depletion
	Pyruvate max. 0.2 g/L acetate max. 0.18 g/L	No acid identified	No acid identified
2 L STR	0.89 AU after 7.5 h with incomplete glucose uptake pH decrease	1.42 AU at glucose depletion after 5.9 h 1.98 AU after 7.5 h Slight pH decrease	0.51 AU at glucose depletion after 8 h 0.94 after 23 h Slight pH increase
	12.5 mM O ₂ uptake	7 mM O ₂ uptake sum 14.8 mM O ₂ uptake	2.7 mM O ₂ uptake (cells) 7.3 mM O ₂ uptake (no cells) sum 20 mM O ₂ uptake
	0.25 g/L acetate RQ 0.9 and 0.7 (two phases), then 0.4	No acid identified RQ 1.0 then 1.4	No acid identified RQ 1.1, shortly 1.4
Small scale STR	1.58 AU at glucose depletion after 7.7 h	1.24 AU at glucose depletion after 7 h 1.73 AU after 8 h	0.48 AU at glucose depletion after 6.6 h 0.55 AU after 12.2 h
	pH decrease	slight pH decrease	biphasic pH
	AA uptake with glucose and after depletion of glucose	AA uptake (1) no, (2) with glucose, (3) without glucose	AA uptake during complete growth phase, with and without glucose
Chemostat (XD graph)	0.5 g/L acetate Washout $D = 0.7 \text{ h}^{-1}$	No acid identified Washout $D = 1.3 \text{ h}^{-1}$	No acid identified Washout $D = 1.1 \text{ h}^{-1}$
	Cells $\sim 6 \cdot 10^8$ cfu/mL, similar to batch yield	Cells $\sim 3.2 \cdot 10^8$ cfu/mL, less than batch yield	Cells $\sim 4.3 \cdot 10^8$ cfu/mL, more than batch yield
	Glc increase for $D > 0.4 \text{ h}^{-1}$, correlated to decrease of cells	Glc and AA increase with D	Glc and AA increase strongly with D
	$AA > Glc$	$Glc > AA$ at low D $Glc < AA$ at high D	$Glc > AA$ at low D $Glc < AA$ at high D
	Acetate $\sim 0.5 \text{ g/L}$	No acid identified	No acid identified
	Plateau at D 0.25 to 0.4 h^{-1} and lower plateau 0.5 to 0.6 h^{-1}	Plateau at D 0.3 to 0.7 h^{-1} and lower plateau 1.0 to 1.2 h^{-1}	Plateau at D 0.2 to 0.9 h^{-1}

Table 4.9: Summary of cultivation experiment results for investigation of specific physiological properties of single-species (4.3.2)

Experiment on physiology	<i>S. a.</i>	<i>B. c.</i>	<i>P. a.</i>
Acetate as carbon source	-	0.2 g/L acetate : no observable cell increase	0.2 g/L acetate : no observable cell increase
		1.0 g/L acetate : uptake with time-delay in parallel with <i>Glc</i>	1.0 g/L uptake in parallel with <i>Glc</i>
		$\Delta AU = 0.4$ shake flask	$\Delta AU = 0.3$ shake flask
		$\Delta AU = 0.49$ STR	$\Delta AU < 0$ STR
pH influence	At constant osmolarity : pH 5.27 decreased cell yield, pH 6.54 and 7.02 o.k.	No significant influence	At constant osmolarity : increase of lag-phase with decrease of pH pH 5.27 decreased cell yield
Use of amino acids (glucose-free medium)	0.35 AU cell yield on <i>AA</i> , not depleted	0.97 AU cell yield on <i>AA</i> , depleted (7.25 h)	0.38 AU cell yield on <i>AA</i> , depleted (7.5 h) <i>Glc</i> pulse : uptake, but no cell formation
	<i>Glc</i> pulse end of stat. phase: uptake, but no cell formation	<i>Glc</i> pulse end of stat. phase: quick uptake and pH decrease, then pH increase and cell formation	<i>Glc</i> pulse end of stat. phase: quick uptake and pH decrease, then pH increase and cell formation
Influence of aeration	Aeration rate increase : decrease of cell yield, increase of by-product formation	-	Aeration rate increase : decrease of cell yield
	Influence of aeration mode (surface/submerge)		Bad reproducibility in STR : influence of level of O_2 limitation (shown in shake flask)

4.3.4 Single-Species Mathematical Models

In the following mathematical models for the description of experimentally determined growth of *S. a.*, *B. c.* and, *P. a.* will be presented. Different assumptions were considered and for these pure culture models the model parameters were determined (3.6.3). The focus of the model formulations were acetate biotrophy and growth on glucose and amino acids as a mixed substrate. The potential uptake of a metabolic product by *B. c.*, and of a medium component apart from glucose by *P. a.* were not taken into account as no quantitative data were available. The results of fits of growth in shake flasks and 2 L STR were not used for mixed culture simulations, as data were influenced by scale-up effects, and will therefore not be presented.

4.3.4.1 Growth on One Substrate: Glucose

The most basic assumption was formulated for growth of *S. a.*, *B. c.*, and *P. a.* in M199+P+NTA medium (eqn. sys. 4.1) on one substrate, namely glucose, based on eqn. 2.14 and eqn. 2.15. The results of the fits for growth of *S. a.*, *B. c.* and *P. a.* in small scale STR (Figure 4.12, Figure 4.15, Figure 4.18, respectively) are given in Table 4.10. The resulting growth rate is denoted by $\mu_{max,199,i}$ to indicate it was determined for growth in this medium.

eqn. sys. 4.1

$$\frac{dX}{dt} = \frac{\mu_{max,199,i} \cdot Glc}{K_{S,i} + Glc} \cdot X$$

$$\frac{dGlc}{dt} = -\frac{1}{Y_{X/Glc,i}} \cdot \frac{\mu_{max,199,i} \cdot Glc}{(K_{S,i} + Glc)} \cdot X$$

In this model formulation the continued cell formation as observed for *B. c.* and *P. a.* after depletion of glucose could not be represented, as no second substrate was considered.

The property of *S. a.* to produce acetate as metabolic product was shown experimentally (4.3.1). The respective model was formulated by extension of the model for growth on glucose as one substrate (eqn. sys. 4.1) by acetate as a growth related product (eqn. 2.16) with the parameter $Y_{Ace/X,Sa}$ as β and α set to zero (eqn. syst. 4.2). Pyruvate was not considered for model formulation to keep the first models as simple as possible.

The parameters were determined for small scale STR cultivation (4.3.1). Two strategies for parameter estimation were performed: at the beginning, all values were determined by optimization, which did not result in biological meaningful values for $\mu_{max,199,Sa}$ and $K_{S,Sa}$.

Therefore, the parameters for growth on glucose as determined before were kept as constraints and the resulting values of acetate yield $Y_{Ace/X,Sa}$ are given (Table 4.10).

eqn. syst. 4.2

$$\frac{dX}{dt} = \frac{\mu_{\max,199,Sa} \cdot Glc}{K_{S,Sa} + Glc} \cdot X$$

$$\frac{dGlc}{dt} = -\frac{1}{Y_{X/Glc,i}} \cdot \frac{\mu_{\max,199,Sa} \cdot Glc}{K_{S,Sa} + Glc} \cdot X$$

$$\frac{dAce}{dt} = Y_{Ace/X,Sa} \cdot \frac{\mu_{\max,199,Sa} \cdot Glc}{K_{S,Sa} + Glc} \cdot X$$

Table 4.10: Kinetic and stoichiometric parameters for growth of *S. a.*, *B. c.*, and *P. a.* on glucose in small scale STR (eqn. sys. 4.1) and acetate production of *S. a.* (eqn. syst. 4.2).

	Unit	<i>S. a.</i>	<i>B. c.</i>	<i>P. a.</i>
$\mu_{\max,199,i}$	h^{-1}	0.83	0.66	0.42
$Y_{X/Glc,i}^*$	AU/(g/L)	1.67	1.45	0.48
$K_{S,i}$	g/L	0.12	0.05	0.07
$Y_{Ace/X,Sa}^{**}$	(g/L)/AU	0.24		

* at the time point of glucose depletion

** for determination of $Y_{Ace/X,Sa}$ the values of $\mu_{\max,199,Sa}$, $\mu_{\max,199,Sa} K_{S,Sa}$ were constraints

eqn. 4.3

$$Y_{Ace/X,Sa} = \frac{\Delta Ace}{\Delta X} = \frac{0.5 \text{ g/L}}{1.803 \cdot 10^{11} \text{ cfu/L}} = 2.77 \cdot 10^{-12} \text{ g/L} / \text{cfu/L} = 3.13 \text{ g/L} / \text{AU}$$

In addition, the yield coefficient of acetate by cell number $Y_{Ace/X,Sa}$ was calculated directly (eqn. 4.3). The value was calculated based on T-RFLP analysis results (cfu/mL). This result was evaluated as the most realistic one and kept in the following.

4.3.4.2 Growth on Two Substrates: Glucose and Acetate

B. c. and of *P. a.* were shown experimentally to grow with glucose and acetate as substrates in shake flasks (data not shown) and small scale STR (Figure 4.22, Figure 4.23).

The respective models for *B. c.* and *P. a.* were formulated by extension of the model for growth on glucose as one substrate (eqn. sys. 4.1) by the assumption of acetate as independent substrate in addition to glucose according to eqn. 2.7 (eqn. syst. 4.4). For parameter estimations lag- and stationary phases were omitted. The growth rates $\mu_{\max,Glc,i}$ and $\mu_{\max,Ace,i}$

together with the affinity constants $K_{S,Glc,i}$ and $K_{S,Ace,i}$ and yields $Y_{X/Glc,i}$ and $Y_{X/Ace,i}$ denote the parameters for independent growth on the two substrates glucose and acetate.

eqn. syst. 4.4

$$\frac{dX}{dt} = \frac{\mu_{\max,Glc,i} \cdot Glc}{K_{S,Glc,i} + Glc} \cdot X + \frac{\mu_{\max,Ace,i} \cdot Ace}{K_{S,Ace,i} + Ace} \cdot X$$

$$\frac{dGlc}{dt} = -\frac{1}{Y_{X/Glc,i}} \cdot \frac{\mu_{\max,Glc,i} \cdot Glc}{K_{S,Glc,i} + Glc} \cdot X$$

$$\frac{dAce}{dt} = -\frac{1}{Y_{X/Ace,i}} \cdot \frac{\mu_{\max,Ace,i} \cdot Ace}{K_{S,Ace,i} + Ace} \cdot X$$

Table 4.11: Parameters for growth of *B. c.* on glucose and acetate (eqn. syst. 4.4)*

	Unit	<i>B. c.</i>		
$\mu_{\max,Glc,Bc}$	h ⁻¹	0.46	0.66	0.66
$\mu_{\max,Ace,Bc}$	h ⁻¹	0.28	0.036	0.036
$K_{S,Glc,Bc}$	g/L	0.07	0.05	0.05
$Y_{X/Glc,Bc}$	AU/(g/L)	1.14	1.45	1.45
$K_{S,Ace,Bc}$	g/L	0.81	0.67	0.67
$Y_{X/Ace,Bc}$	AU/(g/L)	1.78	0.86	0.49

* The parameters that were free for optimization are printed in **bold**.

Table 4.12: Parameters for growth of *P. a.* on glucose and acetate (eqn. syst. 4.4)*

	Unit	<i>P. a.</i>			
$\mu_{\max,Glc,Pa}$	h ⁻¹	0.13	0.42	0.42	0.42
$\mu_{\max,Ace,Pa}$	h ⁻¹	1.09	11.3	8.9E+04	0.34
$K_{S,Glc,Pa}$	g/L	1.10	0.066	0.066	0.066
$Y_{X/Glc,Pa}$	AU/(g/L)	0.04	0.48	0.48	0.26
$K_{S,Ace,Pa}$	g/L	0.27	21.03	1.6E+05	0.22
$Y_{X/Ace,Pa}$	AU/(g/L)	0.43	0.21	0.3	0.11

* Parameters that were free for optimization are printed in **bold**.

The parameters for *B. c.* (Table 4.11) and *P. a.* (Table 4.12) were determined from data of the small scale STR cultivation (Figure 4.22 and Figure 4.23, respectively).

Values determined by optimization of all parameters are given in the first column. Values determined for the acetate growth kinetic with the other parameters as constraints (Table 4.10) are given in the second column. Values for the same parameters as constraints, but the yield

of cells from acetate $Y_{X/Ace,Bc}$ and $Y_{X/Ace,Pa}$, respectively, calculated directly are given in the third column. However, for *P. a.* the resulting values did not appear to be biologically meaningful. Therefore, the yield coefficient on glucose and the one on acetate were set as free variables; the resulting values are given in the fourth column.

4.3.4.3 Growth on One Substrate: Amino Acids

To investigate growth characteristics of *S. a.*, *B. c.* and *P. a.* on amino acids without glucose as carbon and energy source a cultivation experiment on glucose free M199+P+NTA medium was conducted (Figure 4.24, Figure 4.25 and Figure 4.26). The models for growth on amino acids were formulated in line with eqn. sys. 4.1 with the sum of amino acids as single substrate instead of glucose (eqn. syst. 4.5). The respective kinetic parameters of the Monod kinetic only on amino acids are denoted by $\mu_{max,AA,i}$ and $K_{S,AA,i}$ according to eqn. 2.14 and eqn. 2.15. No acetate formation was considered for *S. a.* during growth only on amino acids.

eqn. syst. 4.5

$$\frac{dX}{dt} = \frac{\mu_{max,AA,i} \cdot AA}{K_{S,AA,i} + AA} \cdot X$$

$$\frac{dAA}{dt} = -\frac{1}{Y_{X/AA,i}} \cdot \frac{\mu_{max,AA,i} \cdot AA}{(K_{S,AA,i} + AA)} \cdot X$$

The parameters for growth of *S. a.*, *B. c.* and *P. a.* on amino acids were determined independently as described in 3.6.3 based on experimental data (Figure 4.24, Figure 4.25, Figure 4.26). The direct calculation of the yield coefficients $Y_{X/AA,Sa}$, $Y_{X/AA,Bc}$, and $Y_{X/AA,Pa}$ is given in eqn. 4.6, eqn. 4.7, and eqn. 4.8., respectively. All resulting parameter values are given in Table 4.13.

eqn. 4.6

$$Y_{X/AA,Sa} = \frac{\Delta X}{\Delta AA} = \frac{(4 \cdot 10^{11} - 5.65 \cdot 10^9) \text{ cfu/L}}{(0.6 - 0.073) \text{ g/L}} = 7.48 \cdot 10^{11} \text{ cfu/g}$$

eqn. 4.7

$$Y_{X/AA,Bc} = \frac{\Delta X}{\Delta AA} = \frac{1.8 \cdot 10^{11} \text{ cfu/L} - 1.48 \cdot 10^9 \text{ cfu/L}}{0.6 \text{ g/L}} = 2.98 \cdot 10^{11} \text{ cfu/g}$$

eqn. 4.8

$$Y_{X/AA,Pa} = \frac{\Delta X}{\Delta AA} = \frac{1.57 \cdot 10^{11} \text{ cfu/L} - 3.74 \cdot 10^9 \text{ cfu/L}}{0.6 \text{ g/L}} = 2.55 \cdot 10^{11} \text{ cfu/g}$$

Table 4.13: Kinetic parameters for the growth of *S. a.*, *B. c.* and *P. a.* only on amino acids without glucose (eqn. syst. 4.5 and eqn. 4.6, eqn. 4.7, and eqn. 4.8..

	Unit	<i>S. a.</i>	<i>B. c.</i>	<i>P. a.</i>
$\mu_{max,AA,i}$	h^{-1}	0.5	0.67	0.67
$K_{S,AA,i}$	g/L	0.034	0.056	0.035
$Y_{X/AA,i}$	cfu/g	$7.48 \cdot 10^{11}$	$2.98 \cdot 10^{11}$	$2.55 \cdot 10^{11}$

4.3.4.4 Growth on Two Substrates: Glucose and Amino Acids

For a mathematical description of the experimentally found dependence of *S. a.* growth on glucose and amino acids at the same time (4.3.2.3), the multiplicative formulation (eqn. 2.6) was chosen for the model (eqn. syst. 4.9). This auxotrophy of *S. a.* for certain amino acids has also been reported in literature [152]. An additive formulation for the assumption of glucose and amino acids as independent substrates was applied and tested for the model of *S. a.* as well, but as expected did not yield the possibility to describe the experimental data.

eqn. syst. 4.9

$$\begin{aligned} \frac{dX}{dt} &= \mu_{max,199,Sa} \cdot \left(\frac{Glc}{Glc + K_{S,Glc,Sa}} \cdot \frac{AA}{AA + K_{S,AA,Sa}} \right) \cdot X \\ \frac{dGlc}{dt} &= -\frac{1}{Y_{X/Glc,Sa}} \cdot \mu_{max,199,Sa} \cdot \left(\frac{Glc}{Glc + K_{S,Glc,Sa}} \cdot \frac{AA}{AA + K_{S,AA,Sa}} \right) \cdot X \\ \frac{dAA}{dt} &= -\frac{1}{Y_{X/AA,Sa}} \cdot \mu_{max,199,Sa} \cdot \left(\frac{Glc}{Glc + K_{S,Glc,Sa}} \cdot \frac{AA}{AA + K_{S,AA,Sa}} \right) \cdot X \\ \frac{dAce}{dt} &= Y_{Ace/X,Sa} \cdot \frac{\mu_{max,199,Sa} \cdot Glc}{K_{S,Sa} + Glc} \cdot X \end{aligned}$$

The value for maximum specific growth rate in M199+P+NTA ($\mu_{max,199,Sa}$) was applied and set as constraint for the parameter estimations. The maximum specific growth rate determined for growth only on amino acids ($\mu_{max,AA,Sa}$) was not implemented into the model or simulation, because based on the experimental result for *S. a.* the use of amino acids together with glucose and without glucose was not assumed to be similar (4.3.2.3). As starting point of model development the growth of *S. a.* in M199+P+NTA (amino acids and glucose) and the growth only on amino acids were not required to be described by one mathematical model. The focus was set on the main differences between the species: the independent use of

glucose and the sum of amino acids by *B. c.* and *P. a.* on the one hand, and the dependent use of glucose and the sum of amino acids of *S. a.* on the other hand.

Table 4.14: Parameters for dependent growth of *S. a.* on glucose and amino acids (eqn. syst. 4.9). $\mu_{max,199,Sa} = 0.83 \text{ h}^{-1}$ and $Y_{Ace/X,Sa} = 2.77 \cdot 10^{-12} \text{ g/cfu}$ were set as constraints.

$K_{S,Glc,Sa}$	$K_{S,AA,Sa}$	$Y_{X/AA,Sa}$	$Y_{X/Glc,Sa}$
0.013 g/L	0.011 g/L	$3.56 \cdot 10^{12} \text{ cfu/g}$	$1.75 \cdot 10^{12} \text{ cfu/g}$

The simulation of eqn. syst. 4.9 in comparison to the experimental data for a batch cultivation of *S. a.* in M199+P+NTA medium is given in Figure 4.27. The model simulation represents the experimental data well, with an SES value of 0.1.

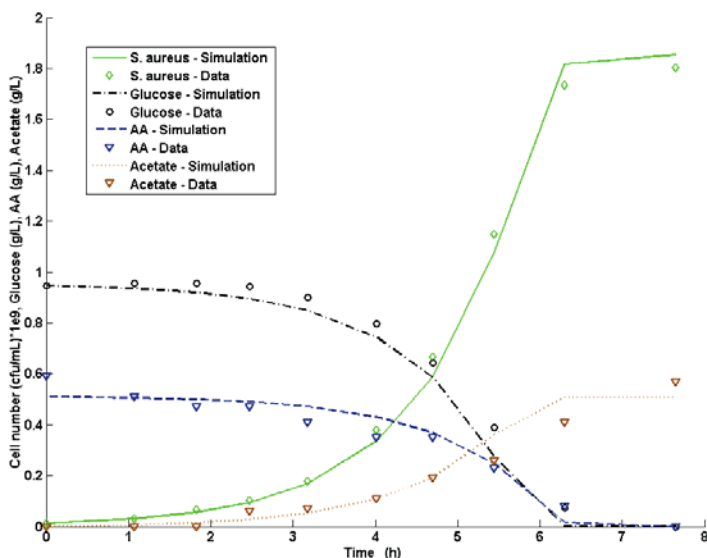


Figure 4.27: Growth of *S. a.* in M199+P+NTA: experimental data and simulation based on eqn. syst. 4.9 and parameters in Table 4.14. SES = 0.1

To characterize *S. a.* growth under chemostat conditions and improve the determination of K_S values, eqn. syst. 4.9 was extended to describe the continuous process mode (eqn. syst. 4.10). For parameter estimation the parameters were determined by an optimized fit to the chemostat experiment with varied dilution rate (XD-graph) (Figure 4.19). The values of the dependent variables at $D = 0 \text{ h}^{-1}$ represent the state at the switch between batch and continuous mode and were not considered for parameter estimation.

The simulation of eqn. syst. 4.10 in comparison to the data for the chemostat experiment with varied dilution rates of *S. a.* in M199+P+NTA medium is given in Figure 4.28.

eqn. syst. 4.10

$$\begin{aligned}\frac{dX}{dt} &= \mu_{\max,199,Sa} \cdot \left(\frac{Glc}{Glc + K_{S,Glc,Sa}} \cdot \frac{AA}{AA + K_{S,AA,Sa}} \right) \cdot X - D \cdot X \\ \frac{dGlc}{dt} &= -\frac{1}{Y_{X/Glc,Sa}} \cdot \mu_{\max,199,Sa} \cdot \left(\frac{Glc}{Glc + K_{S,Glc,Sa}} \cdot \frac{AA}{AA + K_{S,AA,Sa}} \right) \cdot X + D \cdot (Glc_{in} - Glc) \\ \frac{dAA}{dt} &= -\frac{1}{Y_{X/AA,Sa}} \cdot \mu_{\max,199,Sa} \cdot \left(\frac{Glc}{Glc + K_{S,Glc,Sa}} \cdot \frac{AA}{AA + K_{S,AA,Sa}} \right) \cdot X + D \cdot (AA_m - AA) \\ \frac{dAce}{dt} &= Y_{Ace/X,Sa} \cdot \frac{\mu_{\max,199,Sa} \cdot Glc}{K_{S,Sa} + Glc} \cdot X - D \cdot Ace\end{aligned}$$

Table 4.15: Parameters for growth of *S. a.* on glucose and amino acids (eqn. syst. 4.10) for data of chemostat with varied D . $\mu_{\max,199,Sa} = 0.83 \text{ h}^{-1}$ and $Y_{Ace/X,Sa} = 2.77 \cdot 10^{-12} \text{ g/cfu}$ were set as constraints.

$K_{S,Glc,Sa}$	$K_{S,AA,Sa}$	$Y_{X/AA,Sa}$	$Y_{X/Glc,Sa}$
0.006 g/L	0.11 g/L	$6.24 \cdot 10^{12}$ cfu/g	$1.43 \cdot 10^{12}$ cfu/g

The simulation differs from the experimental data in the range of low dilution rates (Figure 4.28). Especially the data of the amino acids do not coincide with the fit in the whole range of D . In comparison to the parameter values determined from the batch experiment, the value determined for the Monod constant for glucose $K_{S,Glc,Sa}$ was now about ten times lower, the Monod constant for amino acids $K_{S,AA,Sa}$ was higher than for the batch data set. The prediction of the washout rate ($D = 0.7 \text{ h}^{-1}$), which was a little lower than the maximum specific growth rate determined from the batch experiment $\mu_{\max,199,Sa} = 0.83 \text{ h}^{-1}$, was very good.

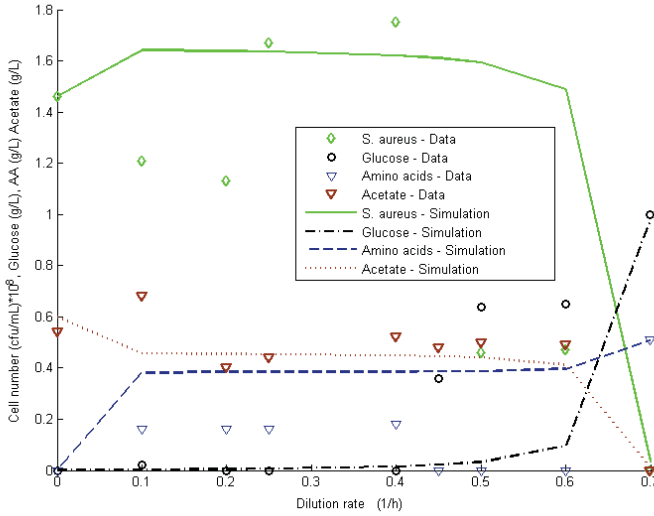


Figure 4.28: XD-Diagram of *S. a.* in M199+P+NTA: experimental data and simulation based on eqn. syst. 4.10 and parameters in Table 4.15. SES = 32.5

To improve the model fit of the XD-diagram for *S. a.* at low dilution rates eqn. syst. 4.10 was extended with terms for maintenance metabolism (eqn. syst. 4.11).

eqn. syst. 4.11

$$\frac{dX}{dt} = \mu_{\max,199,Sa} \cdot \left(\frac{Glc}{Glc + K_{S,Glc,Sa}} \cdot \frac{AA}{AA + K_{S,AA,Sa}} \right) \cdot X - D \cdot X$$

$$\frac{dGlc}{dt} = -\frac{1}{Y_{X|Glc,Sa}} \cdot \mu_{\max,199,Sa} \cdot \left(\frac{Glc}{Glc + K_{S,Glc,Sa}} \cdot \frac{AA}{AA + K_{S,AA,Sa}} \right) \cdot X + D \cdot (Glc_{in} - Glc) - m_{Sa} \cdot X$$

$$\frac{dAA}{dt} = -\frac{1}{Y_{X|AA,Sa}} \cdot \mu_{\max,199,Sa} \cdot \left(\frac{Glc}{Glc + K_{S,Glc,Sa}} \cdot \frac{AA}{AA + K_{S,AA,Sa}} \right) \cdot X + D \cdot (AA_{in} - AA) - m_{Sa} \cdot X$$

$$\frac{dAce}{dt} = Y_{Ace|X,Sa} \cdot \frac{\mu_{\max,199,Sa} \cdot Glc}{K_{S,Sa} + Glc} \cdot X - D \cdot Ace$$

For the determination of the maintenance coefficient the parameters for the model without maintenance (eqn. syst. 4.10) were kept (Table 4.15) and the maintenance coefficient m_{Sa} was determined by fit of the model to the experimental data as $0.04 \cdot 10^{-12} \text{ h}^{-1}$.

The simulation of growth model of *S. a.* in M199+P+NTA with consideration of maintenance metabolism (eqn. syst. 4.11) is given in Figure 4.29. The quality of fit was improved to a SES value of 28.5 compared to the model without maintenance (SES 32.5).

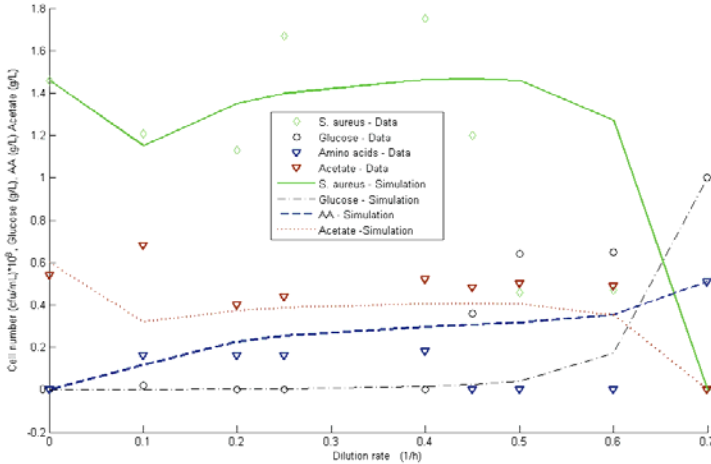


Figure 4.29: XD-Diagram of *S. a.* in M199+P+NTA: experimental data and simulation based on eqn. syst. 4.11 and parameters in Table 4.15 and $m_{Sa} = 0.04 \cdot 10^{-12} \text{ h}^{-1}$. SES = 28.5

The experimental results showed the independent growth of *B. c.* and *P. a.* on the mixed substrates glucose and amino acids (4.3.2). Therefore, the additive formulation of mixed substrate growth kinetic was chosen for the respective models (eqn. 2.7) (2.2.2.2).

Due to some variations in the growth of *P. a.* in small scale STR batch experiments, the determination of $\mu_{max,199,Pa}$ gave varied results : 0.42 h^{-1} , 0.53 h^{-1} , and 0.67 h^{-1} . For the further investigation of mixed substrate use of *P. a.*, the value in the middle of the range was chosen as a representative $\mu_{max,199,Pa} = 0.53 \text{ h}^{-1}$.

For the mathematical description of the growth on glucose and amino acids as two carbon sources, two basic model formulations (A) and (B) were compared for *B. c.* and *P. a.*:

- (A) Use of one $\mu_{max,Bc} = \mu_{max,199,Bc} = 0.66 \text{ h}^{-1}$ (Table 4.10), $\mu_{max,Pa} = \mu_{max,199,Pa} = 0.53 \text{ h}^{-1}$, already determined from the model fits for growth on one substrate, glucose respectively, and with the sum of Monod terms of both substrates (Glc+AA). This

formulation combined the kinetics for dependent growth (one maximum specific growth rate (eqn. 2.6) and independent growth (additive terms) (eqn. 2.7).

- (B) Two separate Monod kinetics for independent growth at low concentrations (eqn. 2.7) for the substrates glucose and amino acids, resulting in $\mu_{max,Glc,Bc}$, $\mu_{max,Glc,Pa}$ respectively, to be determined from experimental data, and $\mu_{max,AA,Bc} = 0.67 \text{ h}^{-1}$, $\mu_{max,AA,Pa} = 0.67 \text{ h}^{-1}$ as already determined (Table 4.13).

Growth on two substrates: glucose and amino acids (A)

The model for growth of *B. c.* and of *P. a.* on glucose and amino acids as mixed substrate based on (A) is given in eqn. syst. 4.12.

The model parameters (Table 4.16) for *B. c.* were determined by optimized fit of the simulation to the experimental data (Figure 4.30). For the Monod constant for amino acids $K_{S,AA,Bc}$ and the yield coefficient on amino acids $Y_{X/AA,Bc}$ the values for growth only on amino acids (Table 4.13) were used as start values.

eqn. syst. 4.12

$$\begin{aligned}\frac{dX}{dt} &= \mu_{max,199,i} \cdot \left(\frac{Glc}{Glc + K_{S,Glc,i}} + \frac{AA}{AA + K_{S,AA,i}} \right) \cdot X \\ \frac{dGlc}{dt} &= -\frac{1}{Y_{X/Glc,i}} \cdot \mu_{max,199,i} \cdot \left(\frac{Glc}{Glc + K_{S,Glc,i}} + \frac{AA}{AA + K_{S,AA,i}} \right) \cdot X \\ \frac{dAA}{dt} &= -\frac{1}{Y_{X/AA,i}} \cdot \mu_{max,199,i} \cdot \left(\frac{Glc}{Glc + K_{S,Glc,i}} + \frac{AA}{AA + K_{S,AA,i}} \right) \cdot X\end{aligned}$$

Table 4.16: Kinetic parameters for growth of *B. c.* on glucose and amino acids (eqn. syst. 4.12) with formulation of mixed substrate growth (A)*

$\mu_{max,199,Bc}$	$K_{S,Glc,Bc}$	$K_{S,AA,Bc}$	$Y_{X/Glc,Bc}$	$Y_{X/AA,Bc}$
0.66 h ⁻¹	0.002 g/L	0.33 g/L	4.05·10¹¹ cfu/g	7.72·10¹¹ cfu/g

* Parameters that were free for optimization are printed in **bold**.

The model of batch growth of *B. c.* on glucose and amino acids (A) was not able to describe the experimental results well. The glucose was taken up too quickly in the model simulation, and the cell formation also took place too quickly. The lag-time of amino acids uptake was not represented at all in the simulation, the amino acid simulation and data show the largest discrepancy.

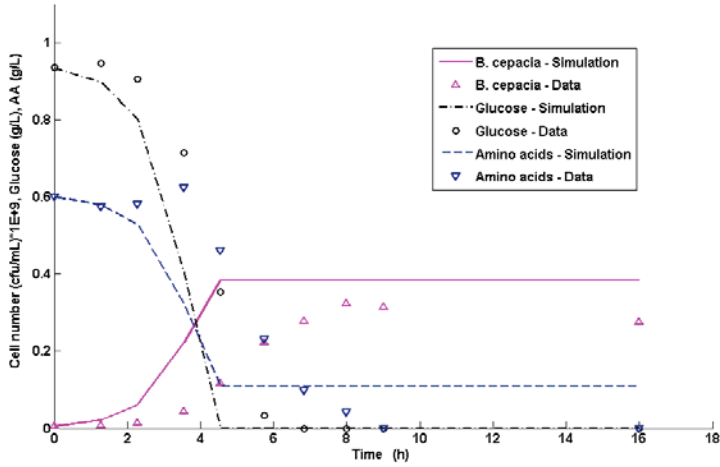


Figure 4.30: Simulation and experimental data for growth of *B. c.* on two substrates: glucose and amino acids. Growth kinetics for two substrates with one $\mu_{max,199,Bc}$ (A). Based on eqn. syst. 4.12 and the parameters in Table 4.16. Sum of error squares (SES) = 0.65

Due to the variations in data of *P. a.* batch experiments the related parameter estimations did not result in meaningful values and are therefore not presented here.

In order to improve the model fit especially concerning the observed lack of fit of the amino acid data, a diauxic kinetic was implemented into the previous model for *B. c.* (eqn. syst. 4.12) to describe the effect of sequential uptake of glucose and amino acids (eqn. syst. 4.13). As it is common, the diauxic growth was formulated as an inhibition (2.2.2.1).

eqn. syst. 4.13

$$\begin{aligned} \frac{dX}{dt} &= \mu_{max,199,Bc} \cdot \left(\frac{Glc}{Glc + K_{S,Glc,Bc}} + \frac{AA}{AA + K_{S,AA,Bc} \cdot (1 + Glc/K_I)} \right) \cdot X \\ \frac{dGlc}{dt} &= -\frac{1}{Y_{X/Glc,Bc}} \cdot \mu_{max,199,Bc} \cdot \left(\frac{Glc}{Glc + K_{S,Glc,Bc}} + \frac{AA}{AA + K_{S,AA,Bc} \cdot (1 + Glc/K_I)} \right) \cdot X \\ \frac{dAA}{dt} &= -\frac{1}{Y_{X/AA,Bc}} \cdot \mu_{max,199,Bc} \cdot \left(\frac{Glc}{Glc + K_{S,Glc,Bc}} + \frac{AA}{AA + K_{S,AA,Bc} \cdot (1 + Glc/K_I)} \right) \cdot X \end{aligned}$$

The model parameters were determined by an optimized fit of the simulation to the experimental data (Table 4.17 and Figure 4.31). The implementation of the diauxic effect of glucose improved the quality of data fit (SES 0.09 compared to 0.65 before) (3.6.3). However, the simulated time course did not result in depletion of amino acids and thereby did not correspond to experimental data. The improvement was not as good as expected compared to the model without diauxic effect, the time-lag of uptake of the amino acids was still too short.

Table 4.17: Parameters for growth of *B. c.* on glucose and amino acids (eqn. syst. 4.13).*

$\mu_{max,199,Bc}$	$K_{S,Glc,Bc}$	$K_{S,AA,Bc}$	K_I	$Y_{X/Glc,Bc}$	$Y_{X/AA,Bc}$
0.66 h^{-1}	0.027 g/L	0.065 g/L	0.018 g/L	$3.02 \cdot 10^{-11} \text{ cfu/g}$	$5.61 \cdot 10^{-11} \text{ cfu/g}$

* parameters that were free for optimization are printed in **bold**.

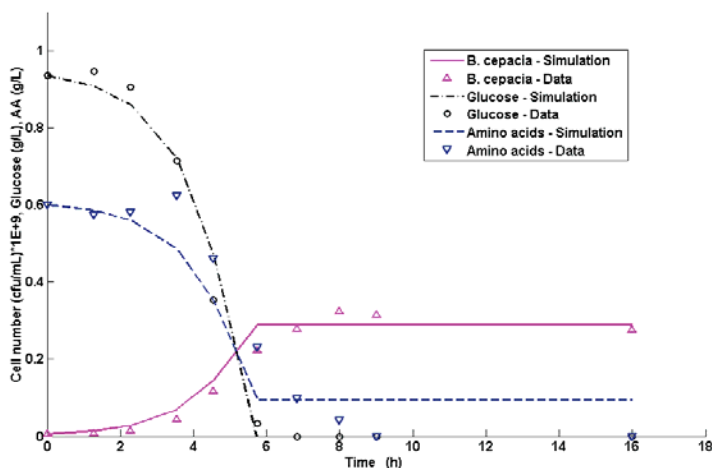


Figure 4.31: Simulation and experimental data for growth of *B. c.* on two substrates: glucose and amino acids. Growth kinetics for two substrates with one $\mu_{max,199,Bc}$ and diauxic growth considered. Based on eqn. syst. 4.13 and with parameters in Table 4.17. SES = 0.09

For simulation of the chemostat experiment with varied dilution rates (Figure 4.20) the previous model for *B. c.* including the diauxic effect (eqn. syst. 4.13) was extended to a continuous process model (eqn. syst. 4.14) by implementation of the dilution rate D .

eqn. syst. 4.14

$$\frac{dX}{dt} = \mu_{max,199,Bc} \cdot \left(\frac{Glc}{Glc + K_{S,Glc,Bc}} + \frac{AA}{AA + K_{S,AA,Bc} \cdot (1 + Glc/K_I)} \right) \cdot X - D \cdot X$$

$$\frac{dGlc}{dt} = -\frac{1}{Y_{X/Glc,Bc}} \cdot \mu_{max,199,Bc} \cdot \left(\frac{Glc}{Glc + K_{S,Glc,Bc}} + \frac{AA}{AA + K_{S,AA,Bc} \cdot (1 + Glc/K_I)} \right) \cdot X + D \cdot (Glc_{in} - Glc)$$

$$\frac{dAA}{dt} = -\frac{1}{Y_{X/AA,Bc}} \cdot \mu_{max,199,Bc} \cdot \left(\frac{Glc}{Glc + K_{S,Glc,Bc}} + \frac{AA}{AA + K_{S,AA,Bc} \cdot (1 + Glc/K_I)} \right) \cdot X + D \cdot (AA_{in} - AA)$$

The model parameters were determined by an optimized fit of the simulation to the experimental data (Table 4.18 and Figure 4.32). The simulation of eqn. syst. 4.14 gave very consistent results for glucose and amino acid concentrations. The cell numbers were not represented exactly concerning the drop at $D = 1.0 \text{ h}^{-1}$ in the simulation. However, as a whole they correlated well and especially the washout point at $D_{crit} = 1.3 \text{ h}^{-1}$ was simulated correctly. This was important, because the washout point was at a higher dilution rate than was to be expected from the value of $\mu_{max,199,Bc}$ of 0.66 h^{-1} . To achieve this, the resulting Monod constant for glucose $K_{S,Glc,Bc}$ was estimated about ten times lower than from the batch experiment and the inhibition constant K_I was higher (Table 4.17).

Table 4.18: Parameters for growth of *B. c.* on glucose and amino acids (eqn. syst. 4.14) *

$\mu_{max,199,Bc}$ 0.66 h^{-1}	$K_{S,Glc,Bc}$	$K_{S,AA,Bc}$	K_I	$Y_{X/Glc,Bc}$	$Y_{X/AA,Bc}$
	0.003 g/L	0.06 g/L	0.51 g/L	$3.21 \cdot 10^{11}$ cfu/g	$4.99 \cdot 10^{11}$ cfu/g

* Parameters that were free for optimization are printed in **bold**.

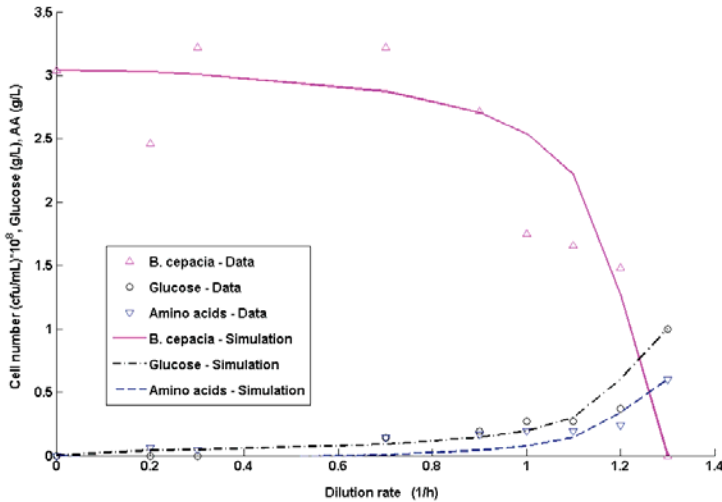


Figure 4.32: XD-Diagram: simulation and experimental data for growth of *B. c.* on two substrates: glucose and amino acids. Growth kinetics for two substrates with $\mu_{max,199,Bc}$ and diauxic growth. Based on eqn. syst. 4.14 and with parameters in Table 4.18. SES = 7.7

An attempt to improve the fit at low dilution rates by implementation of $(-m_{Bc} \cdot X)$ as maintenance term resulted in an SES of 7.54 and was not considered as significant for the model of *B. c.*.

For *P. a.* the chemostat model based on the respective batch model (A) (eqn. syst. 4.12) for growth on glucose and amino acids as mixed substrates was formulated (eqn. syst. 4.15).

eqn. syst. 4.15

$$\begin{aligned} \frac{dX}{dt} &= \mu_{\max,199,Pa} \cdot \left(\frac{Glc}{Glc + K_{S,Glc,Pa}} + \frac{AA}{AA + K_{S,AA,Pa}} \right) \cdot X - D \cdot X \\ \frac{dGlc}{dt} &= -\frac{1}{Y_{X/Glc,Pa}} \cdot \mu_{\max,199,Pa} \cdot \left(\frac{Glc}{Glc + K_{S,Glc,Pa}} + \frac{AA}{AA + K_{S,AA,Pa}} \right) \cdot X + D \cdot (Glc_{in} - Glc) \\ \frac{dAA}{dt} &= -\frac{1}{Y_{X/AA,Pa}} \cdot \mu_{\max,199,Pa} \cdot \left(\frac{Glc}{Glc + K_{S,Glc,Pa}} + \frac{AA}{AA + K_{S,AA,Pa}} \right) \cdot X + D \cdot (AA_{in} - AA) \end{aligned}$$

Table 4.19: Parameters for growth of *P. a.* derived from fit of eqn. syst. 4.15 to data. $\mu_{\max,199,Pa} = 0.54 \text{ h}^{-1}$ was set as constraint.*

$\mu_{\max,199,Pa}$	$K_{S,Glc,Pa}$	$K_{S,AA,Pa}$	$Y_{X/Glc,Pa}$	$Y_{X/AA,Pa}$
0.54 h^{-1}	0.057 g/L	0.027 g/L	$5.85 \cdot 10^{11} \text{ cfu/g}$	$7.22 \cdot 10^{11} \text{ cfu/g}$

* Parameters free for variation are printed in **bold**.

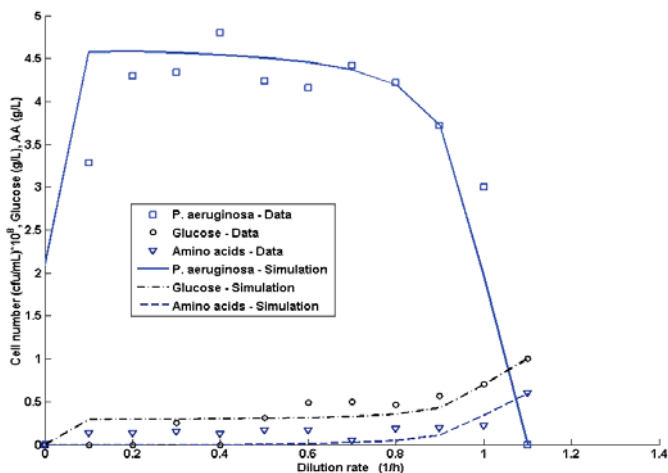


Figure 4.33: XD-Diagram of growth of *P. a.* in M199+P+NTA: experimental data and simulation based on eqn. syst. 4.15 and parameters in Table 4.19. SES = 17.65

The washout of the chemostat experiment took place at a higher value of D than expected from the value for $\mu_{\max,199,Pa}$ of 0.54 h^{-1} . However, the simulation represented well the experimental data, especially the washout point at 1.1 h^{-1} . The step in the curve of glucose at $D = 0.6 \text{ h}^{-1}$ was not represented. The values of the dependent variables at $D = 0 \text{ h}^{-1}$ represent the status at the switch between batch and continuous process mode and were not considered for parameter estimation.

For improvement of the model fit to the experimental data of growth of *P. a.* at low dilution rates, a term for maintenance was implemented into eqn. syst. 4.15 (eqn. syst. 4.16). However, the model fit (SES = 17.15) did not improve significantly by this variation. The parameters were kept from before (Table 4.19) and m_{Pa} was estimated as $0.0024 \cdot 10^{-11} \text{ h}^{-1}$.

eqn. syst. 4.16

$$\frac{dX}{dt} = \mu_{\max,199,Pa} \cdot \left(\frac{Glc}{Glc + K_{S,Glc,Pa}} + \frac{AA}{AA + K_{S,AA,Pa}} \right) \cdot X - D \cdot X$$

$$\frac{dGlc}{dt} = -\frac{1}{Y_{X/Glc,Pa}} \cdot \mu_{\max,199,Pa} \cdot \left(\frac{Glc}{Glc + K_{S,Glc,Pa}} + \frac{AA}{AA + K_{S,AA,Pa}} \right) \cdot X + D \cdot (Glc_{in} - Glc) - m_{Pa} \cdot X$$

$$\frac{dAA}{dt} = -\frac{1}{Y_{X/AA,Pa}} \cdot \mu_{\max,199,Pa} \cdot \left(\frac{Glc}{Glc + K_{S,Glc,Pa}} + \frac{AA}{AA + K_{S,AA,Pa}} \right) \cdot X + D \cdot (AA_{in} - AA) - m_{Pa} \cdot X$$

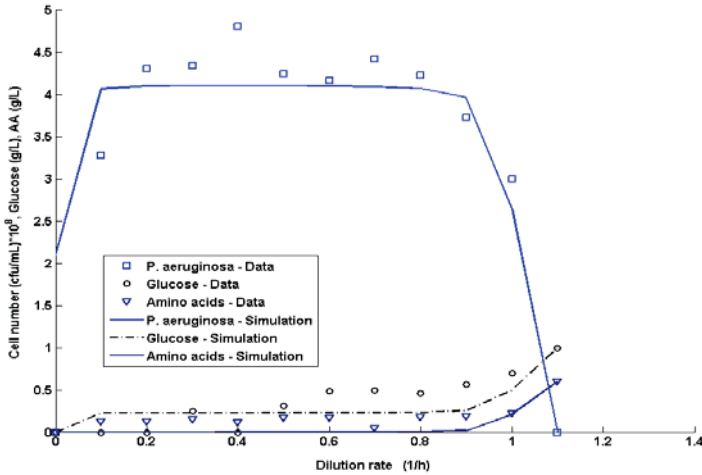


Figure 4.34: XD-Diagram of growth of *P. a.* in M199+P+NTA: experimental data and simulation based on eqn. syst. 4.16 and Table 4.19 and $m_{Pa} = 0.0024 \cdot 10^{-11} \text{ h}^{-1}$. SES = 17.15

Growth on two substrates: glucose and amino acids (B)

The expression for the growth rate as proposed under (B) with the sum of two Monod kinetics separately expressed for glucose and amino acids is given as batch model for *B. c.* in eqn. syst. 4.17. As the implementation of diauxic growth on glucose and amino acids improved model fit for (A), it was directly implemented for (B) as well. The value of the maximum specific growth rate only on amino acids ($\mu_{\max,AA,Bc}$) was taken from the parameter estimation for growth of *B. c.* without glucose (Table 4.13). The maximum specific growth rate only on glucose $\mu_{\max,Glc,Bc}$ could not be assumed to be equal to growth in M199+P+NTA, as glucose was probably taken up together with the amino acids. Therefore, the value of $\mu_{\max,Glc,Bc}$ was determined by fit of data to the model (eqn. syst. 4.17). The resulting parameter values are given in Table 4.20.

eqn. syst. 4.17

$$\begin{aligned}\frac{dX}{dt} &= \left(\frac{\mu_{\max,Glc,Bc} \cdot Glc}{Glc + K_{S,Glc,Bc}} + \frac{\mu_{\max,AA,Bc} \cdot AA}{AA + K_{S,AA,Bc} \cdot (1 + Glc/K_I)} \right) \cdot X \\ \frac{dGlc}{dt} &= -\frac{1}{Y_{X/Glc,Bc}} \cdot \left(\frac{\mu_{\max,Glc,Bc} \cdot Glc}{Glc + K_{S,Glc,Bc}} \right) \cdot X \\ \frac{dAA}{dt} &= -\frac{1}{Y_{X/AA,Bc}} \cdot \left(\frac{\mu_{\max,AA,Bc} \cdot AA}{AA + K_{S,AA,Bc} \cdot (1 + Glc/K_I)} \right) \cdot X\end{aligned}$$

Table 4.20: Parameters for growth of *B. c.* on glucose and amino acids (B) (eqn. syst. 4.18). $\mu_{\max,AA,Bc} = 0.67 \text{ h}^{-1}$ was set as constraint.

$\mu_{\max,Glc,Bc}$	$K_{S,Glc,Bc}$	$K_{S,AA,Bc}$	K_I	$Y_{X/Glc,Bc}$	$Y_{X/AA,Bc}$
0.11 h⁻¹	0.017 g/L	0.017 g/L	0.21 g/L	2.25·10¹¹ cfu/g	1.47·10¹¹ cfu/g

The simulation of growth of *B. c.* for a batch process with the assumption of two separate growth kinetics for glucose and amino acids (Figure 4.35) resulted in an SES value of 0.025. This was an improvement compared with the result for assumption of one growth kinetic on both substrates (SES = 0.09) (eqn. syst. 4.13). The resulting value of $\mu_{\max,Glc,Bc}$ for growth only on glucose was very low compared to $\mu_{\max,AA,Bc}$ for growth only on amino acids (Table 4.20). This was surprising as glucose should lead to a higher specific growth rate than the substrate used second (AA) in a diauxic sequence [105] (2.2.2.1).

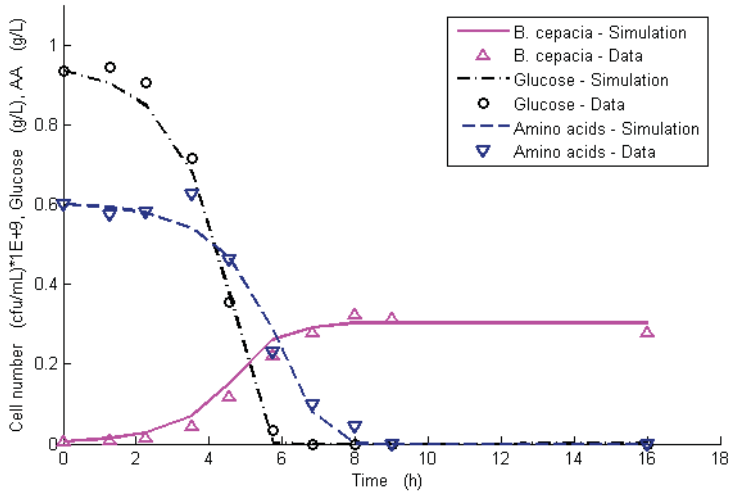


Figure 4.35: Simulation and experimental data for growth of *B. c.* on two substrates: glucose and amino acids. Growth kinetics for two substrates with $\mu_{\max, \text{Glc}, Bc}$ and $\mu_{\max, \text{AA}, Bc}$ and diauxic growth considered. Based on eqn. syst. 4.17 and parameters in Table 4.20. SES = 0.025

For simulation of the chemostat experiment with varied dilution rates for *B. c.* (Figure 4.20) and to determine $K_{S,i}$ values under quasi steady state conditions the batch model was extended to a continuous process model (eqn. syst. 4.18) for formulation (B).

eqn. syst. 4.18

$$\frac{dX}{dt} = \left(\frac{\mu_{\max, \text{Glc}, Bc} \cdot \text{Glc}}{\text{Glc} + K_{S, \text{Glc}, Bc}} + \frac{\mu_{\max, \text{AA}, Bc} \cdot \text{AA}}{\text{AA} + K_{S, \text{AA}, Bc} \cdot (1 + \text{Glc}/K_I)} \right) \cdot X - D \cdot X$$

$$\frac{d\text{Glc}}{dt} = -\frac{1}{Y_{X/\text{Glc}, Bc}} \cdot \left(\frac{\mu_{\max, \text{Glc}, Bc} \cdot \text{Glc}}{\text{Glc} + K_{S, \text{Glc}, Bc}} \right) \cdot X + D \cdot (\text{Glc}_{in} - \text{Glc})$$

$$\frac{d\text{AA}}{dt} = -\frac{1}{Y_{X/\text{AA}, Bc}} \cdot \left(\frac{\mu_{\max, \text{AA}, Bc} \cdot \text{AA}}{\text{AA} + K_{S, \text{AA}, Bc} \cdot (1 + \text{Glc}/K_I)} \right) \cdot X + D \cdot (\text{AA}_{in} - \text{AA})$$

A first estimation of parameters was conducted by fit of model parameters to the experimental data with both maximum specific growth rates $\mu_{\max, \text{Glc}, Bc}$ and $\mu_{\max, \text{AA}, Bc}$ as constraints. This approach was not successful, as the simulated washout point was significantly below the experimentally determined one of $D = 1.3 \text{ h}^{-1}$ (simulation result not shown).

Consequently, for the next approach the value of $\mu_{max,Glc,Bc}$ was free for optimization. The resulting values for all parameters determined from the fit of chemostat data to the model eqn. syst. 4.18 are given in Table 4.21. The value for $\mu_{max,Glc,Bc}$ based on the chemostat data was much higher than from the batch experiment (0.11 h^{-1}), which was biologically more meaningful. Additionally, the value was as expected for a diauxic sequence higher than the growth rate on amino acids.

Table 4.21: Estimated parameters for growth of *B. c.* on glucose and amino acids with two separate Monod kinetics (B) (eqn. syst. 4.18). $\mu_{max,AA,Bc} = 0.67 \text{ h}^{-1}$ was set as constraint.

$\mu_{max,Glc,Bc}$	$K_{S,Glc,Bc}$	$K_{S,AA,Bc}$	K_I	$Y_{X/Glc,Bc}$	$Y_{X/AA,Bc}$
0.74 h^{-1}	0.007 g/L	0.038 g/L	0.34 g/L	$2.35 \cdot 10^{11} \text{ cfu/g}$	$1.84 \cdot 10^{11} \text{ cfu/g}$

The simulation of growth of *B. c.* in a chemostat with varied dilution rates D for two separate growth kinetics for glucose and amino acids (B) is given in Figure 4.36. The resulting SES of 17.9 was more than double the value of the chemostat fit for assumption (A) (7.7) (Figure 4.32). The sum of the resulting maximum growth rates was 1.41 h^{-1} , this was slightly higher than the dilution rate D at the point of wash out (1.3 h^{-1}).

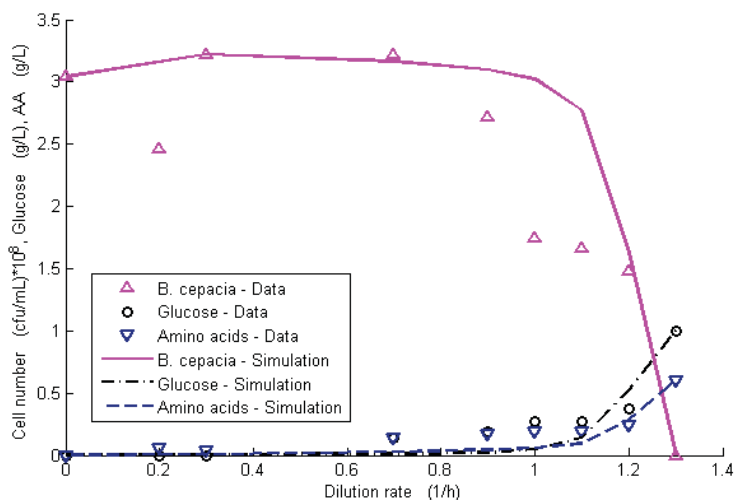


Figure 4.36: XD-Diagram of simulation and experimental data for growth of *B. c.* on two substrates: glucose and amino acids. Growth kinetics for two substrates with two $\mu_{max,Glc,Bc}$ and $\mu_{max,AA,Bc}$ and diauxic growth considered. Based on eqn. syst. 4.18 and with the parameters in Table 4.21. SES = 17.9

The formulation of the growth rate according to (B) with two separate growth rate kinetics for growth of *P. a.* on glucose and amino acids is given in eqn. syst. 4.19.

In line with the procedure for *B. c.*, $\mu_{\max, \text{Glc}, Pa}$ was determined from an optimized fit of the model simulation to the data, whereas $\mu_{\max, AA, Pa}$ was set as constraint as determined from the experimental growth only on amino acids (Table 4.13). This was the method of choice, because there was no experimental data available for growth of *P. a.* only on glucose without amino acids, but only on glucose and amino acids in M199+P+NTA, respectively ($\mu_{\max, 199, Pa}$).

The results of the parameter estimation are given in Table 4.22. The value for $\mu_{\max, \text{Glc}, Pa}$ was low, but within the range of values determined for $\mu_{\max, 199, Pa}$ before (Table 4.10).

eqn. syst. 4.19

$$\begin{aligned}\frac{dX}{dt} &= \left(\frac{\mu_{\max, \text{Glc}, Pa} \cdot \text{Glc}}{\text{Glc} + K_{S, \text{Glc}, Pa}} + \frac{\mu_{\max, AA, Pa} \cdot AA}{AA + K_{S, AA, Pa}} \right) \cdot X - D \cdot X \\ \frac{d\text{Glc}}{dt} &= -\frac{1}{Y_{X/\text{Glc}, Pa}} \cdot \left(\frac{\mu_{\max, \text{Glc}, Pa} \cdot \text{Glc}}{\text{Glc} + K_{S, \text{Glc}, Pa}} \right) \cdot X + D \cdot (\text{Glc}_{in} - \text{Glc}) \\ \frac{dAA}{dt} &= -\frac{1}{Y_{X/AA, Pa}} \cdot \left(\frac{\mu_{\max, AA, Pa} \cdot AA}{AA + K_{S, AA, Pa}} \right) \cdot X + D \cdot (AA_{in} - AA)\end{aligned}$$

Table 4.22: Parameters for growth of *P. a.* on glucose and amino acids (B) derived from fit of eqn. syst. 4.19 to data. $\mu_{\max, AA, Pa} = 0.67 \text{ h}^{-1}$ was set as constraint.

$\mu_{\max, \text{Glc}, Pa}$	$K_{S, \text{Glc}, Pa}$	$K_{S, AA, Pa}$	$Y_{X/\text{Glc}, Pa}$	$Y_{X/AA, Pa}$
0.34 h⁻¹	0.012 g/L	0.001 g/L	2.85·10¹¹ cfu/g	3.27·10¹¹ cfu/g

The simulation based on eqn. syst. 4.19 is given in Figure 4.37. The SES value was improved in comparison to the fit of eqn. syst. 4.15 and eqn. syst. 4.16, namely one kinetic with addition of kinetic expressions for growth on glucose and amino acids (A), without and with maintenance, respectively. Additionally, the simulation for (B) represented the decrease of cell numbers and the increase of glucose concentration, while amino acids were still low, at dilution rates higher than 0.6 h^{-1} much better than (A). The sum of maximum growth rates resulted in 1.01 h^{-1} , which was lower than the dilution rate D at the point of wash out (1.1 h^{-1}).

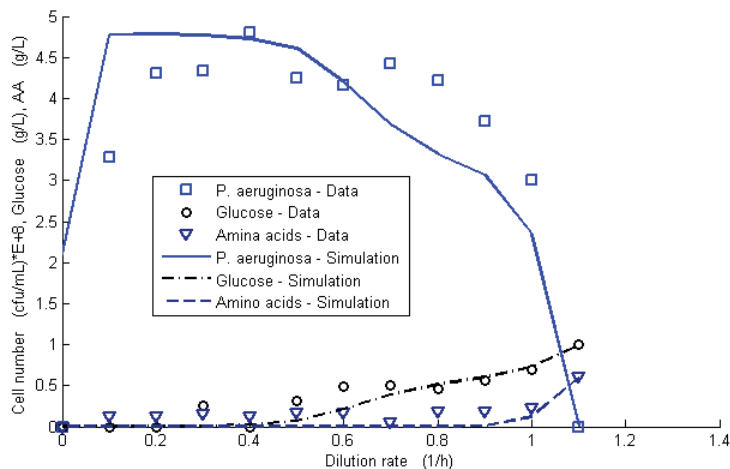


Figure 4.37: XD-Diagram of simulation and experimental data for growth of *P. a.* on two substrates: glucose and amino acids. Growth kinetics for two substrates with two $\mu_{max, Glc, Pa}$ and $\mu_{max, AA, Pa}$ considered. Growth of *P. a.* in M199+P+NTA: experimental data and simulation based on eqn. syst. 4.19 and parameters in Table 4.22. SES = 13.67

4.3.5 Summary of Results for Mathematical Modeling of Single-Species Growth

An overview of the results of the mathematical modeling for the single-species is given in Table 4.23 and Table 4.24.

Table 4.23: Summary I of the established and tested model variants for description of single-species growth dynamics for growth on glucose as single substrate and acetate formation (4.3.4.1).

Model variant	<i>S. a.</i>	<i>B. c.</i>	<i>P. a.</i>
Glc as single substrate	No acetate formation considered	No further cell formation considered	No further cell formation considered
Acetate formation	Varied parameter estimation : best and biologically most meaningful result for parameters from above and direct calculation of acetate yield of cells	-	-

Table 4.24: Summary II of the established and tested model variants for description of single-species growth dynamics considering experimental findings and focusing on acetate biotrophy and mixed substrate growth on amino acids and glucose

Model variant	<i>S. a.</i>	<i>B. c.</i>	<i>P. a.</i>
<i>Glc</i> + <i>Ace</i> as mixed substrate (4.3.4.2)	-	Assumption of independent substrate to <i>Glc</i> : best and biologically most meaningful results for parameters kept from growth on <i>Glc</i> , yield on <i>Ace</i> calculated directly and only $\mu_{max,Ace,Bc}$ and $K_{S,Ace,Bc}$ fitted	Assumption of independent substrate to <i>Glc</i> : best and biologically most meaningful results for parameters kept from growth on <i>Glc</i> , yield on <i>Ace</i> , $\mu_{max,Ace,Bc}$ and $K_{S,Ace,Bc}$ fitted
<i>AA</i> as single substrate (4.3.4.3)	As for glucose, no acetate considered	As for glucose	As for glucose
<i>Glc</i> + <i>AA</i> as mixed substrate (4.3.4.4)	No cell formation considered on <i>AA</i> without <i>Glc</i> <i>Glc</i> and <i>AA</i> as dependent substrates (auxotrophy) : multiplicative kinetic $\mu_{max,199,Sc}$ and yield for <i>Ace</i> kept from before : Batch fit o.k. XD-graph fit o.k. with maintenance fit improved	Further cell formation considered by growth on <i>AA</i> <i>Glc</i> and <i>AA</i> as independent substrates: additive kinetic <i>A.</i> One $\mu_{max,199,Bc}$ from before <i>A.1</i> batch o.k., <i>AA</i> simulation no depletion <i>A.2</i> batch with diauxic effect first <i>Glc</i> than <i>AA</i> , better <i>A.3</i> chemostat with diauxic effect, $D_{crit}=1.3h^{-1}$ fitted <i>B.</i> $\mu_{max,Glc,Bc}$ fitted $\mu_{max,AA,Bc}$ from before <i>B.1</i> batch with $\mu_{max,Glc,Bc}$ $0.1066h^{-1}$, better than <i>A.1</i> <i>B.2</i> chemostat with diauxic effect : new fit necessary for $D=1.3h^{-1}$: $\mu_{max,Glc,Bc}$ $0.73h^{-1}$	Further cell formation considered by growth on <i>AA</i> <i>Glc</i> and <i>AA</i> as independent substrates: additive kinetic <i>A.</i> One $\mu_{max,199,Pa}$ from before <i>A.1</i> chemostat, $D=1.1h^{-1}$ fitted, but not the stepwise decrease in cell number and <i>Glc</i> at $D > 0.6h^{-1}$ <i>B.</i> $\mu_{max,Glc,Pa}$ fitted $\mu_{max,AA,Pa}$ from before <i>B.1</i> chemostat, $D=1.1h^{-1}$ fitted and also the stepwise decrease in cell number and <i>Glc</i> at $D > 0.6h^{-1}$

4.4 Investigation of Biotrophy on Acetate

Acetate was a metabolic product released by *S. a.* during growth on glucose and it was verified experimentally to serve as additional substrate to glucose for *B. c.* (Figure 4.22) and *P. a.* (Figure 4.23). Based on these experimental findings a possible interaction based on acetate could be assumed in a co-cultivation. In the following it was therefore investigated experimentally and by mathematical modeling, if release of acetate resulted in a biotrophy (2.3.3) during mixed culture growth and if it could lead to coexistence in a chemostat culture. In order to clearly identify possible interactions a two-species system was chosen, using *S. a.* as producer and *B. c.* as consumer.

4.4.1 Two-species Chemostat Experiments

S. a. and *B. c.* were co-cultivated in chemostat process mode. Two experiments were conducted in parallel with different dilution rates D , namely 0.05 h^{-1} and 0.2 h^{-1} . Cultivations were conducted in the small scale STR system, with higher aeration (5 NL/h) compared to standard conditions (3.4.5.3), because the experiments were done in an earlier phase of the project. Standard M199+P+NTA medium was used as in single-species experiments (3.2.1.1). Cell numbers from mixed samples were determined by a quantitative T-RFLP (3.5.2.3) and for comparison the overall cell number was determined as optical density (OD_{650}) (3.5.1).

The results of two-species chemostat experiments are given in Figure 4.38 ($D = 0.05\text{ h}^{-1}$) and Figure 4.39 ($D = 0.2\text{ h}^{-1}$).

The results of both two-species mixed culture experiments in chemostat mode with different dilution rates were similar. In both experiments a coexistence of the two species was observed. With a dilution rate of $D = 0.05\text{ h}^{-1}$ both species were detectable until the end of the cultivation (171 h) (Figure 4.38). With a dilution rate of $D = 0.2\text{ h}^{-1}$ *S. a.* was not detectable any more after 124 h. The cell numbers of *S. a.* were close to the quantification limit. It was therefore assumed to be still present in the mixed culture (dotted line). This assumption was also supported by the stable overall biomass (OD_{650}), while the cell numbers of *B. c.* did not increase (Figure 4.39).

At the time point of then switch from batch to continuous process mode *S. a.* had reached a higher cell number ($10^{9.8}\text{ cfu/mL}$; 10^9 cfu/mL) than *B. c.* ($10^{7.6}\text{ cfu/mL}$; $10^{7.3}\text{ cfu/mL}$). Before a quasi steady state of the system was reached, the ratio between the two species changed and the cell number of *B. c.* stayed higher up to the end of the cultivations.

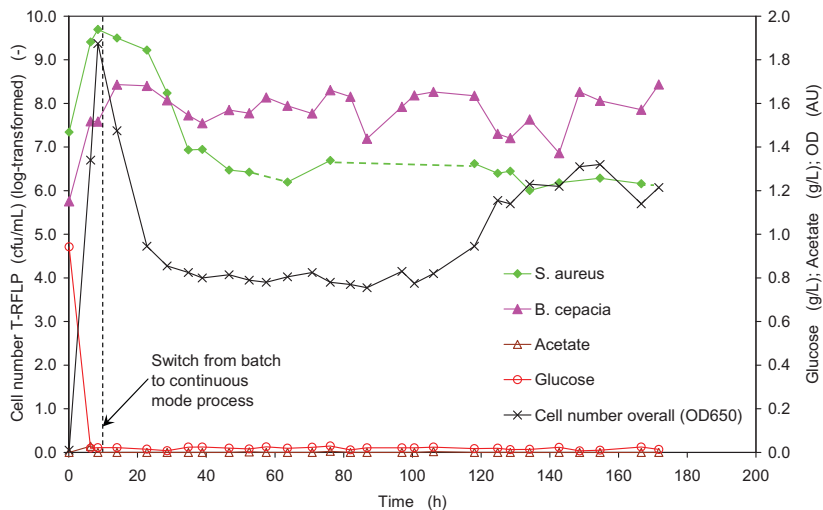


Figure 4.38: Two-species mixed culture in a chemostat ($D = 0.05$ L/h): *B. c.* and *S. a.* in M199+P+NTA medium. Small scale STR: $q = 0.416$ vvm; $n = 300$ rpm, $V_L = 200$ mL. Dotted line indicates interpolation of cell number for *S. a.*.

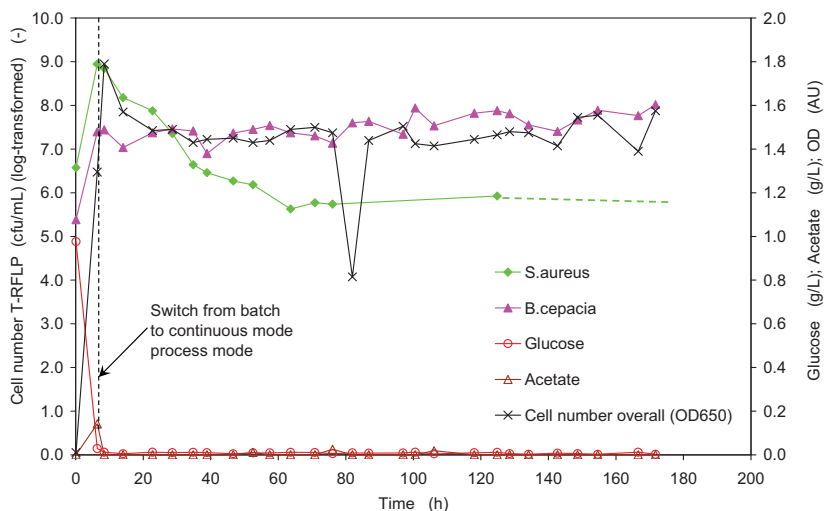


Figure 4.39: Two-species competition in a chemostat ($D = 0.2$ L/h): *B. c.* and *S. a.* in M199+P+NTA medium. Small scale STR: $q = 0.416$ vvm; $n = 300$ rpm, $V_L = 200$ mL. Dotted line indicates interpolation of cell number for *S. a.*.

The overall cell number (OD_{650}) was stable for a dilution rate of $D = 0.2 \text{ h}^{-1}$ at about 1.4 AU. The value of 0.8 AU after 80 h was considered as outlier (Figure 4.39). For a dilution rate of $D = 0.05 \text{ h}^{-1}$ the overall cell number (OD_{650}) was stable at a value of about 0.8 AU for 100 h of cultivation time and then increased to about 1.2 AU (Figure 4.38). This result could not be explained and did not correlate with T-RFLP cell numbers. It might indicate slower start-up behavior of the system for the lower dilution rate.

At both dilution rates glucose concentrations were very low during the whole cultivation time, as it was expected for the assumption of glucose as the main carbon and energy source.

Acetate concentration was very low and in most of the samples not even detected by HPLC analysis in both experiments during the continuous phase. This clearly indicated uptake by *B. c.* of the acetate produced by *S. a.* and confirmed the hypothesis of an acetate based biotrophy in the investigated mixed culture.

4.4.2 Mathematical Models of Two-Species Chemostat

In the two-species mixed cultures an apparent coexistence of *S. a.* and *B. c.* was found. It was also shown that during co-cultivation *B. c.* took up acetate produced by *S. a.*. By mathematical modeling it was evaluated, whether the experimentally assumed acetate biotrophy could be the main cause for the observed coexistence of the two species. For these theoretical considerations the use of the sum of amino acids as substrate was not taken into account for a first approach.

4.4.2.1 Two-Species Chemostat Model without Acetate Biotrophy

Before the acetate food chain was considered the classic chemostat model (Figure 2.2) with the assumption of single substrate competition (2.4.1) was studied as a comparison. The model was formulated (eqn. syst. 4.20) and simulated (Figure 4.40) for the two-species system (4.4.1). The variables X_{Sa} and X_{Bc} denote the cell concentrations of the respective species, the specific growth rates $\mu_{199,Sa}$ and $\mu_{199,Bc}$ are indicated accordingly.

eqn. syst. 4.20

$$\begin{aligned}\mu_{199,Sa} &= \frac{\mu_{\max,199,Sa} \cdot Glc}{K_{S,Sa} + Glc}; & \mu_{199,Bc} &= \frac{\mu_{\max,199,Bc} \cdot Glc}{K_{S,Bc} + Glc} \\ \frac{dX_{Sa}}{dt} &= \mu_{199,Sa} \cdot X_{Sa} - D \cdot X_{Sa}; & \frac{dX_{Bc}}{dt} &= \mu_{199,Bc} \cdot X_{Bc} - D \cdot X_{Bc} \\ \frac{dGlc}{dt} &= -\frac{1}{Y_{X/Glc,Sa}} \cdot \mu_{199,Sa} \cdot X_{Sa} - \frac{1}{Y_{X/Glc,Bc}} \cdot \mu_{199,Bc} \cdot X_{Bc} + D \cdot (Glc_{in} - Glc)\end{aligned}$$

Consequently, for the simulations the parameters determined from single-species experiments in small scale STR for the respective model assumption of single substrate use (glucose) were applied (Table 4.10).

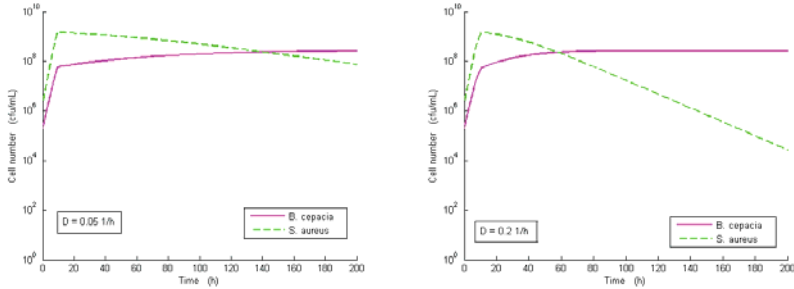


Figure 4.40: Simulation results for two-species chemostat ($D = 0.05 \text{ h}^{-1}$ and $D = 0.2 \text{ h}^{-1}$), the batch phase was simulated for the first 6.5 h. Model assumption of single substrate competition; parameter values from single-species batch experiments (small scale STR).

At the end of the batch phase the relation of species cell numbers was comparable to the experimental results (Figure 4.38; Figure 4.39) in both simulations (Figure 4.40), *S. a.* was higher than *B. c.* The cell numbers of *B. c.* during the continuous phase correlated with the experimental results, whereas the cell numbers of *S. a.* were not well represented by the simulation. The simulations both resulted in survival of *B. c.* and wash out of *S. a.* The effect was more pronounced at a dilution rate $D = 0.2 \text{ h}^{-1}$, which was expected due to system dynamics, which was 4 times faster than with $D = 0.05 \text{ h}^{-1}$.

The simulation results showed that the experimental result of coexistence in a two-species chemostat (Figure 4.38; Figure 4.39) could not be explained by the classic chemostat model assumption of single substrate competition for glucose (Figure 4.40). However, with regard to the simulation the experimental results could also be interpreted as a slow washout of *S. a.* In order to possibly clarify the experimental observation, the effect of an acetate biotrophy on two-species chemostat dynamics was analyzed. The use of amino acids as substrate on the mixed culture growth was not considered here.

4.4.2.2 Two-Species Chemostat Model with Acetate Biotrophy

The two-species chemostat model with glucose competition (eqn. syst. 4.20) was extended with two additional kinetics representing the acetate interaction: (A) acetate formation by *S. a.* as introduced for single-species (eqn. syst. 4.2); (B) acetate uptake as formulated for *B. c.*

single-species (eqn. syst. 4.4). The model of the two-species chemostat with an acetate biotrophy was formulated for the continuous process with the dilution rate D (eqn. syst. 4.21).

eqn. syst. 4.21

$$\begin{aligned}\mu_{199,Sa} &= \frac{\mu_{\max,199,Sa} \cdot Glc}{K_{S,Sa} + Glc}; & \mu_{Glc,Bc} &= \frac{\mu_{\max,Glc,Bc} \cdot Glc}{K_{S,Glc,Bc} + Glc}; & \mu_{Ace,Bc} &= \frac{\mu_{\max,Ace,Bc} \cdot Ace}{K_{S,Ace,Bc} + Ace} \\ \frac{dX_{Sa}}{dt} &= \mu_{199,Sa} \cdot X_{Sa} - D \cdot X_{Sa}; & \frac{dX_{Bc}}{dt} &= \mu_{Glc,Bc} \cdot X_{Bc} + \mu_{Ace,Bc} \cdot X_{Bc} - D \cdot X_{Bc} \\ \frac{dGlc}{dt} &= -\frac{1}{Y_{X/Glc,Sa}} \cdot \mu_{199,Sa} \cdot X_{Sa} - \frac{1}{Y_{X/Glc,Bc}} \cdot \mu_{Glc,Bc} \cdot X_{Bc} + D \cdot (Glc_{in} - Glc) \\ \frac{dAce}{dt} &= Y_{Ace/X,Sa} \cdot \mu_{199,Sa} \cdot X_{Sa} - \frac{1}{Y_{X/Ace,Bc}} \cdot \mu_{Ace,Bc} \cdot X_{Bc} - D \cdot Ace\end{aligned}$$

Simulations for the two-species chemostat model with acetate biotrophy were calculated for the two dilution rates of the experiments ($D = 0.05 \text{ h}^{-1}$ and $D = 0.2 \text{ h}^{-1}$). The batch phase was not included in the model simulation, but the starting values at the end of the batch phase were taken from the experimental data.

By keeping different parameter values as constraints varied parameter sets were determined from the single-species experiments with *B. c.* (Table 4.11) and *S. a.* (Table 4.10). To demonstrate the resulting variation in the predicted growth dynamics all of these values were applied for simulation of the chemostat model (Figure 4.41). The first simulation used the parameters determined by free fit of all values (A). The second simulation used the same parameters as in (A) for *B. c.* and for *S. a.* only the acetate yield $Y_{Ace/X,Sa}$ was fitted (B). For the third and fourth simulation the parameters for *S. a.* were kept the same (C), (D). For the third simulation the parameters for *B. c.* were only fitted for the acetate kinetic (C).

The parameter choice for the fourth variant was considered as biologically meaningful (D). The parameters $K_{S,Ace}$ and $\mu_{\max,Ace,Bc}$ were fitted and the acetate yield $Y_{X/Ace,Bc}$ was calculated directly (eqn. 4.3).

The qualitative results for each of the parameter variants (A, B, C, and D) of the cell number dynamics found with the simulations did not differ for the two dilution rates. For (B) a stable coexistence of *B. c.* and *S. a.* was predicted, with higher cell numbers of *S. a.* than those of *B. c.* This was a significant difference compared to the other variants, which all predicted washout of *S. a.* (A, C, D). The variants (C) and (D), which differed in the cell yield $Y_{X/Ace,Bc}$, still gave very similar simulation results.

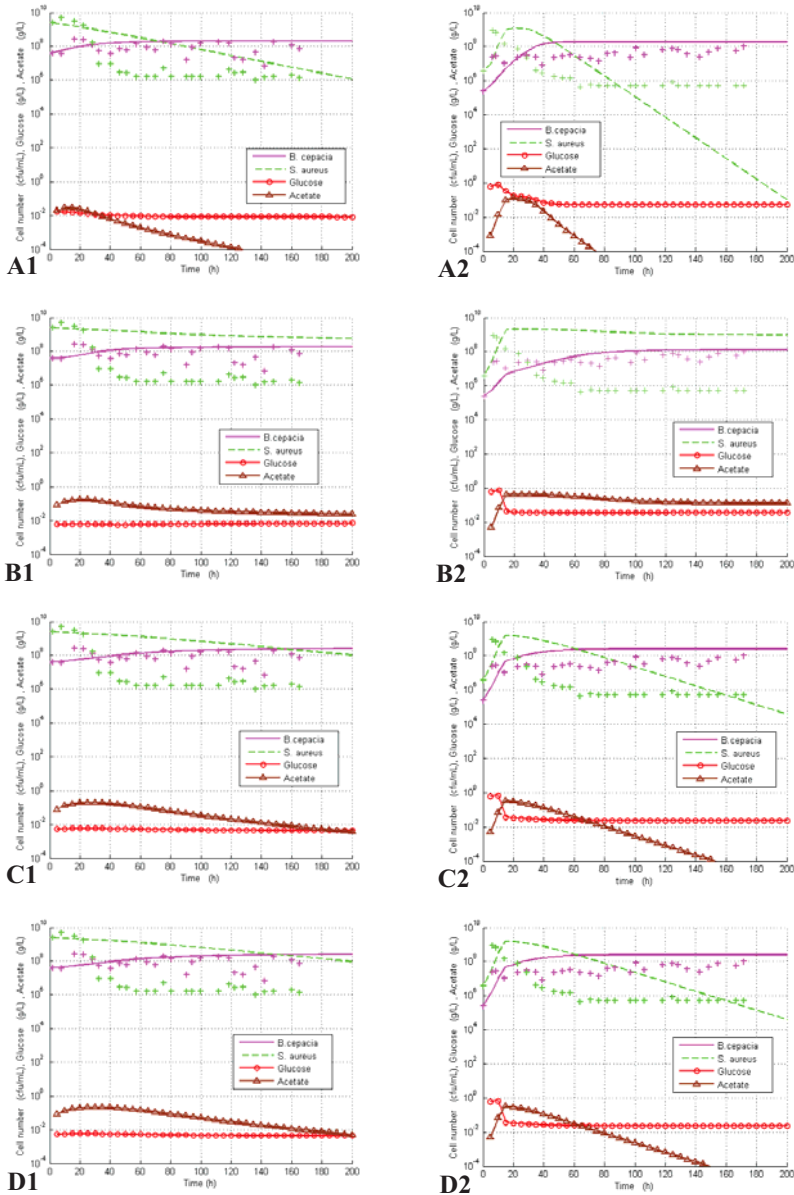


Figure 4.41: Simulation of two-species chemostat with acetate biotrophy (food chain): (1) $D = 0.05 \text{ h}^{-1}$; (2) $D = 0.2 \text{ h}^{-1}$. Different parameter sets from single-species batch experiments (small scale STR) with varied values as constraints (Table 4.10, Table 4.11).

The variants (C) and (D) (Figure 4.41) correlated with the experimental data for the assumption of washout of *S. a.* instead of its presence below the quantification limit. However, the predicted time course for coexistence did not correlate with the range of cell number values of *S. a.* (B).

4.4.3 Summary

Extension of the classic chemostat model with an indirect interaction via acetate biotrophy could explain coexistence of the two species *B. c.* and *S. a.*. However, depending on the chosen parameter set, the model also could explain washout of *S. a.*. Both simulation variants were calculated with parameters directly determined from single-species experiments.

Although coexistence of the two species was assumed from experimental data, *S. a.* was not detectable any more after 124 h in the chemostat experiment with dilution rate $D = 0.2 \text{ h}^{-1}$. Both interpretations of experimental data could be explained with a simulation and the related parameter sets, respectively. It was therefore not resolved yet, which simulation, respective parameter variant, was the correct or more realistic one.

By the explanation of a possible coexistence, depending on the chosen parameter set, the chemostat model with acetate biotrophy was an improvement compared to the classic chemostat model (Figure 4.40), which predicted washout of *S. a.*.

4.5 Investigation of Species Interactions in a Three-Species Chemostat

The three species *S. a.*, *B. c.*, and *P. a.* were co-cultivated in a CSTR in chemostat mode to investigate mixed culture growth dynamics in 2 L STR and small scale STR (0, 3.4.5.3). Cell numbers were determined with quantitative T-RFLP analysis (3.5.2). Afterwards, the observed mixed culture dynamic was analyzed with mathematical modeling and simulation.

4.5.1 Three-Species Chemostat Experiments in 2 L Stirred Tank

A three-species mixed culture chemostat experiments at a dilution rate $D = 0.05 \text{ h}^{-1}$ and a filling volume $V_L = 2.0 \text{ L}$ resulted in an apparently stable coexistence of the two species *B. c.* and *P. a.* (data not shown). After more than 9 volume exchanges (180 h) they were still detected by T-RFLP analysis in a range of $3 \cdot 10^7$ to $2 \cdot 10^8 \text{ cfu/mL}$. The cell numbers of *S. a.* decreased during the first 2.4 volume exchanges (48 h) and were afterwards below the quantification limit of the T-RFLP analysis method ($10^{5.8} \text{ cfu/mL}$; 4.2.2). After 4.5 volume exchanges about 10^5 cfu/mL of *S. a.* cells were still detected by selective agar plates, at the end of the cultivation the cell number of *S. a.* was $2 \cdot 10^4 \text{ cfu/mL}$.

In order to accelerate the system dynamics within the same time range (190 h) the next experiments were conducted at a dilution rate $D = 0.2 \text{ h}^{-1}$. The filling volume was changed to $V_L = 1.0 \text{ L}$ for a reduction of the required medium amount for the feed. The aim was to verify, whether the apparent coexistence phenomenon of *B. c.* and *P. a.* was reproducible and stable.

The result of a three-species chemostat experiment is given in Figure 4.42. At the end of the batch phase all three species were detected, *S. a.* and *P. a.* with about 10^9 cfu/mL and *B. c.* with about 10^8 cfu/mL . After switch to continuous process mode (5.7 h) an instationary phase of system stabilization was observed for about 60 h. After a first decrease of the cell numbers of all three species, *B. c.* stayed in a range of $10^{8.4} \text{ cfu/mL}$ and *S. a.* and *P. a.* decreased similarly until 45 h of cultivation. After this time point *S. a.* was not detected any more with T-RFLP analysis, it was below $10^{5.8} \text{ cfu/mL}$. The cell number of *P. a.* stabilized at about $10^{7.5} \text{ cfu/mL}$ and showed a similar and coherent dynamic as *B. c.* until the end of the cultivation, both then about $10^{8.4} \text{ cfu/mL}$ (170 h). The experiment confirmed the results of an apparent coexistence of at least two species (Figure 4.42) observed before at $D = 0.05 \text{ h}^{-1}$ (data not shown). The stability of the monitored pH value and the overall cell number (OD_{650}) supported the assumption of a stationary phase with at least two species in the chemostat.

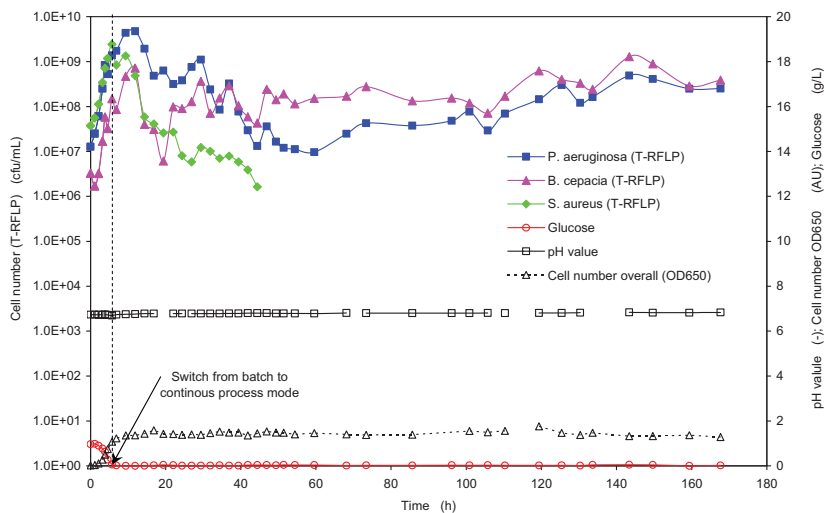


Figure 4.42: Three-species mixed culture in a chemostat: *S. a.*, *B. c.* and *P. a.* in M199+P+NTA medium. 2 L STR: $D = 0.2 \text{ h}^{-1}$, $V_L = 1.0 \text{ L}$, $n = 500 \text{ rpm}$, $q = 1 \text{ vvm}$.

In the experiment described above the inlet tube for the feed supply in the interior of the reactor vessel was short and positioned near the inner wall. This led to formation of a white biofilm above the liquid surface, where the medium flew into the broth. A repetition of the previous experiment under the same experimental conditions was therefore conducted after a constructive change for the feed supply tube (Figure 4.43). It was elongated and positioned closely over the liquid surface almost at the center of the reactor.

The growth dynamics and cell numbers during batch (6 h) and stabilization phase (about 50 h) were comparable to the experiment before. However, the cell number values seemed to differ more pronouncedly: $10^{8.2} \text{ cfu/mL}$ were measured for *B. c.* and $10^{6.5} \text{ cfu/mL}$ for *P. a.* at the end of the cultivation (175 h) in the second experiment compared to the first (both about $10^{8.4} \text{ cfu/mL}$). The time point at which *S. a.* was not detected any more by T-RFLP was almost the same, after 42 h and 45 h, respectively.

A difference between the two repetitive experiments (Figure 4.42 and Figure 4.43) was found in two aspects: a) the biofilm on the interior reactor wall above the culture surface had been successfully avoided by the change of position of the inlet feed tube and b) the dynamics of *B. c.* and *P. a.* in the stationary phase after about 50 h of cultivation were comparable but not equal. In the first experiment the cell numbers of both species reached equal values during the

continuous phase and at the same time showed some kind of oscillating behavior (Figure 4.42). In the experiment with reduced biofilm formation the cell number dynamic of both species had less oscillation, and a pronounced difference between the cell numbers was determined. In both experiments the overall cell number (OD₆₅₀) was stable during the continuous phase at about 1.5 AU.

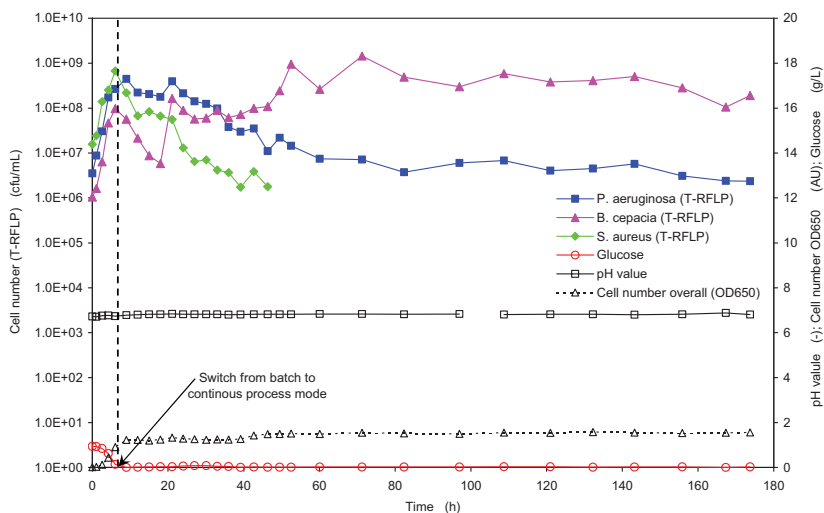


Figure 4.43: Repetition of three-species mixed culture in a chemostat: *S. a.*, *B. c.* and *P. a.* in M199+P+NTA medium. Feed inlet position changed for less biofilm wall growth above liquid surface. 2 L STR: $D = 0.2 \text{ h}^{-1}$, $V_L = 1.0 \text{ L}$, $n = 500 \text{ rpm}$, $q = 1 \text{ vvm}$.

Altogether, the coexistence result was reproducible and the experimental set-up worked very well and therefore could be used for further studies of defined mixed bacterial cultures.

The time courses of OTR and RQ of a three-species chemostat (Figure 4.43) were compared with single-species batch cultivations of *P. a.* (Figure 4.17), *B. c.* (Figure 4.14), and *S. a.* (Figure 4.11) (Figure 4.44 and Figure 4.45). The OTR curve of the mixed culture reached a higher maximum value (5.3 mM/h) than the two similar curves of *B. c.* and *P. a.*.

The time course of RQ of the mixed culture was similar to the one of *P. a.*. Both did not reach values significantly higher than 1.0, which corresponds to the theoretical value for complete glucose oxidation (Figure 4.45).

The comparison of OTR and RQ for the mixed culture and the single-species cultures indicated that the mixed culture had its own metabolic characteristics. These data supported the hypothesis that in the mixed culture interactions between the species occurred.

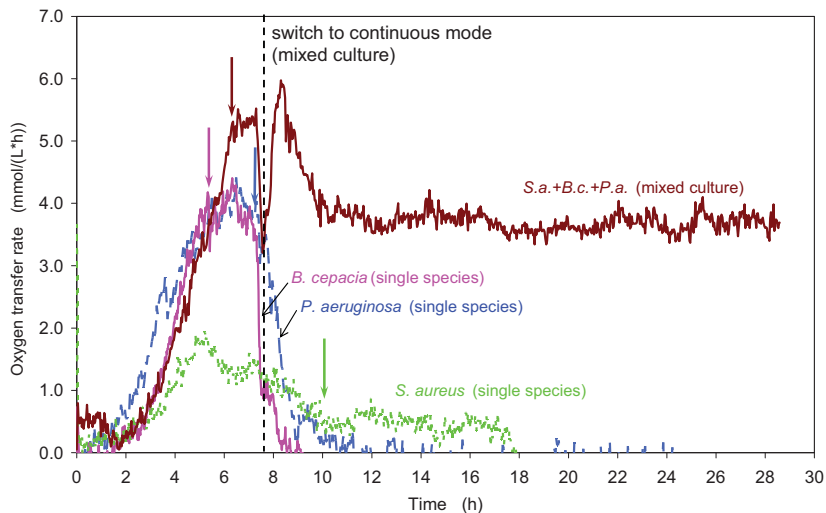


Figure 4.44: OTR during single-species (batch) and three-species mixed (continuous) cultivations in 2 L STR. Broad arrows indicate time points of glucose depletion.

Additional hints on differences in growth characteristics between the mixed culture and the single-species were provided by the HPLC analysis of culture samples. Peak profiles and dynamics differed significantly between the species and the mixed culture (data not shown). Most of the peaks were not identified automatically by the HPLC. As the focus was on cell number dynamics, the identification of the detected substances in the samples was omitted and the obtained raw data will not be presented here.

During continuous mode the RQ of the mixed culture was very stable and supported the assumption of a stable coexistence in the mixed culture. The RQ value of 0.5 indicated a possible uptake of amino acids known to result in low RQ values.

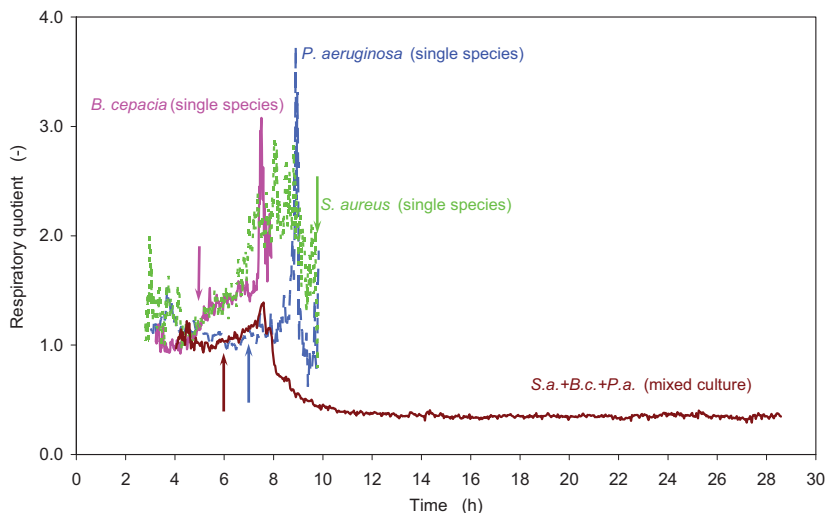


Figure 4.45: Respiratory quotients (RQ) during pure (batch) and mixed (continuous) cultivations in STR. Arrows indicate time point of glucose depletion. Batch data are not shown for beginning and end of cultivations due to high scatter.

4.5.2 Three-Species Chemostat Experiments in Small Scale STR

For further experimental characterization small scale STR were used with a filling volume of $V_L = 0.2$ L, what required less medium in continuous process mode. Additionally, they provided the possibility of four continuous cultivations in parallel.

Two three-species chemostat cultivations were conducted under standard conditions ($q = 0.0416$ vvm) (3.4.5.3) in the small scale STR. A third three-species chemostat cultivation was conducted with an aeration rate of $q = 0.416$ vvm to compare the aeration influence on the mixed cultures with the apparent effects found for the single-species, especially *S. a.* and *P. a.* (4.1.3). The dilution rate was $D = 0.2$ h⁻¹ for comparison with the experimental results of the 2 L scale. Amino acids were quantified in addition to the analysis of cell numbers and glucose in these chemostat experiments.

To investigate the role of glucose and amino acids as substrates for the mixed culture in the chemostat, a glucose pulse (20 g/L final concentration) and an amino acid pulse (10 g/L final concentration) were applied after 192 h and 213 h of cultivation time, respectively.

The results of one of the three chemostat cultivations in small scale STR are given in Figure 4.46. Phase (0) batch phase, phase (I) continuous process mode; phase (II) growth dynamics after the glucose pulse; phase (III) growth dynamics after the amino acid pulse.

At the end of the batch phase (6.5 h) the following cell numbers were determined by T-RFLP (3.5.2): *B. c.* $10^{7.0}$ cfu/mL, *P. a.* $10^{7.9}$ cfu/mL, and *S. a.* $10^{8.6}$ cfu/mL. The decrease in concentration of glucose and amino acids correlated with the increase in cell number. Acetate was not detected during the complete batch phase.

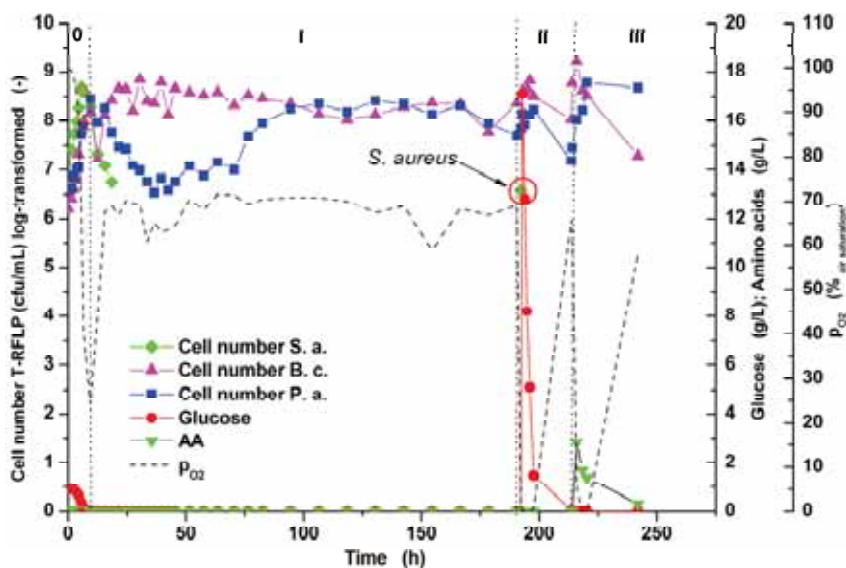


Figure 4.46: Three-species mixed culture experiment in a chemostat: *S. a.*, *B. c.* and *P. a.* in M199+P+NTA medium: (0) batch phase (I) continuous phase; (II) glucose pulse at $t = 192$ h, (III) amino acid pulse at $t = 213$ h. Small scale STR: $D = 0.2 \text{ h}^{-1}$, $V_L = 200 \text{ mL}$, $n = 300 \text{ rpm}$.

In the three-species mixed chemostat cultivation the two species *B. c.* and *P. a.* were detected until the end of the experiment (223 h), the cell numbers were stable and in the same range ($10^{8.0}$ cfu/mL) for both species after a stabilization phase (100 h). After 18 h of cultivation the cell number of *S. a.* was below its limit of quantification with quantitative T-RFLP analysis (about $10^{5.8}$ cfu/mL). With selective agar plates *S. a.* was detectable during the complete cultivation (223 h) in a range of $10^{2.0}$ cfu/mL to $10^{3.0}$ cfu/mL. Apparently, all three species were present in the mixed chemostat culture until the end of the experiment.

The sudden drop of p_{O_2} at about 150 h of cultivation time could not be explained and did not correlate to other data.

After the glucose pulse (192 h) the cell numbers of all three species increased and *S. a.* was detectable again with T-RFLP at about $10^{6.5}$ cfu/mL. In contrast to single-species experiments (4.3) lactate was detected as well.

After the amino acid pulse (213 h) an increase of cell numbers was determined for *B. c.* and *P. a.*, whereas *S. a.* apparently stayed below the quantification limit of the T-RFLP method. *S. a.* did either not form cells as well from amino acids as it did from glucose or *S. a.* was already washed out.

The results of the two parallel cultivation experiments with identical aeration ($q = 0.0416$ vvm) and an increased aeration rate ($q = 0.416$ vvm) were very well comparable and almost identical to the one presented above (Figure 4.46) (data not shown). This reproducibility showed two results: first, the successful establishment of an experimental method for the generation of a defined and controllable mixed culture. Secondly, a difference between mixed culture and single-species cultures regarding their sensitivity towards aeration was found. In contrast to the single-species cultures, no apparent effect of aeration, such as decreased cell numbers of *P. a.* compared to *B. c.* at higher aeration for example, was found for the mixed culture. Again this as already found for OTR and RQ curves indicated a significant change in growth characteristics by co-cultivation of the three species in comparison to the single species growth.

4.5.3 Mathematical Models of Three-Species Chemostat

4.5.3.1 Three-Species Chemostat Model with Single Substrate Competition

The classic chemostat model for competition of three species for one substrate (glucose) was formulated (eqn. syst. 4.22). The parameters applied in the simulations for dilution rates $D = 0.05 \text{ h}^{-1}$ and $D = 0.2 \text{ h}^{-1}$ were determined from single-species experiments with *S. a.*, *B. c.*, and *P. a.* (Table 4.10).

eqn. syst. 4.22

$$\begin{aligned} \frac{dX_{Sa}}{dt} &= \left(\frac{\mu_{\max,199,Sa} \cdot Glc}{Glc + K_{S,Sa}} \right) \cdot X_{Sa} - D \cdot X_{Sa}; & \frac{dX_{Bc}}{dt} &= \left(\frac{\mu_{\max,199,Bc} \cdot Glc}{Glc + K_{S,Bc}} \right) \cdot X_{Bc} - D \cdot X_{Bc}; \\ \frac{dX_{Pa}}{dt} &= \left(\frac{\mu_{\max,199,Pa} \cdot Glc}{Glc + K_{S,Pa}} \right) \cdot X_{Pa} - D \cdot X_{Pa}; \end{aligned}$$

$$\frac{dGlc}{dt} = \frac{1}{Y_{X/Glc,Sa}} \left(\frac{\mu_{max,199,Sa} \cdot Glc}{Glc + K_{S,Sa}} \right) \cdot X_{Sa} - \frac{1}{Y_{X/Glc,Bc}} \left(\frac{\mu_{max,199,Bc} \cdot Glc}{Glc + K_{S,Bc}} \right) \cdot X_{Bc} - \frac{1}{Y_{X/Glc,Pu}} \left(\frac{\mu_{max,199,Pu} \cdot Glc}{Glc + K_{S,Pu}} \right) \cdot X_{Pu} + D \cdot (Glc_m - Glc)$$

Simulations for the two dilution rates $D = 0.05 \text{ h}^{-1}$ and $D = 0.2 \text{ h}^{-1}$ for comparison with the experimental data (Figure 4.47), both predicted washout of the two species *S. a.* and *P. a.*. The washout of *P. a.* was more pronounced. *B. c.* was predicted to stay in the system as only species. At a dilution rate of $D = 0.2 \text{ h}^{-1}$ the simulated cell numbers of the two washed out species were below the quantification limit of T-RFLP analysis (about $10^{5.8} \text{ cfu/mL}$) at the end of the simulated cultivation time.

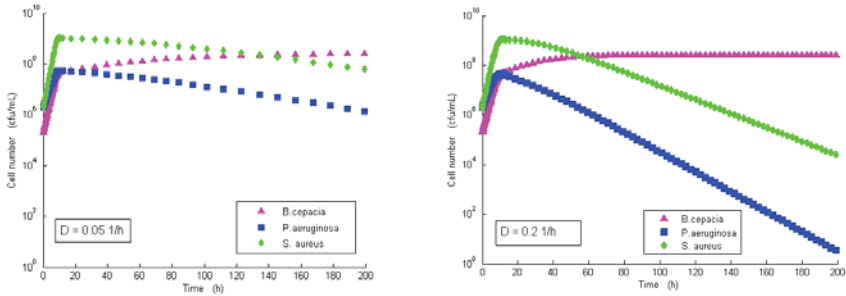


Figure 4.47: Simulation of three-species competition for one substrate, glucose in a chemostat (eqn. syst. 4.22). Parameters from single-species experiments.

The simulations with the classic chemostat model of competition for one substrate (2.4.1) (eqn. syst. 4.22) for the three-species mixed chemostat contradicted the experimental results of an apparent coexistence of at least two of the species, *B. c.* and *P. a.* (4.5.1).

4.5.3.2 Three-Species Chemostat Model with Acetate Biotrophy

For *S. a.* as acetate producer and *B. c.* as acetate consumer the hypothesis of a food chain was studied experimentally and mathematically (4.4). For the three-species mixed chemostat the respective model including *P. a.* as a second acetate consumer was formulated (eqn. syst. 4.23). It was investigated, if an acetate food chain could explain the observed coexistence phenomenon in the three-species chemostat experiment (Figure 4.46). Instead of the variation presented in the two-species analysis, here the biologically most meaningful parameters for each species were applied for the simulation (Figure 4.48) *S. a.* (Table 4.10, third column), *B. c.* (Table 4.11, third column), and *P. a.* (Table 4.12, fourth column).

eqn. syst. 4.23

$$\begin{aligned}\mu_{199,Sa} &= \frac{\mu_{\max,199,Sa} \cdot Glc}{K_{S,Sa} + Glc} \\ \mu_{199,Bc} &= \frac{\mu_{\max,199,Bc} \cdot Glc}{K_{S,Glc,Bc} + Glc}; & \mu_{Ace,Bc} &= \frac{\mu_{\max,Ace,Bc} \cdot Ace}{K_{S,Ace,Bc} + Ace} \\ \mu_{199,Pa} &= \frac{\mu_{\max,199,Pa} \cdot Glc}{K_{S,Glc,Pa} + Glc}; & \mu_{Ace,Pa} &= \frac{\mu_{\max,Ace,Pa} \cdot Ace}{K_{S,Ace,Pa} + Ace} \\ \frac{dX_{Sa}}{dt} &= \mu_{199,Sa} \cdot X_{Sa} - D \cdot X_{Sa}; & \frac{dX_{Bc}}{dt} &= \mu_{199,Bc} \cdot X_{Bc} + \mu_{Ace,Bc} \cdot X_{Bc} - D \cdot X_{Bc} \\ \frac{dX_{Pa}}{dt} &= \mu_{199,Pa} \cdot X_{Pa} + \mu_{Ace,Pa} \cdot X_{Pa} - D \cdot X_{Pa} \\ \frac{dGlc}{dt} &= -\frac{1}{Y_{X/Glc,Sa}} \cdot \mu_{199,Sa} \cdot X_{Sa} - \frac{1}{Y_{X/Glc,Bc}} \cdot \mu_{199,Bc} \cdot X_{Bc} - \frac{1}{Y_{X/Glc,Pa}} \cdot \mu_{199,Pa} \cdot X_{Pa} + D \cdot (Glc_{in} - Glc) \\ \frac{dAce}{dt} &= Y_{Ace/X,Sa} \cdot \mu_{199,Sa} \cdot X_{Sa} - \frac{1}{Y_{X/Ace,Bc}} \cdot \mu_{Ace,Bc} \cdot X_{Bc} - \frac{1}{Y_{X/Ace,Pa}} \cdot \mu_{Ace,Pa} \cdot X_{Pa} - D \cdot Ace\end{aligned}$$

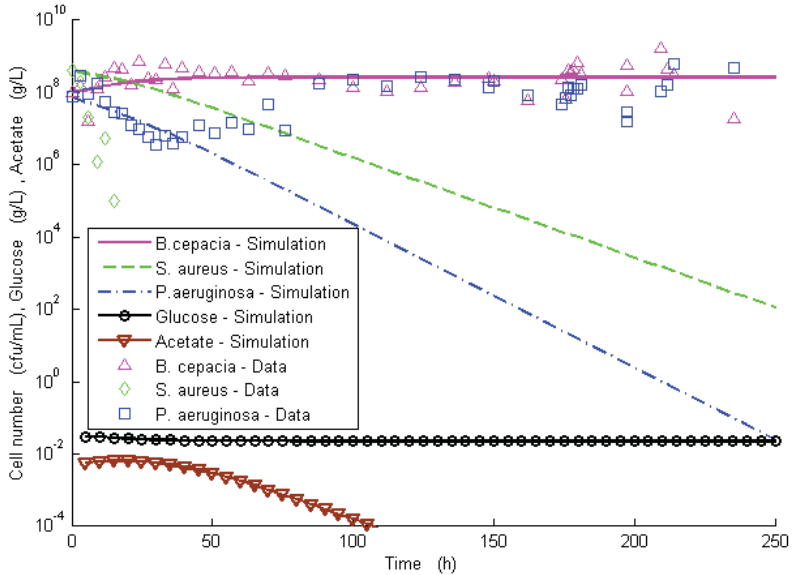


Figure 4.48: Simulation of three-species chemostat assuming competition for glucose and acetate biotrophy with *S. a.* as acetate producer, *B. c.* and *P. a.* as acetate consumers (eqn. syst. 4.23). Parameters determined from single-species experiments. Experimental data from three-species mixed culture experiment (Figure 4.46).

The simulation of competition for glucose together with an acetate food chain still predicted washout of the two species *P. a.* and *S. a.*. Again it did not describe the experimental result of apparent coexistence of the two species *B. c.* and *P. a.*. The cell number of *B. c.* of about $10^{8.3}$ cfu/mL as remaining species, however was represented very well by the model simulation.

4.5.3.3 Three-Species Chemostat Models with Mixed Substrate Growth

In single-species analysis amino acids were found to serve as additional substrate to glucose for *P. a.* (Figure 4.26) and *B. c.* (Figure 4.25). *S. a.* consumed amino acids as well, but was known and found to require amino acids together with glucose, which led to a formulation of the respective kinetic for dependent use of mixed substrates (eqn. syst. 4.10).

In the following it was therefore investigated what possible affect the mixed substrate use had on the three-species growth dynamics in the chemostat. In order to separately investigate different assumptions the acetate biotrophy was not considered in a first approach. The input concentrations of glucose and of the sum of amino acids were $Glc_{in} = 1$ g/L and $AA_{in} = 0.6$ g/L, respectively. The cell numbers at the switch between batch and process mode were taken from experimental data as: *B. c.* 10^8 cfu/mL, *P. a.* $10^{7.88}$ cfu/mL and *S. a.* $10^{8.61}$ cfu/mL. The batch phase itself was not included in the model simulation to reduce the number of possible variations to the chemostat mode.

Two basic models for mixed substrate growth on glucose and amino acids were formulated. For *S. a.* in both variants the same kinetic for dependent growth on the two substrates was used (eqn. syst. 4.10). For *B. c.* in both variants the formulation with diauxic growth was used (eqn. syst. 4.13).

Mixed substrate chemostat model No. 1 (eqn. syst. 4.24) was based on the kinetic formulation (A) with one $\mu_{max,199,i}$ proposed for single-species kinetics of *B. c.* (eqn. syst. 4.14) and *P. a.* (eqn. syst. 4.15).

Mixed substrate chemostat model No. 2 (eqn. syst. 4.25) was based on the kinetic formulation (B) with two separate kinetic expressions for growth on glucose and amino acids for *B. c.* (eqn. syst. 4.18) and *P. a.* (eqn. syst. 4.19).

eqn. syst. 4.24

$$\begin{aligned}\frac{dX_{Sa}}{dt} &= \mu_{\max,199,Sa} \cdot \left(\frac{Glc}{Glc + K_{S,Glc,Sa}} \cdot \frac{AA}{AA + K_{S,AA,Sa}} \right) \cdot X_{Sa} - D \cdot X_{Sa} \\ \frac{dX_{Bc}}{dt} &= \mu_{\max,199,Bc} \cdot \left(\frac{Glc}{Glc + K_{S,Glc,Bc}} + \frac{AA}{AA + K_{S,AA,Bc} \cdot (1 + Glc/K_I)} \right) \cdot X_{Bc} - D \cdot X_{Bc} \\ \frac{dX_{Pa}}{dt} &= \mu_{\max,199,Pa} \cdot \left(\frac{Glc}{Glc + K_{S,Glc,Pa}} + \frac{AA}{AA + K_{S,AA,Pa}} \right) \cdot X_{Pa} - D \cdot X_{Pa}\end{aligned}$$

Substrates:

$$\begin{aligned}\frac{dGlc}{dt} &= \frac{1}{Y_{X/Glc,Sa}} \cdot \mu_{\max,199,Sa} \cdot \left(\frac{Glc}{Glc + K_{S,Glc,Sa}} \cdot \frac{AA}{AA + K_{S,AA,Sa}} \right) \cdot X_{Sa} - \frac{1}{Y_{X/Glc,Bc}} \cdot \mu_{\max,199,Bc} \cdot \left(\frac{Glc}{Glc + K_{S,Glc,Bc}} + \frac{AA}{AA + K_{S,AA,Bc} \cdot (1 + Glc/K_I)} \right) \cdot X_{Bc} - \dots \\ &\dots \frac{1}{Y_{X/Glc,Pa}} \cdot \mu_{\max,199,Pa} \cdot \left(\frac{Glc}{Glc + K_{S,Glc,Pa}} + \frac{AA}{AA + K_{S,AA,Pa}} \right) \cdot X_{Pa} + D \cdot (Glc_m - Glc) \\ \frac{dAA}{dt} &= -\frac{1}{Y_{X/AA,Sa}} \cdot \mu_{\max,199,Sa} \cdot \left(\frac{Glc}{Glc + K_{S,Glc,Sa}} \cdot \frac{AA}{AA + K_{S,AA,Sa}} \right) \cdot X_{Sa} - \frac{1}{Y_{X/AA,Bc}} \cdot \mu_{\max,199,Bc} \cdot \left(\frac{Glc}{Glc + K_{S,Glc,Bc}} + \frac{AA}{AA + K_{S,AA,Bc} \cdot (1 + Glc/K_I)} \right) \cdot X_{Bc} - \dots \\ &\dots \frac{1}{Y_{X/AA,Pa}} \cdot \mu_{\max,199,Pa} \cdot \left(\frac{Glc}{Glc + K_{S,Glc,Pa}} + \frac{AA}{AA + K_{S,AA,Pa}} \right) \cdot X_{Pa} + D \cdot (AA_m - AA)\end{aligned}$$

Metabolite:

$$\frac{dAce}{dt} = Y_{Ace/X,Sa} \cdot \mu_{\max,199,Sa} \cdot \left(\frac{Glc}{Glc + K_{S,Glc,Sa}} \cdot \frac{AA}{AA + K_{S,AA,Sa}} \right) \cdot X_{Sa} - D \cdot X_{Sa}$$

The simulation of the mixed substrate chemostat model variant No. 1 was performed (Figure 4.49) with the respective parameters from the single-species experiments for *S. a.* (Table 4.15), *B. c.* (Table 4.18), and *P. a.* (Table 4.19). A summary is given in Table 4.25.

The simulation of the three-species chemostat experiment included the glucose and amino acid pulses as described in the experimental section for comparison of the system dynamics.

Table 4.25: Parameters determined from single-species data and applied for the simulation of mixed substrate chemostat model No. 1 (eqn. syst. 4.24).

Parameter	Unit	<i>S. a.</i>	<i>B. c.</i>	<i>P. a.</i>
$\mu_{\max,199,i}$	h^{-1}	0.83	0.67	0.54
$K_{S,AA,i}$	g/L	0.0055	0.003	0.057
$K_{S,Glc,i}$	g/L	0.11	0.063	0.027
$Y_{X/AA,i}$	cfu/g	$6.2 \cdot 10^{12}$	$4.9 \cdot 10^{11}$	$7.2 \cdot 10^{11}$
$Y_{X/Glc,i}$	cfu/g	$1.4 \cdot 10^{12}$	$3.2 \cdot 10^{11}$	$5.8 \cdot 10^{11}$
K_I	g/L		0.51	
$Y_{Ace/X,Sa}$	g/cfu	$2.77 \cdot 10^{-12}$		

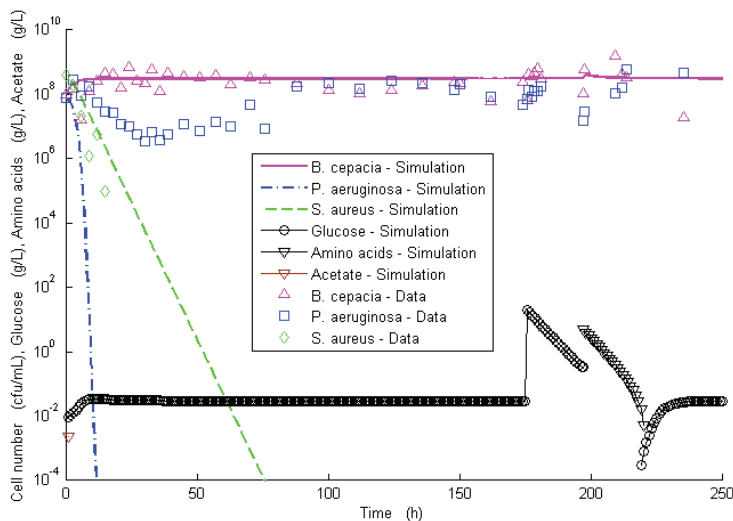


Figure 4.49: Simulation three-species chemostat model variant No. 1 (eqn. syst. 4.24) for mixed substrate growth on glucose and amino acids. Parameters determined from single-species experiments with the same model assumptions (Table 4.25). Experimental data from three-species mixed culture experiment (Figure 4.46). Glucose and amino acid pulse included in the simulation and the experimental data.

The simulation of the three-species chemostat with mixed substrate use (No. 1; eqn. syst. 4.24) predicted a very quick washout of *P. a.* and afterwards of *S. a.*. This simulation result did not describe the experimental result of an apparent coexistence of at least two of the three species (Figure 4.49). However, the cell numbers of *S. a.* and of *B. c.* were well represented.

The reaction of the mixed culture to the glucose and amino acid pulse was less pronounced in this simulation than in the experimental result. Additionally, at the time point of the pulses in the simulation only *B. c.* was still in the chemostat. In the experiment both species, *B. c.* and *P. a.* were affected by the pulses. Surprisingly, the predicted increase in cell number of *B. c.* by the pulsed substrates was less pronounced than the one observed in the experiment.

The simulation of the mixed substrate chemostat model variant No. 2 (eqn. syst. 4.25) was performed (Figure 4.50) with the respective parameters determined from the single-species experiments for *S. a.* (Table 4.15), *B. c.* (Table 4.21), and *P. a.* (Table 4.22). The summary of parameters is given in Table 4.26.

The simulation of the three-species chemostat experiment included the glucose and amino acid pulses as described in the experimental section for comparison of the system dynamics.

eqn. syst. 4.25

$$\frac{dX_{Sa}}{dt} = \mu_{\max,199,Sa} \cdot \left(\frac{Glc}{Glc + K_{S,Glc,Sa}} \cdot \frac{AA}{AA + K_{S,AA,Sa}} \right) \cdot X_{Sa} - D \cdot X_{Sa}$$

$$\frac{dX_{Bc}}{dt} = \left(\frac{\mu_{\max,Glc,Bc} \cdot Glc}{Glc + K_{S,Glc,Bc}} + \frac{\mu_{\max,AA,Bc} \cdot AA}{AA + K_{S,AA,Bc} \cdot (1 + Glc/K_I)} \right) \cdot X_{Bc} - D \cdot X_{Bc}$$

$$\frac{dX_{Pa}}{dt} = \left(\frac{\mu_{\max,Glc,Pa} \cdot Glc}{Glc + K_{S,Glc,Pa}} + \frac{\mu_{\max,AA,Pa} \cdot AA}{AA + K_{S,AA,Pa}} \right) \cdot X_{Pa} - D \cdot X_{Pa}$$

Substrate:

$$\begin{aligned} \frac{dGlc}{dt} = & \frac{1}{Y_{X/Glc,Sa}} \cdot \mu_{\max,199,Sa} \cdot \left(\frac{Glc}{Glc + K_{S,Glc,Sa}} \cdot \frac{AA}{AA + K_{S,AA,Sa}} \right) \cdot X_{Sa} - \frac{1}{Y_{X/Glc,Bc}} \cdot \left(\frac{\mu_{\max,Glc,Bc} \cdot Glc}{Glc + K_{S,Glc,Bc}} \right) \cdot X_{Bc} - \dots \\ & \dots \frac{1}{Y_{X/Glc,Pa}} \cdot \left(\frac{\mu_{\max,Glc,Pa} \cdot Glc}{Glc + K_{S,Glc,Pa}} \right) \cdot X_{Pa} + D \cdot (Glc_{in} - Glc) \end{aligned}$$

$$\begin{aligned} \frac{dAA}{dt} = & \frac{1}{Y_{X/AA,Sa}} \cdot \mu_{\max,199,Sa} \cdot \left(\frac{Glc}{Glc + K_{S,Glc,Sa}} \cdot \frac{AA}{AA + K_{S,AA,Sa}} \right) \cdot X_{Sa} - \frac{1}{Y_{X/AA,Bc}} \cdot \left(\frac{\mu_{\max,AA,Bc} \cdot AA}{AA + K_{S,AA,Bc} \cdot (1 + Glc/K_I)} \right) \cdot X_{Bc} - \dots \\ & \dots \frac{1}{Y_{X/AA,Pa}} \cdot \left(\frac{\mu_{\max,AA,Pa} \cdot AA}{AA + K_{S,AA,Pa}} \right) \cdot X_{Pa} + D \cdot (AA_{in} - AA) \end{aligned}$$

Metabolite:

$$\frac{dAce}{dt} = Y_{Ace/X,Sa} \cdot \mu_{\max,199,Sa} \cdot \left(\frac{Glc}{Glc + K_{S,Glc,Sa}} \cdot \frac{AA}{AA + K_{S,AA,Sa}} \right) \cdot X_{Sa} - D \cdot X_{Sa}$$

Table 4.26: Parameters determined from single-species experimental data and applied for the simulation of mixed substrate chemostat model No. 2 (eqn. syst. 4.25).

Parameter	Unit	S. a.	B. c.	P. a.
$\mu_{\max,199,Sa}$	h^{-1}	0.83		
$\mu_{\max,Glc,i}$	h^{-1}		0.74	0.34
$\mu_{\max,AA,i}$	h^{-1}		0.67	0.67
$K_{S,Glc,i}$	g/L	0.006	0.007	0.012
$K_{S,AA,i}$	g/L	0.11	0.04	0.001
$Y_{X/AA,i}$	cfu/g	$6.2 \cdot 10^{12}$	$1.8 \cdot 10^{11}$	$3.2 \cdot 10^{11}$
$Y_{X/Glc,i}$	cfu/g	$1.4 \cdot 10^{12}$	$2.3 \cdot 10^{11}$	$2.8 \cdot 10^{11}$
K_I	g/L		0.34	
$Y_{Ace/X,Sa}$	g/cfu	$2.77 \cdot 10^{-12}$		

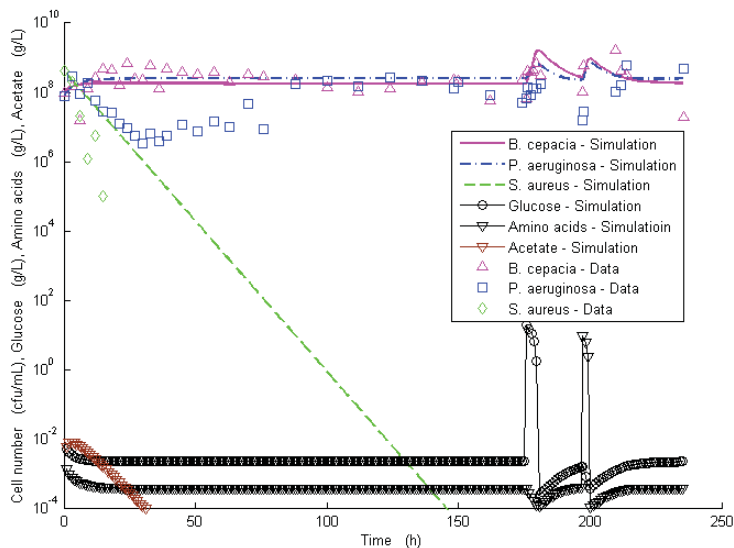


Figure 4.50: Simulation of three-species chemostat model variant No. 2 (eqn. syst. 4.25) for mixed substrate growth on glucose and amino acids. Parameters determined from single-species experiments with the same model assumptions (Table 4.26). Experimental data from three-species mixed culture experiment (Figure 4.46). Glucose and amino acid pulse included in the simulation and the experimental data.

The mixed substrate chemostat model variant No. 2 predicted stable coexistence of the two species *B. c.* and *P. a.* (Figure 4.50), which very well correlated with the experimental finding. The experimental cell number value range was very well represented by the simulation as well as the reaction to the glucose and amino acid pulses. The washout of *S. a.* was described, but slower than seen in the experiment. However, the growth dynamics of *P. a.* during the instationary phase in the continuous cultivation directly after the batch phase was not described by the simulation.

The reaction of the mixed culture to the glucose and the amino acid pulse was represented comparatively well concerning cell number increase of *B. c.* and *P. a.*. The appearance of *S. a.* above the quantification limit, as observed in the experiment, was not predicted. This was probably due to the predicted washout of *S. a.* (very low cell number) at the time point of glucose and amino acid pulses.

To test for stability of the coexistence of two populations, a simulation of 1000 h cultivation time was performed (data not shown), which did not indicate washout of either one of the apparently coexisting species *B. c.* and *P. a.* (Figure 4.46).

4.5.3.4 Studies of the Properties of Model Variant No. 2 to Explain Coexistence

Two variations of the mixed substrate model No. 2 were simulated to evaluate the function of the two substrates glucose and amino acids (no graphs shown). For the first variation the amino acid concentration in the feed AA_{in} was set to zero, for the second the glucose concentration in the feed Glc_{in} was set to zero.

As a result of the first scenario (glucose) *B. c.* stayed in the reactor and *P. a.* was washed out. For the second scenario (amino acids) *P. a.* survived and *B. c.* was washed out. As expected *S. a.* was washed out in both simulations, because the model assumption considered its growth to be dependent on the presence of the two substrates, glucose and amino acids.

In a further simulation study of the system it was tested, why *S. a.* was the species to be washed out of the system and how in theory with model No. 2 at least this could be circumvented. For this investigation single kinetic parameters and model assumptions concerning *S. a.* were changed compared to the original model No. 2. The model equations and parameters for *B. c.* and *P. a.* were applied as given in eqn. syst. 4.25 and Table 4.26, respectively. The results of the different variants are given in Figure 4.51.

A change of the three-species dynamic simulated with the pure culture parameters was achieved for a different affinity of *S. a.* for amino acids (B) and (E). The assumption of a different growth kinetic of *S. a.* on amino acids to consider the experimentally found property to grow on amino acids without glucose did not result in a change of the overall dynamic (C).

Varied model assumption	Simulation result	Effect
<p>(A) assumption: <i>S. a.</i> had highest affinity for glucose</p> <p>$K_{S,Glc,Sa} = 0.0001 \text{ g/L}$</p>		No changes
<p>(B) assumption: <i>S. a.</i> had highest affinity for amino acids</p> <p>$K_{S,AA,Sa} = 0.0001 \text{ g/L}$</p>		<i>S. a.</i> stayed in longer, but no stable three-species coexistence
<p>(C) consideration of growth of <i>S. a.</i> only on amino acids (Figure 4.24): extension of growth kinetic with</p> $\mu_{AA,Sa} = \frac{\mu_{max,AA,Sa} \cdot AA}{AA + K_{S,AA,Sa}}$ <p>$\mu_{max,AA,Sa} = 0.5 \text{ h}^{-1}$ (Table 4.13)</p>		No changes
<p>(D) combination of (A) and (C)</p>		No changes
<p>(E) combination of (B) and (C)</p>		<i>S. a.</i> and <i>B. c.</i> formed stable two-species coexistence, <i>P. a.</i> was washed out.

Figure 4.51: Simulations of mixed substrate model No. 2 with varied assumptions for properties of *S. a.* concerning consumption of glucose and amino acids to test for the dependencies among the species in the mixed culture and possibilities to circumvent the CEP.

4.5.3.5 Chemostat Model Variants to Generate Three-Species Coexistence

The experimental three-species chemostat data obtained with selective agar plates for *S. a.* (3.2.2.2) indicated the presence of the respective species below the quantification limit of quantitative T-RFLP analysis method. It was therefore theoretically investigated with three-species chemostat models, which could be an explanation for such a three-species coexistence in the system of interest (4.5.3.5).

As a first variant of the mixed substrate chemostat model No. 2 (eqn. syst. 4.25) was formulated by integration of the acetate biotrophy, which had been analyzed separately before for the two- and three-species chemostat (4.4.2 and 4.5.3.2). The resulting model equations were formulated as given in eqn. syst. 4.26 as a combination of the assumptions before. The same parameters as in single-species experiments were used (Table 4.27). The simulation result is given in Figure 4.52.

eqn. syst. 4.26

$$\begin{aligned}\frac{dX_{Sa}}{dt} &= \mu_{\max,199,Sa} \cdot \left(\frac{Glc}{Glc + K_{S,Glc,Sa}} \cdot \frac{AA}{AA + K_{S,AA,Sa}} \right) \cdot X_{Sa} - D \cdot X_{Sa} \\ \frac{dX_{Bc}}{dt} &= \left(\frac{\mu_{\max,Glc,Bc} \cdot Glc}{Glc + K_{S,Glc,Bc}} + \frac{\mu_{\max,Ace,Bc} \cdot Ace}{Ace + K_{S,Ace,Bc}} + \frac{\mu_{\max,AA,Bc} \cdot AA}{AA + K_{S,AA,Bc} \cdot (1 + Glc/K_I)} \right) \cdot X_{Bc} - D \cdot X_{Bc} \\ \frac{dX_{Pa}}{dt} &= \left(\frac{\mu_{\max,Glc,Pa} \cdot Glc}{Glc + K_{S,Glc,Pa}} + \frac{\mu_{\max,Ace,Pa} \cdot Ace}{Ace + K_{S,Ace,Pa}} + \frac{\mu_{\max,AA,Pa} \cdot AA}{AA + K_{S,AA,Pa}} \right) \cdot X_{Pa} - D \cdot X_{Pa}\end{aligned}$$

Substrate:

$$\begin{aligned}\frac{dGlc}{dt} &= \frac{1}{Y_{X/Glc,Sa}} \cdot \mu_{\max,199,Sa} \cdot \left(\frac{Glc}{Glc + K_{S,Glc,Sa}} \cdot \frac{AA}{AA + K_{S,AA,Sa}} \right) \cdot X_{Sa} - \frac{1}{Y_{X/Glc,Bc}} \cdot \left(\frac{\mu_{\max,Glc,Bc} \cdot Glc}{Glc + K_{S,Glc,Bc}} \right) \cdot X_{Bc} - \dots \\ &\dots \frac{1}{Y_{X/Glc,Pa}} \cdot \left(\frac{\mu_{\max,Glc,Pa} \cdot Glc}{Glc + K_{S,Glc,Pa}} \right) \cdot X_{Pa} + D \cdot (Glc_{in} - Glc) \\ \frac{dAA}{dt} &= \frac{1}{Y_{X/AA,Sa}} \cdot \mu_{\max,199,Sa} \cdot \left(\frac{Glc}{Glc + K_{S,Glc,Sa}} \cdot \frac{AA}{AA + K_{S,AA,Sa}} \right) \cdot X_{Sa} - \frac{1}{Y_{X/AA,Bc}} \cdot \left(\frac{\mu_{\max,AA,Bc} \cdot AA}{AA + K_{S,AA,Bc} \cdot (1 + Glc/K_I)} \right) \cdot X_{Bc} - \dots \\ &\dots \frac{1}{Y_{X/AA,Pa}} \cdot \left(\frac{\mu_{\max,AA,Pa} \cdot AA}{AA + K_{S,AA,Pa}} \right) \cdot X_{Pa} + D \cdot (AA_{in} - AA)\end{aligned}$$

Metabolite:

$$\begin{aligned}\frac{dAce}{dt} &= Y_{Ace/X,Sa} \cdot \mu_{\max,199,Sa} \cdot \left(\frac{Glc}{Glc + K_{S,Glc,Sa}} \cdot \frac{AA}{AA + K_{S,AA,Sa}} \right) \cdot X_{Sa} \\ &- \frac{1}{Y_{X/Ace,Bc}} \cdot \frac{\mu_{\max,Ace,Bc} \cdot Ace}{Ace + K_{S,Ace,Bc}} \cdot X_{Bc} - \frac{1}{Y_{X/Ace,Pa}} \cdot \frac{\mu_{\max,Ace,Pa} \cdot Ace}{Ace + K_{S,Ace,Pa}} \cdot X_{Pa} - D \cdot X_{Sa}\end{aligned}$$

Table 4.27: Parameters for simulation of mixed substrate chemostat model No. 2 (Table 4.26) extended with acetate biotrophy (food chain) (eqn. syst. 4.26), extended with competition for three substrates: glucose, valine (*Val*) and the rest of amino acids (eqn. syst. 4.27), and extended with a biotrophy (*Pr*) between *P. a.* and *S. a.* (eqn. syst. 4.28)

Parameter	Unit	<i>S. a.</i>	<i>B. c.</i>	<i>P. a.</i>
$\mu_{max,M199,i}$	h^{-1}	0.83	0.67	0.54
$\mu_{max,Glc,i}$	h^{-1}		0.74	0.34
$\mu_{max,AA,i}$	h^{-1}		0.67	0.67
$K_{S,Glc,i}$	g/L	0.006	0.007	0.012
$K_{S,AA,i}$	g/L	0.11	0.04	0.001
$Y_{X/AA,i}$	cfu/g	$6.2 \cdot 10^{12}$	$1.8 \cdot 10^{11}$	$3.3 \cdot 10^{11}$
$Y_{X/Glc,i}$	cfu/g	$1.4 \cdot 10^{12}$	$2.3 \cdot 10^{11}$	$2.9 \cdot 10^{11}$
K_I	g/L		0.34	
$Y_{Ace/X,i}$	g/cfu	$2.77 \cdot 10^{-12}$		
$\mu_{max,Ace,i}$	h^{-1}		0.04	0.34
$K_{S,Ace,i}$	g/L		0.67	0.22
$Y_{X/Ace,i}$	cfu/g		$0.92 \cdot 10^{11}$	$0.45 \cdot 10^{11}$
$\mu_{max,Val,i}$	h^{-1}	1	0.1	0.1
$K_{S,Val,i}$	g/L	0.008	0.8	0.8
$Y_{X/Val,i}$	cfu/g	$1.0 \cdot 10^{11}$	$1.0 \cdot 10^{11}$	$1.0 \cdot 10^{11}$
$\mu_{max,Pr,Sa}$	h^{-1}	0.4		
$K_{S,Pr,Sa}$	g/L	0.01		
$Y_{X/Pr,i}$	cfu/g	$1.0 \cdot 10^{10}$		
$Y_{Pr/X,Pa}$	g/cfu			$1.0 \cdot 10^{-11}$

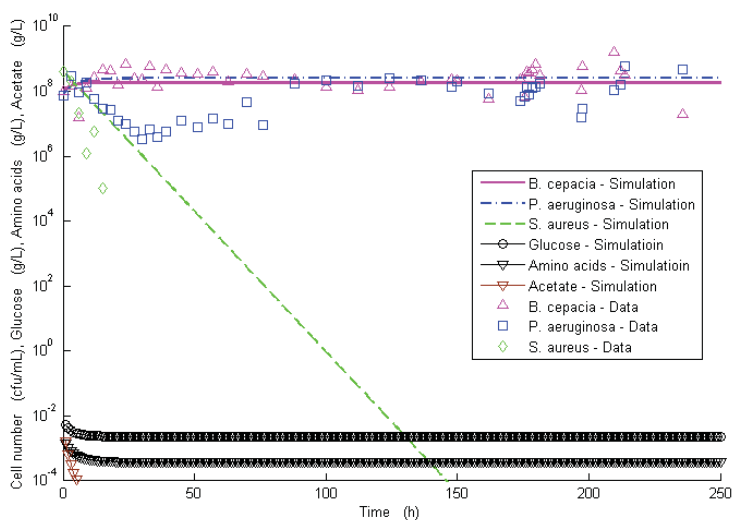


Figure 4.52: Simulation of mixed substrate three-species chemostat model No. 2 extended with acetate biotrophy for *S. a.*, *B. c.* and *P. a.* (Table 4.27 and eqn. syst. 4.26).

The combined model assumptions of the experimentally found properties of the single-species so far, mixed substrate use and acetate biotrophy did not predict a three-species coexistence (Figure 4.52). It was therefore no possible explanation for the observed experimental results in the three-species chemostat experiment.

The next model variation to test for an explanation of the possible three-species coexistence was based on the hypothesis *S. a.* had a very high affinity for one of the amino acids, namely valine. The assumption was based on own experimental results and reports in literature, valine was taken up quickest of all amino acids by *S. a.* (2.1.3.1). The model described therefore the competition of all three species, *S. a.*, *P. a.*, and *B. c.* for three substrates: glucose, valine and the other amino acids (eqn. syst. 4.27). The parameters for all kinetics were kept the same as before (4.5.3.3) determined from single-species data. The parameters for valine consumption were deliberately chosen with highest affinity for *S. a.* (Table 4.27).

eqn. syst. 4.27

$$\begin{aligned}\frac{dX_{Sa}}{dt} &= \mu_{\max,199,Sa} \cdot \left(\frac{Glc}{Glc + K_{S,Glc,Sa}} \cdot \frac{AA}{AA + K_{S,AA,Sa}} \right) \cdot X_{Sa} + \mu_{\max,Val,Sa} \cdot \frac{Val}{Val + K_{S,Val,Sa}} \cdot X_{Sa} - D \cdot X_{Sa} \\ \frac{dX_{Bc}}{dt} &= \frac{\mu_{\max,Glc,Bc} \cdot Glc}{Glc + K_{S,Glc,Bc}} \cdot X_{Bc} + \frac{\mu_{\max,AA,Bc} \cdot AA}{AA + K_{S,AA,Bc} \cdot (1 + Glc/K_I)} \cdot X_{Bc} + \frac{\mu_{\max,Val,Bc} \cdot Val}{Val + K_{S,Val,Bc}} \cdot X_{Bc} - D \cdot X_{Bc} \\ \frac{dX_{Pa}}{dt} &= \frac{\mu_{\max,Glc,Pa} \cdot Glc}{Glc + K_{S,Glc,Pa}} \cdot X_{Pa} + \frac{\mu_{\max,AA,Pa} \cdot AA}{AA + K_{S,AA,Pa}} \cdot X_{Pa} + \frac{\mu_{\max,Val,Pa} \cdot Val}{Val + K_{S,Val,Pa}} \cdot X_{Pa} - D \cdot X_{Pa}\end{aligned}$$

Substrate:

$$\begin{aligned}\frac{dGlc}{dt} &= \frac{1}{Y_{X/Glc,Sa}} \cdot \mu_{\max,199,Sa} \cdot \left(\frac{Glc}{Glc + K_{S,Glc,Sa}} \cdot \frac{AA}{AA + K_{S,AA,Sa}} \right) \cdot X_{Sa} - \frac{1}{Y_{X/Glc,Bc}} \cdot \left(\frac{\mu_{\max,Glc,Bc} \cdot Glc}{Glc + K_{S,Glc,Bc}} \right) \cdot X_{Bc} - \dots \\ &\dots \frac{1}{Y_{X/Glc,Pa}} \cdot \left(\frac{\mu_{\max,Glc,Pa} \cdot Glc}{Glc + K_{S,Glc,Pa}} \right) \cdot X_{Pa} + D \cdot (Glc_{in} - Glc) \\ \frac{dAA}{dt} &= \frac{1}{Y_{X/AA,Sa}} \cdot \mu_{\max,199,Sa} \cdot \left(\frac{Glc}{Glc + K_{S,Glc,Sa}} \cdot \frac{AA}{AA + K_{S,AA,Sa}} \right) \cdot X_{Sa} - \frac{1}{Y_{X/AA,Bc}} \cdot \left(\frac{\mu_{\max,AA,Bc} \cdot AA}{AA + K_{S,AA,Bc} \cdot (1 + Glc/K_I)} \right) \cdot X_{Bc} - \dots \\ &\dots \frac{1}{Y_{X/AA,Pa}} \cdot \left(\frac{\mu_{\max,AA,Pa} \cdot AA}{AA + K_{S,AA,Pa}} \right) \cdot X_{Pa} + D \cdot (AA_{in} - AA) \\ \frac{dVal}{dt} &= \frac{1}{Y_{X/Val,Sa}} \cdot \mu_{\max,Val,Sa} \cdot \left(\frac{Val}{Val + K_{S,Val,Sa}} \right) \cdot X_{Sa} - \frac{1}{Y_{X/Val,Bc}} \cdot \left(\frac{\mu_{\max,Val,Bc} \cdot Val}{Val + K_{S,Val,Bc}} \right) \cdot X_{Bc} - \dots \\ &\dots \frac{1}{Y_{X/Val,Pa}} \cdot \left(\frac{\mu_{\max,Val,Pa} \cdot Val}{Val + K_{S,Val,Pa}} \right) \cdot X_{Pa} + D \cdot (Val_{in} - Val)\end{aligned}$$

$$\text{Metabolite: } \frac{dAce}{dt} = Y_{Ace/X,Sa} \cdot \mu_{\max,199,Sa} \cdot \left(\frac{Glc}{Glc + K_{S,Glc,Sa}} \cdot \frac{AA}{AA + K_{S,AA,Sa}} \right) \cdot X_{Sa} - D \cdot X_{Sa}$$

The extension of the mixed substrate model with the hypothetical property of *S. a.* to take up valine with highest affinity compared to the two competitors, *B. c.* and *P. a.* could explain and describe a three-species coexistence in a chemostat. The cell numbers of the three species were in the experimentally observed and assumed ranges (Figure 4.53). This result was not unexpected, as the CEP predicts possible coexistence of i species on at least i substrates (2.4.2). However, coexistence of course is not possible for a deliberate parameter set and therefore this result for parameters from single-species experiments and other values chosen in a meaningful range were not considered trivial.

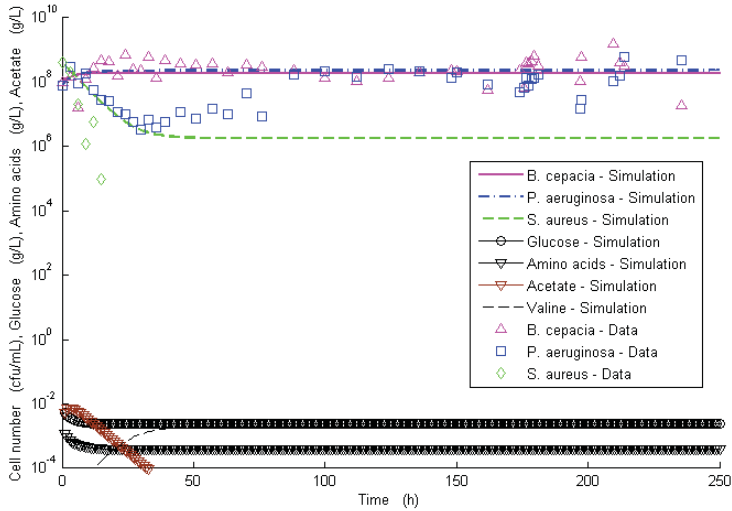


Figure 4.53: Simulation of mixed substrate model No. 2 with extension of valine as third substrate (eqn. syst. 4.27), for which *S. a.* had the highest affinity (parameters deliberately chosen). All other parameters as before, determined from pure cultures (Table 4.27).

Another theoretical model extension of the mixed substrate model No. 2 to test for explanation and generation of a three-species coexistence was the assumption of a biotrophy on a metabolic product (*Pr*) of *P. a.* serving as an exclusive substrate additionally to glucose and amino acids for *S. a.* (eqn. syst. 4.28). This assumption was not supported by experimental findings so far. The parameters were applied as before as determined from

single-species experiments, the kinetic parameters of the biotrophy were deliberately chosen in a biologically meaningful range (Table 4.27).

eqn. syst. 4.28

$$\begin{aligned}\frac{dX_{Sa}}{dt} &= \mu_{\max,199,Sa} \cdot \left(\frac{Glc}{Glc + K_{S,Glc,Sa}} \cdot \frac{AA}{AA + K_{S,AA,Sa}} \right) \cdot X_{Sa} + \mu_{\max,Pr,Sa} \cdot \left(\frac{Pr}{Pr + K_{S,Pr,Sa}} \right) \cdot X_{Sa} - D \cdot X_{Sa} \\ \frac{dX_{Bc}}{dt} &= \frac{\mu_{\max,Glc,Bc} \cdot Glc}{Glc + K_{S,Glc,Bc}} \cdot X_{Bc} + \frac{\mu_{\max,AA,Bc} \cdot AA}{AA + K_{S,AA,Bc} \cdot (1 + Glc/K_i)} \cdot X_{Bc} - D \cdot X_{Bc} \\ \frac{dX_{Pa}}{dt} &= \frac{\mu_{\max,Glc,Pa} \cdot Glc}{Glc + K_{S,Glc,Pa}} \cdot X_{Pa} + \frac{\mu_{\max,AA,Pa} \cdot AA}{AA + K_{S,AA,Pa}} \cdot X_{Pa} - D \cdot X_{Pa}\end{aligned}$$

Substrate:

$$\begin{aligned}\frac{dGlc}{dt} &= \frac{1}{Y_{X/Glc,Sa}} \cdot \mu_{\max,199,Sa} \cdot \left(\frac{Glc}{Glc + K_{S,Glc,Sa}} \cdot \frac{AA}{AA + K_{S,AA,Sa}} \right) \cdot X_{Sa} - \frac{1}{Y_{X/Glc,Bc}} \cdot \left(\frac{\mu_{\max,Glc,Bc} \cdot Glc}{Glc + K_{S,Glc,Bc}} \right) \cdot X_{Bc} - \dots \\ &\dots \frac{1}{Y_{X/Glc,Pa}} \cdot \left(\frac{\mu_{\max,Glc,Pa} \cdot Glc}{Glc + K_{S,Glc,Pa}} \right) \cdot X_{Pa} + D \cdot (Glc_{in} - Glc) \\ \frac{dAA}{dt} &= \frac{1}{Y_{X/AA,Sa}} \cdot \mu_{\max,199,Sa} \cdot \left(\frac{Glc}{Glc + K_{S,Glc,Sa}} \cdot \frac{AA}{AA + K_{S,AA,Sa}} \right) \cdot X_{Sa} - \left(\frac{\mu_{\max,AA,Bc} \cdot AA}{AA + K_{S,AA,Bc} \cdot (1 + Glc/K_i)} \right) \cdot X_{Bc} \cdot \frac{1}{Y_{X/AA,Bc}} - \dots \\ &\dots \frac{1}{Y_{X/AA,Pa}} \cdot \left(\frac{\mu_{\max,AA,Pa} \cdot AA}{AA + K_{S,AA,Pa}} \right) \cdot X_{Pa} + D \cdot (AA_{in} - AA)\end{aligned}$$

Metabolite:

$$\begin{aligned}\frac{dAce}{dt} &= Y_{Ace/X,Sa} \cdot \mu_{\max,199,Sa} \cdot \left(\frac{Glc}{Glc + K_{S,Glc,Sa}} \cdot \frac{AA}{AA + K_{S,AA,Sa}} \right) \cdot X_{Sa} - D \cdot X_{Sa} \\ \frac{dPr}{dt} &= Y_{Pr/X,Pa} \cdot \left(\frac{\mu_{\max,Glc,Pa} \cdot Glc}{Glc + K_{S,Glc,Pa}} + \frac{\mu_{\max,AA,Pa} \cdot AA}{AA + K_{S,AA,Pa}} \right) \cdot X_{Pa} - \frac{1}{Y_{X/Pr,Sa}} \cdot \left(\frac{\mu_{\max,Pr,Sa} \cdot Pr}{Pr + K_{S,Pr,Sa}} \right) \cdot X_{Sa} - D \cdot X_{Sa}\end{aligned}$$

The assumption of mixed substrate kinetics for glucose and amino acids extended with a hypothetical food chain based on a product of *P. a.* taken up by *S. a.* could describe and explain a three-species coexistence in the mixed culture (Figure 4.54).

Further experimental investigations will be required for validation of the proposed model variants.

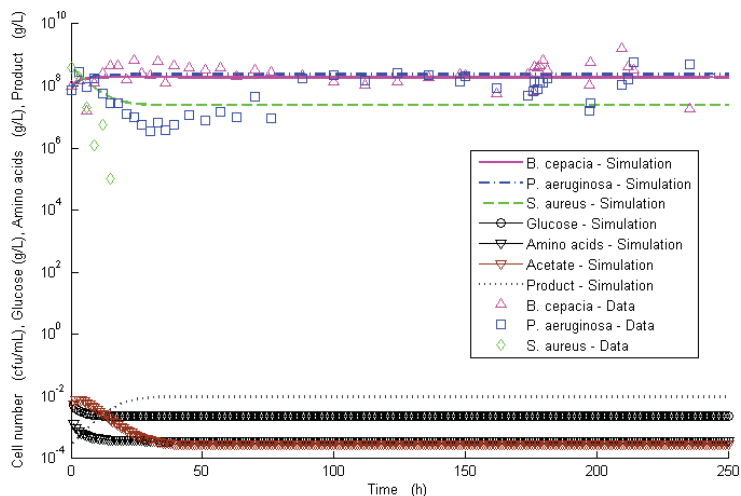


Figure 4.54: Simulation of mixed substrate model No. 2 with product formation by *P. a.* and uptake of this product with biomass formation by *S. a.* (eqn. syst. 4.28), (parameters deliberately chosen). Other parameters as before, determined from pure cultures (Table 4.27).

4.5.4 Summary

An overview of the main results of the experimental three-species chemostat cultivations is given in Table 4.28. A stable coexistence of at least two of the three species, *B. c.* and *P. a.*, was found for a time-period of more than 35 volume exchanges independent of the cultivation vessel. This result was reproducible. Selective dilution plating for *S. a.* even indicated the presence of this third species in the mixed culture, but below the quantification limit of the T-RFLP analysis method.

Table 4.28: Three-species chemostat experiments in 2 L and small scale STR at $D = 0.2 \text{ h}^{-1}$.

Experiment	Three-species mixed culture, consisting of ...		
	<i>S. a.</i>	<i>B. c.</i>	<i>P. a.</i>
Chemostat cultivation in 2 L STR (4.5.1)	Not detected (below $10^{5.8}$ cfu/mL) after about 50 h	Stable at about $10^{8.5}$ cfu/mL for at least 180 h (36 volume exchanges)	Stable at about $10^{6.5}$ cfu/mL for at least 180 h (36 volume exchanges)
Chemostat cultivation in small scale STR (4.5.2); parallel cultivations : two with $q = 0.5 \text{ NL/h}$, one with $q = 5 \text{ NL/h}$	Not detected (below $10^{5.8}$ cfu/mL) after about 19 h	Stable at about 10^8 cfu/mL for at least 190 h (38 volume exchanges)	stable at about 10^8 cfu/mL for at least 190 h (38 volume exchanges)
	After <i>Glc</i> pulse : uptake of <i>Glc</i> and ...		
	Detected at $10^{6.5}$ cfu/mL (at one time point)	Increased to 10^9 cfu/mL	Increased to $10^{8.5}$ cfu/mL
	After <i>AA</i> pulse : uptake of <i>AA</i> and ...		
	Not detected	Increased	Increased

The model variants and respective simulation results, which were formulated and tested for their capability of description of the determined experimental results, are given in Table 4.29 and Table 4.30. The assumption of competition for two substrates, glucose and amino acids, between the three species with two independent uptake kinetics for each of the substrates in the *B. c.* and *P. a.* model described the observed two-species coexistence. This validation of the model was achieved with model parameters completely based on the pure culture analysis.

Extension of this successful mixed substrate model No. 2 with the assumption of a third substrate valine, for which *S. a.* had the highest affinity, could explain a possible three-species coexistence. This could also be done by introducing a hypothetical biotrophy between *S. a.* and *P. a.*. The extension of the mixed substrate model with the acetate biotrophy between *S. a.* and the two other species was not able to explain a possible three-species coexistence.

Table 4.29: Summary I of three-species chemostat model variants and their respective simulation results (4.5.3).

Model	Simulation of a three-species mixed culture, consisting of ...		
	<i>S. a.</i>	<i>B. c.</i>	<i>P. a.</i>
Single substrate competition for <i>Glc</i> (classic chemostat)	$D = 0.05 \text{ h}^{-1}$;		
	After 200 h still present, but washed out afterwards 2 nd :	After 200 h still present, no washout :	After 200 h below quantification limit, washed out 1 st :
	<i>washout not definitely confirmed by experimental data</i>	<i>confirmed by experimental data</i>	<i>not confirmed by experimental data</i>
	$D = 0.2 \text{ h}^{-1}$;		
Single substrate competition for <i>Glc</i> and acetate biotrophy ($D = 0.2 \text{ h}^{-1}$)	After 200 h below quantification limit, washed out 2 nd :	After 200 h still present, no washout :	After 200 h below quantification limit, washed out 1 st :
	<i>washout not definitely confirmed by experimental data</i>	<i>confirmed by experimental data</i>	<i>not confirmed by experimental data</i>
	Washed out 2 nd :	No washout :	Washed out 1 st :
	<i>washout not definitely confirmed by experimental data</i>	<i>confirmed by experimental data</i>	<i>not confirmed by experimental data</i>
Mixed substrate competition for <i>Glc</i> and <i>AA</i> (Model No. 1)	Assumption of dependent growth on <i>Glc</i> and <i>AA</i>	Assumption of independent uptake of <i>Glc</i> and <i>AA</i> : one $\mu_{\max, 199, Bc}$ and diauxic effect	Assumption of independent uptake of <i>Glc</i> and <i>AA</i> : one $\mu_{\max, 199, Pa}$
	Washout predicted :	No washout :	Washout before <i>S. a.</i> predicted :
	<i>washout not definitely confirmed by experimental data</i>	<i>confirmed by experimental data</i>	<i>not confirmed by experimental data</i>
Mixed substrate competition for <i>Glc</i> and <i>AA</i> (Model No. 2)	Assumption of dependent growth on <i>Glc</i> and <i>AA</i>	Assumption of independent uptake of <i>Glc</i> and <i>AA</i> : $\mu_{\max, Glc, Bc}$ and $\mu_{\max, AA, Bc}$ and diauxic effect	Assumption of independent uptake of <i>Glc</i> and <i>AA</i> : $\mu_{\max, Glc, Pa}$ and $\mu_{\max, AA, Pa}$
	Washout predicted :	Stable coexistence of <i>B. c.</i> and <i>P. a.</i> predicted :	
	<i>washout not definitely confirmed by experimental data, slower in simulation than in experiment</i>	<i>confirmed by experimental data</i>	
		cell numbers predicted as $10^{8.3} \text{ cfu/mL}$:	
		<i>confirmed by experimental data</i>	

Table 4.30: Summary II of three-species chemostat model variants and their respective simulation results (4.5.3).

Model	Simulation of a three-species mixed culture, consisting of ...		
	<i>S. a.</i>	<i>B. c.</i>	<i>P. a.</i>
Analysis of	Only <i>Glc</i> in the chemostat feed		
Model No. 2	Washout predicted due to assumption for dependence on both substrates	<i>B. c.</i> stays in predicted : growth rather on <i>Glc</i>	Washout predicted : growth rather on <i>AA</i>
	Only <i>AA</i> in the chemostat feed		
	Washout predicted due to assumption for dependence on both substrates	Washout predicted : growth rather on <i>Glc</i>	<i>P. a.</i> stays in predicted : growth rather on <i>AA</i>
	A. for <i>S. a.</i> : $K_{S,Glc} = 0.0001$ (lower than experimentally determined) :		
	No change of simulation outcome		
	B. for <i>S. a.</i> : $K_{S,AA} = 0.0001$ (lower than experimentally determined) :		
	Almost stable coexistence of the three species		
	C. for <i>S. a.</i> : extension of single-species kinetics for growth only on <i>AA</i> without <i>Glc</i> : No change of simulation outcome		
	Combination of A. + B. :		
	No change of simulation outcome		
	Combination of B. + C. :		
	Stable two-species coexistence of <i>B. c.</i> + <i>S. a.</i> , washout of <i>P. a.</i> predicted		
Variants of mixed substrate Model No. 2 for explanation of possible three-species coexistence			
Model No. 2	No three-species coexistence, simulation result as for model No. 2		
<u>and</u> acetate biotrophy			
Model No. 2	Prediction of three-species coexistence		
<u>and</u> valine as a third substrate	Predicted cell numbers in the range of experimental results		
Model No. 2	Prediction of three-species coexistence		
<u>and</u> metabolic product of <i>P. a.</i> as substrate for <i>S. a.</i>	Predicted cell numbers in the range of experimental results		

5 Discussion

5.1 *Systems Analysis by Combining Mathematical Modeling and Experiments*

The methodological approach of characterization of a mixed culture presented here comprised the iterative combination of mathematical modeling and experiments (Figure 1.2).

I. The kinetic growth parameters of the bacterial strains of interest were not known from literature (2.1.3). Therefore, the respective experimental data were used to determine pure culture parameter values based on single-species models. The parameters from single-species experiments, $Y_{X/S,i}$, $\mu_{max,i}$ and $K_{S,i}$, were determined by separate experiments, when possible, to prevent mutual effects of dependence. Furthermore K_S was determined additionally from chemostat experiments with varied dilution rate (XD-graphs) to avoid the negative influence on parameter estimation of the instationarity of batch experiment at low substrate concentrations. The arbitrary properties of the species were identified by the experimental analysis and by lack of fit of the single-species data to the model simulation. This characterization led to a change of the model assumptions in addition to properties potentially relevant as interactions, which were identified from mixed culture growth.

II. The mixed culture chemostat models for different assumptions of interactions among the single species were formulated by the combination of the respective single-species models. All mixed culture simulations were calculated with the parameter sets for single-species growth derived in the presented work from optimized fit of the respective models to the experimental data (4.3.4). With those simulations of the different mixed culture model variants the theoretical outcome of co-cultivation specifically for the varied assumptions of single-species properties were compared.

III. The result of the mixed chemostat experiment was compared with the mixed culture simulations. By evaluation of the consistency between simulation and experiment it was tested which assumptions were required to describe the mixed culture experiment. This procedure was used to describe interactions among the species in the mixed culture based on their pure culture behavior. In contrast to the studies reported so far (2.3.4), here the differences found between simulation and the respective mixed culture experiments could be assumed to be related to interspecies interactions and not to parameter errors.

Furthermore, these differences were used to identify those interactions, which were required to describe the main interactions responsible for the observed mixed culture behavior. It has

to be stressed here that it was not the aim to obtain a parameter set from a fit of mixed culture data to describe the experimental result. The potential lack of fit between the simulation and the experimental result was the special advantage and it was used to deduce the knowledge for the mixed culture about potential interactions or properties different from the pure cultures. And in order to improve the consistency, further research on pure culture properties or possible species interactions was conducted.

Not all interactions can be directly deduced from a detailed experimental analysis of single-species cultures, but only become apparent by comparison with the mixed culture. However, the mixed culture data alone would not lead to the hypothesis of a certain interaction either, as for example the substrate of a biotrophy would not be detected in the mixed cultivation.

From HPLC data (3.5.3) it was apparent that the mixed culture physiological properties were different from each of the pure cultures. The chromatographic results for dynamics of the supernatant's composition (data not shown) during cultivations indicated further metabolic interactions or competitions. This was supported by the OTR and RQ data from pure and mixed cultivation experiments (Figure 4.44; Figure 4.45). In the follow-up research of the project, the peaks should be identified and quantified to get a complete substrate and product balance. Afterwards the relevant ones will have to be included in the mathematical models to study, if these could contribute to the explanation of the overall dynamics of the mixed culture.

In order to be able to perform the comparison for identification of possible interactions, it was obvious that the data of single-species experiments as well as the resulting parameters had to be of high quality as well as comparable to the data of the mixed cultures. The analytical methods for off-line determination were statistically validated for their quantification range and error (3.5), especially the cell enumeration by quantitative T-RFLP (4.2). This was evaluated as important for the quality of the estimated parameters and the comparability between a resulting simulation and the respective experiment (pure and mixed cultures). Such evaluation of data quality for the mathematical parameter estimation was hardly reported in literature for mixed culture studies (2.3.4, 2.4.3.3).

Biofilms are very commonly applied for experimental mixed culture studies, as mixed biofilm cultures are closer to the natural mode of growth. However, a quantitative description of the bacterial interactions with their environment and other species is difficult to determine quantitatively in a complex system such as a biofilm. It was therefore decided here to study

the respective species in an STR in suspension mode of growth to ensure homogeneous, controllable and defined conditions. Monitoring and control of cultivation conditions such as pH, p_{O_2} , OTR, CTR, RQ, dilution rate D , mixing n , aeration q was possible with the process control system of the STR systems. This possibility has not been reported for biofilm mixed cultures and has not been considered in the chemostat mixed cultures reported in literature (2.3.4, 2.4.3.3). The culture parameters pH, p_{O_2} , OTR, CTR, and RQ served as indicators of metabolic differences between the single-species and mixed cultures. Additionally, here mixing n and aeration q were controlled at fixed values, which were chosen as standard conditions to ensure comparability between results (4.1.3). However, it will have to be considered in a later stage of the project, which additional effects for example control of the p_{O_2} by n or q or growth as biofilms can have on the mixed culture.

Theory predicts extinction of all but one species for growth on one substrate by the mathematical model of the competitive exclusion principle (CEP) [50]. Contrarily, environmental observation prove the coexistence of more than one species in a surrounding with little substrate, what was termed the “paradox of the plankton” [67]. Consequently, numerous theoretical considerations are available on the dynamics of mixed cultures based on mathematical models for up to an infinite number of species [3, 48, 64, 82, 112, 132]. In contrast to the laboratory set-up with biofilms these models are mainly set in a chemostat. The chemostat model as a theoretical environment for mixed culture growth “occupies a central place in mathematical ecology” [132].

Studies of bacterial population dynamics with absolute cell numbers for more than two species were conducted by Gottschal et al. [41], Gottschal and Thingstad [42], McKee et al. [94] and McDermid et al. [93]. Of the above named four studies only one presented a mathematical model for the description of the results [42]. However, in these investigations the strains were specifically chosen for their known use of substrate and their expected interaction. No investigations have been reported of interaction effects for mixed cultures with arbitrary properties by the combination of quantitative experimental results and use of mathematical modeling. It rather seems, the lack of reliable data for mixed culture hinders the development of mathematical models, which would be closer to experiments than the ones reported to date. Chen and Weimerer [18] examined a defined mixed culture of three species, but their quantification referred to the content of RNA and was evaluated only relatively.

In contrast to the studies above, the species chosen here for the mixed cultures had arbitrary and unknown properties. Their characteristics potentially relevant for interactions were

characterized for and with the help of the mixed cultivations, as for example the growth on amino acids and glucose. In contrast to the study with three strains and mathematical modeling [42] instead of only two-species experiments for characterization of interactions here growth properties were derived by single-species analysis.

5.2 *Cell Number Quantification with T-RFLP*

The lack of an efficient and species-specific enumeration method for cell numbers in mixed cultures is a key reason for the paucity of studies with more than two species. Such a method would be invaluable for a broad range of investigations of mixed culture dynamics as well as for fundamental research on competition and coexistence [110]. That would support the development of an understanding of underlying mechanisms of community dynamics in ecological, medical as well as in biotechnological applications. For this, the quantitative analysis of absolute species numbers and their population dynamics would be necessary, because the kinetics derived from pure cultures are in many cases not sufficient for the description of mixed culture kinetics and dynamics [121].

For the quantitative monitoring of compositional changes in microbial communities specific methods for species enumeration are applied in microbial ecology. However, these methods are so far focused on the diversity of the species, not on cell concentrations. T-RFLP analysis is one of these methods and, so far, has been mainly used in semi-quantitative investigations to determine the relative species abundance from fragment peak areas [87, 88, 108, 148]. Other quantitative T-RFLP approaches refer to community diversity profiling and data set comparisons [11, 72]. Evaluation of T-RFLP described so far in literature is mainly focusing on profiling quality and often based on DNA as starting material rather than bacterial suspension samples [11, 31, 72, 88, 108].

One approach to use T-RFLP analysis for quantification of absolute cell numbers of single species was presented. However, analysis of mixed sample data and corresponding error analysis were not included in the respective study [145]. For the presented project, a T-RFLP analysis method was established based on the one from literature for quantification of absolute cell numbers in mixed culture samples and its application was evaluated.

5.2.1 Requirements for Mixed Culture Cell Enumeration

For comparability of growth dynamic results within one cultivation and between different cultivations, precision of a possible quantification method was considered much more important than accuracy. The main requirements for the establishment of quantitative T-RFLP

method in growth studies of defined mixed cultures were therefore reproducibility and consistency of quantifications as independent as possible of the number of species or their relative amounts in samples. The same value had to be measured with little error for one cell number independent of the kind and time point of cultivation for single-, two-, or three-species experiments as well as for repetition of experiments. If cell numbers were all determined with T-RFLP, it was not as important that the result was correct with regard to an external standard. Consequently, the consistency of quantification results with T-RFLP was evaluated (4.2.3 and 4.2.4) and only limited effort was taken to verify cell numbers against a reference. Here, a dilution plating method was applied as reference [93].

5.2.2 Evaluation of Error within T-RFLP Quantification

With a relative SD of about 1.3 % (Table 4.2) errors for quantification of single-species replicates by T-RFLP were in a similar range as errors reported in literature. For example, a value better than 3 % for single-species sample replicates and absolute cell number quantification was reported by Trotha et al. [145], while Lukow et al. [89] report an error of 1.5 % for relative peak area of three replicate soil samples.

To reduce the influence of pipetting, dilutions were prepared independently (each step out of the same undiluted suspension) and then the dilution steps were pooled before analysis. This reduced the observed error in lower concentration ranges significantly. However, part of the estimated errors (Table 4.2) were still considered to be due to the error of dilution and it needs to be emphasized that for quantifications of actual culture samples no dilutions need to be prepared. Correspondingly, the error of T-RFLP for samples taken from shake flasks or bioreactors was even lower (maximum CV 1.7 %; 8.4 ± 0.13 log-transformed cfu/mL) than the error estimated from defined sample replicates (maximum CV 4.4 %; 8.8 ± 0.39 log-transformed cfu/mL).

5.2.3 Means of Impact on T-RFLP Quantification Quality and Range

Efficiency of PCR was reported to vary and thereby to prevent the use of T-RFLP for absolute quantifications [88]. In addition species specific efficiencies are known to induce PCR bias of amplicons from 16S rDNA mixtures [140]. In the presented project these species-specific parameters, such as the efficiency quotient and 16S rRNA gene copy number, were determined and taken into account for the adaptation of T-RFLP for quantification of absolute cell numbers. In contrast to results reported before [140], no obvious PCR bias for mixed template samples was found here. An unbiased quantification of samples consisting of up to three species was found to be possible after selection of appropriate and constant parameter

values for T-RFLP analysis, namely the efficiency quotient (eqn. 3.7). The influence of the template ratio on PCR results was described and modeled [140]. The experimental evaluation for the T-RFLP analysis did not show a significant influence on quantification results. However, the lower initial template amounts per species in mixed sample PCR resulted in lower peak heights for the species and the IQS compared to pure samples. This might be a reason for the tendency of mixed sample dilution series to show regression slopes closer to 1.0 (Table 4.3; Table 4.4; Table 4.5).

Consistency of single-, two-, and three-species T-RFLP results was evaluated by comparison of defined two- and three-species bacterial dilutions with the corresponding T-RFLP quantifications of the single-species samples. An influence of the relative and absolute amounts of the species in mixed samples was not apparent; mixed sample results were consistent with those of single-species (Figure 4.6). The result of linear regression did not significantly change for two- or three-species compared to single-species dilution series (Table 4.3; Table 4.4; Table 4.5). This indicated the comparability of growth dynamics as well.

One drawback of quantification with T-RFLP is that its quantification limit is not close to zero but about 10^5 cfu/mL, meaning species can still be present in a significant number, but are not detected. Here, the limit was not found to depend on the number of species. However, the limit is expected to depend on the ratio between the number of the species of interest and the sum of other species cells. The number of other species cells might depend on both, number of species and number of cells. As the absolute DNA concentration for PCR is constant, a small ratio means a little amount of template DNA. For a defined number of cycles this leads to a small amount of PCR product and possibly to a fluorescent intensity below the detection limit of the DNA sequencer.

The quantification limit became apparent in the T-RFLP results for *S. a.* in the chemostat experiment (Figure 4.9), where it could be of specific interest to differentiate between a constant decrease down to extinction and a possible stabilization of cell numbers below 10^5 cfu/mL. It was tried to overcome the lower and also the upper quantification limit by an increase, respectively decrease, of the standard sample volume of 1 mL, by a change of the ratio between cell number of interest and of the IQS. However, no improvement was found. Furthermore, while quantification results were expected to be independent of the sample volume, the results with 5 mL, 2 mL and 0.5 mL sample volume differed about 0.5 log-scales compared to the 1 mL standard sample, but results were consistent for each volume (data not

shown). This phenomenon cannot be explained at present and requires further research. For future development of quantitative T-RFLP the preparation of different sets of IQS with ten-fold dilutions of the reference strain could be a way to overcome this limitation. Therefore, sample volumes should be kept constant according to the calibration protocols and samples below quantification limit analyzed by the plating counting method if required.

The quantification range of T-RFLP largely depends on the DNA extraction and PCR amplification. As all fragments are derived from these steps, it would not be possible to quantify a mixture containing one species with a very high cell number (e.g. 10^{20} cfu/mL) together with another species with a low cell number (e.g. 10^6 cfu/mL). While dilution would allow quantification of the species with the high cell number, the other species would be amplified in negligible amounts as its ratio towards the other species remains constant. Here, a possible ratio between two species was found to be $10^{10}/10^5$ cells, the limits of quantification were found to be 10^{10} cfu/mL and 10^5 cfu/mL for the three species. The number of species, which could be analyzed with T-RFLP without narrowing of this range was not investigated. This will have to be done in further experiments. Another option could be the use of specific primers to exclude and include species specific fragments from the mixed DNA templates in the PCR. However, this would present a difficulty to coamplify the IQS with the specific primer set.

In eqn. 3.7 peak areas are directly used to calculate cell numbers. Fragment peaks, which are out of the linear range (below 10^5 cfu/mL or above 10^{10} cfu/mL) often could not be used for this calculation as some of their “real” area is cut off, which means lost for calculation resulting in outliers. Loss of either one of the peaks (species or IQS) was additionally observed for concentrations out of the linear range. After change from the older ABIPrism 3100 analyzer, which was used in the beginning of the project as well as in the study reported in literature [145], to ABIPrism 3100Avant [126] the loss of peak area of the higher peak occurred more frequently. Instead positively an highly improved data quality for mixed sample analysis was achieved with the new analyzer, no peaks were lost anymore for single-, two-, and three-species samples with concentrations within the linear range. With the old ABIPrism 3100 analyzer the linear range of quantification of mixed samples had been reduced in comparison to pure samples. Either one of the peaks, species or IQS respectively, was not detectable anymore, if mixtures contained high concentrations (10^{10} or 10^9 cfu/mL) of one species and low concentrations (10^6 or 10^5 cfu/mL) of a second (data not shown). With the new ABIPrism 3100Avant the quantification range was the same for mixed and for pure

samples (4.2). This was most likely due to increased sensitivity of the ABIPrism 3100Avant, which has an improved hardware (photo detector) compared to the other analyzer. In addition, the laser beam split was used only on four instead of 16 capillaries.

The following options were investigated to decrease peak heights (areas) and thereby cut off of high peaks in chromatograms: reduction of template amount in PCR, reduction of amplicon amount in restriction digest, dilution of restriction digest before fragment analysis, decrease of injection voltage or injection time for fragment analysis sample loading. However, none of these modifications improved results. Quantification either did not change significantly or quantification became impossible due loss of small peaks (data not shown). It seems that once the DNA is extracted, quantification is quite robust against these variations. For method improvement it was therefore not required to treat samples differently depending on species composition, which is an advantage because less time-consuming.

Genome size was reported to be the main influencing factor for PCR efficiency [145]. Here, this was not confirmed, as T-RFLP quantifications calculated with efficiency factors taken from the literature [145] did not fit to the reference values (Figure 3.6, open symbols). This might be explained by the hypothesis that a) genomic DNA is reduced to a maximal size of 50 kbp by DNA extraction procedure (pers. com. Qiagen, Hilden, Germany) or b) PCR efficiency depends on parameters such as primer specificity, polymerase affinity, and PCR conditions in general.

5.2.4 Application of T-RFLP for Monitoring Cultivations

For single-species cultures T-RFLP was found to function well as a quantification method (Figure 4.8) with similar results in the logarithmic scale as with OD measurement. However, curves of T-RFLP were not as smooth as OD measurements, especially for *B. c.* (Figure 4.8). Very likely this did not indicate data scatter, as monitoring of two completely independent shake flask cultures with quantitative T-RFLP gave comparable results. It should be investigated in further experiments, if the observed difference between T-RFLP and OD could be due to physiological or genetic effects. For example, the effect of accumulation of genomes during high growth rates as known for *E. coli* [125] would have an impact on quantitative T-RFLP results. Another possible explanation would be T-RFLP and OD measure the cell number and cell mass density, respectively. And since cells can increase in size and mass without dividing, this would result in a lag of T-RFLP behind OD measurements.

Concerning the comparison of the two methods for cell enumeration in the XD-experiments (4.3.1.4), the cell numbers determined with T-RFLP analysis confirmed the overall picture of the OD data. As T-RFLP analysis method was validated for log-transformed values, the results were compared in the respective form. The values were very much in the same range or even consistent with the values calculated from OD. The washout points determined with T-RFLP analysis also were the same as for OD method for all strains.

The quantitative T-RFLP method presented would be applicable for monitoring growth of pure cultures, as well as every simple microbial community or mixed culture of known composition (4.2). The only prerequisite would be the determination of the species specific efficiency factors by calibration against a reference method (Figure 3.6) and copy numbers of 16S rDNA gene for the respective species. Even in case the composition would not be completely known a quantitative comparison of unspecified T-RFLP peaks as absolute cell number would be possible by setting efficiency and copy number as constants. For natural communities it would be necessary to assure that no pseudo T-RFLP fragment was quantified as bacterial species [30]. For mixed cultures in biotechnology or model systems of microbial ecology with known composition this would not pose a problem as each peak could be assigned to a specific and known species.

5.2.5 Benefit of T-RFLP Quantification for Mixed Culture Studies

Quantification of a three-species mixed culture chemostat with T-RFLP quantification showed stable and consistent results (Figure 4.9). Moreover, T-RFLP quantification can be used as a species specific enumeration method for monitoring mixed species growth dynamics in a time-efficient and reproducible way. This will be beneficial especially to the field of theoretical ecology, mathematical biology and bioprocess engineering by providing quantitative and absolute cell numbers of population dynamics [132]. In particular, it will allow comparing growth dynamics between pure and mixed cultures and can therefore be considered as an important tool to analyze interspecies interactions in microbial communities.

There are several general advantages of quantitative T-RFLP method for mixed culture studies in comparison to enumeration methods such as selective dilution plating or microscopic image analysis after staining with FISH probes [121]: First, a quantification range of 10^6 to 10^{10} cfu/mL (*S. a.*), of 10^5 to 10^{10} cfu/mL (*P. a.*) and of 10^4 to 10^9 cfu/mL (*B. c.*) is available via one sample preparation after the method has been adapted once to a certain application. Also, samples have not to be diluted during processing and therefore, no additional dilution errors are introduced. Secondly, sample preparation and centrifugation

require only about 20 min, which reduces workload and allows short sampling intervals. Third, processed samples can be collected over one sampling period or cultivation and stored at -20 °C for quantitative T-RFLP analysis of the complete data set. Fourth, no additional incubation steps resulting in additional bias are introduced, for example by growth dependence on selective media [94]. Finally, an increase of species number within a community does not result in additional time cost or consumption of consumables for quantitative T-RFLP as it would be the case, for example for additional selective agars, real-time PCR or fluorescent probes.

Real-time PCR was not chosen for the mixed culture quantification, as it has to be considered that for cell enumeration in mixed samples the results obtained can usually not be compared to quantitative T-RFLP for two reasons: a) real-time PCR quantifies the copies of a target gene in a sample of extracted DNA. However, the result is not necessarily correlated to the absolute cell number before DNA extraction, as the PCR can not take into account the loss of DNA during extraction; b) real-time PCR quantification uses standard curves obtained with the target gene inserted in a plasmid, whose amplification kinetic usually differs from that of the genomic target gene.

In contrast, the T-RFLP method used here quantifies gene copies in the culture sample prior to extraction using *C. jejuni* as internal standard thereby accounting for losses during all sample preparation steps.

5.3 *Growth Characteristics of the Single Species*

The investigated species were chosen for their medical relevance in CF related mixed cultures, where they are assumed to exist as microbial communities (2.1). In order to learn about possible interactions between the species in a mixed culture, first the pure culture growth properties of the species were characterized and afterwards the results were implemented in mathematical models. By comparison of the model simulations with the experimental results selected assumptions could be validated or rejected.

5.3.1 *Single-Species Experiments with *S. aureus*, *B. cepacia*, and *P. aeruginosa**

In literature not much was available with regard to quantitative analysis of growth dynamics for the selected organisms. They have almost been exclusively studied for their medical impact and properties such as infection mechanisms, virulence factors and genetic diversity (2.1.3). Furthermore the available studies were not conducted in the defined full medium established here (M199+P+NTA, 4.1.2), but mostly in complex media, such as LB or

Columbia Blood medium (3.2). For the generation of the required basis for the mathematical modeling on the one hand the growth dynamics of the strains were analyzed in batch and continuous cultivations (4.3.1). On the other hand additional experiments were performed aiming at the characterization of properties potentially relevant for interactions during mixed cultivations (4.3.2).

5.3.1.1 Acetate, Pyruvate and Influence of pH Value

S. a. was found to form acetate during aerobic growth on glucose in batch and chemostat experiments (4.3.1). This was also reported in literature [35]. In contrast to a report by Somerville et al. [136] the uptake of acetate by *S. a.* after the exponential growth phase was not observed. This could be due to inactivation of the enzyme aconitase, which is required for acetate uptake and the activity of which depends on the iron concentration in the medium as reported by the same authors. If this was relevant for the *S. a.* strain used here, could not be clarified in the presented work. However, the release of acetate into the medium provided the possibility of an acetate biotrophy between the three species, as *B. c.* and *P. a.* took up acetate as an additional carbon source to glucose (4.3.2.1).

Additionally, pyruvate formation was found for *S. a.* in shake flask and STR cultivations. Secretion of pyruvate was not reported in literature. The increase of pyruvate concentration seemed to correlate with the occurrence of a phase of decreased growth (linear growth phase) after the phase of exponential growth (Figure 4.10, Figure 4.11). Which effect leads to the increase of pyruvate in *S. a.* cultures should be characterized further.

The RQ below 1.0 during growth of *S. a.* on glucose (Figure 4.11) correlated to the formation of acetate and pyruvate as metabolic products, which were less oxidized than carbon dioxide. It was not experimentally verified, if *B. c.* and *P. a.* took up pyruvate as a possible carbon source. However, as the two organisms are reported to be metabolically very versatile, this is possible. Pyruvate thereby provides another possibility of biotrophy between the strains in a mixed cultivation and should therefore be investigated further.

Both metabolic products of *S. a.*, acetate and pyruvate, decreased the pH value of culture broth to about pH 6.4 for the conditions used here. The pH optimum for *S. a.* was reported to be about 7.0 (2.1.3.1). The uptake of the metabolites by *B. c.* and *P. a.* consequently would affect the pH adversely, which could affect growth of the strains positively. However, in the experiments performed (4.3.2.2) it was not confirmed that a) growth of *S. a.* was affected negatively by the decreased pH in single-species batch cultures; and b) that consequently a

higher pH value due to acetate uptake in the mixed culture would support growth of *S. a.*, which would have been a synergistic effect.

5.3.1.2 Growth on Two Substrates: Glucose and Amino Acids

All strains of *S. a.* have been reported to be auxotrophic for several amino acids, about 5 to 12 depending on the strain, for most strains arginine and valine in any case [107, 152]. This was confirmed by experimental results with M199+P+NTA.

Cultivation in glucose-free M199+P+NTA and namely growth on amino acids resulted in formation of a small cell number (Figure 4.24). This indicated use of amino acids as both, energy and carbon source and monomers for protein synthesis. Different metabolic pathways and use for amino acids during growth with and without glucose need to be assumed as the requirement for amino acids is reported to change depending on growth conditions [152]. In comparison to growth on glucose together with amino acids the use of glucose as carbon and energy source was advantageous concerning cell number formation compared to the growth only on amino acids [13], as was to be expected.

For the two species *B. c.* and *P. a.* it was shown that independent growth took place on the two substrates, glucose and amino acids (Figure 4.15 and Figure 4.25 ; Figure 4.18 and Figure 4.26, respectively). Selective media for *B. c.* or *P. a.* do not contain amino acids (Table 9.3), confirming that amino acids are not required by the two strains in contrast to *S. a.*. The question remains, if the substrates have to be considered as mixed substrates serving different metabolic purposes or multiple substrates with homologous purposes (2.2.2.1 ; 2.2.2.2). In literature no information on the use of single amino acids in culture media by *P. a.* or *B. c.* was available. A common feature of the two strains is their versatility concerning their range of possible carbon and energy sources (2.1.3.2 ; 2.1.3.3), which could mean the use of the two substrates as independent carbon sources.

Most bacteria, including *P. a.* and *B. c.*, synthesize all 20 amino acids internally and use them as monomers for protein synthesis. If amino acids are present in the environment (culture medium), they can be used directly for the intracellular polypeptide synthesis [13]. Additionally, as was shown experimentally here (4.3.2.3), they can serve as carbon and energy source additionally to glucose. However, in presence of glucose, the function of amino acids cannot be clearly defined [44]. The individual use of amino acids could even vary with the amount of glucose additionally present.

A diauxic behavior for the uptake of glucose and amino acids was found for *B. c.* (Figure 4.15), but not for *P. a.* (Figure 4.18); glucose was taken up during the first hours of cultivation without a decrease of amino acid concentration.

5.3.1.3 Other Substrates and Metabolites

For *B. c.* an additional carbon and energy source was assumed, which was formed during glucose uptake and its consumption after depletion of glucose led to a RQ value of 1.4. The value indicated a substrate, which was more oxidized than glucose. However, its formation should have generated an RQ below 1.0, which was not observed (Figure 4.14). The assumption was further supported by the results of O₂ consumption and pH curve: the uptake of 0.1 g/L of amino acids after glucose depletion (III) would not lead to uptake of about 50 % of the overall O₂ consumption of the cultivation (7.8 mM of 14.8 mM). Furthermore, the uptake of amino acids would result in a release of ammonia and thereby an increase of pH. In the experiment pH decreased during consumption of glucose indicating formation of an acidic substance. The pH increase in the second growth phase was then possibly due to uptake of the acidic substance (Figure 4.14). Additionally, amino acid consumption normally leads to an RQ of about 0.5 and not an increase as it was observed. However, during the present work the hypothetical substance was not identified and in literature no potentially metabolic products were reported.

Cell formation and O₂ uptake continued after depletion of glucose and amino acids, which indicated use of an unknown carbon source by *P. a.*. Additionally, a minimum of the pO₂ value before depletion of glucose and amino acids indicated a substrate apart from these two substrates in the medium. This was supported by the overall O₂ consumption of 20 mM, which was higher than the one stoichiometrically required for 1 g/L glucose (Figure 4.17). The shift from 1.1 to 1.0 of RQ could indicate the depletion of a second substrate before glucose. A formation of such a substance could, however, not be concluded from the O₂ uptake, which supported the assumption that it was present in the medium. In literature a diauxic growth of *P. a.* was reported, where citric acid was preferred to glucose [44]. However, citric acid is no component of the M199+P+NTA medium. The OTR curve of *P. a.* was characterized by a large number of peaks (Figure 4.17), which could represent diauxic effects as reported by Anderlei and Büchs [1]. However, the hypothetical substrates were not identified during the present work.

A possible explanation for the observed growth dynamics of *P. a.* could be its property of extracellular formation of gluconate from glucose. The gluconate is further dehydrogenated

extracellularly to 2-ketogluconate, which is then taken up as substrate [66]. The oxidation leads to very high O_2 demand, which was observed in all cultivations of *P. a.* (4.3.1.3). Furthermore, the intermediates could be responsible for the diauxic peaks of the OTR curve and 2-ketogluconate could be the substrate of cell formation after depletion of glucose. These proposed effects will have to be investigated in a follow-up project.

The obtained results of the single-species experiments gave information on the growth properties of these non-biotechnologically used microorganisms under defined conditions. Furthermore they provided a data basis for mathematical modeling and ideas of possible interactions required for the description of the mixed cultures.

5.3.2 Model Assumptions and Simulation Results for the Single-Species

The models for description of single-species growth were formulated to represent the most prominent properties found in the experiments with the species. Iteratively further kinetics were introduced to improve the mathematical models for description of the growth of the microorganisms.

5.3.2.1 Estimated Kinetic Parameters for Growth on Glucose

The estimation of the kinetic parameters for growth of *P. a.* on one substrate, glucose, resulted in $\mu_{max,199,Pa}$ of 0.42 h^{-1} , which was comparable to the values in literature : 0.29 h^{-1} , 0.40 h^{-1} or 0.45 h^{-1} (Table 2.1). The value for *S. a.* of $\mu_{max,199,Sa}$ of 0.83 h^{-1} was comparable to the lower range of growth rates given in literature : $0.81\text{ h}^{-1} - 1.81\text{ h}^{-1}$ (2.1.3.1). However, the latter were determined with *S. a.* strains in LB medium, which also in the experiments of the study presented here, led to improved growth compared to the defined medium (Table 4.1). No further values of kinetic parameters for the strains were available in literature.

The washout rates in the XD-experiments (4.3.1.4) for *B. c.* and *P. a.* were 1.3 h^{-1} and 1.1 h^{-1} , respectively. These values could not be described by a simulation for growth on a single substrate glucose with the $\mu_{max,199, is}$ which were 0.66 h^{-1} for *B. c.* and 0.42 h^{-1} for *P. a.*. For *S. a.* the values were more comparable, the washout was at $D = 0.7\text{ h}^{-1}$ and $\mu_{max,199,Sa}$ was 0.83 h^{-1} . As discussed in the following, the observed use of amino acids as substrate additional to glucose was evaluated for an explanation of the observed phenomenon of increased washout rate.

5.3.2.2 Mixed Substrate Kinetics for Glucose and Amino Acids

For growth of bacteria not only a carbon and energy source such as glucose is required, but nitrogen and phosphor sources, trace elements and other components depending on the

species are required as well [125]. However, the mathematical description of the kinetics is reduced for sufficient description to the main effects of the bacterial growth depending on the context (2.2). Most approaches take into account the main influencing medium component, namely a) the substrate, which determines the cell yield (limiting substrate, no increase in cell number after depletion) and b) the substrate, which determines the specific growth rate (rate determining substrate) [99] (2.2.1). The two functions have been assumed to be fulfilled by the same medium component, namely glucose or another carbon source, by most research groups. However, it has not been reported, whether the assumption was verified [73, 105].

The function of amino acids as additional substrate as shown experimentally and as discussed in the preceding part (5.3.1.2) had to be described mathematically for the strains of interest.

The kinetics for growth on glucose and amino acids of the three species *S. a.*, *B. c.*, and *P. a.* were established for the description of growth in standard medium M199+P+NTA. Based on the considerations on the various possibilities to use of glucose and amino acids by the single species in 5.3.1.2, the growth dynamics in glucose-free medium (4.3.2.3), only on amino acids, could not be described with the same model. However, parameters of single substrate growth were determined for amino acids (4.3.4.3). The values were applied in the mixed substrate kinetics and improved the data basis of the parameter estimations; as starting values for the optimized fit (Monod constants, yield constants) and constraints (maximum growth rate on amino acids, where applicable) (4.3.4.4).

For *S. a.* the formulation of the growth on glucose and amino acids as dependent substrates resulted in a good description of the batch experiment curves (Figure 4.27). The Monod constants for glucose and amino acids were very similar, that for amino acids $K_{S,AA,Sa}$ was 0.011 g/L, that for glucose $K_{S,Glc,Sa}$ was 0.013 g/L. When the parameters were determined from the XD-data (Figure 4.28), the respective constants differed, that of glucose $K_{S,Glc,Sa}$ was then 0.006 g/L and that for amino acids $K_{S,AA,Sa}$ was 0.11 g/L. The simulation of the XD-data as a whole was good. The washout rate of 0.7 h^{-1} was represented well, as expected it was a little lower than the $\mu_{max,199,Sa}$ of 0.83 h^{-1} [51]. It failed in the detailed description of the experimental data, the amino acids were predicted too high, the steps in glucose and cell numbers at higher dilution rates were not simulated. The differences most probably result from properties of *S. a.*, which have not yet been considered in the model, for example formation of pyruvate, or were not deducible from the experiments. They will have to be experimentally quantified and determined in further investigations.

The models of *B. c.* and *P. a.* were formulated for the assumption of the use of glucose and amino acids as independent multiple substrates (2.2.2.2). Two variants of the respective additive kinetic were compared, (A) with one $\mu_{max,199,i}$ and (B) with two $\mu_{max,Glc,i}$ and $\mu_{max,AA,i}$ (4.3.4.4).

For *B. c.* the description of the experimental batch data by the model simulation (A) was improved significantly by implementation of a diauxic kinetic for glucose and amino acids (Figure 4.31). The diauxic effect could be due not only to amino acids, but to another substrate as discussed before (5.3.1.3). However, as no quantitative data was available on this, the first approach was formulated just with the amino acids. The model simulation (A) with diauxic growth still described the uptake of amino acids earlier than found in the experiments. And the simulated growth of *B. c.* stopped, when glucose was depleted and left amino acids unused, which did not describe experimental curves well (Figure 4.31). In comparison the simulation (B) of diauxic growth and use of glucose and amino acids as multiple substrates was a very good description of the time courses of cell number, glucose and amino acids for *B. c.* (Figure 4.35).

For the kinetic variants (A) and (B) the estimated values for the Monod constants of *B. c.* were in a similar range : (A) for glucose 0.027 g/L, for amino acids 0.065 g/L, (B) for both 0.017 g/L. However, the estimated $\mu_{max,Glc,Bc}$ for variant (B) was very low (0.11 h⁻¹) compared to the respective $\mu_{max,AA,Bc}$ of 0.67 h⁻¹. The growth rate on amino acids as single substrate was used as constraint from the experiment without glucose (4.3.4.3). The value could be different, when glucose was present. However, estimation of all parameters including $\mu_{max,AA,Bc}$ from the one experiment with glucose and amino acids present did not give meaningful results (data not shown). Therefore, the presented methodology was chosen. For the parameter estimation from the XD-data the resulting $\mu_{max,Glc,Bc}$ for variant (B) was 0.74 h⁻¹, which was considered a meaningful value (Figure 4.36).

The applied kinetics were chosen for uptake of multiple substrates at low concentrations (2.2.2.2). This assumption is valid especially under continuous cultivation conditions [44]. This was confirmed, as the simulation with *B. c.* and *P. a.* for both kinetic variants (A) and (B) described the XD-experiments very well. The resulting maximum specific growth rate in the both kinetics consequently is the sum of the growth rates on glucose and amino acids. Thereby, especially the increased washout rates of 1.3 h⁻¹ and 1.1 h⁻¹, respectively, were predicted with the kinetics of amino acids and glucose as independent multiple substrates. For *P. a.* with kinetic (B) even the step in cell number at higher dilution rates was represented

successfully (Figure 4.37). The results confirmed the assumption of growth on glucose and amino acids as multiple substrates.

As discussed above for all three strains, the predicted washout rates were consistent with the ones experimentally found for *S. a.*, *B. c.*, *P. a.* : 0.7 h^{-1} ; 1.3 h^{-1} ; 1.1 h^{-1} . The resulting values were not exactly the same as the related μ_{max} (*S. a.* 0.83 h^{-1}), respectively twice the sum $\mu_{max,199}$ or $\mu_{max,Glc} + \mu_{max,AA}$ for *B. c.* ($0.66 \text{ h}^{-1} + 0.66 \text{ h}^{-1}$ (A) ; $0.74 \text{ h}^{-1} + 0.67 \text{ h}^{-1}$ (B)) and for *P. a.* ($0.53 \text{ h}^{-1} + 0.53 \text{ h}^{-1}$ (A) ; $0.34 \text{ h}^{-1} + 0.67 \text{ h}^{-1}$ (B)). This relates to the impact of the terms for glucose and amino acids in the solution of the equation $\mu = D$ for the washout point: $\mu(Glc; AA) = D_{crit}$. The resulting values for the maximum growth rates depend on the applied kinetic terms, which was also reported for the standard chemostat model (2.4.1) [51].

The higher maximum specific growth rate in the chemostat experiments compared to the maximum growth rates from batch results was surprising, as standard textbooks predict the washout for a value close to the maximum specific growth rate determined by batch experiments. However, the influence of mixed substrates on chemostat dynamics was rarely considered. The use of the additive kinetic was especially suggested for description of multiple substrate uptake at low concentrations as in the chemostat [44]. And the resulting effect of increased growth rates on multiple substrates as observed here was reported [73]. However, the authors have pointed out the drawback of too high values predicted from the kinetic formulation of the sum of individual Monod terms for high numbers of mixed substrates. It might seem inappropriate with regard to standard laboratory experiments to generate a higher growth rate by the sum of Monod kinetics terms in the chemostat than for the batch experiment. However, one has to keep in mind that the models applied here are phenomenologically derived [104]. They do not fulfill the task to describe the cell with all its properties and potentials in various environmental conditions, as for example a biosystems approach would. Altogether, the good description found here for the XD experimental results with the application of the additive mixed substrate kinetic was evaluated as successful.

On the whole the data curves of the XD-graphs were not as expected from the presentations in textbook theory [20]. In contrast, they had significant differences to the ideal curves such as decrease in cell number at low dilution rates or a strong increase of assumed substrates with increasing dilution rate (4.3.1.4). It was assumed, that these differences were due to the specific growth kinetics of the single-species. However, as the model simulations did not represent the curves characteristics too well, additional properties have to be assumed in the model equations. These new assumptions could, for example take into account the additional

substrates or metabolites for *B. c.* and *P. a.* as discussed above (5.3.1.3). It would be helpful, if possible single-species properties could in addition be deduced from the specific curve characteristics in the XD-graphs. The different formulations of growth kinetics are mostly either presented as batch dynamics or for chemostat cultivations at one dilution rate, but not as XD-graph. Mixed substrate use was discussed in a number of publications [19, 43, 49, 157], but the consequences on parameter estimation methods or change in the resulting XD-graphs have not been discussed by the authors. For follow-up of the project these effects on XD-graphs could be established as « chemostat archetypes » for different kinetics as already known for batch culture curves.

Alternatively, the increase of maximum specific growth rate respectively specific growth rate at wash out in the chemostat compared to the batch experiments could also be a result of biofilm formation as reported by Bryers [14]. During the performed experiments some cell adhesion was visible on the pO_2 probe and at the phase border between liquid and head space in the reactor. However, the verification of possible quantitative effects of the observed biofilm cells on the experimental outcome was not studied here. It will have to be investigated in the follow-up project.

Some experimental results have not yet been considered in the mathematical modeling. For example the hypothetical additional substrates apart from glucose and amino acids for *B. c.* and *P. a.* as discussed above (5.3.1.3), which will have to be studied in further projects.

In pure culture studies amino acids or polypeptides are very often part of the culture media. However, they are mostly not considered as a mixed substrate for formulation of the growth models. This is due to the fact that they are not considered as limiting cell yield or as determining growth rate. Growth in the medium as a whole with all its components determines the maximum specific growth rate, which is then described by the standard kinetics (2.2.1). However, it remains an open question, if the neglect of substrates apart from glucose, has always been the right choice for modeling of growth dynamics presented in literature (2.4.3.3). Because in contrast to the standard approach, the potential importance of the amino acids in the medium as additional substrate to glucose for a complete description of growth characteristics was shown here.

5.4 *Apparent Coexistence Phenomenon in the Mixed Cultures*

Chemostat experiments with mixed cultures of the two species *S. a.* and *B. c.* resulted in an apparent two-species coexistence (4.4.1). The mixed cultivation of the three species *S. a.*,

B. c., and *P. a.* resulted in apparent coexistence phenomena, as well. Here, at least two of the three species, *B. c.* and *P. a.*, remained in the system (4.5.1). However, due to the quantification limit of the T-RFLP analysis method the results for *S. a.* in both mixed cultivations were not completely straightforward. The limit of quantification of the T-RFLP analysis is about $10^{5.8}$ cfu/mL, which was in the same range as the cell numbers of *S. a.*. It could therefore not be decided, if *S. a.* was washed out or just below the limit of quantification in the experiment. Especially the two-species chemostat result for $D = 0.2 \text{ h}^{-1}$ could be coexistence of *B. c.* and *S. a.*, or possibly washout of *S. a.* (4.4.1). Detection of *S. a.* was shown in a three-species chemostat cultivation by T-RFLP after the application of a glucose pulse (Figure 4.46) and additionally by selective plating after more than 44 volume exchanges, which indicated a possible three-species coexistence (4.5.1).

The coexistence results were unexpected, as coexistence of species in a chemostat is generally assumed to occur only for well defined parameter relations. Additionally, it is an instable stability point in mathematical terms, which would lead to the necessity to apply a controller to sustain it [20]. In order to possibly explain and understand these unexpected experimental results they were compared to mathematical simulations with different assumptions.

For the assumption of growth on glucose as single substrate the mathematical simulations (classic chemostat model) (eqn. syst. 4.20) predicted washout of all but one species : *B. c.* was predicted to stay in for the two-species chemostat (4.4.2.1) and as expected in the three-species chemostat (4.5.3.1), as well. The simulations were consistent with the CEP (2.4.2) of competition for one substrate (glucose). And if in the two-species chemostat washout was considered as experimental result, the simulation predicted the correct species to survive (*B. c.*) (Figure 4.40). However, the simulations for glucose as single substrate could not explain the results of apparent coexistence in the mixed culture experiments. The results were in line with the findings during the single-species characterization, where it became obvious that glucose alone was not sufficient to describe the growth properties of the single species (4.3 ; 5.3). The additional properties of the single species found there, were investigated further for their potential to explain the experimental results of the mixed cultivations and solve the contradiction with the simulation.

5.4.1 Mixed Cultures with Acetate as Additional Carbon Source

S. a. produced acetate during its growth on glucose (4.3.1), which posed the possibility of an acetate biotrophy with the other species, *B. c.* and *P. a.* that were shown experimentally to take up acetate as carbon source (4.3.2.1). These findings led to the assumption and

investigation of an acetate biotrophy (2.3.3) (4.4). In chemostat cultivations with *S. a.* and *B. c.* as producer and consumer of acetate an apparent coexistence was found for the dilution rates $D = 0.05 \text{ h}^{-1}$ (Figure 4.38) and for $D = 0.2 \text{ h}^{-1}$. However, the coexistence result for the higher D was not as explicit; this could possibly also be washout of *S. a.* (Figure 4.39) (see above 5.4). The hypothesis that acetate produced by *S. a.* was taken up by the other species was supported by the fact, that no or only little acetate was detected in mixed cultures (batch and continuous mode) in comparison to cultivations of *S. a.* as single species (Figure 4.19).

Simulations with the assumption acetate biotrophy improved the description of the experiments of the two-species chemostat (4.4.2.2). Depending on the applied parameter set from the single-species experiments the simulation results varied (Figure 4.41 A-D). Clearly, a completely free fit of all parameters did not lead to biologically meaningful results. However, with those values determined from single-species experiments coexistence of *S. a.* and *B. c.* as one possible experimental result was shown (Figure 4.41 B). More appropriately in the following values were used as constraints, which physiologically should not differ between growth with or without acetate. The resulting biologically meaningful parameter sets predicted washout of *S. a.* and, therefore, could explain the second possible interpretation of the experimental observation (Figure 4.41 C, D).

Within the presented project the biotrophy on acetate was analyzed mathematically for the mixed culture of *S. a.* and *B. c.* (4.4.2) [54]. It was shown by bifurcation analysis of stability that for a dilution rate D of 0.05 h^{-1} acetate biotrophy can lead to coexistence for *B. c.* and *S. a.*. The parameter sets for the respective numerical scenario simulations were not completely identical with those used here (4.3.4.1 ; 4.3.4.2), because the work was done in an earlier phase of the project. And the yield of acetate per cell by *S. a.* needed to be higher than determined from the experiments to achieve the coexistence.

Depending on the applied parameters, respectively their way of determination, coexistence or washout of *S. a.* was predicted. Consequently, the protocols of determination of the parameters from the single-species experiments will be crucial for further studies.

As a hypothesis this discrepancy between simulation and experiment could possibly be solved by including pyruvate biotrophy in the model. If instead of an increased acetate yield pyruvate formation could be included in the model, it would possibly yield the same effect on the potential consumer *B. c.* and thereby explain the experimentally found coexistence with parameters from the experiments.

A three-species chemostat model including acetate biotrophy was formulated accordingly to the two-species model (eqn. syst. 4.23). The simulation based on the biologically meaningful parameters from single-species experiments predicted *B. c.* as the remaining species, which was consistent with the result from the two-species simulation. The washout of *P. a.* was predicted to take place even before *S. a.* (Figure 4.48). The assumption of acetate biotrophy therefore could not explain a three-species coexistence, which was consistent with the CEP. The CEP predicts growth of only i (here : 2) species on i substrates (here ; 2, acetate and glucose). However, obviously the parameters of *S. a.* could not explain a stable coexistence with *B. c.*. The acetate biotrophy could neither explain the experimentally found two-species coexistence of *P. a.* and *B. c.*, because after washout of the acetate producer (*S. a.*) no interaction based on acetate was possible and just glucose as substrate was available. It was not resolved, if acetate was not detected in the three-species chemostat cultivation due to washout of *S. a.* or further uptake of acetate by *B. c.* and *P. a.*.

Altogether, it was found that acetate biotrophy is an interaction in the mixed culture of *S. a.*, *B. c.* and *P. a.*. However, the assumption of acetate biotrophy could not explain the apparent coexistence of at least two species in the chemostat.

5.4.2 Evaluation of Mixed Culture with Multiple Substrate Use

Amino acids are used as additional substrate to glucose by the single species (4.3.2.3, 5.3.1.2). And the CEP states that coexistence of a number of species only is possible on at least the same number of substrates [50]. Consequently, two substrates, amino acids and glucose, could possibly explain the experimentally observed two-species coexistence (4.5.1) in theory.

One kinetic (A) was formulated with one maximum specific growth rate with the terms of Monod for glucose and amino acids added together. A second kinetic (B) added two separate Monod terms with two maximum growth rates. With the respective parameter values of the single-species experiments for the respective kinetic formulations of mixed substrate use two three-species models No. 1 with kinetic (A) (eqn. syst. 4.24) and No. 2 with kinetic (B) (eqn. syst. 4.25) have been set up. The model variant No. 1 could not describe the experimental result (Figure 4.49), but predicted washout of *P. a.* even before *S. a.*. The mixed chemostat model variant No. 2 gave a good description of the apparent two species coexistence (Figure 4.50).

It is noteworthy that the achieved prediction of the experiment by the simulation No. 2 was not only a result of the assumption of growth on mixed substrates. The simulation No. 1 with

the same assumption could not describe the cultivation results. The applied formulation of the mixed substrate (A) or (B) was responsible for this difference. This result showed that mathematically for the same physiological assumption coexistence could be generated or prevented. In model No. 1 the kinetics are coupled, thereby growth of *B. c.* on glucose results in an increased uptake of amino acids by *B. c.*, as well. As a consequence *P. a.* does not have any of the two substrates left to grow. In model No. 2 the kinetics are uncoupled, *B. c.* grows on glucose and at the same time leaves amino acids to *P. a.* (4.5.3.4). However, both species grow on both substrates parallel, while they coexist. This was analyzed and confirmed by the simulation of the applied pulses of glucose and amino acids, which led to an increase in cell number of both species (Figure 4.50).

One experimental investigation of three-species growth in a chemostat on two substrates, thiosulfate and acetate, was reported [41] in analogy to the presented project. One of the species, *Thiobacillus neapolitanus*, was a specialist, which means it only grew on thiosulfate, the second, a spirillum-shaped heterotroph, only grew on acetate, and the third was a generalist, a versatile *Thiobacillus* A2, which grew on acetate and thiosulfate. As already stated, such choice of strains according to their known properties has been the standard case in theoretical ecology (2.3.2). The authors investigated two-species combinations of the three and confronted them with different ratios of the substrates at different dilution rates D . For the three-species chemostat the ratios of cell numbers for different ratios of acetate and thiosulfate at steady state were presented for a constant $D = 0.75 \text{ h}^{-1}$. The authors found a three-species coexistence that lasted for 20 volume exchanges. In a second publication the authors presented a mathematical model for the experiments [42]. Their parameter identification was based on the two-species experiments and did not predict the observed three-species coexistence. As a possible reason for this discrepancy the low system dynamics or the high sensitivity of parameters of the mixed culture towards fluctuations in the dilution rate were proposed by the authors.

A «sharing» of substrates as presented here for amino acids and glucose, for which three species compete, has not been investigated before for a three-species mixed culture.

In pure culture studies amino acids or polypeptides are very often part of the culture media. However, they are mostly not considered as a mixed substrate for formulation of the growth models, which means that they are not assumed to limit the cell yield or determine the growth rate. The assumption to model growth in a medium as a whole to determine the maximum specific growth rate is generally applied (2.2.1). In contrast here, the importance to consider

the amino acids with regard to the mixed culture outcome became evident. It was shown that the amino acids present in the medium generated a competitive interaction in addition to glucose between the members of the mixed culture. This mixed substrate competition could explain the observed coexistence of two species in the three-species chemostat.

5.4.3 Explanations for a Possible Three-Species Coexistence

A possible coexistence of all species including *S. a.* during the complete cultivation time could be assumed in the three-species chemostat (5.4) based on the applied pulses (Figure 4.46) and positive selective dilution platings (4.5.2).

By variation of parameters of model No. 2 (4.5.3.4), it was found that possible three-species coexistence could not be achieved for the mixed substrate assumption. This was in accordance to the CEP, which states that coexistence can be achieved just on at least as many substrates as species (2.4.2). However, the affinity of *S. a.* towards amino acids ($K_{S,AA,So}$) had the most relevant impact on the outcome of the simulation. Even a two-species coexistence of *B. c.* and *S. a.* was predicted, if *S. a.* had the highest affinity towards amino acids compared to *B. c.* and *P. a.* and *S. a.* could grow on amino acids only without glucose.

A combination of the assumption of growth on glucose and amino acids (model No. 2) with an acetate biotrophy between the three species (eqn. syst. 4.26) did not predict three-species coexistence. Extensions of model No. 2 (eqn. syst. 4.25) could explain three-species coexistence (4.5.3.5) with: a) valine considered separately from the other amino acids as third substrate (eqn. syst. 4.27), b) a hypothetical product formed by *P. a.*, which could be used as substrate by the two other species (eqn. syst. 4.28).

Assumption a) was based on the experimental observation that *S. a.* had a high affinity to the amino acid valine, which was taken up as the quickest in different experiments. This was also confirmed in literature [107]. The simulation result was confirmed by the theoretical analysis of three species growing on three complementary substrates, which showed the possibility of coexistence over a wide parameter range [147]. Assumption b) was based on the hypothetical formation of gluconate and 2-ketogluconate by *P. a.* (5.3.1.3) [66] and additionally on the fact, that in HPLC analysis many peaks for compounds were observed in pure cultures of *P. a.*, whereas in the chemostat mixed cultures only few peaks were detectable. Thus either the related substances were not produced or they were consumed by the other species.

The presented simulations could qualitatively explain or generate (mathematically) coexistence of three-species. However, further experimental investigations will first have to

validate and quantify the proposed interactions. On the one hand, the hypothetical model extensions for the valine kinetics of *S. a.* and the product formation by *P. a.* together with consumption by *B. c.* and *S. a.* have to be characterized with single-species data. Afterwards, their effect concerning the outcome of the mixed culture dynamics could be evaluated by comparison to the three-species experiment. This on the other hand requires a more detailed investigation on the presence of *S. a.* three-species mixed culture during the cultivation. It has to be determined, whether *S. a.* stays in the chemostat at low cell number or is actually slowly washed out.

Up to now, the effect of biofilm formation on the three-species mixed culture has not been considered. For continuous cultivations biofilms have been reported as a possible impact on the outcome of system dynamics [14]. Although biofilm formation was closely observed during the cultivations and none was visible on the reactor wall, there still was cell material at the gas-liquid phase border and also on the p_{O_2} probe (5.3.1.2). It should be further investigated, what effect possible cell retention and biofilm formation could have on the chemostat dynamics and the possible three-species coexistence. This will have to be quantified and considered in a model variant for testing of possible influences of the found cell numbers on the outcome of the competition.

5.5 *Comparison to the Original System - CF Lungs*

The mixed culture in the chemostat displays some differences in comparison to a potential mixed culture existing in the lungs of a CF patient. One of the major challenges in CF research is the identification of antibiotics and therapies to overcome the high resistance of the bacterial infections in CF patients against the existing treatments.

It is known that tests for such antibiotics on a mixed culture as batch or chemostat would be closer to the “real” system than on single-species cultures on agar plates [38]. Tests on mouse models are probably closer to CF lungs than those *in vitro* systems. Rat and mice models without CF mutation are used as animal models for biofilm bacteria in lungs [60]. Unfortunately, as reported in literature CF knockout mice do not display comparable clinic symptoms as human CF patients, and the same is valid for animal cell models such as MDCK and others [141]. Therefore, antibiotic testing by application of an experimental protocol on the mixed culture presented here in addition to the established methods could be a tribute to the search for new antibiotics and therapeutic strategies.

The bronchial mucus in lungs is a water rich gel (over 97 % water) containing numerous macromolecules such as proteins, glycoproteins, lipids together with inorganic salts [114]. This composition is different compared to the culture medium in the presented study. However, the defined medium established here for the cultivation experiments (4.1.2) would provide the option to add defined components of the “real” system and study their possible impact on the mixed culture.

Compared to the findings in the chemostat cultivations *S. a.* is a frequent infection in CF lungs (2.1.3.1). The apparent weakness of *S. a.* in the chemostat cultivations in this study, which led to washout or at least to very low cell numbers, could be a definite advantage in the natural lung system. First, *S. a.* is auxotroph for many amino acids and additionally requires nucleic acids as substrates [107]. These components are typically present in the lung environment out of lysed host cells [137]. Secondly, *S. a.* withstands very high osmolarity (equivalent to 20 % NaCl) [152]. The increased salt and lower water content is the typical characteristic of the secretory liquids of CF patients, including the lung mucus. This would mean advantageous growth conditions to *S. a.*

The availability of iron is required for the growth of all three strains used in the presented study, which is significant for the lung environment (2.1.3). *S. a.* was reported to react to iron depletion with decrease of growth [144]. *B. c.* and *P. a.* form different siderophores and compete with the host tissue for iron, which is one form of their virulence (2.1.3.2, 2.1.3.3). As a confirmation in the experiments for medium development only weak growth was observed in a medium after formation of a white precipitate (4.1.2), which presumably contained iron as co-precipitate, together with calcium and magnesium phosphates. Therefore, the competition for iron among the three species could be assumed to take place in the chemostat mixed culture as well as in the lungs.

An additional effect could be a possible synergistic use of macromolecules existing in the bronchial mucus. Not all bacteria are capable to express the necessary enzymes to degrade those into the respective monomers. Therefore, the property of *S. a.* to synthesize a variety of such enzymes as virulence factors [4] could be an advantage for other species present, leading to mutual support.

A susceptibility of *P. a.* towards O₂ supply conditions was found in the experiments (4.1.3) and was reported in literature [122]. In the epithelial areas of lung, O₂ reduced conditions do often occur [156]. Consequently, an effect on growth of *P. a.* in lungs of CF patients based on

the p_{O_2} could be expected, but has so far not been and probably can not be studied *in situ* due to the localization of the cultures in patients.

In biofilms the imbedded bacteria are confronted with spatial and temporal gradients of environmental conditions concerning pH, p_{O_2} , substrate, and product concentrations. These gradients could lead to local advantages of species and therefore on the whole to stable coexistence.

The approach to study a mixed culture consisting of CF relevant bacteria in a laboratory chemostat system has not been presented before. It provides the possibility to analyze the reaction of the mixed culture quantitatively for the individual species depending on the different influencing parameters. In further studies the effect of elevated osmolarity, O_2 limitation, iron limitation, pH values, substrate variation and especially antibiotics on growth dynamics and the outcome of the competition can be investigated and evaluated both, quantitatively and separately for each parameter.

6 Summary

In the presented project the growth dynamics of a three-species mixed culture were investigated, both experimentally and by mathematical modeling. With the three strains, *S. a.*, *B. c.*, and *P. a.*, known from the context of infections in lungs of CF patients, a reproducible chemostat was set up under defined conditions in an STR. The concept was to identify possible interspecies interactions that might occur when strains are co-cultivated by comparison of experimental mixed culture results and simulations based on single-species data (model assumptions). Data on cell numbers in mixed culture samples with high accuracy were essential for this aim. Therefore, a quantitative analysis method had to be established.

A quantitative T-RFLP method was evaluated and applied for specific and absolute cell number enumerations. The method allowed reproducible enumerations of mixed cultures and was tested to be unbiased by quantitative sample composition. Log-transformed absolute cell numbers of single-species dilutions were linear within a lower working range of 10^4 to 10^6 cfu/mL (species-dependent) and an upper working range of 10^{10} cfu/mL. The error of three-species samples was 6.95 ± 0.20 log-transformed cfu/mL (mean \pm SD). A maximum error of 8.60 ± 0.39 log-transformed cfu/mL was determined for two-species samples.

A defined, but full medium based on a basal cell culture medium was adjusted with phosphate buffer and NTA and established for cultivation of bacterial strains that are frequent in lungs of CF patients. The resulting composition M199+P+NTA provided good growth for all chosen strains and five further strains additionally surveyed. At the same time it facilitated analysis of all educts and substrates of interest, as it contained no complex components.

Mixed culture experiments were performed as chemostat cultures for two species, *S. a.* and *B. c.*, and the three species, *S. a.*, *B. c.*, and *P. a.* at dilution rates 0.05 h^{-1} and 0.2 h^{-1} . In the two-species experiments the results were not definite, whether stable coexistence for *S. a.* and *B. c.* or a very slow washout of *S. a.* was the case. In the three-species experiments a stable coexistence of at least two of the three species, namely *B. c.* and *P. a.*, was achieved for more than 35 volume exchanges. Additionally, selective dilution plating for *S. a.* indicated the presence of *S. a.* in the mixed culture chemostat up to the end of the cultivation.

As the experimentally found stable coexistence was not explained by a classical chemostat model based on one substrate (glucose), investigations with single-species on possible interactions and on the formulation of the related model extensions were conducted. The

parameter values applied in mixed culture chemostat models were determined completely from separate pure culture experiments.

An acetate biotrophy was simulated for both the two-species and the three-species chemostat. For a parameter set determined from single-species cultures without constraints coexistence for the two-species chemostat was theoretically explained. For biologically meaningful parameter sets no coexistence was predicted for the two- and the three-species chemostat by the assumption of acetate biotrophy. However, the acetate biotrophy was assumed to take place, as no acetate was detected in mixed culture experiments during batch- and during the continuous phase. The acetate interaction was not sufficient to explain coexistence.

The assumption of mixed substrate growth on glucose and amino acids that are used independently of each other by *P. a.* and *B. c.* (diauxic) was formulated mathematically in two variants: coupled ($\mu_{max,199,i}$) (A) and uncoupled ($\mu_{max,Glc,i}$ and $\mu_{max,AA,i}$) (B) use and dependently for *S. a.*. A very good consistency between the experimental result and the simulation for the proposed model variant No. 2 (eqn. syst. 4.25) based on formulation (B) ("substrate sharing") was achieved. It confirmed the apparent coexistence of at least two of the species, *B. c.* and *P. a.*, and the washout of the third, *S. a.* This assumption also allowed to describe the effect of an enhanced specific growth rate at the point of washout D_{crit} observed in the chemostat cultures compared to the batch experiments for *P. a.* and *B. c.* as single-species.

A possible three-species coexistence, as could be assumed by selective plates for *S. a.*, was not explained based on the mixed substrate model variant No. 2. A model, which combined the models of acetate biotrophy and mixed substrate growth, did not describe three-species coexistence either. Extensions of model No. 2 with another (additional) theoretical interaction a) competition for valine or b) a biotrophy with a hypothetical product formed by *P. a.* were qualitatively able to explain or generate (mathematically) coexistence of three-species. However, further experiments will have to investigate the proposed interactions.

Within this project it was shown that by comparison of the mathematical description of a mixed culture chemostat with experimental data derived by rapid and reliable enumeration of absolute cell numbers from mixed samples potential species interactions were successfully identified. The research was conducted for three species with arbitrary and unknown properties, which was not presented in literature before. The detailed experimental analysis and mathematical description of the pure cultures was found as an additionally required prerequisite of the performed investigations.

7 Outlook

The presented project successfully demonstrated that the quantitative T-RFLP for cell number enumeration delivered an important prerequisite for mixed culture investigations. For low cell numbers of *S. a.* additional selective dilution plating were necessary due to the limiting quantification range of T-RFLP. In order to be independent from such additional quantification methods it would be desirable to extend the T-RFLP quantification range, for example by application of specific primers for each species to prevent competition for primers during the PCR reaction. Additionally, other methods for mixed sample analysis such as flow cytometry could be evaluated for their applicability on the investigated system.

The experimental and mathematical analyses of the interactions of the bacterial species led to a good description of the observed behavior of the three-species mixed culture (two-species coexistence). In order to explain stable three-species coexistence the growth characteristics and metabolites of the pure cultures need to be closer understood and characterized. For example a possible pyruvate biotrophy could be investigated in addition to the already tested acetate biotrophy between *S. a.* and the other two species. The uptake of individual amino acids, for example valine, by the single species should be experimentally analyzed in more detail and afterwards be implemented accordingly into the models. Additionally, the presence of possible other substrates for *B. c.* and *P. a.* or metabolites of these species (gluconate, 2-ketogluconate) should be investigated. The possibility of polysaccharide production and secretion of quorum-sensing signaling molecules should also be considered. Such macromolecules could represent a possible substrate for *S. a.* and another possible synergistic interaction, if they were degraded by one species and afterwards used by more than one species.

For this purpose the HPLC data analysis, which was established within the presented project, but only few peaks have yet been identified, should be used in more detail for growth analysis of the cultures. Additionally, a medium containing fewer components could be helpful to identify the substances actually required by the strains.

Care should be taken not to extend the pure culture models with all properties, which can be found in the data. Only those which have a significant impact on the overall dynamic behavior and can therefore be identified as an important property of the species should be included and tested for their impact in the mixed culture as well.

The possibility of bacterial growth on the wall of the bioreactor should be quantified experimentally for cell number and viability in the biofilm and afterwards be considered in the mathematical models. The resulting possible impact on mixed chemostat and single-species cultures, especially with regard to the observed increase of washout in XD compared to one expected from the maximum specific growth rate of batch cultures will have to be evaluated.

An operating diagram for a model of two species growing on two substitutable substrates was proposed in literature [117]. It could be evaluated, if such a theoretical analysis could be applied for the experimental system presented in this project, as well. Additionally, for the further project an application of other parameter estimation method in particular for μ_{max} and K_s , as for example proposed by Baltes et al. [7], could be tested, as it was found that the values were crucial for the predicted outcome of the competition. To evaluate the impact of the parameters on the system dynamics, sensitivity analyses and parameters variation studies should be conducted.

In the long term the answer of the mixed culture system to externally applied disturbances, for example antibiotic pulses could be analyzed. The results of model analysis could contribute to the development of new therapeutic approaches towards the typically very complex clinic manifestations of bacterial mixed infections. The reproducible heterogeneous bacterial chemostat culture in a quasi-stationary condition will be useable, for example as a model test system for efficacy studies using antibiotics.

The experimental set-up and protocol will function for other mixed cultures of interest or an extension of the presented system with additional strains as well. The T-RFLP analysis quantification parameters and the choice of a suitable defined medium will have to be adapted for different species in the mixed culture. Afterwards, the overall methodology presented here, allows quantitatively analyzing mixed cultures consisting of more than two species. The achieved quality of data provides the comparability with mathematical simulations for the validation of mathematical models or for the identification of potentially required model extensions. Thereby it can contribute to other fields in which mixed cultures are studied, especially for validation of proposed models in mathematical biology projects.

8 References

1. Anderlei, T. and J. Büchs. 2001. Device for Sterile Online Measurements of the Oxygen Transfer Rate in Shaking Flasks. *Biochemical Engineering Journal* 7:157-162.
2. Andrews, J.F. 1968. A Mathematical Model for Continuous Culture of Microorganisms Utilizing Inhibitory Substrates. *Biotechnology and Bioengineering* 10:707 - 723.
3. Armstrong, R.A. and R. McGehee. 1980. Competitive Exclusion. *The American Naturalist* 115(2):151-170.
4. Arvidson, S., A. Björklind, R. Eriksson, and T. Holme. 1976. Enzymes from *Staphylococcus aureus*. In: D. A.C.R., E. D.C., E. C.G.T., and M. J., editors. *Continuous Culture Vol. 6: Applications and New Fields*. Chichester: Ellis Horwood.
5. Bader, F.B. 1982. Kinetics of Double-Substrate Limited Growth. In: M.J. Bazin, editor. *Microbial Population Dynamics*. Boca Raton, Florida: CRC Press, Inc. p 1-31.
6. Bakke, R., M.G. Trulear, J.A. Robinson, and W.G. Characklis. 1984. Activity of *Pseudomonas aeruginosa* in Biofilms. *Biotechnology and Bioengineering* 26:1418-1424.
7. Baltes, M., R. Schneider, C. Sturm, and M. Reuss. 1994. Optimal Experimental Design for Parameter Estimation in Unstructured Growth Models. *Biotechnol. Prog.* 10:480-488.
8. Bazin, M.J., P.T. Saunders, and J.I. Prosser. 1976. Models of Microbial Interactions in the Soil. *Critical Reviews in Microbiology*:463-498.
9. Beckmann, W. and T.G. Lessie. 1979. Response of *Pseudomonas aeruginosa* to beta-Lactam Antibiotics: Utilization of Penicillin G as the Carbon Source. *Journal of Bacteriology* 140(3):1126-1128.
10. Beyenal, H., S.N. Chen, and Z. Lewandowski. 2003. The Double Substrate Growth Kinetics of *Pseudomonas aeruginosa*. *Enzyme and Microbial Technology* 72:92-98.
11. Blackwood, C.B., T. Marsh, S.-H. Kim, and E.A. Paul. 2003. Terminal Restriction Fragment Length Polymorphism Data Analysis for Quantitative of Microbial Communities. *Applied and Environmental Microbiology* 69(2):926-932.
12. Breidt, F. and H.P. Fleming. 1998. Modeling of the Competitive Growth of *Listeria monocytogenes* and *Lactococcus lactis* in Vegetable Broth. *Applied and Environmental Microbiology* 64(9):3159-3165.
13. Brock, T.D. 2001. *Mikrobiologie*. Berlin: Spektrum Akademischer Verlag Heidelberg.
14. Bryers, J.D. 1984. Biofilm Formation and Chemostat Dynamics: Pure and Mixed Culture Considerations. *Biotechnol Bioeng* 26:948-958.
15. Burkhardt, F. 1992. *Mikroskopische Diagnostik* Stuttgart: Thieme Verlag. 94; 142-144 p.
16. Butler, G.J., S.B. Hsu, and P. Waltman. 1985. A Mathematical Model of the Chemostat with Periodic Washout Rate. *Journal of Applied Mathematics* 45(3):435-449.
17. Chandler, D.P., J.K. Fredrickson, and F.J. Brockman. 1997. Effect of PCR Template Concentration on the Composition and Distribution of Total Community 16S rDNA Clone Libraries. *Molecular Ecology* 6:475-482.
18. Chen, J. and P.J. Weimerer. 2001. Competition among Three Predominant Ruminant Cellulolytic Bacteria in the Absence or Presence of Non-Cellulolytic Bacteria. *Microbiology* 147:21-30.
19. Chian, S.K. and R.I. Mateles. 1968. Growth of Mixed Cultures on Mixed Substrates. *Applied Microbiology* 16(9):1337-1342.
20. Chmiel, H. 2006. *Bioprozesstechnik*. München: Elsevier GmbH. 144-145 p.
21. Costerton, J.W., P.S. Stewart, and E.P. Greenberg. 1999. Bacterial Biofilms: A Common Cause of Persistent Infections. *Science* 284:1318-1322.
22. de Bentzmann, S., C. Plotkowski, and E. Puchelle. 1996 Receptors in the *Pseudomonas aeruginosa* Adherence to Injured and Repairing Airway Epithelium. *American Journal of Respir. Crit. Care Med.* 154:155-162.
23. de Leenheer, P. and H.L. Smith. 2003. Feedback Control for Chemostat Models. *Journal of Mathematical Biology* 46:48-70.
24. de Rose, V. 2002. Mechanisms and Markers of Airway Inflammation in Cystic Fibrosis. *European Respiration Journal* 19:333-340.
25. deFreitas, M.J. and A.G. Fredrickson. 1978. Inhibition as a Factor in the Maintenance of the Diversity of Microbial Ecosystems. *J. Gen. Microbiol.* 106:307-320.
26. Dunne, W.M. 2002. Bacterial Adhesion: Seen any good Biofilms lately? *Clinical Microbiology Reviews* 15(2):155-166.
27. Duthoit, F., J.J. Godon, and M.C. Montel. 2003. Bacterial Community Dynamics During Production of Registered Designation of Origin Salers Cheese as Evaluated by 16S rRNA Gene Single-strand Conformation Polymorphism Analysis. *Applied and Environmental Microbiology* 69(7):3840-3848.
28. Dykhuizen, D. and M. Davies. 1980. An experimental model: Bacterial Specialists and Generalists Competing in Chemostats. *Ecology* 61:1213.

29. Eberl, L. and B. Tümmler. 2004. *Pseudomonas aeruginosa* and *Burkholderia cepacia* in Cystic Fibrosis: Genome Evolution, Interactions and Adaptation International Journal of Medical Microbiology 294:123-131.
30. Egert, M. and M.W. Friedrich. 2003. Formation of Pseudo-Terminal Restriction Fragments, a PCR-Related Bias Affecting Terminal Restriction Fragment Length Polymorphism Analysis of Microbial Community Structure. Applied and Environmental Microbiology 69(5):2555-2562.
31. Farrelly, V., F.A. Rainey, and E. Stackebrandt. 1995. Effect of Genome Size and *rm* Gene Copy Number on PCR Amplification of 16S rRNA Genes from a Mixture of Bacterial Species. Applied and Environmental Microbiology 61(7):2798-2801.
32. Fogel, G.B., C.R. Collins, J. Li, and C.F. Brunk. 1999. Prokaryotic Genome Size and SSU rDNA Copy Number: Estimation of Microbial Relative Abundance from a Mixed Population. Microbial Ecology 38:93-113.
33. Fredrickson, A.G. 1977. Behavior of Mixed Cultures of Microorganisms. Annual Review Microbiology: 31:63-87.
34. Fredrickson, A.G. 1982. Interactions of Microbial Populations in Mixed Culture Situations. In: B.H. W., P.E. T., and S. G., editors. Foundations of Biochemical Engineering Kinetics and Thermodynamics in Biological Systems: ACS Symposium Series 207.
35. Gardner, J.F. and J. Lascelles. 1962. The Requirement for Acetate of a Streptomycin-resistant Strain of *Staphylococcus aureus*. Journal of Gen. Microbiol. 29:157-164.
36. Gause, G.F. 1932. Experimental Studies on the Struggle for Existence. Journal of Experimental Biology.
37. Genzel, Y., S. Koenig, and U. Reichl. 2004. Amino Acid Analysis in Mammalian Cell Culture Media Containing Serum and High Glucose Concentrations by Anion Exchange Chromatography and Integrated Pulsed Amperometric Detection. Analytical Biochemistry 335:119-125.
38. Ghani, M. and J.S. Soothill. 1997. Ceftazidime, Gentamicin, and Rifampicin, in Combination, Kill Biofilms of Mucoid *Pseudomonas aeruginosa*. Canadian Journal of Microbiology 43(11):999-1004.
39. Gilligan, P.H. 1991. Microbiology of Airway Disease in Patients with Cystic Fibrosis. Clinical Microbiology Reviews 4(1):35-51.
40. Gilliland, G., S. Perrin, K. Blanchard, and H.F. Bunn. 1990. Analysis of Cytokine mRNA and DNA: Detection and Quantitation by Competitive Polymerase Chain Reaction. Proceedings of National Academic Sciences USA 87:2725-2729.
41. Gottschal, J.C., S. de Vries, and J.G. Kuenen. 1979. Competition Between the Facultatively Chemolithotrophic *Thiobacillus* A2, an Obligately Chemolithotrophic *Thiobacillus* and a Heterotrophic *Spirillum* for Inorganic and Organic Substrates. Archives of Microbiology 121:241-249.
42. Gottschal, J.C. and T.F. Thingstad. 1982. Mathematical Description of Competition between Two and Three Bacterial Species under Dual Substrate Limitation in the Chemostat: A Comparison with Experimental Data. Biotechnology and Bioengineering 24:1403-1418.
43. Gottschal, J.C. 1986. Mixed Substrate Utilization by Mixed Cultures. In: J.S. Poindexter and E.R. Leadbetter, editors. Methods and Special Applications in Bacterial Ecology. New York: Plenum Press. p 261-292.
44. Gottschal, J.C. and L. Dijkhuizen. 1988. The Place of the Continuous Culture in Ecological Research. In: W. J.W.T., editor. Handbook of Laboratory Model Systems for Microbial Ecosystems. Boca Raton, Florida: CRC Press, Inc. p 19ff.
45. Gottschal, J.C. 1990. Different Types of Continuous Culture in Ecological Studies. In: G. R. and N.J. R., editors. Methods in Microbiology (Vol. 22): Techniques in Microbial Ecology. London: Academic Press Ltd.
46. Gottschal, J.C. 1993. Growth Kinetics and Competition – some Contemporary Comments. Antonie van Leeuwenhoek 63(3-4):299-313.
47. Haefner, J.W. 2005. Modeling Biological Systems. New York: Springer Verlag.
48. Hansen, S.R. and S.P. Hubbell. 1980. Single-Nutrient Microbial Competition: Qualitative Agreement between Experimental and Theoretically Forecast Outcomes. Science 207(4438):1491-1493.
49. Harder, W. and L. Dijkhuizen. 1976. Mixed Substrate Utilization. In: D. A.C.R., E. D.C., E. C.G.T., and M. J., editors. Continuous Culture Vol. 6: Applications and New Fields. Chichester U.K.: Ellis Horwood.
50. Hardin, G. 1960. The Competitive Exclusion Principle. Science 131:1292-1298.
51. Herbert, D., R.C. Elsworth, and G. Telling. 1956. The Continuous Culture of Bacteria: a Theoretical and Experimental Study. Journal General Microbiology 14:601-622.
52. Herbert, D. 1958. Continuous Culture of Microorganisms; some Theoretical Aspects. In: I. Málek, editor. Continuous Cultivations of Microorganisms. Prague, Czech Republic: Czech Academy of Sciences.
53. Herbert, D. 1961. The Chemical Composition of Micro-organisms as a Function of Their Environment. Microbial reaction to environment: eleventh symposium of the Society of Gen. Cambridge: University Press. p 391-416.

54. Hessel, J., J.K. Schmidt, U. Reichl, and D. Flockerzi. 2006. Coexistence in the Chemostat as a Result of Metabolic By-Products. *Journal of Mathematical Biology* 53(4):556-584.
55. Heydorn, A., B.K. Ersboll, M. Hentzer, M.R. Parsel, M. Givskov, and S. Molin. 2000. Experimental Reproducibility in Flow-chamber Biofilms. *Microbiology* 149:2409-2415.
56. Higuchi, R., C. Fockler, G. Dollinger, and R. Watson. 1993. Kinetic PCR Analysis: Real-time Monitoring of DNA Amplification Reactions. *Biotechnology* 11:1026-1030.
57. Hogardt, M., K. Trebesius, A.M. Geiger, M. Hornef, J. Rosenecker, and J. Heesemann. 2000. Specific and Rapid Detection by Fluorescent In Situ Hybridization of Bacteria in Clinical Samples Obtained from Cystic Fibrosis Patients. *Journal of Clinical Microbiology* 38(2):818-825.
58. Hoiby, N., G. Döring, and P.O. Schoitz. 1987. Pathogenic Mechanisms of Chronic *Pseudomonas aeruginosa* Infections in Cystic Fibrosis Patients. *Antibiot. Chemother* 39:60-76.
59. Hoiby, N., *Pseudomonas in Cystic Fibrosis: Past, Present, Future*, in The Joseph Levy Memorial Lecture (internet: http://www.ecfsoc.org/pa_review/nh_lect.html). 1998.
60. Hoiby, N., H.K. Johansen, C. Moser, Z. Song, O. Ciofu, and A. Kharazmi. 2001. *Pseudomonas aeruginosa* and the *In Vitro* and *In Vivo* Biofilm Mode of Growth. *Microbes and Infection* 3:23-25.
61. Hsu, S.B., S.P. Hubbell, and P. Waltman. 1977. A Mathematical Theory for Single-nutrient competition in continuous cultures of micro-organisms *SIAM Journal of Applied Mathematics* 32(2):366-383.
62. Hsu, S.B. 1980. A Competition Model for a Seasonally Fluctuating Nutrient. *Journal of Mathematical Biology* 9:115-132.
63. Hsu, S.B., Y.-S. Li, and P. Waltman. 2000. Competition in the Presence of a Lethal External Inhibitor. *Mathematical Biosciences* 167(2):177-199.
64. Huisman, J. and F.J. Weissing. 2001. Biological Conditions for Oscillations and Chaos Generated by Multispecies Competition. *Ecology* 82(10):2682-2695.
65. Huisman, J. and F.J. Weissing. 2002. Oscillations and Chaos Generated by Competition for Interactively Essential Resources. *Ecological Research* 17:175-181.
66. Hunt, J.C. and P. Pibbs. 1983. Regulation of Alternate Peripheral Pathways of Glucose Catabolism during Aerobic and Anaerobic Growth of *Pseudomonas aeruginosa*. *Journal of Bacteriology* 154(2):793-802.
67. Hutchinson, G.E. 1961. The Paradox of the Plankton. *The American Naturalist* 95(882):137-145.
68. Jannasch, H.W. 1967. Enrichment of Aquatic Bacteria in Continuous Culture. *Journal General Microbiology* 59:165-173.
69. Jannasch, H.W. and T. Egli. 1993. Microbial Growth Kinetics: a Historical Perspective. *Antonie van Leeuwenhoek* 63:213-224.
70. Kendall, A.I., T.E. Friedemann, and M. Ishikawa. 1930. Quantitative Observations on the Chemical Activity of "Resting" *Staphylococcus aureus*. *Journal of Infectious Diseases* 47:223-228.
71. Kerem, B.S., J.M. Rommans, J.A. Buchanam, D. Markiewicz, T.K. Cox, A. Chakravarti, M. Buchwald, and L.C. Tsu. 1989. Identification of the Cystic Fibrosis Gene: Genetic Analysis. *Science* 245:1073-1080.
72. Kitts, C.L. 2001. Terminal Restriction Fragment Patterns: A Tool for Comparing Microbial Communities and Assessing Community Dynamics. *Curr. Issues Intest. Microbiol.* 2(1):17-25.
73. Kovarova-Kovar, K. and T. Egli. 1998. Growth Kinetics of Suspended Microbial Cells: From Single-Substrate-Controlled Growth to Mixed-Substrate Kinetics. *Microbiology and Molecular Biology Reviews* 62(3):646-666.
74. Krebs, H.A. 1937. Dismutation of Pyruvic Acid in *Gonococcus* and *Staphylococcus*. *Biochemistry Journal* 31:661-671.
75. Kuehn, M., K. Lent, J. Haas, J. Hagenzieker, M.U. Cervin, and A.L. Smith. 1992. Fimbriation of *Pseudomonas cepacia*. *Infections and Immunology* 60 2002 - 2007.
76. Kuennen, J.G. 1981. Mixed Substrates and Mixed Culture. *Antonie van Leeuwenhoek* 47:187-189.
77. Laanbroek, H.J., A.J. Smit, G. Klein Nulend, and H. Veldkamp. 1979. Competition for L-Glutamate between Specialised and Versatile *Clostridium* Species. *Archives of Microbiology* 120:61-66.
78. Lee, I.H., A.G. Fredrickson, and H.M. Tsuchiya. 1976. Dynamics of Mixed Cultures of *Lactobacillus plantarum* and *Propionibacterium shermanii*. *Biotechnology and Bioengineering* 18:513.
79. Lenas, P. and S. Pavlou. 1995. Coexistence of Three Competing Microbial Populations in a Chemostat with Periodically Varying Dilution Rate. *Mathematical Biosciences* 129:111-142.
80. Levin, S.A. 1970. Community Equilibria and Stability, and an Extension of the Competitive Exclusion Principle. *American Naturalist* 104(939):413-423.
81. Lewenza, S., B. Conway, E.P. Greenberg, and P.A. Sokol. 1999. Quorum Sensing in *Burkholderia cepacia*: Identification of the LuxRI Homologs CepRI *Journal of Bacteriology* 181 748-756.
82. Lobry, C. and J. Harmand. 2006. A New Hypothesis to Explain the Coexistence of *n* Species in the Presence of a Single Resource. *Comptes Rendus Biologies* 329(1):40-46.
83. Loladze, I., Y. Kuang, W.F. Fagan, and J.J. Elser. 2004. Competition and Stoichiometry: Coexistence of Two Predators on One Prey. *Theoretical Population Biology* 65:1-14.

84. Lu, Z. and K.P. Haderl. 1998. Model of Plasmid-Bearing, Plasmid-Free Competition in the Chemostat with Nutrient Recycling and an Inhibitor. *Mathematical Biosciences* 148:147-159.
85. Lubin, M.B., J.D. Elashoff, S.-J. Wang, W.I. Rotter, and H. Toyoda. 1991. Precise Gene Dosage Determination by Polymerase Chain Reaction: Theory, Methodology, and Statistical Approach. *Molecular and Cellular Probes* 5:307-317.
86. Luedeking, R. and E.L. Piret. 1959. A Kinetic Study of Lactic Acid Fermentation. Batch Process at Controlled pH. *Journal of Biochemical and Microbiological Technology and Engineering* 1(4):393-412.
87. Lueders, T. and M. Friedrich. 2000. Archaeal Population Dynamics during Sequential Reduction Processes in Rice Field Soil. *Applied and Environmental Microbiology* 66(7):2732-2742.
88. Lueders, T. and M.W. Friedrich. 2003. Evaluation of PCR Amplification Bias by Terminal Restriction Fragment Length Polymorphism Analysis of Small-subunit rRNA and mcr A Genes by Using Defined Template Mixtures of Methanogenic Pure Cultures and Soil DNA Extracts. *Applied and Environmental Microbiology* 1(1):320-6.
89. Lukow, T., P. Dunfield, and W. Liesack. 2000. Use of the T-RFLP Technique to Assess Spatial and Temporal Changes in the Bacterial Community Structure within an Agricultural Soil Planted with Transgenic and Non-transgenic Potato Plants. *FEMS Microbiol. Ecology* 32:241-247.
90. Mai, V. and J.G.J. Morris. 2004. Colonic Bacterial Flora: Changing Understandings in the Molecular Age. *Journal of Nutrition* 134(2):459-464.
91. Marsh, P.D. and G.H.W. Bowden. 2000. Microbial Community Interactions in Biofilms. In: D.G. Allison, P. Gilbert, H.M. Lappin-Scott, and M. Wilson, editors. *Community Structure and Co-operation in Biofilms*. Cambridge: University Press. p 167-198.
92. May, R.M. and W.J. Leonard. 1975. Nonlinear Aspects of Competition between Three Species. *Journal of Applied Mathematics* 29(4):243-253.
93. McDermid, A.S., A.S. McKee, and P.D. Marsh. 1985. A Mixed-culture Chemostat System to Predict the Effect of Anti-microbial Agents on the Oral Flora: Preliminary Studies using Chlorhexidine. *Journal of Dental Research* 66(8):1315-1320.
94. McKee, A.S., A.S. McDermid, D.C. Ellwood, and P.D. Marsh. 1985. The Establishment of Reproducible Complex Communities of Oral Bacteria in the Chemostat Using Defined Inocula. *Journal of Applied Bacteriology* 59:263-275.
95. McKenney, D., K.E. Brown, and D.G. Allison. 1995. Influence of *Pseudomonas aeruginosa* Exoproducts on Virulence Factor Production in *Burkholderia cepacia*: Evidence of Interspecies Communication. *Journal of Bacteriology* 177(23):6989-6992.
96. Megee, R.D., J.F. Drake, A.G. Fredrickson, and H.M. Tsuchiya. 1972. Studies in Intermicrobial Symbiosis. *Saccharomyces cerevisiae* and *Lactobacillus casei*. *Canadian Journal of Microbiology* 18:1733-?
97. Mikx, F.H.M. and J.S. Van der Hoeven. 1975. Symbiosis of *Streptococcus mutans* and *Veillonella alcalescens* in Mixed Continuous Cultures. *Archives of Oral Biology* 20:407.
98. Miura, Y., H. Tanaka, and M. Okazaki. 1980. Stability Analysis of Commensal and Mutual Relations with Competitive Assimilation in Continuous Mixed Culture. *Biotechnology and Bioengineering* 22:929-948.
99. Monod, J. 1949. The Growth of Bacterial Cultures. *Annual Review Microbiology* 3:371-394.
100. Monod, J. 1950. La Technique de Culture Continu; Théorie et Applications. *Ann. Inst. Pasteur* 79:390.
101. Mortimer, C.E. 1996. *Chemie. U. Mueller*, translator. Stuttgart - New York: Georg Thieme Verlag.
102. Mueller, S., A. Loesche, T. Bley, and T. Scheper. 1995. A Flow Cytometric Approach for Characterization and Differentiation of Bacteria during Microbial Processes. *Applied Microbiology and Biotechnology* 43:93-101.
103. Munack, A. Optimal Feeding Strategy for Identification of Monod-type Models by Fed Batch Experiments. in *Reprints of the 4th International Congress on Computer Applications in Fermentation Technology*. 1988: Ellis Horwood Limited.
104. Narang, A. 1998. The Steady States of Microbial Growth on Mixtures of Substitutable Substrates in a Chemostat. *Journal of Theoretical Biology* 190:241-261.
105. Narang, A. 2005. Toward an Integrated Physiological Theory of Microbial Growth: from Subcellular Variables to Population Dynamics. *Mathematical Biosciences and Engineering* 2(1):169-206.
106. Novick, A. and L. Szilard. 1950. Description of the Chemostat. *Science* 112:715.
107. Onoue, Y. and M. Mori. 1997. Amino Acid Requirements for the Growth and Enterotoxin Production by *Staphylococcus aureus* in Chemically Defined Media. *International Journal of Food Microbiology* 36:77-82.
108. Osborn, A.M., E.R.B. Moore, and K.N. Timmis. 2000. An Evaluation of Terminal-Restriction Fragment Length Polymorphism (T-RFLP) Analysis for the Study of Microbial Community Structure and Dynamics. *Environmental Microbiology* 2(1):39-50.
109. Palleroni, N.J., R.W. Ballard, E. Ralston, and M. Doudoroff. 1972. Deoxyribonucleic Acid Homologies Among Some *Pseudomonas* Species. *Journal of Bacteriology* 110(1):1-11.

110. Passarge, J. and J. Huisman. 2002. Competition in Well-Mixed-Habitats. In: U. Sommer and B. Worm, editors. Competition and Coexistence. Berlin Heidelberg: Springer Verlag. p Chapter 2.
111. Pier, G.B. 2000. Role of the Cystic Fibrosis Transmembrane Conductance Regulator in Innate Immunity to *Pseudomonas aeruginosa* Infections Proceedings of the National Academic Science USA 97 8822-8828.
112. Pilyugin, S.S., G.T. Reeves, and A. Narang. 2004. Predicting Stability of Mixed Microbial Cultures from Single Species Experiments: 2. Physiological Model. Mathematical Biosciences 192(2):111-136.
113. Pirt, S.J. 1975. Principles of Microbe and Cell Cultivation. Oxford.
114. Plotkowski, M.C., S. de Bentzmann, and E. Puchelle. 2000. Studying Bacterial Adhesion to Respiratory Mucosa. In: Y.H. An and R.J. Friedmann, editors. Handbook of Bacterial Adhesion: Principles, Methods, and Applications. Totowa, New Jersey: Humana Press Inc. p 457-485.
115. Pschyrembel, W. 2002. Klinisches Woerterbuch. Berlin: Walter de Gruyter.
116. Qazi, S., B. Middleton, S.H. Muharram, A. Cockayne, P. Hill, P. O'Shea, S.R. Chhabra, M. Camara, and P. Williams. 2006. N-Acyl-Homoserine Lactones Antagonize Virulence Gene Expression and Quorum Sensing in *Staphylococcus aureus*. Infection and Immunity 74(2):910-919.
117. Reeves, T.G., A. Narang, and S.S. Pilyugin. 2004. Growth of Mixed Cultures on Mixtures of Substitutable Substrates: the Operating Diagram for a Structured Model. Journal of Theoretical Biology 226:143-157.
118. Renders, N., H. Verbrugh, and A. van Belkum. 2001. Dynamics of Bacterial Colonisation in the Respiratory Tract of Patients with Cystic Fibrosis. Infection, Genetics and Evolution 1:29-39.
119. Riedel, K., M. Hentzer, O. Geisenberger, B. Huber, A. Steidle, H. Wu, N. Hoiby, M. Givskov, S. Molin, and L. Eberl. 2001. N-Acyl-Homoserine Lactone Mediated Communications between *Pseudomonas aeruginosa* and *Burkholderia cepacia* in Mixed Biofilms. Microbiology 174(Pt12):3249-62.
120. Robinson, J.A., M.G. Trulear, and W.G. Characklis. 1984. Cellular Reproduction and Extracellular Polymer Formation by *Pseudomonas aeruginosa* in Continuous Culture. Biotechnology and Bioengineering 26:1409-1417.
121. Rogers, J.B., N.M. Duteau, and K.F. Reardon. 2000. Use of 16S-rRNA to Investigate Microbial Population Dynamics During Biodegradation of Toluene and Phenol by a Binary Culture. Biotechnology and Bioengineering 70(4):436-445.
122. Sabra, W., E.-J. Kim, and A.-P. Zeng. 2002. Physiological Responses of *Pseudomonas aeruginosa* PAO1 to Oxidative Stress in Controlled Microaerobic and Aerobic Cultures. Microbiology 148:3195-3202.
123. Saiman, L., G. Cacalano, and A. Prince. 1990. *Pseudomonas cepacia* Adherence to Respiratory Epithelial Cells is Enhanced by *Pseudomonas aeruginosa*. Infection and Immunity 58:2578-2584.
124. Schaal, K.P. and A. Graevenitz. 1994. *Pseudomonaden* und andere anspruchsllose, nicht-fermentierende, gram-negative Bakterien. In: H. Brandes, W. Köhler, H.J. Eggers, and G. Pulverer, editors. Lehrbuch der Medizinischen Mikrobiologie. Stuttgart Jena New York: Gustav Fischer Verlag. p 463-472.
125. Schlegel, H.G. 1992. Allgemeine Mikrobiologie. Stuttgart, New York: Thieme. 634 p.
126. Schmidt, J.K., B. Koenig, and U. Reichl. 2007. Characterization of a Three Bacteria Mixed Culture in a Chemostat: Evaluation and Application of a Quantitative Terminal-Restriction Fragment Length Polymorphism (T-RFLP) Analysis for Absolute and Species Specific Cell Enumeration. Biotechnology and Bioengineering 96(4):738-758.
127. Schneegurt, M.A. and C.F. Kulpa. 1998. The Application of Molecular Techniques in Enviromental Biotechnology for Monitoring Microbial Systems. Biotechnology and Applied Biochemistry 27:73-79.
128. Shapiro, H.M. 2000. Multiparameter Flow Cytometry of Bacteria: Implications for Diagnostics and Therapeutics. Cytometry 43:223-226.
129. Shapiro, H.M. and G. Nebe-von-Caron. 2004. Multiparameter Flow Cytometry of Bacteria. . Methods in Molecular Biology 263:33-44.
130. Shimizu, H., T. Mizuguchi, E. Tanaka, and S. Shioya. 1999. Nisin Production by a Mixed-culture System Consisting of *Lactococcus lactis* and *Kluyveromyces marxianus*. Applied and Environmental Microbiology 65(7):3134-3141.
131. Smith, H.L. 1981. Competitive Coexistence in an Oscillating Chemostat. Journal of Applied Mathematics 40:498-522.
132. Smith, H.L. and P. Waltman. 1995. The Theory of the Chemostat : Dynamics of Microbial Competition. H.L. Smith, editor. Cambridge: Cambridge University Press.
133. Smith, J.J., S.M. Travis, E.P. Greenberg, and M.J. Welsh. 1996. Cystic Fibrosis Airway Epithelia Fail to Kill Bacteria because of Abnormal Airway Surface Fluid Cell 85:229-236.
134. Smith, R.S. and B.H. Iglewski. 2003. *Pseudomonas aeruginosa* Quorum Sensing as a Potential Antimicrobial Target. Journal of Clinical Investigations 112(10):1460-1465.
135. Sokol, P.A., C.J. Lewis, and J.J. Dennis. 1992. Isolation of a Novel Siderophore from *Pseudomonas cepacia*. Journal of Medical Microbiology 36(184 - 189).

136. Somerville, G.A., M.S. Chaussee, C.I. Morgan, J.R. Fitzgerald, D.W. Dorward, L.J. Reitzer, and J.M. Musser. 2002. *Staphylococcus aureus* Aconitase Inactivation Unexpectedly Inhibits Post-exponential-phase Growth and Enhance Stationary-phase Survival. *Infection and Immunity* 70(11):6373-6382.
137. Somerville, G.A., B. Said-Salim, J.M. Wickman, S.J. Raffels, B.N. Kreiswirth, and J.M. Musser. 2003. Correlation of Acetate catabolism and growth yield in *Staphylococcus aureus*: implications for host-pathogen interactions. *Infection and Immunity* 71(8):4724-4732.
138. Spiegelman, D., G. Whissel, and C.W. Greer. 2005. A Survey of the Methods for the Characterization of Microbial Consortia and Communities. *Canadian Journal of Microbiology* 51:355-386.
139. Storhas, W. 2003. *Bioverfahrenentwicklung*: Wiley-VCH. 400 p.
140. Suzuki, M.T. and S.J. Giovannoni. 1996. Bias Caused by Template Annealing in the Amplification of Mixtures of 16S rRNA Genes by PCR. *Applied and Environmental Microbiology* 62(2):625-630.
141. Tattersson, L.E., J.F. Poschet, A. Firoved, J. Skidmore, and V. Deretic. 2001. CFTR and *Pseudomonas* Infections in Cystic Fibrosis. *Frontiers in Bioscience* 6:D890-897.
142. Tjihuis, L., E. Rekswinkel, M.C.M. Van Loosdrecht, and J.J. Heijnen. 1994. Dynamics of Population and Biofilm Structure in the Biofilm Airlift Suspension Reactor for Carbon and Nitrogen Removal. *Water Sci Tech* 29:377-384.
143. Tilman, D. 1982. *Resource Competition and Community Structure*. Princeton, New Jersey: Princeton University Press.
144. Trivier, D., M. Davril, N. Houdret, and R.J. Courcol. 1995. Influence of Iron Depletion on Growth Kinetics, Siderophore Production, and Protein Expression of *Staphylococcus aureus*. *FEMS Microbiology Letters* 127:195-200.
145. Trotha, R., U. Reichl, F.L. Thies, D. Sperling, W. Koenig, and B. Koenig. 2002. Adaption of a Fragment Analysis Technique to an Automated High-throughput Multicapillary Electrophoresis Device for the Precise Qualitative and Quantitative Characterization of Microbial Communities. *Electrophoresis* 23(7-8):1070-79.
146. Tümmler, B. and C. Kiewitz. 1999. Cystic Fibrosis: an Inherited Susceptibility to Bacterial Respiratory Infections. *Molecular Medicine Today* 5:351-358.
147. Vayenas, D.V. and S. Pavlou. 1999. Coexistence of Three Microbial Populations Competing for Three Complementary Nutrients in a Chemostat. *Mathematical Biosciences* 161:1-13.
148. Wang, M., S. Ahmé, M. Antonsson, and G. Molin. 2004. T-RFLP Combined with Principal Component Analysis and 16S rRNA Gene Sequencing: an Effective Strategy for Comparison of Fecal Microbiota Infants of Different Ages. *Journal of Microbiological Methods* 59:53-69.
149. Weber, J., J. Buehner, T. Bley, and R. Goehde. 2006. Populationen überwachen - Durchflußzytometrisches Online-Monitoring zur Prozesssteuerung. *BioTec* 5-6:32-33.
150. Welti, M., K. Jaton, M. Altwegg, R. Sahli, A. Wenger, and J. Bille. 2003. Development of a Multiplex Real-time Quantitative PCR Assay to Detect *Chlamydia pneumoniae*, *Legionella pneumophila* and *Mycoplasma pneumoniae* in Respiratory Tract Secretions. *Diagnostic Microbiology & Infectious Diseases* 45(2):85-95.
151. Whiteley, M., J.R. Ott, E.A. Weaver, and R.J.C. McLean. 2001. Effects of Community Composition and Growth Rate on Aquifer Biofilm Bacteria and Their Susceptibility to Betadine Disinfection. *Environmental Microbiology* 3(1):43-52.
152. Wilkinson, G.J. 1997. *Biology. The Staphylococci in Human Disease*. New York. p 1-38.
153. Williams, F.M. 1971. Dynamics of Microbial Populations In: B.C. Patten, editor. *Systems Analysis and Simulation in Ecology*. New York: Academic Press. p 147-267.
154. Wimpenny, J.W.T. and R. Colasanti. 1997. A Unifying Hypothesis for Biofilm Structures Based on Cellular Automaton Models. *FEMS Microbiology Ecology* 22(1):1-16.
155. Wolkowicz, G.S.K. and X.-Q. Zhao. 1998. N-species Competition in a Periodic Chemostat. *An International Journal for Theory and Applications* 11:465-491.
156. Worlitzsch, D., R. Tarran, M. Ulrich, U. Schwab, A. Cekici, K.C. Meyer, P. Birrer, G. Bellon, J. Berger, T. Weiss, K. Botzenhart, J.R. Yankaskas, S. Randell, R.C. Bouocher, and G. Döring. 2002. Effects of Reduced Mucus Oxygen Concentration in Airway *Pseudomonas* Infections of Cystic Fibrosis Patients. *The Journal of Clinical Investigations* 109(9):317-325.
157. Yoon, H., G. Klinzing, and H.W. Blanch. 1977. Competition for Mixed Substrates by Microbial Populations. *Biotechnology and Bioengineering* 19:1193-1977.
158. Yu, H. and N.E. Head. 2002. Persistent Infections and Immunity in Cystic Fibrosis. *Frontiers in Bioscience* 7:442-457.
159. Zeng, J.R., A.M. Saunders , Z. Yuan, L.L. Blackall, and J. Keller. 2002. Identification and Comparison of Aerobic and Dentrifying Polyphosphate-Accumulating Organisms. *Biotechnology and Bioengineering* 83(2):140-148.

9 Appendix

A. Chemicals and Equipment

Table 9.1: List of applied Chemicals

Name	Catalogue No./Supplier/Manufacturer
T-RFLP method	
LiChrosolv® water	Merck, Darmstadt, Germany
TRIS-HCl	No. 9090, Carl Roth, Karlsruhe, Germany
TRIS Ultra Qualität	No. 5429.3, Carl Roth, Karlsruhe, Germany
EDTA (Titrplex® III)	No. 1.08418, Merck, Darmstadt, Germany
Triton X-100	No. 1.08603, Merck, Darmstadt, Germany
Ortho-Phosphoric acid (H ₃ PO ₄), 85 %	No. 1.00573, Merck, Darmstadt, Germany
Glycerol, 87 %	No. 1.04094, Merck, Darmstadt, Germany
Bromphenolblau	No. 114421, Sigma, Taufkirchen, Germany
Xylencyanol	No. X-4126, Sigma, Taufkirchen, Germany
Lysozyme	No. L7651, Sigma, Taufkirchen, Germany
Lysostaphine	No. L0761, Sigma, Taufkirchen, Germany
RNAase A	No. 10109169001, Roche Diagnostics, Mannheim, Germany
Proteinase K (>600 mAU/mL)	No. 19133, Qiagen, Hilden, Germany
Ethanol (99,8 %, undenatured)	No. 9065.2, Carl Roth, Karlsruhe, Germany
QIAamp DNA blood Mini Kit	No. 51106, Qiagen, Hilden, Germany
hhaI-solution (10 U/μL)	No. R0139 L, New England Biolabs, Frankfurt a. M., Germany
NEB buffer 4	New England Biolabs, Frankfurt a. M., Germany
BSA solution (100x conc.) (10 mg/mL)	New England Biolabs, Frankfurt a. M., Germany
QIAquick Gel Extraction Kit	No. 28706, Qiagen, Hilden, Germany
10x PCR buffer	Takara Shiuzo, Cambrex Bioscience, Verviers, Belgium
MgCl ₂ (25 mM)	Takara Shiuzo, Cambrex Bioscience, Verviers, Belgium
primer 8f FAM	MWG, Ebersberg, Germany
5'-AGA GTT TGA TCC TGG CTC AG-3'	
primer 1492r	MWG, Ebersberg, Germany
5'-TAG CTT GTT ACG ACT T-3'	
dNTPs (2.5 mM each)	Takara Shiuzo, Cambrex Bioscience, Verviers, Belgium
Takara Ex Taq DNA polymerase (5 U/μL)	No. RR001, Takara Shiuzo, Cambrex Bioscience, Verviers, Belgium
1 kb ladder size standard	No. D-0428, Sigma, Taufkirchen, Germany

HiDi formamide	No. 4311320, Applied Biosystems, Darmstadt, Germany
Genescan [®] 500 ROX sizing standard	No. 401734, Applied Biosystems, Darmstadt, Germany
Polymer 3100 POP-6	No. 4316357, Applied Biosystems, Darmstadt, Germany
Media	
Q-Guard 2 Ultrapure water	Millipore, Schwalbach, Germany
α -D(+)-Glucose monohydrate	No. X997.2, Carl Roth, Karlsruhe, Germany
Sodium acetate anhydrous	No. 71183, Fluka Chemie, Buchs SG, Switzerland
Sodium hydroxide (NaOH)	No. 1.06482.1000 Merck, Darmstadt, Germany
Sodium hydrogen carbonate	No. 1.06329.1000, Merck, Darmstadt, Germany
Nitrilotriacetate (NTA)	No. A1280, AppliChem, Darmstadt
Sodium dihydrogenphosphate (NaH_2PO_4)	No. K300.2, Carl Roth, Karlsruhe
Dipotassium hydrogenphosphate (K_2HPO_4)	No. T875.2, Carl Roth, Karlsruhe
Casaminoacids	No. 0230-15-5, Difco
L-Methionine	No. 64320, Fluka Chemie, Buchs SG, Switzerland
GMEM basal medium	No. 22100, Gibco/Invitrogen, Karlsruhe, Germany
DMEM	Ready-made, provided by IDT company
Ham's F12	No. 21700, Gibco/Invitrogen, Karlsruhe, Germany
MEM α basal medium	No. 11900, Gibco/Invitrogen, Karlsruhe, Germany
M199 basal medium	No. 10012, Gibco/Invitrogen, Karlsruhe, Germany
Agar	No. 1.01616, Merck, Darmstadt, Germany
Sodium chloride (NaCl)	No. 3957, Carl Roth, Karlsruhe, Germany
Tryptone	No. 211705, Becton Dickinson, Heidelberg, Germany
Yeast extract	No. 212750, Becton Dickinson, Heidelberg, Germany
Potassium chloride (KCl)	No. 1.04936, Merck, Darmstadt, Germany
Columbia blood agar plates	No. PB5008A, Oxoid, Wesel, Germany
Chocolate agar plates (Vitox)	No. P05090A, Oxoid, Wesel, Germany
Charcoal agar plates (<i>C. jejuni</i>)	Oxoid, Wesel, Germany
CCDA <i>Campylobacter</i> plates	No. P05091A, Oxoid, Wesel, Germany
PCN agar plates	source: Institute of Medical Microbiology, Magdeburg, Germany
<i>B.c.</i> agar plates	source: Int. of Medical Microbiology,

<i>Staphylococcus</i> plates Columbia CNA	Magdeburg, Germany
Sodium di-hydrogenphosphate monohydrate (NaH ₂ PO ₄ *H ₂ O)	No. PB5049A, Oxoid, Wesel, Germany
Dipotassium hydrogenphosphate (K ₂ HPO ₄)	No. K300.2, Roth, Karlsruhe, Germany
Agarose	No. P749.2, Roth, Karlsruhe, Germany
	No. 2267.4, Roth, Karlsruhe, Germany
Cultivations	
Antifoam liquid	Contraspum 210, Zschimmer & Schwarz, Germany
Analytics	
Ammonium standard solution	Conc. 1000 mg/L NH ₄ ⁺ , Merck KGaA, Darmstadt, Germany
GMEM without glutamine	Sigma-Aldrich, Taufkirchen, Germany
Sodium acetate	No. 71180, Fluka Chemie, Buchs SG, Switzerland
Sodium formiate	No. 17841, Fluka Chemie, Buchs SG, Switzerland
Fumarate	No. F-2752, Sigma-Aldrich, Taufkirchen, Germany
Sodium fumarate	No. 47970, Fluka Chemie, Buchs SG, Switzerland
Malate	No. M-0375, Sigma-Aldrich, Taufkirchen, Germany
Sodium propionate	No. 18108, Riedel-de-Haen, Taufkirchen, Germany
Pyruvate (sodium salt)	No. P-8574, Sigma-Aldrich, Taufkirchen, Germany
Di-sodium-succinate	No. S 2378, Sigma, Buchs SG, Switzerland

Table 9.2: List of equipment

Name	Catalogue No./Supplier/Manufacturer
T-RFLP method	
Biofuge Fresco (1.5 – 2.0 mL tubes)	Heraeus Instruments, Hanau, Germany
Biofuge Stratos (15 mL centrifuge tubes, MTP)	Heraeus Instruments, Hanau, Germany
Vortexer Reax Top	Heidolph Instruments, Kelheim, Germany
Varioclav	H+P Labortechnik, Oberschleißheim, Germany
T3 Thermocycler	Biometra, Göttingen, Germany
Thermomixer	Eppendorf, Hamburg, Germany
Genetic Analyzer ABI Prism 3100Avant	Applied Biosystems, Darmstadt, Germany
Ultrospec 3000 UV/VIS Spectrophotometer	Pharmacia Biotech, Cambridge, UK
Ultra-Microcuvette	No. 5144575, Omnilab, Gehrden, Germany

DataCollection software 2.0	Applied Biosystems, Darmstadt, Germany
GeneMapper software 3.5	Applied Biosystems, Darmstadt, Germany
Media	
CampyGen sachets	No. CN0025; Oxoid, Wesel, Germany
Plastic anaerobic jar (2.5 L)	Oxoid, Wesel, Germany
0.2 µm sterile membrane filter	Nalgene Nunc International, USA
Static incubator	Modell 400, Memmert, Schwabach, Germany
Cultivations	
Biostat B2 STR	B.B. Biotech, Melsungen, Germany
Thermic mass flow controller	Bronkhorst High-Tech B. V., Netherlands
pH probe	405 DPAS SC, Mettler Toledo, Switzerland
Water cooling thermostat	F12, Julabo, Seelbach, Germany
Gas analysis module CO ₂	Uras 14, ABB Automation Products GmbH, Germany
Gas analysis module O ₂	Magnos 16, ABB Automation Products GmbH, Germany
Sterile filters gas (hydrophob)	Millex [®] FG, Millipore, Schwalbach, Germany
Flowmeter	Krohne AG, Basel, Switzerland
Return valve	EM Technik, Maxdorf, Germany
Process control system PCS 7	Siemens AG, München, Germany
Hose pump 101U/R	Watson-Marlow Limited, GB
Sterile coupling STT	B.B. Biotech, Melsungen, Germany
Oneway filtration Unit	Nalgene Nunc International, Rochester, USA
Milligard filter candle	Millipore, Schwalbach, Germany
Feed- and harvest bottles (25 L)	Nalgene Nunc International, Rochester, USA
Balance SG 32001 (max: 320,000 +/- 0.1 g)	Mettler Toledo, Greifensee, Switzerland
Dasgip fedbatch pro [®]	Dasgip AG, Jülich, Germany
StirrerPro [®] reactor vessels (470 mL)	Dasgip AG, Jülich, Germany
Bioblock [®] tempering and agitation unit	Dasgip AG, Jülich, Germany
PH4PO4 [®] monitoring unit	Dasgip AG, Jülich, Germany
MX4/4 [®] gas mixing unit	Dasgip AG, Jülich, Germany
GA4 [®] off-gas analysis unit	Dasgip AG, Jülich, Germany
MP8 [®] multipump unit	Dasgip AG, Jülich, Germany
Software EasyAccess [®]	Dasgip AG, Jülich, Germany
Orbital shaking incubator	ISF-W-1 with humidity, Kuehner AG, Basel, Switzerland
Brita water filter	Brita AG, Taunusstein, Germany
Shake flasks (unbaffled)	Schott, Mainz, Germany
pH meter for small vessels	WTW inoLab, Weilheim, Germany
Eppendorf centrifuge	
Spectrophotometer Ultrospec 500	Amersham, Munich, Germany
One-way Plastibrand 1.5 mL halfmicro	Brand, Wertheim, Germany

PMMA cuvettes, Vortexer Reax	Heidolph, Kelheim, Germany
Analytics	
Automated enzymatic glucose and lactate measurement biosensor	YSI 7100 MBS, Kreienbaum Wissenschaftliche Meßsysteme, Langenfeld, Germany
Ammonia measurement	Vitros DT60 II System Chemistry, Ortho- Clinical Diagnostics, Neckargemünd, Germany
NH ₃ analysis plates for Vitros DT60	Ortho-Clinical Diagnostics, Neckargemünd, Germany
Vitros DT pipettes and tips	Ortho-Clinical Diagnostics, Neckargemünd, Germany
Reversed phase HPLC (organic acids)	Agilent 1100 series, Agilent Technologies, Böblingen, Germany
Syringe filter Spartan 13/0,2 C: pore size 0,2 µm	Whatmann Schleicher und Schuell, Dassel, Germany
Reversed-phase column	Inertsil ODS-3, Particle size: 5 µm, MZ Analyzentechnik, Mainz, Germany
HPLC software (RP column)	ChemStation for LC 3d Rev. A. 09.03, Agilent Technologies, Böblingen, Germany

B. Media compositions

a) Recipes of defined media for selected strains

Table 9.3: Media compositions for *S. a.*, *P. a.*, *B. c.*, and *S. m.* as reported in literature

	Def. Medium für <i>S. aureus</i>	Def. Medium für <i>S. aureus</i>	Def. Medium für <i>S. aureus</i>	Def. Medium für <i>S. aureus</i>	Minimalmedium für <i>P. aeruginosa</i> und <i>B. cepacia</i>	ABC-Medium für Pseudomonaden	Def. Medium Stenotrophomonas
	MM (g/mol)	[mmol/L]	[mg/L]	[mg/L]	[mmol/L]	Teil 2, AG Eberl)	(Palleroni und Dubroff, 1972)
C-Quellen							
Glucose	180,16	27,8*	5008 *	27,75	5000,00	11,1*	-
Glycerol	92,09	68,4*	6298 *	-	-	-	-
Citronensäure*H ₂ O	210,14	0,2	42,03	-	-	-	-
Citronensäure	192,1	-	-	-	-	10*	10,0
Eisenammoniumsulfat	263	-	-	-	-	-	0,190
Natriumcitrat*2H ₂ O	294,1	-	1,390	-	400,000	-	-
Maltol (Apfelsäure)	134	-	0	-	0,000	-	0,037
			0	-	0	-	-
anorg. Salze			0	-	0	-	-
CaCl ₂	110,99	-	-	-	0,1	-	0,450
CaCl ₂ *2H ₂ O	129	-	-	-	-	0,1	-
Fe(NO ₃) ₃ *9H ₂ O	404	-	-	-	-	-	-
FeCl ₃ *6H ₂ O	270,33	0,09	24,3297	-	0,01	0,003	-
FeSO ₄ *7H ₂ O	278,02	-	-	-	-	-	-
KCl	74,55	-	-	-	-	-	-
K ₂ HPO ₄	174,18	40,2	7002,036	40,2	7000,0	-	-
KH ₂ PO ₄	136,09	-	14,7	2000,0	22,0	22,0	33
MgCl ₂ *6H ₂ O	203,3	-	-	-	1,0	2,0	-
MgSO ₄	120,37	-	0,4	50,0	-	-	-
MgSO ₄ *7H ₂ O	246,48	2,03	500,3544	-	-	-	2,029
NiCl ₂	58,44	-	-	-	51,3	51,3	-
Na ₂ HPO ₄	141,96	-	-	-	42,3	42,3	33,000
NaH ₂ PO ₄ *H ₂ O	138,07	14,5	2002,015	-	-	-	-
NaHCO ₃	84,01	-	-	-	-	-	-
NH ₄ Cl	53,49	-	0	-	0,0	-	18,695
(NH ₄) ₂ SO ₄	132,14	7,6	1004,254	7,6	1000,0	15,1	-
CuSO ₄ *5H ₂ O	249,68	-	-	-	-	-	-
ZnSO ₄ *7H ₂ O	287,54	-	-	-	-	-	-
			0	-	0,000	-	-
Aminosäuren							
L-Alanin	89,09	0,67	59,6903	0,673	60,000	-	-
L-Arginin	174,2	0,24	41,806	0,267	50,000	-	-
L-Arginin*HCl	210,86	-	-	-	-	-	-
L-Asparagin*H ₂ O	150,14	-	-	-	-	-	-
L-Asparaginsäure	133,1	0,68	90,506	0,676	90,000	-	-
L-Cystein*HCl*H ₂ O	175,64	-	-	-	-	-	-
L-Cystin	240,3	0,083	19,9449	0,083	20,000	-	-
L-Cystin*2HCl	276,96	-	-	-	-	-	-
L-Glutamin	146,15	0,61	89,1515	-	-	-	-
L-Glutaminsäure	147,13	-	-	0,690	100,000	-	-
Glycin	75,07	0,67	50,2969	0,696	50,000	-	-
L-Histidin	155,16	0,095	14,7402	0,129	20,000	-	-
L-Histidin HCl*H ₂ O	209,63	-	-	-	-	-	-
L-Isoleucin	131,17	0,23	30,1691	0,229	30,000	-	-
L-Leucin	131,18	0,68	89,2024	0,686	90,000	-	-
L-Lysin	146,19	0,27	39,4713	0,342	50,000	-	-
L-Lysin*HCl	182,65	-	-	-	-	-	-
L-Methionin	149,21	0,07	10,4447	0,020	3,000	-	0,268
L-Phenylalanin	165,19	0,24	39,6456	0,242	40,000	-	-
L-Prolin	115,13	0,09	10,3617	0,695	80,000	-	-
L-Serin	105,09	0,29	30,4761	0,000	0,000	-	-
L-Threonin	119,12	0,25	29,78	0,252	30,000	-	-
L-Tryptophan	204,23	0,05	10,2115	0,049	10,000	-	-
L-Tyrosin	181,19	0,28	50,7332	0,276	50,000	-	-
L-Tyrosin (D-Natriumsalz)	261,22	-	-	-	-	-	-
L-Valin	117,15	0,68	79,662	0,683	80,000	-	-
Casaminocacids	-	-	-	-	2 g/L	-	0,5 g/L
Vitamine							
Biotin	244,31	0,00002	0,0048862	0,00002	0,00500	-	0,00008
Cholindchlorid	139,63	-	-	-	-	-	-
D-Ca-Pantothenat	476,56	0,001	0,47656	0,001	0,250	-	0,0001
Folsäure	441,4	-	-	-	-	-	0,00005
Inositol	180,2	-	-	-	-	-	-
Nicotinamid	122,1	-	-	-	-	-	-
Nikotininsäure (Niacin)	123,1	0,01	1,231	0,010	1,200	-	0,0004
Pyridoxin*HCl	205,6	-	-	-	-	-	0,0005
Pyridoxal*HCl	203,6	0,02	4,072	-	-	-	-

b) Commercially available cell culture media

Table 9.4: Compositions of commercially available basal cell culture media and the variations introduced for bacterial cultivations. *

Vollmedien		GMEM	GMEM+P	GMEM+P-Gluc	GMEM+P-Gluc+NTA	DMEM	HAM'S F12	MEMO Medium
	[g/mol]	[mmol/L]	[mmol/L]	[mmol/L]	[mmol/L]	[mmol/L]	[mmol/L]	[mmol/L]
C-Quellen								
Glucose	180,16	25,0	31,1	25,0	25,0	25,0	10,0	5,6
Glycerol	92,09	-	-	-	-	-	-	-
anorg. Salze								
CaCl ₂	110,99	1,8	1,8	1,8	1,8	1,8	-	1,8
CaCl ₂ ·2H ₂ O	129	-	-	-	-	-	0,34	-
Fe(NO ₃) ₃ ·9H ₂ O	404	0,00025	0,00024	0,00024	0,00024	0,00025	-	-
FeSO ₄ ·7H ₂ O	278,02	-	-	-	-	-	0,003	-
KCl	74,55	5,4	5,4	5,4	5,4	5,37	3,00	5,4
K ₂ HPO ₄	174,18	-	37,5	37,5	37,5	-	-	-
KH ₂ PO ₄	136,09	-	-	-	-	-	-	-
MgCl ₂ ·6H ₂ O	203,3	-	-	-	-	-	0,61	-
MgSO ₄	120,37	0,8	0,81	0,81	0,81	0,81	-	0,8
MgSO ₄ ·7H ₂ O	246,48	-	-	-	-	-	-	-
NaCl	58,44	109,5	109,5	109,5	109,5	109,51	130,0	116,4
Na ₂ HPO ₄	141,96	-	-	-	-	-	1,0	-
NaH ₂ PO ₄	119,98	-	-	-	-	-	-	-
NaH ₂ PO ₄ ·H ₂ O	138,07	0,9	38,4	38,4	38,4	0,91	-	1,0
NaHCO ₃	84,01	-	-	-	-	-	14,0	-
(NH ₄) ₂ SO ₄	132,14	-	-	-	-	-	-	-
CuSO ₄ ·5H ₂ O	249,68	-	-	-	-	-	1,00128E-05	-
ZnSO ₄ ·7H ₂ O	287,54	-	-	-	-	-	0,003	-
Aminosäuren								
L-Alanin	89,09	-	-	-	-	-	0,101	0,28
L-Arginin	174,2	-	-	-	-	-	-	-
L-Arginin·HCl	210,86	0,2	0,20	0,20	0,20	0,40	1,00	0,60
L-Asparagin·H ₂ O	150,14	-	-	-	-	-	0,10	0,33
L-Asparaginsäure	133,1	-	-	-	-	-	0,10	0,23
L-Cistein·HCl·H ₂ O	175,64	-	-	-	-	-	0,20	0,57
L-Cystin	240,3	-	-	-	-	-	-	-
L-Cystin·2HCl	276,96	0,1	0,10	0,10	0,10	0,23	-	0,11
L-Glutamin	146,15	2,0	2,00	2,00	2,00	4,00	-	2,00
L-Glutaminsäure	147,13	-	-	-	-	-	0,10	0,51
Glycin	75,07	-	-	-	-	0,40	0,10	0,67
L-Histidin	155,15	-	-	-	-	-	-	-
L-Histidin HCl·H ₂ O	209,63	0,1	0,10	0,10	0,10	0,20	0,10	0,20
L-Hydroxyprolin	131,13	-	-	-	-	-	-	-
L-Isoleucin	131,17	0,4	0,40	0,40	0,40	0,80	0,03	0,40
L-Leucin	131,18	0,4	0,40	0,40	0,40	0,80	0,10	0,40
L-Lysin	146,19	-	-	-	-	-	-	-
L-Lysin·HCl	182,65	0,4	0,40	0,40	0,40	0,80	0,20	0,40
L-Methionin	149,21	0,1	0,10	0,10	0,10	0,20	0,03	0,10
L-Phenylalanin	165,19	0,2	0,20	0,20	0,20	0,40	0,03	0,19
L-Prolin	115,13	-	-	-	-	-	0,30	0,35
L-Serin	105,09	-	-	-	-	0,40	0,10	0,24
L-Threonin	119,12	0,4	0,40	0,40	0,40	0,80	0,10	0,40
L-Tryptophan	204,23	0,0	0,04	0,04	0,04	0,08	0,01	0,05
L-Tyrosin	181,19	-	-	-	-	-	-	-
L-Tyrosin (Di-Natriumsalz)	261,22	0,2	0,23	0,23	0,23	0,40	0,03	0,20
L-Valin	117,15	-	0,40	0,40	0,40	0,80	0,10	0,39
Vitamine								
L-Ascorbinsäure	176,13	-	-	-	-	-	-	0,284
p-Aminobenzoessäure	137,14	-	-	-	-	-	-	-
Biotin	244,31	-	-	-	-	-	0,00003	0,0004
Calciferol	396,66	-	-	-	-	-	-	-
D-Ca-Pantothemat	476,56	0,004	0,004	0,004	0,004	0,008	0,001	0,002
Chollinchlorid	139,63	0,014	0,014	0,014	0,014	0,029	0,100	0,007
Folsäure	441,4	0,005	0,0045	0,0045	0,0045	0,009	0,003	0,002
Inositol	180,2	0,020	0,02	0,02	0,02	0,040	0,100	0,011
Menadion	172,18	-	-	-	-	-	-	-
Nikotinamid	122,1	0,016	0,016	0,016	0,016	0,033	0,0003	0,008
Nikotinsäure (Niacin)	123,1	-	-	-	-	-	-	-
Pyridoxin·HCl	205,6	-	-	-	-	-	0,0003	-
Pyridoxal·HCl	203,6	0,010	0,01	0,01	0,01	0,020	-	0,005
Pyridoxamin·2HCl	241,1	-	-	-	-	-	-	-
Riboflavin	376,37	0,001	0,001	0,001	0,001	0,001	0,0001	0,0003
Thiamin	300,6	-	-	-	-	-	-	-
Thiamin·HCl	337,3	0,006	0,006	0,006	0,006	0,012	0,004	0,003

Vollmedien (Fortsetzung)		GMEM	GMEM+P	GMEM+P-Gluc	GMEM+P-Gluc+NTA	DMEM	HAM'S F12	MEMO Medium
	[g/mol]	[mmol/L]	[mmol/L]	[mmol/L]	[mmol/L]	[mmol/L]	[mmol/L]	[mmol/L]
<i>sonstige B.</i>								
Phenolrot	354,38	0,04	0,042	0,042	0,042	0,042	0,004	0,028
Adeninsulfat	368,34	-	-	-	-	-	-	-
Adenosin-5-Triphosphat	489	-	-	-	-	-	-	-
Adenosin-5-Phosphat	347	-	-	-	-	-	-	-
Cholesterin	386,7	-	-	-	-	-	-	-
2-desoxy-D-Ribose	134,13	-	-	-	-	-	-	-
Gluthadion (reduziert)	307,33	-	-	-	-	-	-	-
Guanin*HCl	187,59	-	-	-	-	-	-	-
HEPES	238,31	-	-	-	-	-	-	-
Hypoxanthin	136,11	-	-	-	-	-	-	-
Hypoxanthin (Natriumsalz)	159,1	-	-	-	-	-	0,030	-
Ribose	150,13							
Natriumacetat	82,03	-	-	-	-	-	-	-
Thymin	126,12	-	-	-	-	-	-	-
Tween 80	-	-	-	-	-	-	-	-
Uracil	112,09	-	-	-	-	-	-	-
Xanthin (Natriumsalz)	174	-	-	-	-	-	-	-
Linolsäure	280,46	-	-	-	-	-	0,0003	-
DL-68-Thiocitinsäure	206,33	-	-	-	-	-	0,001	0,001
Natriumpyruvat	110	-	-	-	-	-	1,000	1,0
Putrescin*2HCl	161,1	-	-	-	-	-	0,001	-
Thymidin	242,23	-	-	-	-	-	0,003	-
Nitritriessigsäure	191,1	-	-	-	4	-	-	-
Tryptone Peptone	-	-	-	-	-	-	-	-
Yeast Extract	-	-	-	-	-	-	-	-
<i>Ribonukleotide</i>								
Adenosin	267,2	-	-	-	-	-	-	0,04
Cytidin	243,2	-	-	-	-	-	-	0,04
Guanosin	283,2	-	-	-	-	-	-	0,04
Uridin	244,2	-	-	-	-	-	-	0,04
<i>Desoxyribonukleotide</i>								
2' Desoxyadenosin	251,25	-	-	-	-	-	-	0,04
2' Desoxycytidin	263,68	-	-	-	-	-	-	0,04
2' Desoxyguanosin	267,24	-	-	-	-	-	-	0,04
2' Desoxythymidin	208,21	-	-	-	-	-	-	0,05

* yellow marked are components that were added to the “original” composition

Volllmedium	MEM 111 Medium+P+NTA	MEM 111 Medium+P+NTA	Medium 199	Medium 199+P+NTA	Medium 199+P+NTA	LB	Casaminoacids
	[mmol/L]	[mg/L]	[mmol/L]	[mmol/L]	[mg/L]	[g/L]	Endkonz. 1g/L [mg/L]_{casam}
G-Quellen							
Glucose	5,55	1000,00	5,55	5,55	1000,00	-	-
Glycerol	-	-	-	-	-	-	-
anorg. Salze							
0	0	0	0	0	0	-	-
CaCl ₂	1,8	200,0	1,3	1,3	140,1	-	-
CaCl ₂ ·2H ₂ O	-	-	-	-	-	-	-
Fe(NO ₃) ₃ ·9H ₂ O	-	-	0,002	0,002	0,720	-	-
FeSO ₄ ·7H ₂ O	-	-	-	-	-	-	-
KCl	5,4	400,0	5,4	5,4	400,0	-	-
K ₂ HPO ₄	37,5	6531,8	-	37,5	6531,8	-	-
KH ₂ PO ₄	-	-	0,4	0,4	60,0	-	-
MgCl ₂ ·6H ₂ O	-	-	-	-	-	-	-
MgSO ₄	0,8	97,7	-	-	-	-	-
MgSO ₄ ·7H ₂ O	-	-	0,4	0,4	97,9	-	-
NaCl	116,4	6800,0	128,3	128,3	7500,0	5,00	-
Na ₂ HPO ₄	-	-	-	-	-	-	-
NaH ₂ PO ₄	-	-	0,4	0,4	47,7	-	-
NaH ₂ PO ₄ ·H ₂ O	39,4	5441,9	-	39,4	5301,9	-	-
NaHCO ₃	-	-	-	-	-	-	-
(NH ₄) ₂ SO ₄	-	-	-	-	-	-	-
CuSO ₄ ·5H ₂ O	-	-	-	-	-	-	-
ZnSO ₄ ·7H ₂ O	-	-	-	-	-	-	-
0	0	0	0	0	0	-	-
Aminosäuren							
0	0	0	0	0	0	-	-
L-Alanin	0,28	25,00	0,28	0,28	25,00	-	30
L-Arginin	-	-	-	-	-	-	25
L-Arginin·HCl	0,60	126,98	0,33	0,33	70,00	-	-
L-Asparagin·H ₂ O	0,33	50,00	-	-	-	-	-
L-Asparaginsäure	0,23	30,00	0,23	0,23	30,00	-	50
L-Asparagin·HCl·H ₂ O	0,57	100,00	0,00	0,00	0,11	-	-
L-Cystin	-	-	-	-	-	-	-
L-Cystin·2HCl	0,11	31,00	0,09	0,09	26,06	-	-
L-Glutamin	2,00	292,00	0,68	0,68	100,00	-	-
L-Glutaminsäure	0,51	75,00	0,45	0,45	66,82	-	159
Glycin	0,67	50,00	0,67	0,67	50,00	-	14
L-Histidin	-	-	-	-	-	-	19
L-Histidin HCl·H ₂ O	0,20	41,88	0,10	0,10	21,88	-	-
L-Hydroxyprolin	-	-	0,08	0,08	10,00	-	-
L-Isoleucin	0,40	52,40	0,15	0,15	20,00	-	40
L-Leucin	0,40	52,40	0,46	0,46	60,00	-	50
L-Lysin	-	-	-	-	-	-	59
L-Lysin·HCl	0,40	72,47	0,38	0,38	70,00	-	-
L-Methionin	0,10	15,00	0,10	0,10	15,00	-	14
L-Phenylalanin	0,19	32,00	0,15	0,15	25,00	-	36
L-Prolin	0,35	40,00	0,35	0,35	40,00	-	80
L-Serin	0,24	25,00	0,24	0,24	25,00	-	20
L-Threonin	0,40	48,00	0,25	0,25	30,00	-	17
L-Tryptophan	0,05	10,00	0,05	0,05	10,00	-	-
L-Tyrosin	-	-	-	-	-	-	4
L-Tyrosin (Di-Natriumsalz)	0,20	52,09	0,22	0,22	57,88	-	-
L-Valin	0,39	46,00	0,21	0,21	25,00	-	56
0	0	0	0	0	0	-	-
Vitamine							
0	0	0	0	0	0	-	-
L-Ascorbinsäure	0,284	50,000	0,0003	0,0003	0,0500	-	-
p-Aminobenzoesäure	-	-	0,0004	0,0004	0,0500	-	-
Biotin	0,0004	0,1000	0,00004	0,00004	0,01000	-	-
Calciferol	-	-	0,00025	0,00025	0,10000	-	-
D-Ca-Pantothenat	0,002	1,000	0,00002	0,00002	0,01000	-	-
Cholinchlorid	0,007	1,000	0,004	0,004	0,500	-	-
Folsäure	0,002	1,000	0,00002	0,00002	0,01000	-	-
L-Inositol	0,011	2,000	0,0003	0,0003	0,0500	-	-
Menadin	-	-	0,0001	0,0001	0,0100	-	-
Nikotinamid	0,008	1,000	0,0002	0,0002	0,0250	-	-
Nikotinsäure (Niacin)	-	-	0,0002	0,0002	0,0250	-	-
Pyridoxin·HCl	-	-	-	-	-	-	-
Pyridoxal·HCl	0,005	1,000	0,0001	0,0001	0,0250	-	-
Pyridoxamin·2HCl	-	-	-	-	-	-	-
Riboflavin	0,0003	0,1000	0,0003	0,0003	0,1000	-	-
Thiamin	-	-	-	-	-	-	-
Thiamin·HCl	0,003	1,000	0,00003	0,00003	0,01000	-	-

Vollmedien (Fortsetzung)	MEM \square Medium+P+NTA	MEM \square Medium+P+NTA	Medium 199	Medium 199+P+NTA	Medium 199+P+NTA	LB	Casaminoacids
	(mmol/L)	(mg/L)	(mmol/L)	(mmol/L)	(mg/L)	(g/L)	Endkonz. 1g/L (mg/L) _{gesamt}
sonstige B.							
Phenolrot	0,028	10,000	0,06	0,06	20,00		-
		0			0		-
Adeninsulfat	-		0,03	0,03	10,00		-
Adenosin-5-Triphosphat	-		0,002	0,002	1,000		-
Adenosin-5-Phosphat	-		0,0006	0,0006	0,2000		-
Cholesterin	-		0,001	0,001	0,200		-
2-Desoxy-D-Ribose	-		0,004	0,004	0,500		-
Glutathion (reduziert)	-		0,0002	0,0002	0,0500		-
Guanin*HCl	-		0,002	0,002	0,300		-
HEPES	-		25,00	25,00	5958,00		-
Hypoxanthin	-		-	-			-
Hypoxanthin (Natriumsalz)	-		0,002	0,002	0,354		-
Ribose	-		0,003	0,003	0,500		-
Natriumacetat	-		0,33	0,33	27,32		-
Thymin	-		0,002	0,002	0,300		-
Tween 80	-		20 mg/L	20 mg/L			-
Uracil	-		0,00	0,00	0,30		-
Xanthin (Natriumsalz)	-		0,002	0,002	0,344		-
Linolsäure	-		-	-			-
DL-68-Thiocitinsäure	0,001	0,200	-	-			-
Natriumpyruvat	1,0	110,0	-	-			-
Putrescin*2HCl	-		-	-			-
Thymidin	-		-	-			-
					0		-
Nitrothessapsäure	4	764,4	-	4	764,4		-
Tryptone Peptone	-		-	-		10	-
Yeast Extract	-		-	-		5	-
					0		-
Ribonukleotide					0		-
Adenosin	0,04	10,00	-	-			-
Cytidin	0,04	10,00	-	-			-
Guanosin	0,04	10,00	-	-			-
Uridin	0,04	10,00	-	-			-
					0		-
Desoxyribonukleotide					0		-
2' Desoxyadenosin	0,04	10,00	-	-			-
2' Desoxycytidin	0,04	11,00	-	-			-
2' Desoxyguanosin	0,04	10,00	-	-			-
2' Desoxythymidin	0,05	10,00	-	-			-

LEBENS LAUF

JULIA KRISTIANE SCHMIDT

ANSCHRIFT Käfertaler Straße 21, 68167 Mannheim**GEBURTSDATUM** 12. Okt. 1971**GEBURTSORT** Bad Oeynhausen (NRW, Deutschland)**SCHULISCHER WERDEGANG**

1982 – 1991 Immanuel-Kant-Gymnasium Bad Oeynhausen

PRAXIS

1991 – 1992 Metalltechnisches Praktikum, Fa. Buschjost Ventiltechnik, Bad Oeynhausen

Gießereitechnisches Praktikum, Fa. Brockfeld & Meyer, Bünde

Metalltechnisches Praktikum Fa. Vesuvius-Flocon, Apparatebau für Flüssigstahlverarbeitung, Champaign, Illinois, USA

STUDIUM

1992 – 2001 RWTH Aachen, Studium Maschinenbau (Dipl.-Ing.) mit Vertiefungsrichtung Bioverfahrenstechnik

Diplomarbeit am Lehrstuhl Bioverfahrenstechnik, RWTH Aachen

1998 – 1999 Verfahrenstechnische Studienarbeit am Institut de Chimie et Génie des Procédés, Ecole Centrale Paris, Frankreich

1994 – 2001 RWTH Aachen, Studium Biologie (Dipl.-Biol.) mit Vertiefung Molekularbiologie, Mikrobiologie und Biotechnologie

Diplomarbeit Fa. Henkel KGaA, Enzymtechnologie, Düsseldorf

WISSENSCHAFTLICHER WERDEGANG

2002 – 2007 Otto-von-Guericke-Universität Magdeburg, Wissenschaftliche Mitarbeiterin (Promotion) des Lehrstuhls Bioprozesstechnik am Max-Planck-Institut Dynamik komplexer technischer Systeme, Magdeburg

BERUFLICHER WERDEGANG

2007 – dato BASF SE, Ludwigshafen, Verfahrensentwicklung Industrielle Biotechnologie

Mannheim, 28.05.2008